LEVEL II

(12)

AD A108795

RADC-TR-81-282
Final Technical Report
November 1981

DESIGN, FABRICATION AND TEST OF A METAL-GRID ANGULAR FILTER

Hazeltine Corporation

John F. Pedersen
Peter W. Hannan

ROME AIR DEVELOPMENT CENTER
Air Force Systems Command
Griffiss Air Force Base, New York 13441

This report has been reviewed by the RADC Public Affairs Office (PA) and is releasable to the National Technical Information Service (NTIS). At NTIS it will be releasable to the general public, including foreign nations.

RADC-TR-81-282 has been reviewed and is approved for publication.

APPROVED: Peter R Franchi

PETER R. FRANCHI
Project Engineer

APPROVED: Allan C Schell

ALLAN C. SCHELL
Chief, Electromagnetic Sciences Division

FOR THE COMMANDER: John P. Huss

JOHN P. HUSS
Acting Chief, Plans Office

UNCLASSIFIED

SECURITY CLASSIFICATION OF THIS PAGE (When Data Entered)

REPORT DOCUMENTATION PAGE

READ INSTRUCTIONS BEFORE COMPLETING FORM

1. REPORT NUMBER RADC-TR-81-282	2. GOVT ACCESSION NO. AD-A108 795	3. RECIPIENT'S CATALOG NUMBER
4. TITLE (and Subtitle) DESIGN, FABRICATION AND TEST OF A METAL-GRID ANGULAR FILTER		5. TYPE OF REPORT & PERIOD COVERED Final Technical Report June 1980 - May 1981
		6. PERFORMING ORG. REPORT NUMBER 6436
7. AUTHOR(s) John F. Pedersen Peter W. Hannan		8. CONTRACT OR GRANT NUMBER(s) F19628-78-C-0152
9. PERFORMING ORGANIZATION NAME AND ADDRESS Hazeltine Corporation Pulaski Road Greenlawn NY 11740		10. PROGRAM ELEMENT, PROJECT, TASK AREA & WORK UNIT NUMBERS 62702F 46001436
11. CONTROLLING OFFICE NAME AND ADDRESS Deputy for Electronic Technology (RADC/EEAA) Hanscom AFB MA 01731		12. REPORT DATE November 1981
		13. NUMBER OF PAGES 176
14. MONITORING AGENCY NAME & ADDRESS (if different from Controlling Office) Same		15. SECURITY CLASS. (of this report) UNCLASSIFIED
		15a. DECLASSIFICATION/DOWNGRADING SCHEDULE N/A

16. DISTRIBUTION STATEMENT (of this Report)

Approved for public release; distribution unlimited

17. DISTRIBUTION STATEMENT (of the abstract entered in Block 20, if different from Report)

Same

18. SUPPLEMENTARY NOTES

RADC Project Engineer: Peter R. Franchi (RADC/EEAA)

19. KEY WORDS (Continue on reverse side if necessary and identify by block number)

Metal-Grid
Spatial Filter
Angular Filter

20. ABSTRACT (Continue on reverse side if necessary and identify by block number)

This final report describes the design, fabrication and test of a metal-grid spatial filter. The filter is a 5x5 foot flat panel incorporating 4 layers of crossed wire grids in a supporting structure of dielectric skins and dielectric honeycomb material.
The spatial filter passes an electromagnetic wave incident within its angular passband centered on normal incidence, but reflects the wave if it is incident beyond about 30° in the angular reject band. This result is

DD FORM 1473, 1 JAN 73 EDITION OF 1 NOV 65 IS OBSOLETE

UNCLASSIFIED

SECURITY CLASSIFICATION OF THIS PAGE (When Data Entered)

406 1'11

obtained for any polarization of the wave. The filter operates at 9 GHz, and has a bandwidth of about 1 GHz for passing a wave at normal incidence.

The measured characteristics of the spatial filter are close to those expected from analysis and previous tests of metal grids. There is more rejection for angles of incidence in the H plane than for incidence in the E plane.

Placement of the spatial filter in front of a reflector antenna results in a significant reduction of antenna sidelobes beyond 30° from the main beam in both the H plane and the E plane. There is only a slight degradation of the antenna sidelobes within the angular passband of the filter.

By
Dist
A

CONTENTS

CONTENTS (Cont)

LIST OF ILLUSTRATIONS

LIST OF ILLUSTRATIONS (Cont)

LIST OF TABLES

SECTION 1
INTRODUCTION

Spatial filters offer the potential for reducing sidelobes in the radiation patterns of directive antennas. An investigation of metal-grid spatial filters has been conducted by Hazeltine Corporation for RADC/ET. The program included study of metal grids, analysis of spatial filter designs, study of filter/antenna performance, and the design, fabrication and testing of a 5' x 5' filter.

Reference 1 reported the results of the first phase of this program. In that report the basic features of a metal-grid spatial filter were first described; then the results of a study and computer analysis were presented. This analysis included consideration of many filter characteristics and the important question of their sensitivity to tolerances. Also described were measurements of metal grids and dielectric supports in waveguides simulating angles near grazing in the E plane and angles near broadside.

The following report presents the results of the second phase of the program: the design, fabrication and test of a metal grid spatial filter. First this report reviews the concept of a spatial filter and then it outlines the choices available to construct the elements comprising the filter. Next is a discussion of the relationship between certain filter characteristics (reflection coefficient, insertion phase) and tolerances on the filter elements (layer susceptance and layer spacing). The results of the tolerance analysis (presented in detail in reference 1) were applied in selecting the filter fabrication technique, and in choosing the "strength" of the filter.

Ref. 1 - P. W. Hannan, P. L. Burgmyer, "Metal-Grid Spatial Filter", Interim Technical Report RADC-TR-79-295, by Hazeltine Corp., July 1980.

The test results on a 5 ft. square metal-grid spatial filter, and a comparison with theoretical calculations, is presented in Section 6. In addition, measurements of the spatial filter in conjunction with a reflector antenna are also presented in this section. Figure 1-1 is a photograph of the spatial filter being tested on the antenna range. Finally, concluding remarks are given in Section 7.

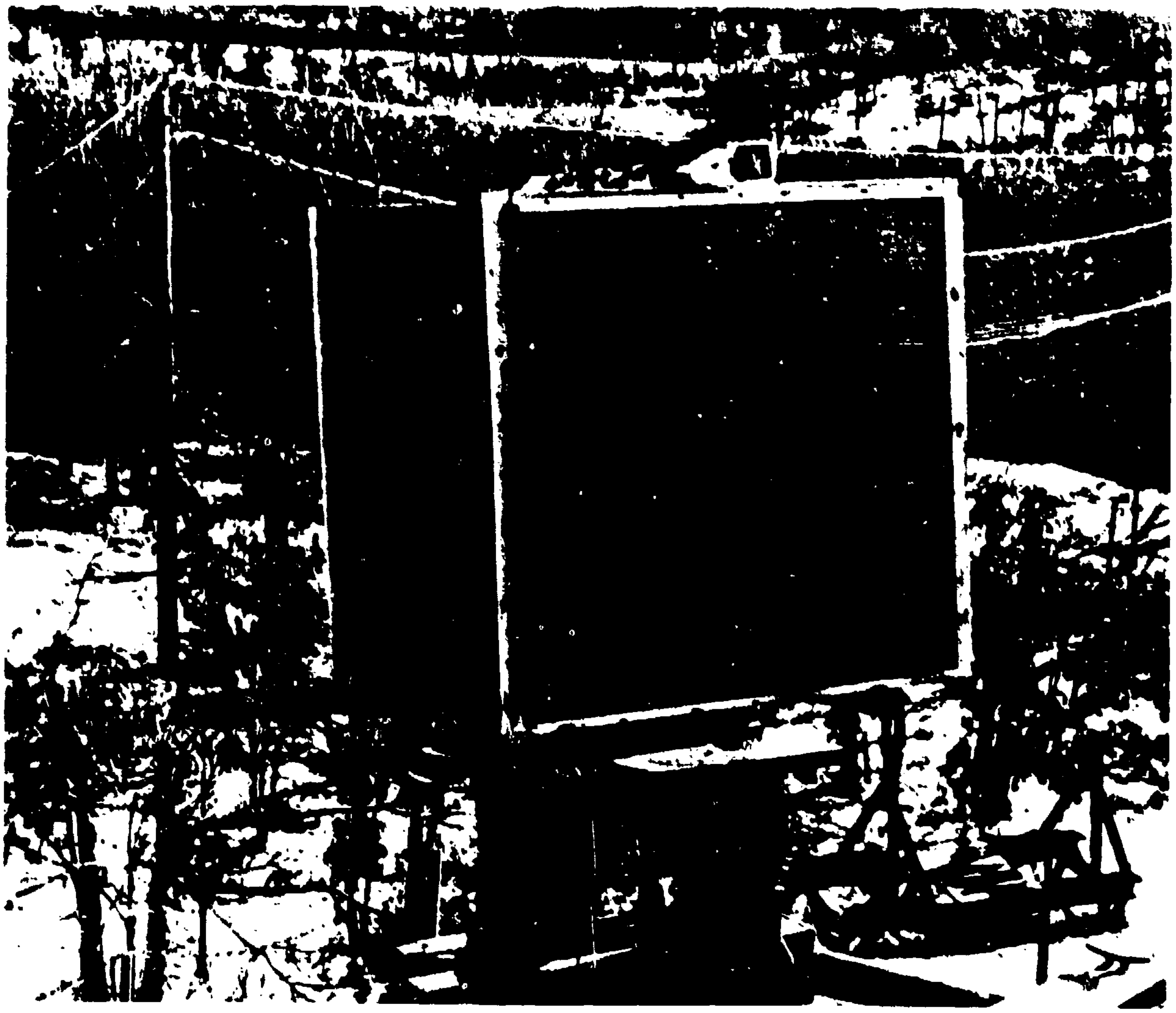

Figure 1-1 Photograph of Spatial Filter in Front of Antenna on Antenna Range

SECTION 2

THE METAL GRID SPATIAL FILTER

2.1 BACKGROUND

Spatial filters comprising layers of dielectric have been synthesized and analyzed by Mailloux (Ref.2). Raytheon, under contract to RADC, has extended this synthesis and has tested an experimental model of a dielectric filter (Ref. 3, 4).

Spatial filters utilizing layers of metal grids have been proposed by Schell et al (Ref. 5) and studied by Mailloux (Ref. 6). Experiments with some metal-grid filters have been performed by Rope et al (Refs. 7, 8). Mailloux and Franchi have analyzed and

Ref. 2 - R. J. Mailloux, "Synthesis of Spatial Filters with Chebyshev Characteristics", IEEE Trans. Antennas and Propagation, pp. 174-181; March, 1976.

Ref. 3 - J. H. Pozgay, S. Zamoscianyk, L. R. Lewis, "Synthesis of Plane Stratified Dielectric Slab Spatial Filters Using Numerical Optimization Techniques", Final Technical Report RADC-TR-76-408 by Raytheon Co., December, 1976.

Ref. 4 - J. H. Pozgay, "Dielectric Spatial Filter Experimental Study", Final Technical Report RADC-TR-78-248 by Raytheon Co., November, 1978.

Ref. 5 - A. C. Schell et al, "Metallic Grating Spatial Filter for Directional Beamforming Antenna" AD-D002-623; April, 1976.

Ref. 6 - R. J. Mailloux, "Studies of Metallic Grid Spatial Filters", IEEE AP-S Int. Symp. Digest, p. 551; 1977.

Ref. 7 - E. L. Rope, G. Tricoles, O-C Yue, "Metallic Angular Filters for Array Economy", IEEE AP-S Int. Symp. Digest, pp. 155-157; 1976.

Ref. 8 - E. L. Rope, G. Tricoles, "An Angle Filter Containing Three Periodically Perforated Metallic Layers", IEEE AP-S Int. Symp. Digest, pp. 818-820; 1979.

tested experimental models of metal-grid filters (Ref. 9).

In comparison with dielectric filters, filters that use metal grids offer reduced weight and fabrication cost. Also, pure metal grids do not have the dielectric Brewster-angle effect that can cause a spurious passband for E-plane incidence. However, metal grids are generally supported by dielectric layers, so the question of spurious passbands remains; this was addressed in the first phase of this investigation (Ref. 1, 10).

Ref. 9 - R. J. Mailloux and P. R. Franchi, "Metal Grid Angular Filters for Sidelobe Suppression", RADC-TR-79-10; January 1979.

Ref. 10 - P. W. Hannan and J. F. Pedersen, "Investigation of Metal-Grid Angular Filters", Proceedings of the 1980 Antenna Applications Symposium, Allerton Park, Illinois; September 1980.

2.2 PURPOSE OF SPATIAL FILTER

A spatial filter is a device which passes or rejects an electromagnetic wave depending on the angle of incidence of this wave relative to the filter surface. A representative spatial filter is indicated in Figure 2-1(a), in which waves incident at and near broadside (normal incidence) are passed by the filter but waves incident at angles further from broadside are rejected by the filter.

If a spatial filter is placed in front of a directive antenna, it can reduce those sidelobes of the directive antenna that correspond to waves that are incident in the angular reject band of the filter. The main lobe of the antenna corresponds to a wave that is incident in the angular passband of the antenna, and is not substantially affected by the filter. This case is indicated in Figure 2-1(b).

The antenna may have either a fixed main beam or a main beam that is scanning over a limited angular region. For a scanning beam antenna, the angular passband of the spatial filter can encompass the scan region so that the main beam is always passed but potential grating lobes may be rejected. This application was considered by Mailloux (Ref. 2). For a fixed-beam antenna such as the reflector antenna indicated in Figure 2-1(b), the spatial filter can reduce the sidelobes caused by feed spillover, feed-support scattering, and reflector contour errors while retaining a strong main beam. The reflector antenna application is the principal one that is considered in this program.

2.3 PRINCIPLE OF SPATIAL FILTER

The spatial filters investigated in this program operate in accordance with a single basic principle. This principle appears in Reference 5, and is repeated in the following. As indicated in Figure 2-2 the spatial filter comprises a series of layers. Each layer acts essentially as a shunt susceptance to an incident plane wave. Between these susceptance layers are regions of essentially free space in which the plane wave travels in almost the same direction as its incidence direction.

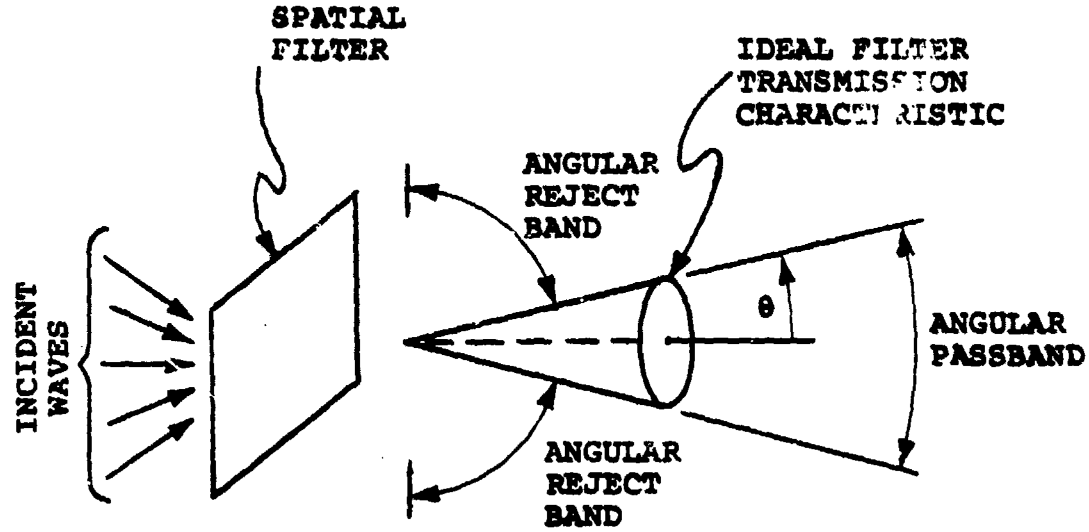

(a) basic function

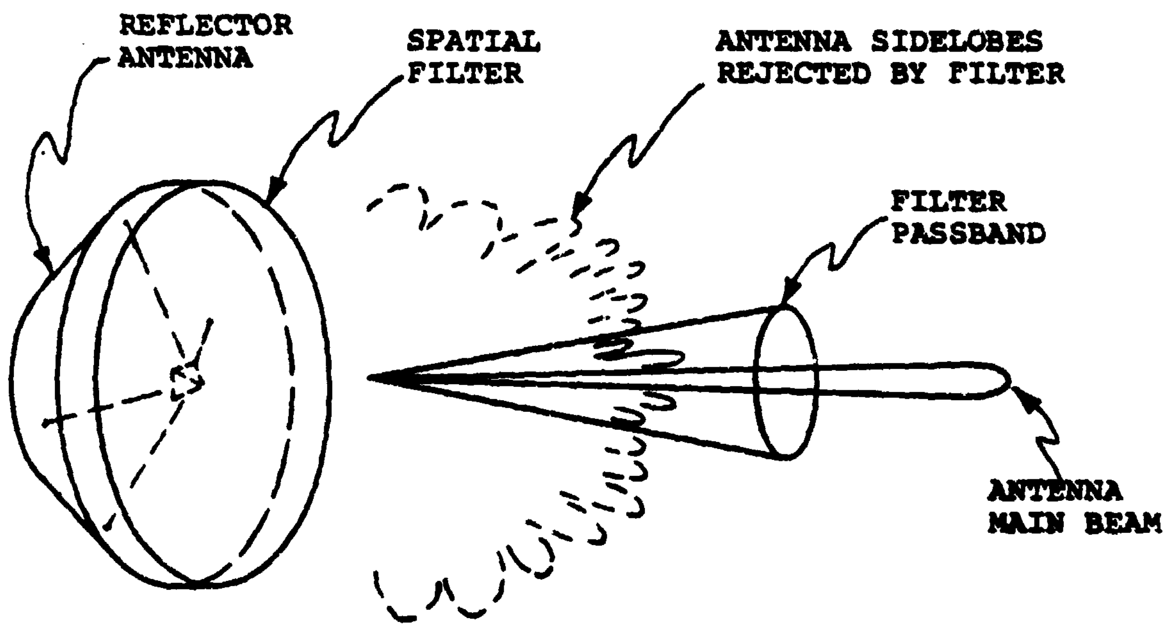

(b) application to reflector antenna

Figure 2-1 Purpose of Spatial Filter

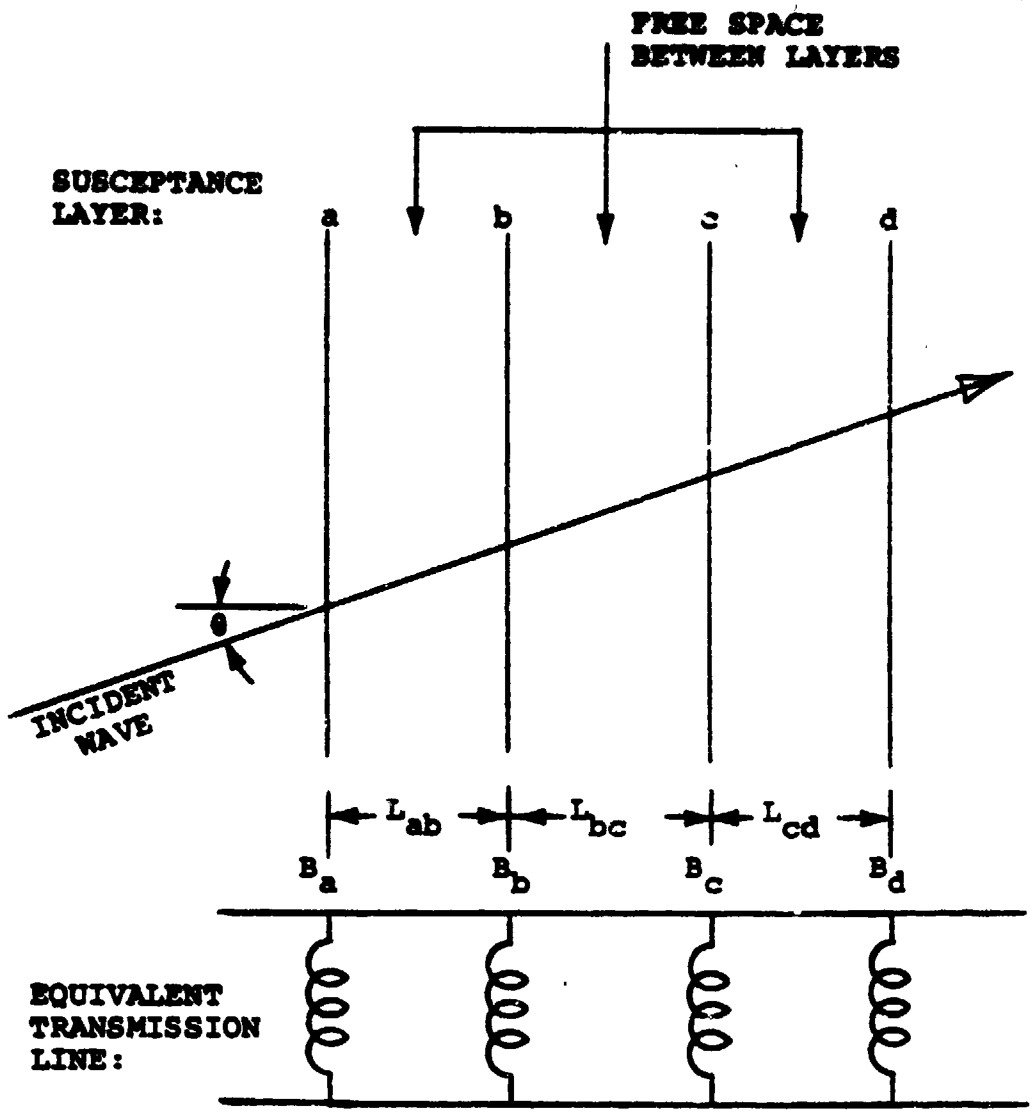

EQUIVALENT WAVELENGTH $= \lambda_g = \dfrac{\lambda}{\cos\theta}$

EQUIVALENT PHASE SHIFT BETWEEN LAYERS $= \dfrac{2\pi L}{\lambda_g}$

$$= \frac{2\pi L \cos\theta}{\lambda} = \frac{2\pi L}{c} f \cos\theta$$

Figure 2-2 Principle of Metal-Grid Spatial Filter

In a transmission-line equivalent circuit of this spatial filter the equivalent wavelength or "guide" wavelength (λ_g) is equal to the free-space wavelength divided by cos θ where θ is the angle of incidence. The phase shift between layers is therefore proportional to cos θ as well as to frequency. The nominal values for the susceptance layers and the phase shifts between layers can be specified so as to yield a conventional frequency filter. However, because the phase shifts between layers are proportional to cos θ as well as to frequency, the structure will also act an an angle-sensitive filter in which the term cos θ is the variable of significance. The net result is that the spatial filter can be designed on the basis of a conventional frequency filter.

SECTION 3
CONSTRUCTION OF A METAL-GRID SPATIAL FILTER

3.1 INTRODUCTION

It is the purpose of this section to discuss the choices available to fabricate a metal-grid spatial filter. First, the alternatives that may be used to construct the metallic-grid layers will be compared to the practical considerations of realizing the susceptance values of typical filters. Consideration will also be given to filter size and its relationship to the choice of crossed grids or parallel grids.

This section will also discuss the effect that dielectric material has on the performance of a spatial filter. Dielectric material is needed to support the susceptance layers and to space the layers from each other. The specific dielectric material selected for the filter fabricated during this program will be discussed in Section 5.

3.2 LAYER SUSCEPTANCE

A metal-grid spatial filter comprises a series of metal-grid susceptance layers. Each susceptance layer is spaced from the others in accordance with the design equations of conventional frequency filters. The susceptance layer of a spatial filter may be made from several types of metallic grids. An early selection can be made between certain types of metallic grids for those cases where the performance is clearly preferable to another. In other cases the choice is more complex and the selection depends upon factors relating to the physical dimensions of the filter as well as the electrical specification of frequency, angular pass-band width, angular rejection etc.

Inductive or Capacitive Grid

One choice that can be made is between an inductive susceptance or a capacitive susceptance for the metal grid, as indicated in Figure 3-1. The central layers in a spatial filter typically require rather large values of susceptance. These large values are easily obtainable with a non-resonant inductive grid by using a closely-spaced grid. On the other hand large

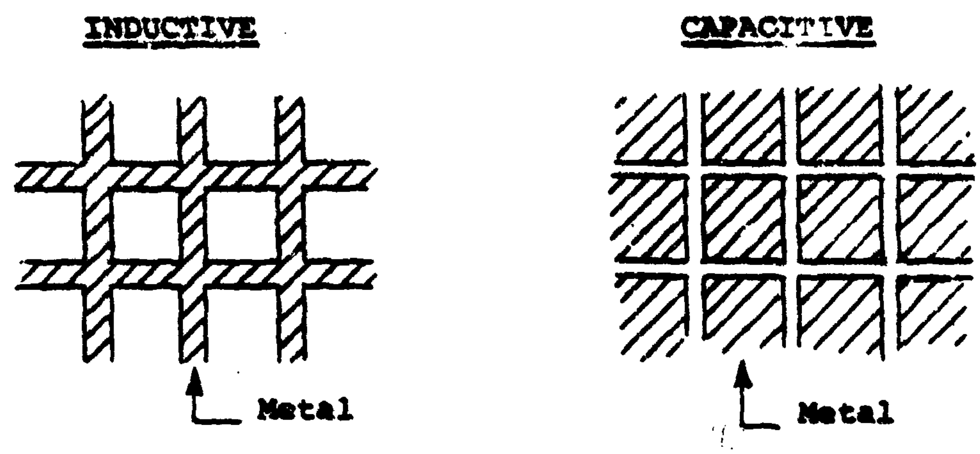

Figure 3-1 Inductive and Capacitive Metal Grids

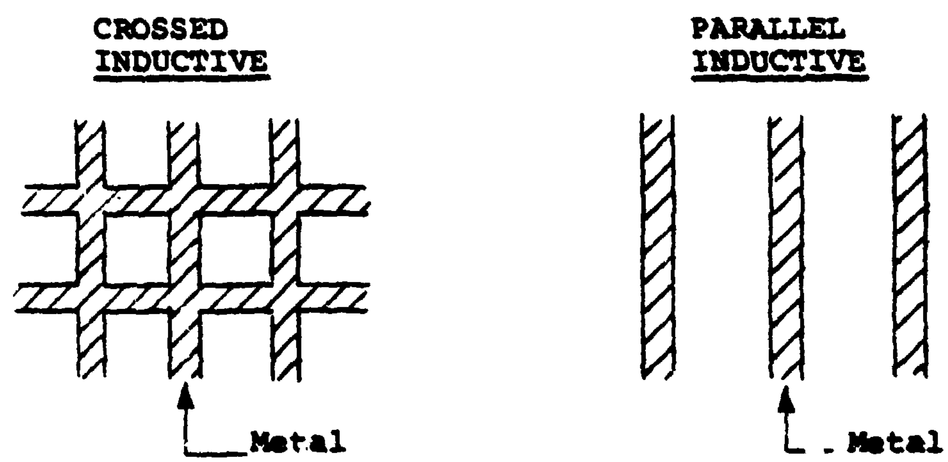

Figure 3-2 Crossed and Parallel Inductive Metal Grids

susceptance values with a non-resonant capacitive grid require very small capacitive gaps that would be difficult to control to an acceptable tolerance. The alternative, a resonant capacitive grid, would degrade the frequency behavior of the filter and would also have a problem of tolerance control.

Another factor of significance is the strong potential for spurious passbands in the E-plane of incidence with a capacitive metal grid supported by a dielectric skin. With an inductive metal grid this potential also exists but to a lesser degree. For these reasons an inductive susceptance has been selected for the metal-grid spatial filter.

Crossed Grid or Parallel Grid

Another choice that can be made is between a crossed inductive grid and a parallel inductive grid, as indicated in Figure 3-2. A spatial filter using crossed grids is capable of providing the desired rejection outside the passband for incident waves of any polarization. With a spatial filter using only parallel grids, incident waves polarized perpendicular to the wires would pass through the filter virtually unaffected.

In a reflector antenna designed for linear polarization, some of the sidelobe radiation can be cross polarized. For example, wide-angle radiation from currents in the feed supports and from spillover beyond the edge of the reflector can contain appreciable cross-polarized components. A spatial filter using parallel grids would not reject these cross-polarized sidelobes. Of course, with a reflector antenna designed for circular polarization or dual polarization a spatial filter using parallel wire grids would not adequately reject even the normally-polarized sidelobes. A spatial filter using crossed grids is clearly more effective for these applications.

A crossed inductive grid has some problems of construction in large sizes as well as some complexities of behavior vs. angle of incidence. However, the crossed grid has been selected for the metal-grid spatial filter, because of its capability for providing a spatial filter having adequate rejection for all polarizations.

Configuration of Crossed Grid

There are several practical configurations that are capable of providing an inductive crossed metal grid. These configurations may be separated into two categories: (1) contacting crossed grids, and (2) insulated crossed grids. With the contacting crossed grids, the crossed sets of parallel conductors have electrical contact at all the crossing points. With the insulated crossed grids there is no conductive path between the crossed sets of parallel conductors, although there is some capacitance. Also the two crossed sets of parallel conductors in an insulated crossed grid are typically slightly displaced from each other.

Two configurations for the contacting crossed grids are of interest. One configuration is flat metal strips on a sheet of dielectric, as indicated in Figure 3-3(a). A good method for obtaining this configuration is to use conventional printed-circuit technology in which a copper-clad sheet of thin dielectric is selectively etched, leaving the desired pattern of copper on the dielectric sheet. This method is best suited to structures which are flat. which is expected to be the case for a typical spatial filter. A limitation of this method is that an area as large as that typically required for a spatial filter cannot be obtained from a single printed-circuit panel. Assembling several printed-circuit sheets is possible but presents some practical difficulties of securing the necessary electrical contact in all the conductors across adjacent sheets.

The other configuration for a contacting crossed grid is holes in a metal sheet, as indicated in Figure 3-3(b). A thin dielectric sheet bonded to the holed metal sheet may be needed for strength and for assembly in a multi-layer spatial filter. A limitation of the holed metal sheet configuration again is the area that can be constructed with a single sheet; however, this area is typically larger than that available with the strip construction described above. Round holes, as shown in the figure,

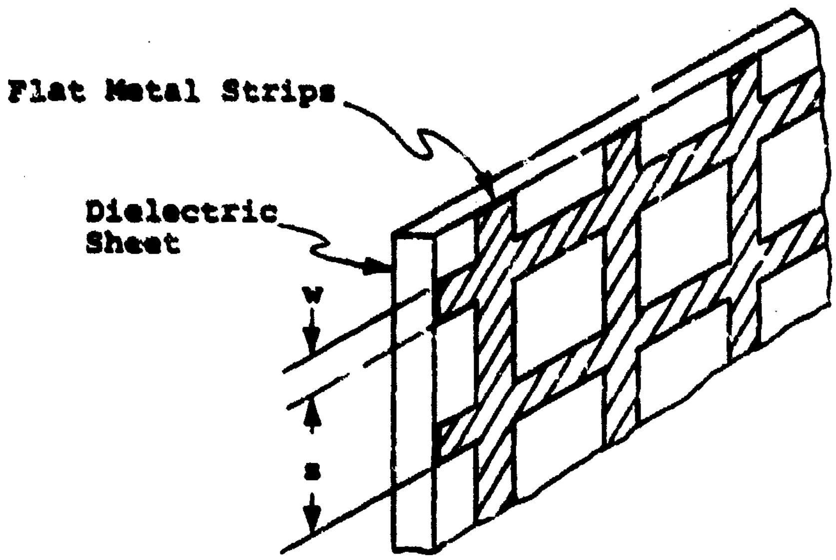

(a) strip configuration

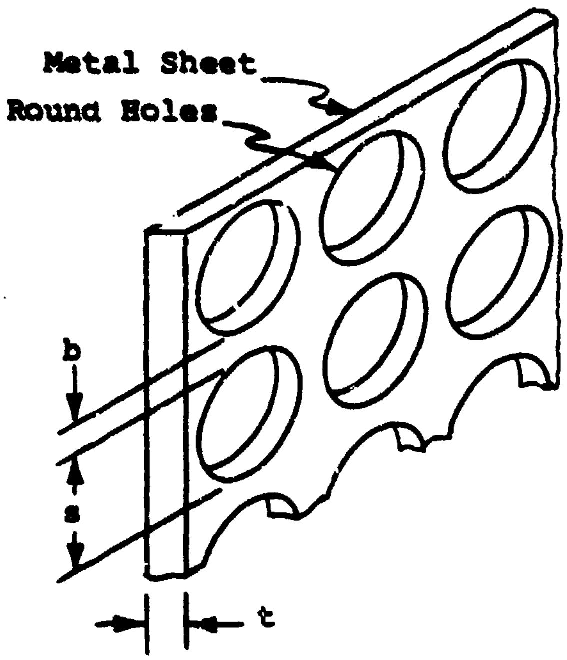

(b) hole configuration

Figure 3-3 Contacting Inductive Crossed Metal Grids

are easily obtainable with rather good control of tolerances when large susceptance is desired. However, small values of susceptance with round-non-resonant holes requires the holes to be nearly touching which may be difficult to achieve reliably. Approaching resonance by the addition of a major amount of dielectric would reduce the susceptance of the round holes but would complicate the frequency behavior of the filter and would create problems of dielectric tolerance control. An approach that can overcome this problem is to use a procedure for constructing the holes that makes them nearly square instead of round.

For the insulated crossed grids there are also two configurations of interest. One configuration is crossed grids of round metal wires embedded in a thin dielectric sheet as indicated in Figure 3-4(a). Many different antennas have used this type of construction for their reflecting surfaces, and curved as well as flat surfaces can be made. There is not a clear limitation of area with this wire configuration, although very large areas would require special construction techniques. The behavior of this insulated crossed grid for E-plane incidence is more complex than that of a contacting crossed grid, and may be more subject to possible spurious passbands

The other insulated crossed grid configuration is flat metal strips on different dielectric sheets for the two crossed grids, as indicated in Figure 3-4(b). This configuration avoids some of the area limitation inherent with printed-circuit construction because printed circuits can usually be made longer in one dimension than the other. If the long dimension is parallel to the conductors in each grid, a larger area can be assembled while avoiding the need for providing electrical contact across adjacent sheets. As with the crossed wires, the behavior of this insulated crossed strip grid for E-plane incidence is more complex than that of the contacting crossed strip grid, and may be more subject to possible spurious passbands.

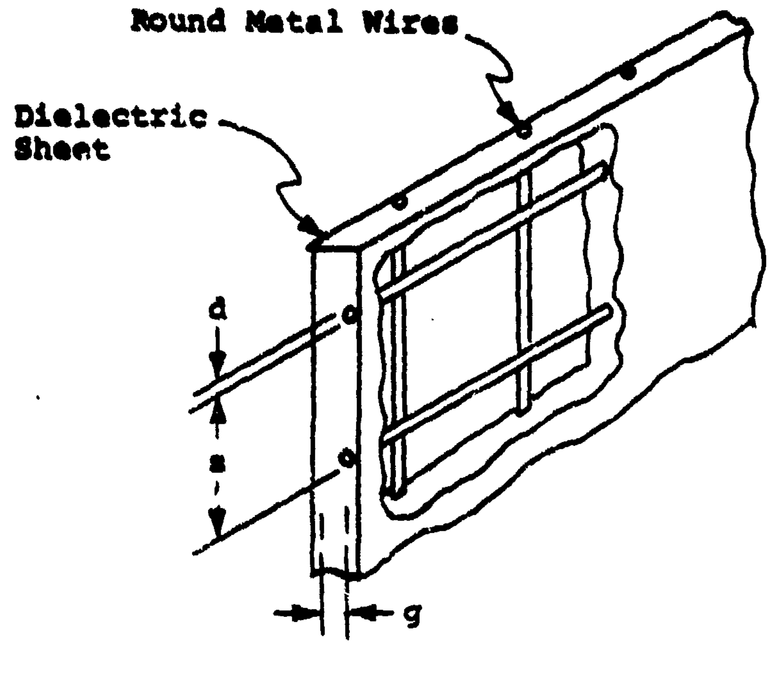

(a) wire configuration

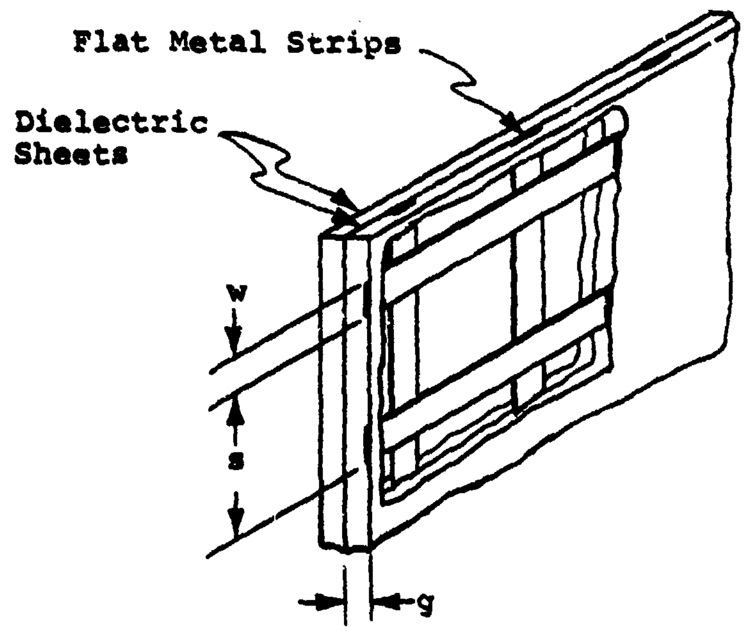

(b) strip configuration

Figure 3-4 Insulated Inductive Crossed Metal Grids

3.3 DIELECTRIC SUPPORT STRUCTURE

Ideally the metal-grid spatial filter comprises several layers of metal grids separated by regions of essentially free space. For a structure that is mechanically sound, it is necessary to support the metal-grid layers with dielectric material. A representative construction is indicated in Figure 3-5. To separate the metal-grid layers a dielectric core material such as honeycomb or foam is used. To lend mechanical strength to the metal grid, it is typically bonded to or embedded in a thin dielectric skin. Both the spacers and the skins can have an effect on the performance of the spatial filter.

Dielectric Core Effects

The dielectric core material has a dielectric constant k only slightly greater than unity. This low dielectric constant is desired in order to retain the wave angle within the spatial filter as close as possible to the angle of the wave incident on the spatial filter. The principal effect of a low-k core on the passband of the spatial filter can be compensated by a simple change of the separation between the metal-grid layers. The dissipative loss of the core material, while usually not substantial for ordinary radome-type applications, can be appreciable in the spatial filter because of the increased electric field in the core material caused by the resonant behavior of the spatial filter in its passband. Also, variations of the dielectric constant of the core material caused by non-uniform density or by anisotropy, although small, can contribute to a degradation of spatial-filter performance.

An additional effect of the dielectric core material is the modification of the spatial filter rejection for large angles of incidence in the E-plane. While the reflection of a crossed metal grid tends toward zero at $\theta = 90°$ in the E-plane, the reflection of a dielectric tends toward unity at $\theta = 90°$. This is true for the low-k spacer material even though such material has a very small reflection near broadside. It happens that beyond

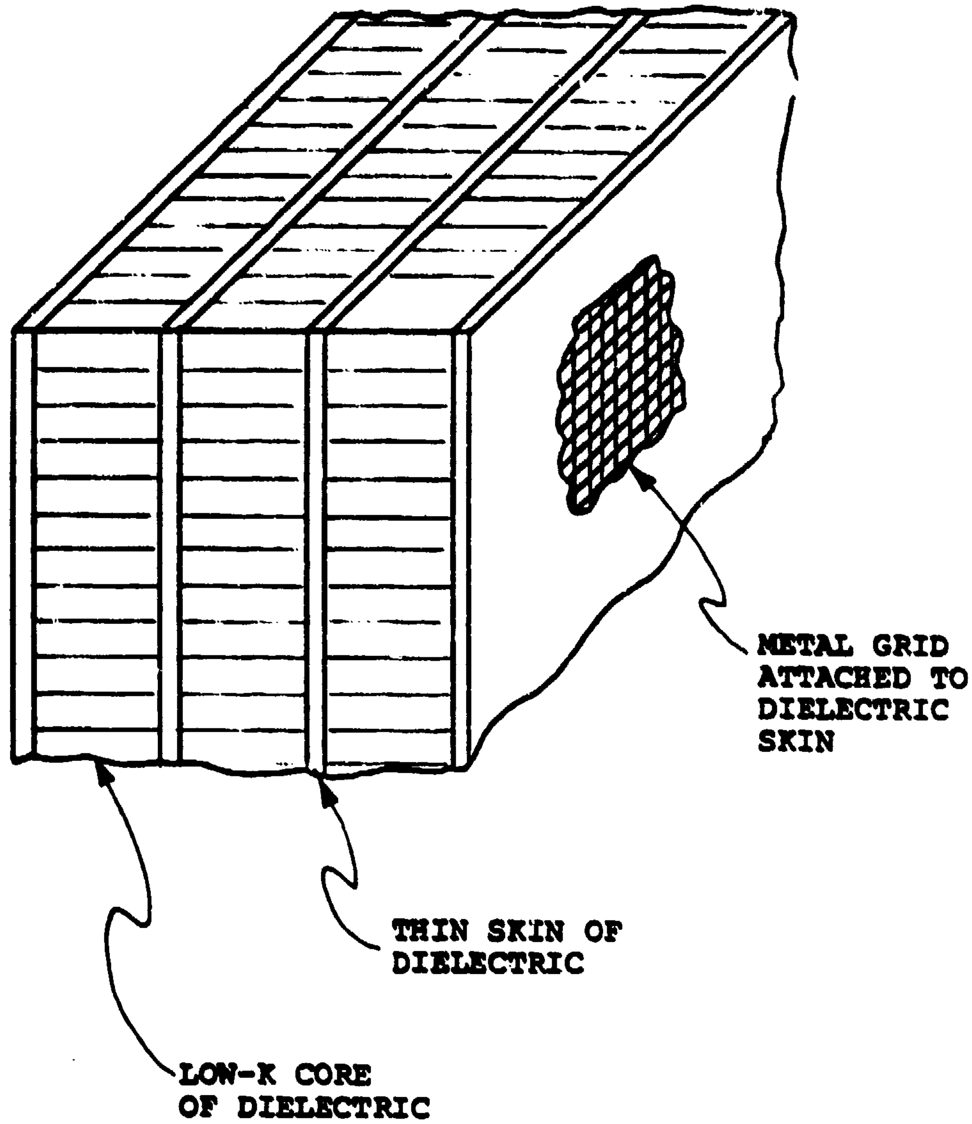

Figure 3-5 Dielectric Support Structure for Metal Grids in a Spatial Filter

the Brewster angle in the E-plane of incidence the reflection of the dielectric core material tends to reinforce the reflection of an inductive metal grid. This is fortunate for the rejection performance of a spatial filter, because otherwise the grid and spacer reflections could cancel at some large angle of incidence in the E-plane, giving a spurious passband. Instead, the rejection of the filter is enhanced by the core material at large incidence angles in the E-plane.

In the H-plane of incidence, the reflection of dielectric material tends to subtract from the reflection of a crossed metal grid. However, the reflection of the metal grid tends toward unity at $\theta = 90°$ in the H-plane, and it predominates over the dielectric reflection. Therefore, there is no opportunity for a spurious passband in the H-plane of incidence. Also, the modification of the H-plane rejection characteristic of the metal grid by the dielectric material is not very important because the rejection provided by a crossed metal grid at large angles in the H-plane is large compared with that in the E-plane.

Dielectric Skin Effects

Metal grids consisting of thin strips or small-diameter wires should be bonded to or embedded in a dielectric skin in order to have mechanical integrity. Holes in a metal sheet are also likely to need a dielectric skin because of the thin metal cross-section between holes required to obtain low values of non-resonant susceptance. A typical dielectric skin is fiberglass with a dielectric constant of about 4 and a thickness of about 0.030 inches.

The basic effect of a dielectric skin on the passband of the spatial filter can be compensated approximately by a change in the susceptance of the metal grid. A thin dielectric skin behaves approximately as a capacitive susceptance with the following value at broadside incidence:

$$B_{skin} \approx \frac{2\pi t(k-1)}{\lambda}$$

where t is the thickness of the skin and k is its dielectric constant. The inductive susceptance of the metal grid should be increased by approximately this value in order to retain the original filter behavior at broadside incidence. The dissipative loss of the skin, in contrast to that of the core, is not enhanced by the filter resonance.

The dielectric skin also modifies the spatial filter rejection for large angles of incidence in the E-plane. At incidence angles very close to grazing incidence in the E-plane the dielectric skin can increase the filter rejection. However at other incidence angles in the E-plane, the dielectric skin can decrease the filter rejection.

For a more detailed discussion that includes computed and measured results on E-plane rejection of metal grids with dielectric support, the reader should refer to reference 1.

SECTION 4
SPATIAL FILTER DESIGN ANALYSIS

4.1 PURPOSE OF DESIGN ANALYSIS

It was the objective of the analysis completed during the first phase of this investigation (ref. 1) to examine the basic tradeoffs between the filter parameters of passband width, passband ripple, and number of poles, and the related qualities such as stop-band rejection, cutoff slope, frequency bandwidth, and sensitivity to tolerances. For this purpose only the essential elements of the filter, the susceptances and the lengths, were considered, without the perturbing effect of the dielectric materials that would be needed in a self-supporting construction. A basic factor that limits the performance available from the spatial filter is the sensitivity to tolerances; this subject is considered later in this section.

4.2 BASIC FILTER DESIGN

The design of the spatial filter follows conventional frequency filter methods, which are well-documented in the literature (Ref. 11). The narrowband design technique of Ref. 11 is used since it is straightforward and is adequate for the major purposes of this study. A Chebyshev equal-ripple type has been selected by reason of its characteristic sharp cutoff beyond the passband. For any desired combination of passband width, number of poles, and passband ripple, the filter element values can be determined. For speed and accuracy, a computer provides the nominal filter element values, i.e., the various lengths and susceptances in each filter.

Ref. 11 - G. L. Matthaei, L. Young, E. M. T. Jones, "Microwave Filters, Impedance-Matching Networks, and Coupling Structures", McGraw-Hill, pp. 85-101, 450-452; 1964.

Nominal element values have been obtained for a number of 2-, 3-, and 5-pole filters of various passband widths and ripple values. The passband widths are grouped in three representative values within a $\pm 10°$ to $\pm 20°$ range, and ripple values range upward and downward from a typical value of .01 dB transmission loss. Table 4-1 lists the various designs and identifies each with a code indicating the design values. The letters A, B, and C denote passband widths of ±11.5, ±14 or ±18 degrees; the first number indicates the number of poles; and the second number counts the number of zeroes in the ripple dB value.

The element designations for the various filters are illustrated in Figure 4-1 and are tabulated in Table 4-2. In this table the lengths are given both in electrical degrees and in inches at a design frequency of 9.5 GHz (lengths in inches are needed in some tolerance studies). It can be seen from the table that the lengths approach a half wavelength as the susceptance values become large.

4.3 NOMINAL FILTER PERFORMANCE

For each of the selected filter designs, performance with nominal element values has been computed and plotted in reference 1. The plots include transmission loss, reflection coefficient, and insertion phase as a function of incidence angle in both the H-plane and the E-plane. In addition, computed values of cut-off slope at the -6 dB transmission point, rejection at 25° and 45° off broadside, and reflection coefficient and insertion phase at broadside (or nominal) incidence have been obtained and tabulated in reference 1.

An interesting correlation relating the sum of all the susceptive elements of a filter to the rejection that the filter provides at 45° incidence is shown in Figure 4-2. For a given quantity of poles a single curve relates the rejection to the total susceptance, regardless of passband width or ripple level. More poles tend to give greater rejection for a given total susceptance, particularly for filters with large rejection. An example of the complete transmission characteristics of an all metal-grid filter is shown in Figure 4-3 for a B_{32} filter.

TABLE 4-1

FILTER IDENTIFICATION CODE

Filter Code	Passband Width (deg)	Quantity of Poles	Ripple (dB)
A20	± 11.5	2	.1
A21	"	"	.01
A22	"	"	.001
B20	± 14.0	"	.1
B21	"	"	.01
B22	"	"	.001
C20	± 18.0	"	.1
C21	"	"	.01
C22	"	"	.001
A31	± 11.5	3	.01
A32	"	"	.001
B31	± 14.0	"	.01
B32	"	"	.001
C31	± 18.0	"	.01
C32	"	"	.001
A51	± 11.5	5	.01
A52	"	"	.001
A54	"	"	.00001
A56	"	"	.0000001
B51	± 14.0	"	.01
B52	"	"	.001
B54	"	"	.00001
B56	"	"	.0000001
C51	± 18.0	"	.01
C52	"	"	.001
C54	"	"	.00001
C56	"	"	.0000001

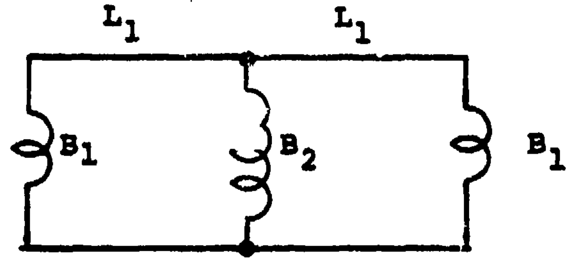

(a) Two-pole filter

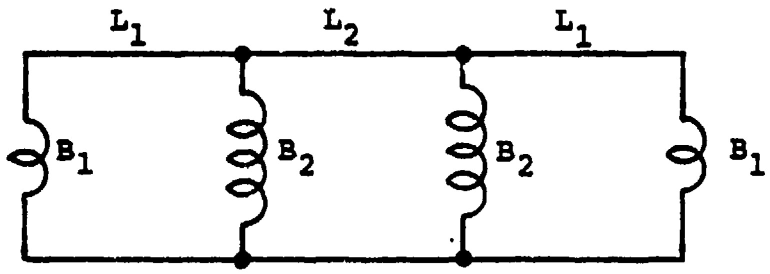

(b) Three-pole filter

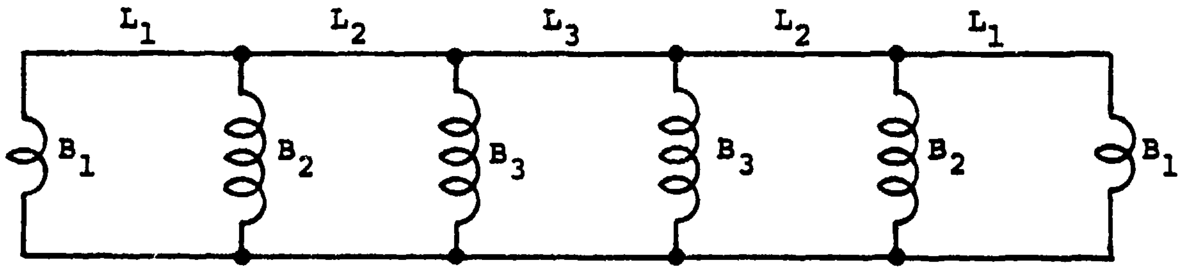

(c) Five-pole filter

Figure 4-1 Filter Elements for 2-, 3-, and 5-Pole Filters

TABLE 4-2

ELEMENT VALUES FOR BROADSIDE-CENTERED FILTERS

FILTER CODE	B_1	L_1 (deg.)	@ 9.5 GHz L_1 (in.)	B_2	L_2 (deg.)	@ 9.5 GHz L_2 (in.)	B_3	L_3 (deg.)	@ 9.5 GHz L_3 (in.)
A20	3.3827	159.726	.5511	11.3950					
A21	2.2930	151.067	.5212	6.6366					
A22	1.4800	138.788	.4789	3.6191					
B20	2.6730	154.255	.5322	7.6312					
B21	1.7373	143.186	.4940	4.3668					
B22	1.0179	127.598	.4403	2.2386					
C20	1.9145	144.887	.4999	4.4973					
C21	1.1234	129.894	.4482	2.4232					
C22	0.4837	109.635	.3783	0.9614					
A31	2.8419	157.817	.5445	12.3081	170.770	.5892			
A32	2.1531	151.954	.5243	8.5252	166.797	.5755			
B31	2.2115	152.127	.5249	8.2534	166.378	.5741			
B32	1.6152	144.745	.4994	5.6687	160.566	.5540			
C31	1.5285	142.562	.4919	4.8848	157.734	.5442			
C32	1.0172	132.723	.4579	3.2621	148.488	.5123			
A51	3.1742	160.261	.5529	15.6887	173.850	.5998	22.7039	174.966	.6037
A52	2.5924	156.554	.5402	12.2909	172.401	.5948	19.1715	174.044	.6005
A54	1.7720	148.333	.5118	7.5296	168.150	.5802	12.8832	171.176	.5906
A56	1.1574	138.232	.4769	4.5793	161.416	.5569	8.2827	166.425	.5742
B51	2.4957	155.280	.5358	10.5520	170.912	.5897	15.3088	172.557	.5954
B52	1.9968	150.657	.5198	8.2417	168.778	.5823	12.9150	171.197	.5907
B54	1.2793	140.570	.4843	4.9839	162.554	.5609	8.6450	166.974	.5761
B56	0.7241	127.779	.4409	2.9270	152.840	.5273	5.5022	160.024	.5521
C51	1.7670	146.932	.5070	6.3063	165.085	.5696	9.2234	167.765	.5788
C52	1.3463	140.826	.4859	4.8775	161.624	.5577	7.7581	165.544	.5712
C54	0.7204	127.250	.4390	2.8237	151.692	.5234	5.1279	158.693	.5475
C56	0.2101	111.015	.3830	1.4548	136.835	.4721	3.1561	147.638	.5094

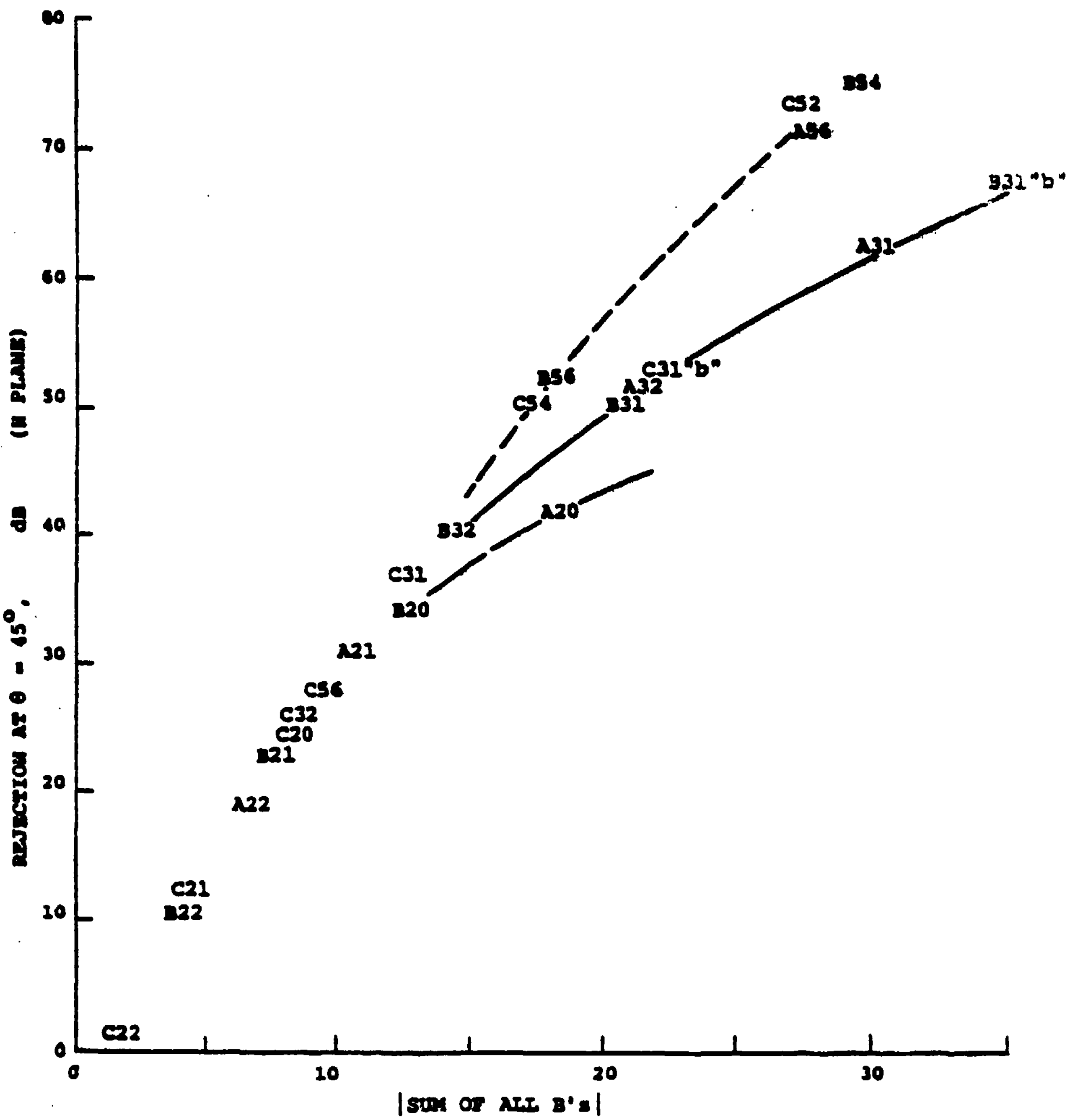

Figure 4-2 Rejection vs. Susceptance Sum for Various Filters

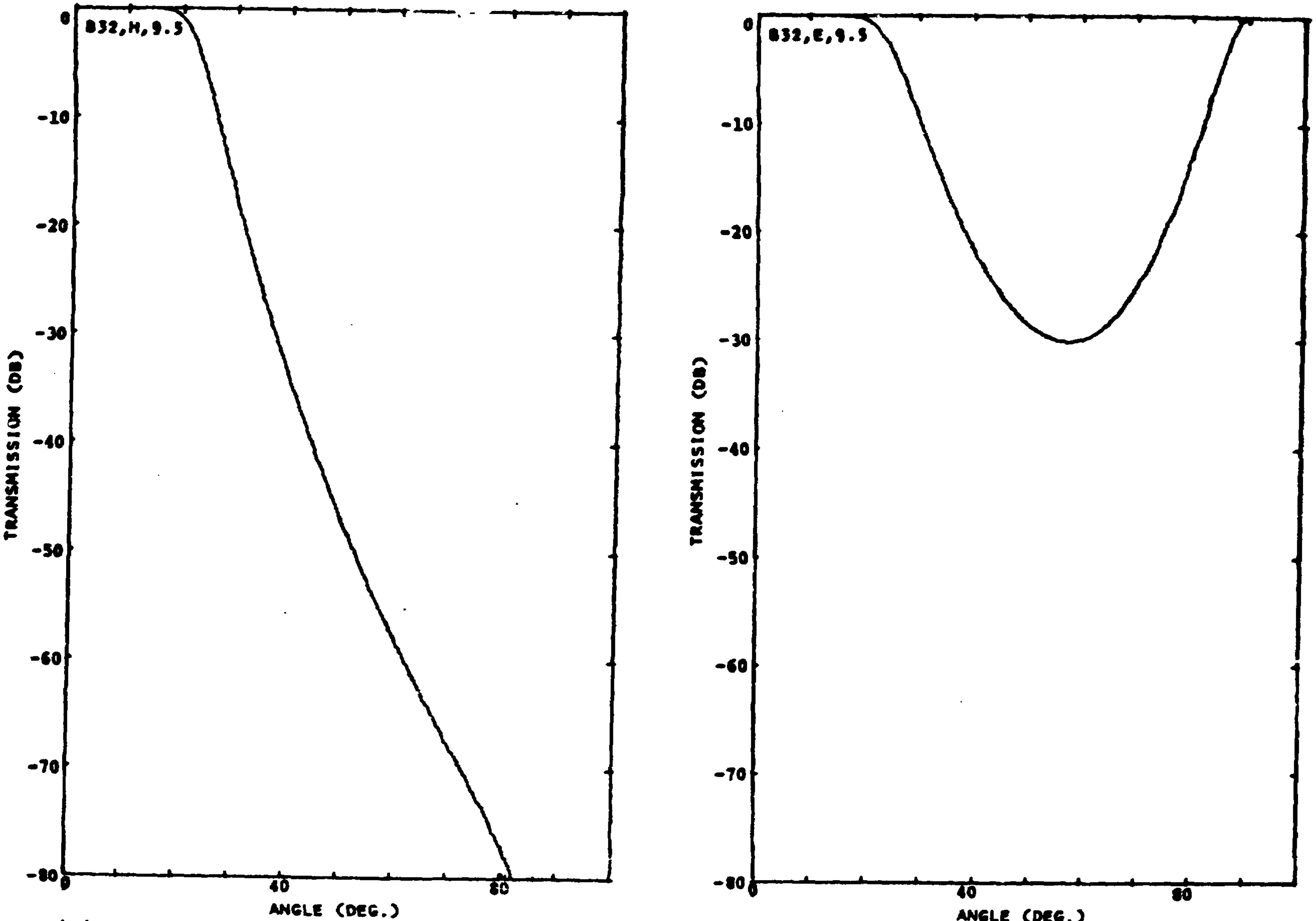

(a) H Plane (b) E Plane

Figure 4-3 Transmission, Filter B32, H and E Planes

4.4 FILTER ELEMENT TOLERANCES

For all the filter designs considered, the variation in reflection and insertion phase with percentage changes in element values have been computed at broadside (or nominal) incidence. The results have been expressed as "standard tolerances", or the percentage change in all susceptances or all lengths causing either 5° change in insertion phase or 0.2 change in reflection coefficient of the filter. The 5° $\Delta\phi i$ and 0.2 ΔR have been arbitrarily chosen as standard allowable errors of filter performance at broadside. In this way, a common "medium of exchange" that can be related to mechanical or material-property tolerances in practical filters has been established.

The significance of the properties considered lies in the application of the spatial filter in passing the main beam of a reflector antenna while reducing the sidelobe radiation that occurs in the stopband of the filter. The filter reflection at the main-beam incidence angle (broadside) usually passes directly back into the antenna, and therefore must be limited. The filter insertion phase at broadside, if not uniform over the entire area of the antenna aperture, will perturb the aperture illumination and generate sidelobes in the radiation pattern of the antenna/filter combination.

Computation of the "standard tolerance" based on insertion phase is illustrated in Figure 4-4. Filter performance with a length increased 1% was computed, and the change in insertion phase from the nominal-length performance was calculated (2.7 degrees in the example illustrated). Next, the performance with a length increased 3% was compared with nominal; the insertion-phase change at broadside incidence was again calculated (8.3 degrees). A simple linear interpolation yields 1.8% as the "standard tolerance" on length for this example, based on 5° insertion phase. Standard tolerances based on reflection were determined in a similar manner.

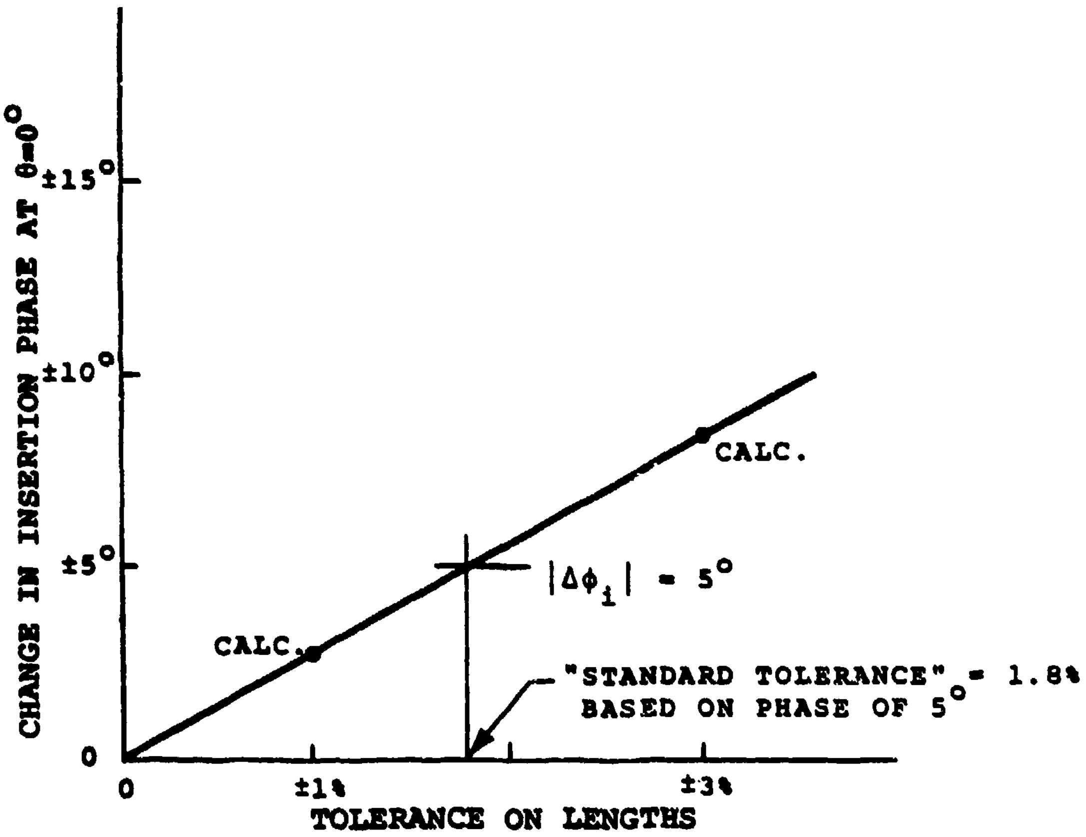

Figure 4-4 Method for Determination of Tolerance

Single-Element Deviations

The most critical length in a Chebyshev filter is the center length because this length corresponds to the highest Q resonator. Figure 4-5 shows the percent standard tolerance on one center length, based on 5° $\Delta\phi i$, plotted vs. the nominal rejection at 45° in the H-plane for various filters. A clear trend of tighter tolerances required for greater rejection is evident, regardless of passband width or ripple level. Increasing the number of poles yields greater rejection for a given tolerance in most cases.

A similar presentation is given in Figure 4-6 for the percent standard tolerance on one center length, based on 0.2 ΔR. Again, a clear trend of tighter tolerances required for greater rejection is evident, as well as a greater rejection-tolerance product with increasing number of poles. For any particular filter the tolerances based on 0.2 ΔR are looser than the tolerances based on 5° $\Delta\phi i$.

The tolerances on susceptance have trends similar to those given above when the case of susceptance at the edge of the filter is considered. Figure 4-7 shows the percent standard tolerance on one edge susceptance, based on 5° $\Delta\phi i$, plotted vs. the rejection at 45°. Figure 4-8 shows the tolerance based on 0.2 ΔR. It is evident that on a percentage basis, these edge susceptance tolerances are substantially looser than the center length tolerance. Center susceptance tolerances, not shown here, do not have a clear trend of tigher tolerances with increasing rejection. Instead, the center susceptance tolerances are typically 8 to 10% based on 5° $\Delta\phi i$, and are typically 20% or more based on 0.2 ΔR.

All-Element Cumulative Deviations

The "standard tolerances" discussed so far have assumed that only one length or one susceptance in the filter deviates from the nominal value. This assumption is obviously optimistic. Another assumption that can be made is that all the lengths or

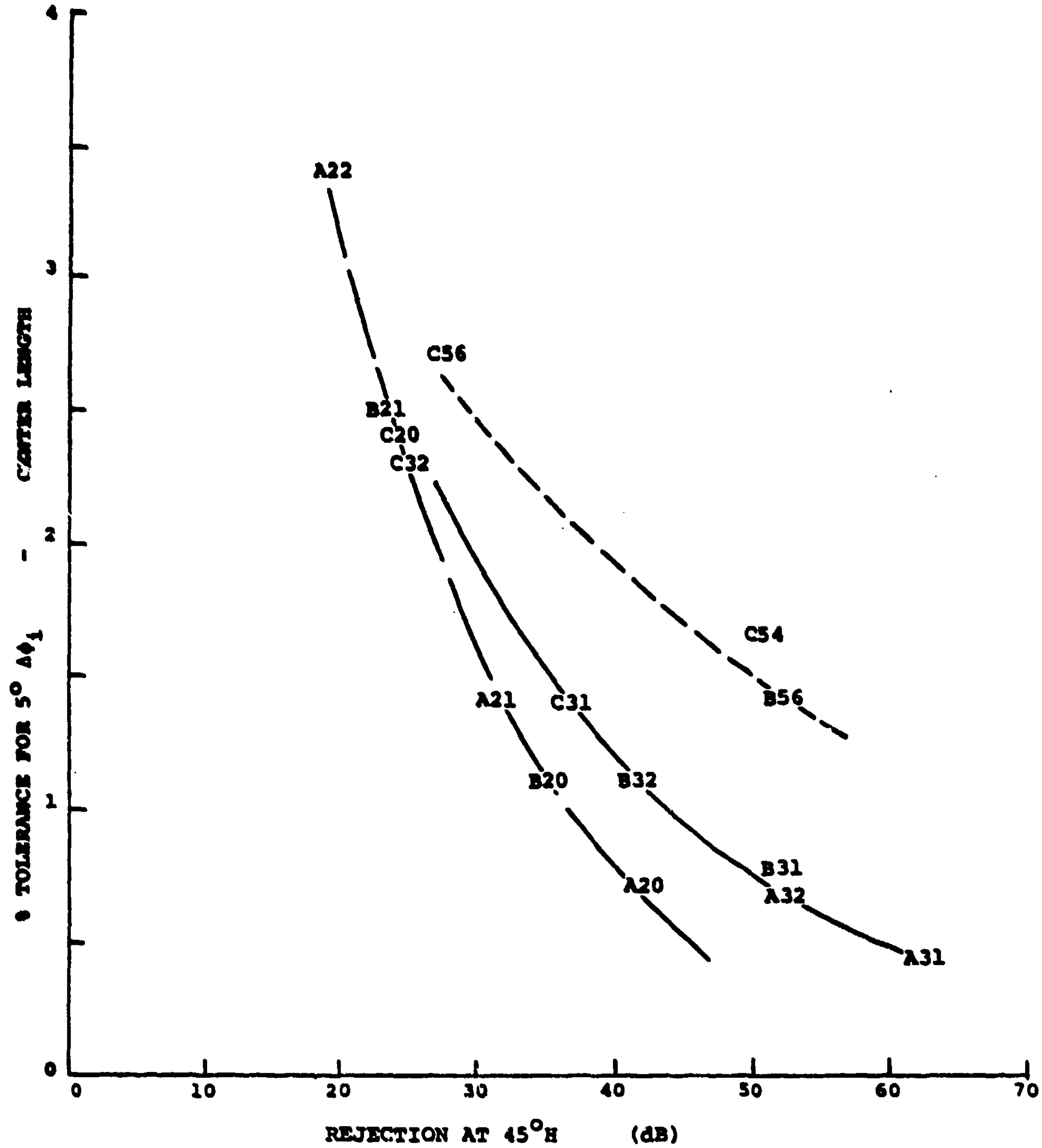

Figure 4-5 Tolerance on Center Length vs. Rejection, for 5° $\Delta\phi_i$ Allowable

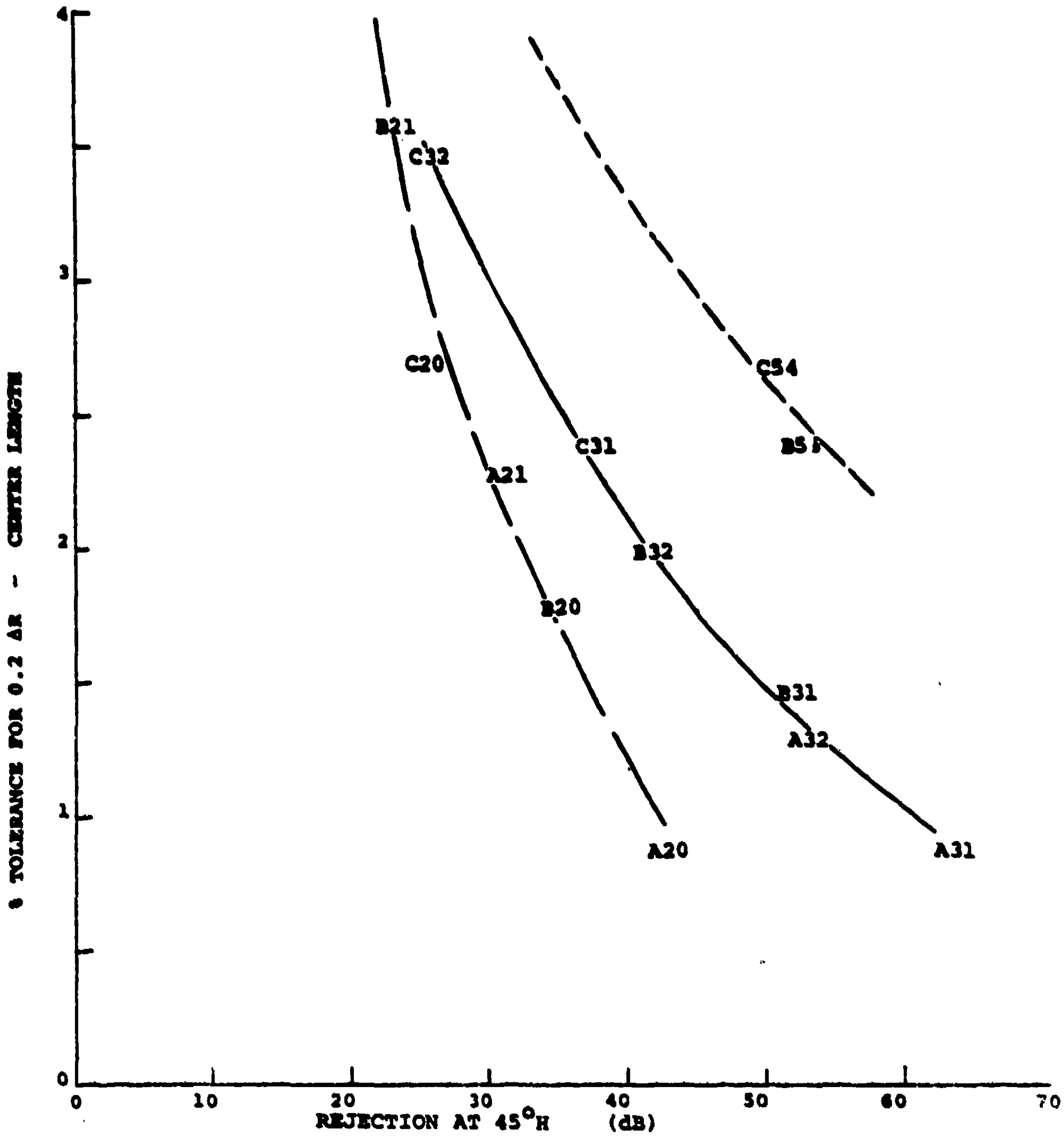

Figure 4-6 Tolerance on Center Length vs. Rejection, for 0.2 ΔR Allowable

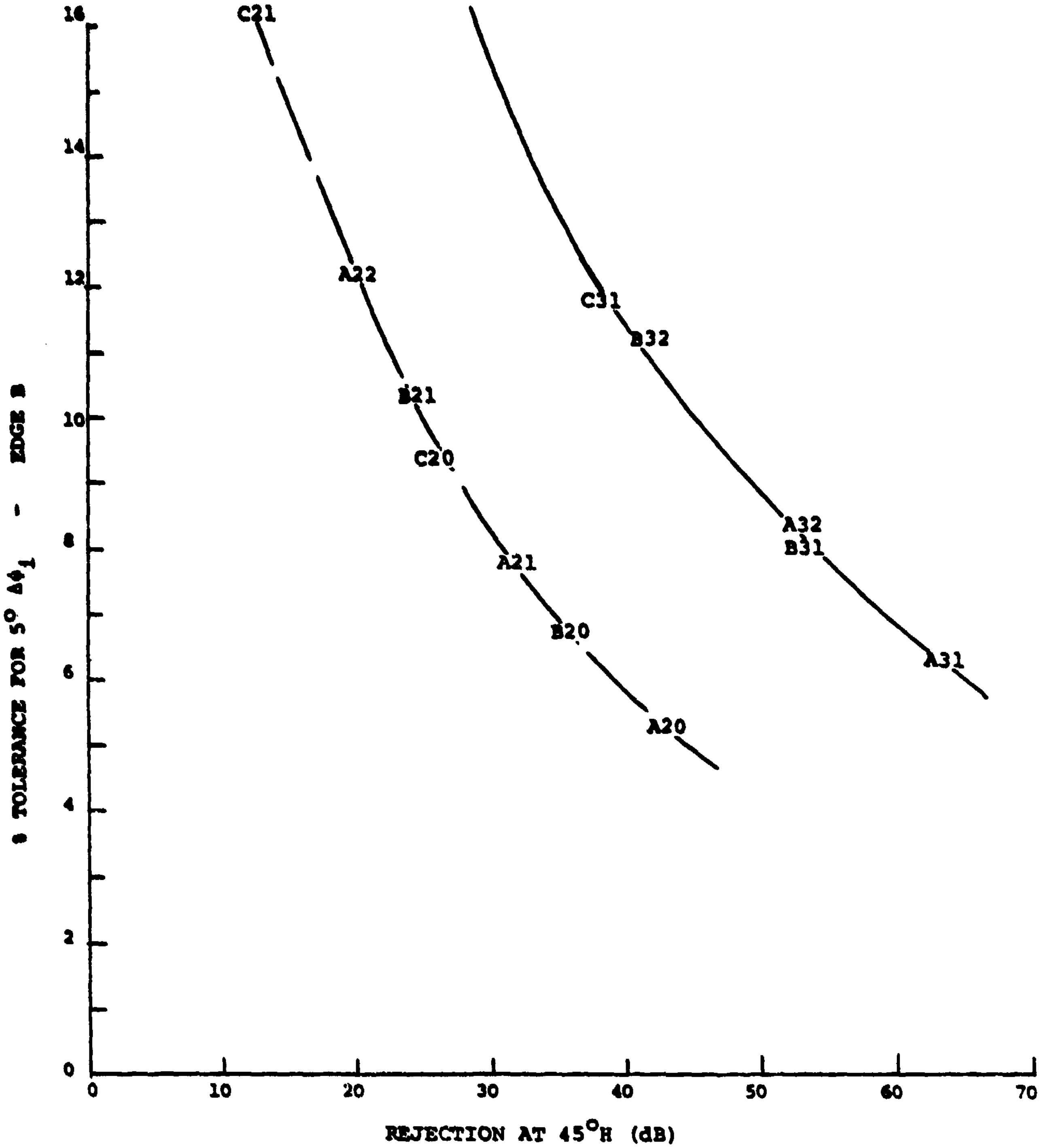

Figure 4-7 Tolerance on Edge Susceptance vs. Rejection, for 5° $\Delta\phi_i$ Allowable

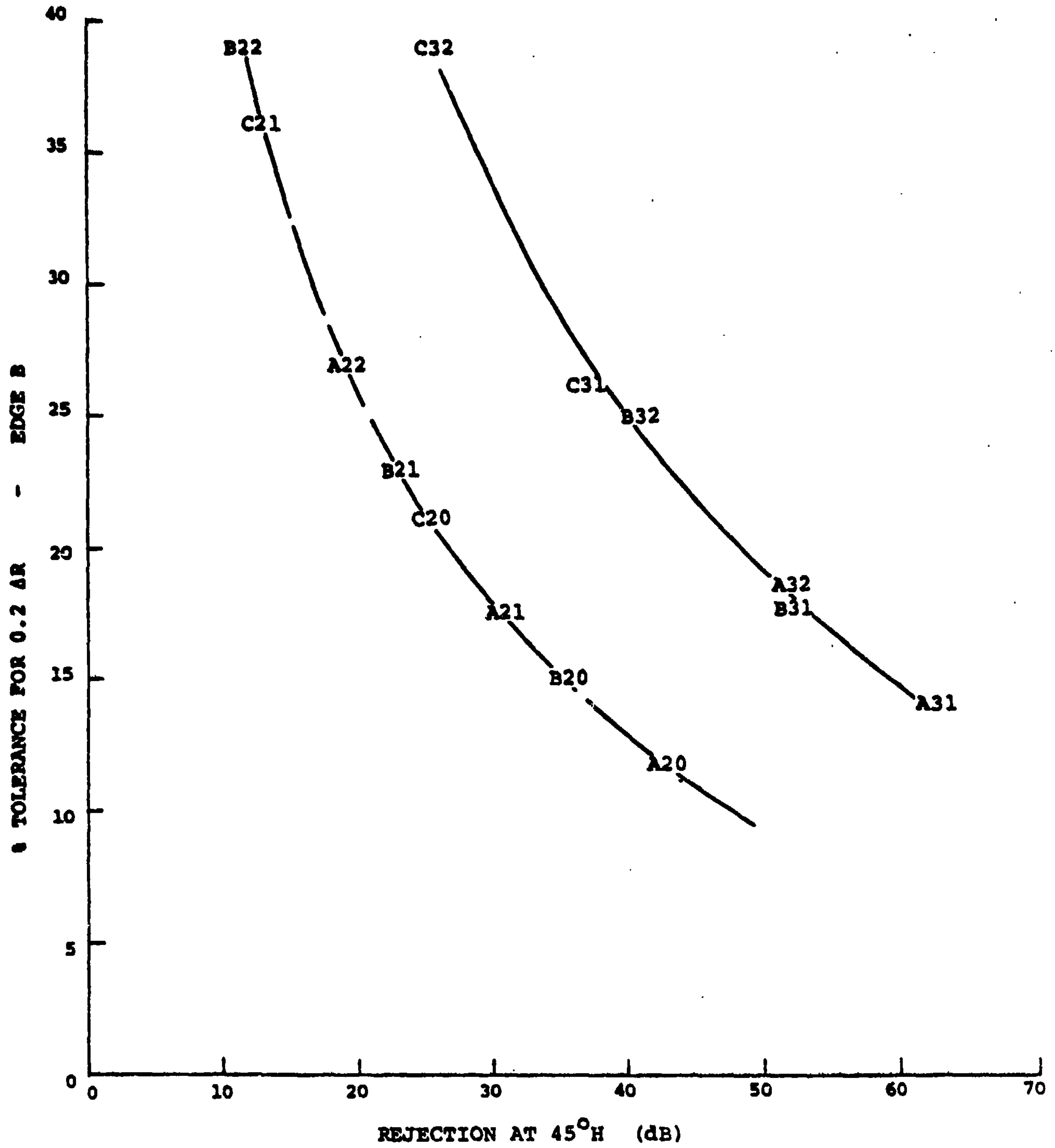

Figure 4-8 Tolerance on Edge Susceptance vs. Rejection, for 0.2 ΔR Allowable

all the susceptances deviate in such a way as to create the greatest effect. This assumption is used in the following.

For the length tolerances based on $\Delta\phi i$, the greatest deviation of ϕi occurs when all the length deviations have the same sign. Figure 4-9 shows this case, based on a 5° $\Delta\phi i$. As expected, the allowable tolerance on length is tighter for this worst-case assumption than it is when only one length deviates, as may be seen by comparison with Figure 4-5.

For the length tolerances based on ΔR, the greatest deviation of R occurs when successive length deviations have alternating signs. Figure 4-10 shows this case, based on a 0.2 ΔR. Again, the allowable tolerance on length is tighter for this worst-case assumption than it is when only one length deviates, as may be seen by comparison with Figure 4-6.

For the susceptance tolerances based on $\Delta\phi i$, the greatest deviation of ϕi appears to occur when all the susceptance deviations have the same sign. For the susceptance tolerances based on ΔR, the greatest deivation of R is expected to occur when successive susceptance deviations have alternating signs.

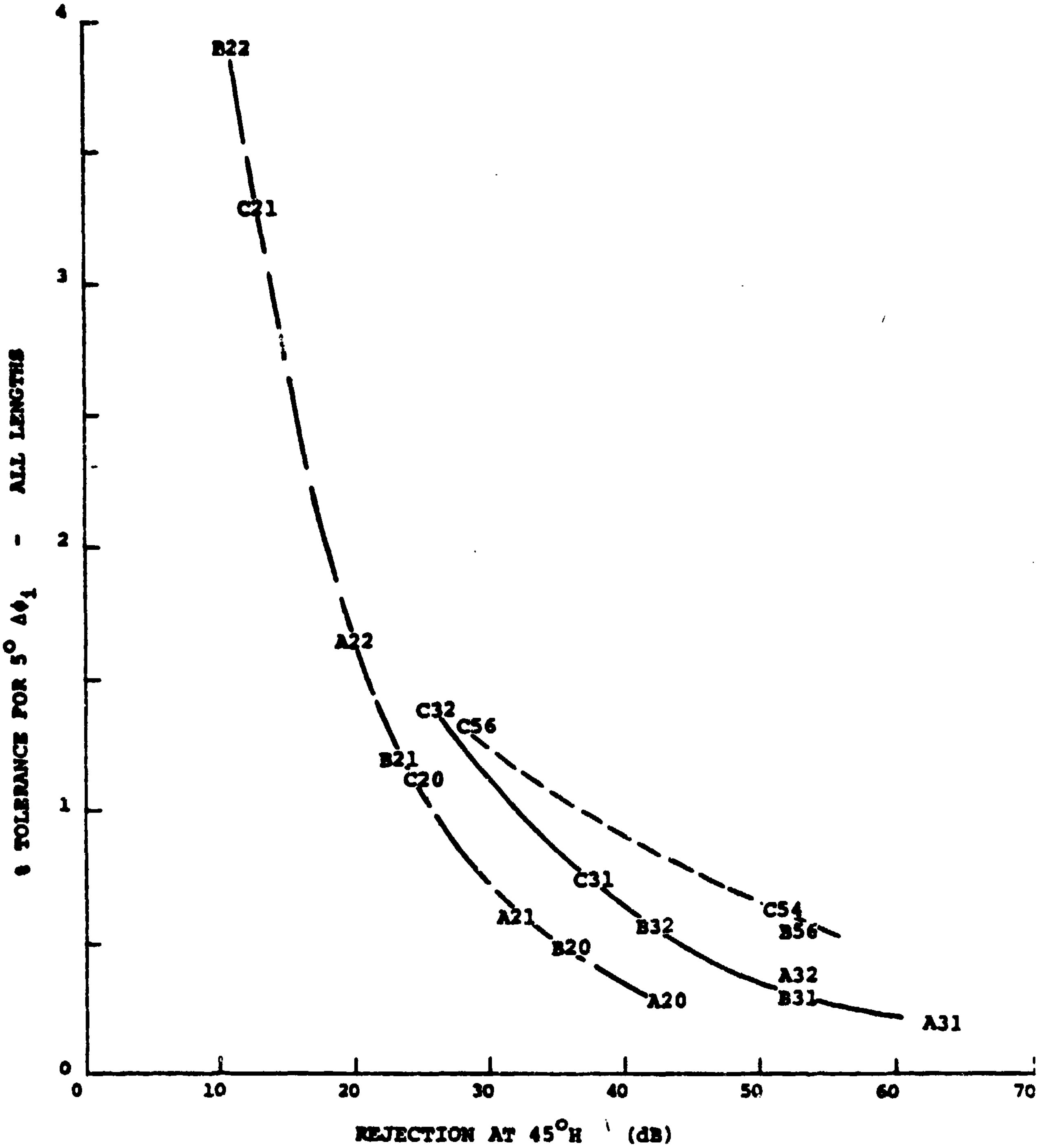

Figure 4-9 Tolerance on All Lengths Cumulative vs. Rejection for 5° $\Delta\phi_i$ Allowable

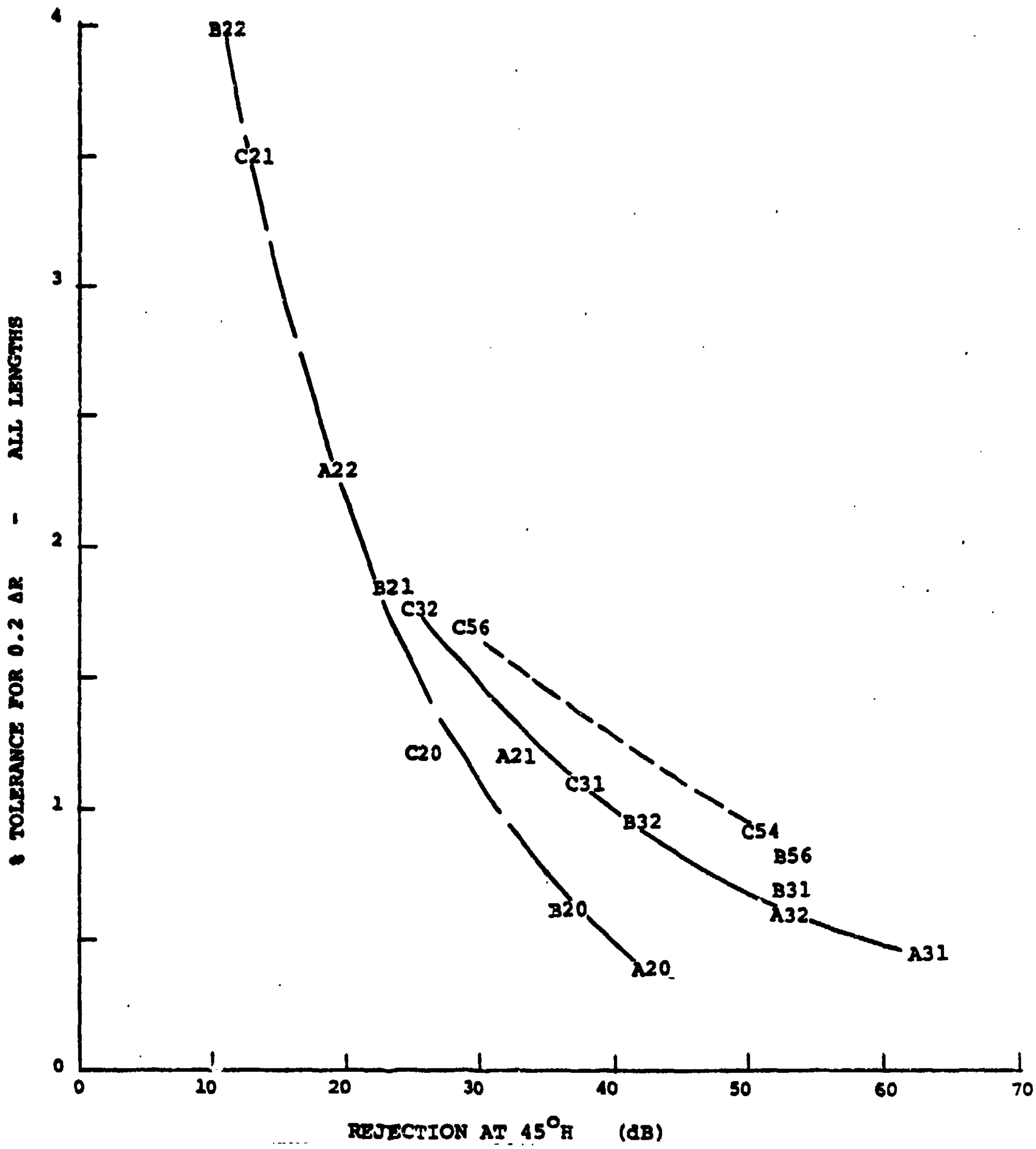

Figure 4-10 Tolerance on All Lengths Cumulative vs. Rejection, for 0.2 ΔR Allowable

SECTION 5

FILTER FABRICATION

5.1 INTRODUCTION

In the previous sections of this report the spatial filter was discussed in general terms with minimal detail given to practical considerations of materials, filter size and fabrication techniques. It is the objective of this section to apply the results reported in section 4 to the limitations of some of the methods of fabricating the elements comprising a spatial filter.

5.2 FILTER STRENGTH

In section 4 of this report a design philosophy is outlined that emphasizes using the filter's affect on the antenna characteristics of reflection coefficient and near-in sidelobe levels as the principal considerations in selecting the most appropriate filter type (A_{31},B_{32}, etc.). This is accomplished by requiring filter dimensions to vary within "standard tolerances". The standard tolerances are based upon criteria of acceptable antenna performance. The criteria used for this report are arbitrary, however they would be acceptable for many applications. In some cases, more stringent requirements may be warranted, or alternatively, for other applications less stringent criteria would be acceptable. In any event the "standard tolerance" provides a convenient method of comparing various filters. It is felt that by adhering to the "standard tolerance" for a particular application, the filter will have the desirable features of rejecting antenna far sidelobes with minimal harmful affect within the filter passband.

Consider figure 4-5, which shows the percentage tolerance on center layer spacing required to maintain the insertion phase variation within 5°. A B_{32} filter requires the center length to be held within 1.1% of its nominal value. An A_{31}

filter requires the center length be maintained to ±.45%, while a C_{31} filter has a tolerance of 1.4%. Clearly a C_{31} filter would be the easiest to construct; however, this filter would provide the least rejection of far sidelobes, especially in the E-plane. Conversely an A_{31} filter would provide the greatest reduction in far sidelobes, but it is the most sensitive to tolerances and therefore may substantially degrade the sidelobes within the filter passband. For the purpose of comparing the rejection capability of various filters, the term "filter strength" is defined as the rejection provided at a 45° angle of incidence. Table 5-1 summarizes the filter strength and standard tolerances for some representative filters.

Note in table 5-1 that the standard tolerances are specified as a percentage. Since the layer spacings are approximately a half-wave length for all filter types, the standard tolerance expressed in inches increases as frequency decreases. Mechanical tolerances on length are in general fixed; they are determined by the capabilities of the fabrication process and are specified directly rather than as a percentage of the length. Therefore, one would expect that a "strong" filter that would significantly degrade antenna performance at a high frequency could be fabricated at a lower frequency with minimal harmful effect within the filter passband and substantial rejection of far sidelobes. This is true, eventhough a larger filter may be required for lower frequency operation. This trend is shown in figure 5-1 as a graph of allowable rejection vs. frequency with the tolerances on insertion phase and center length as parameters.

One of the requirements of this investigation was to design and fabricate a 5 ft. x 5 ft. filter to operate at approximately 9.5 GHz. The selection of filter strength would be based upon results of a tolerance analysis and a survey of existing fabrication techniques that emphasized the tolerances that could be

TABLE 5-1 FILTER STRENGTH AND STANDARD TOLERANCES FOR SOME REPRESENTATIVE FILTERS

	FILTER CODE*	A31	A32 B31	B32	C31
	Tolerance Center Layer Length ($\pm \Delta L_{CEN}$)				
$\pm \Delta L_{CEN}$ for a $\pm 5^{\circ}$ Δ Insertion Phase		±0.45%	±0.7%	±1.1%	±1.4%
Above at 9.5 GHz		±0.002"	±0.0035"	±0.0055"	±0.007"
	Filter Rejection				
dBT	45° H-Plane	-63.	-52.	-40.	-37.
	25° H-Plane	-28	-17.	- 7.	- 4.
dBT	45° E-Plane**	-47.	-37.	-26.	-22.
	25° E-Plane	-22.	-11.	- 3.	- 1.

* A 3 1

1 — Number of Zero's in Ripple dB Value

3 — Number of Poles

A — Width of Passband

** Dielectric Skins Will Substantially Reduce Rejection (See Fig. 4-4 Reference 1)

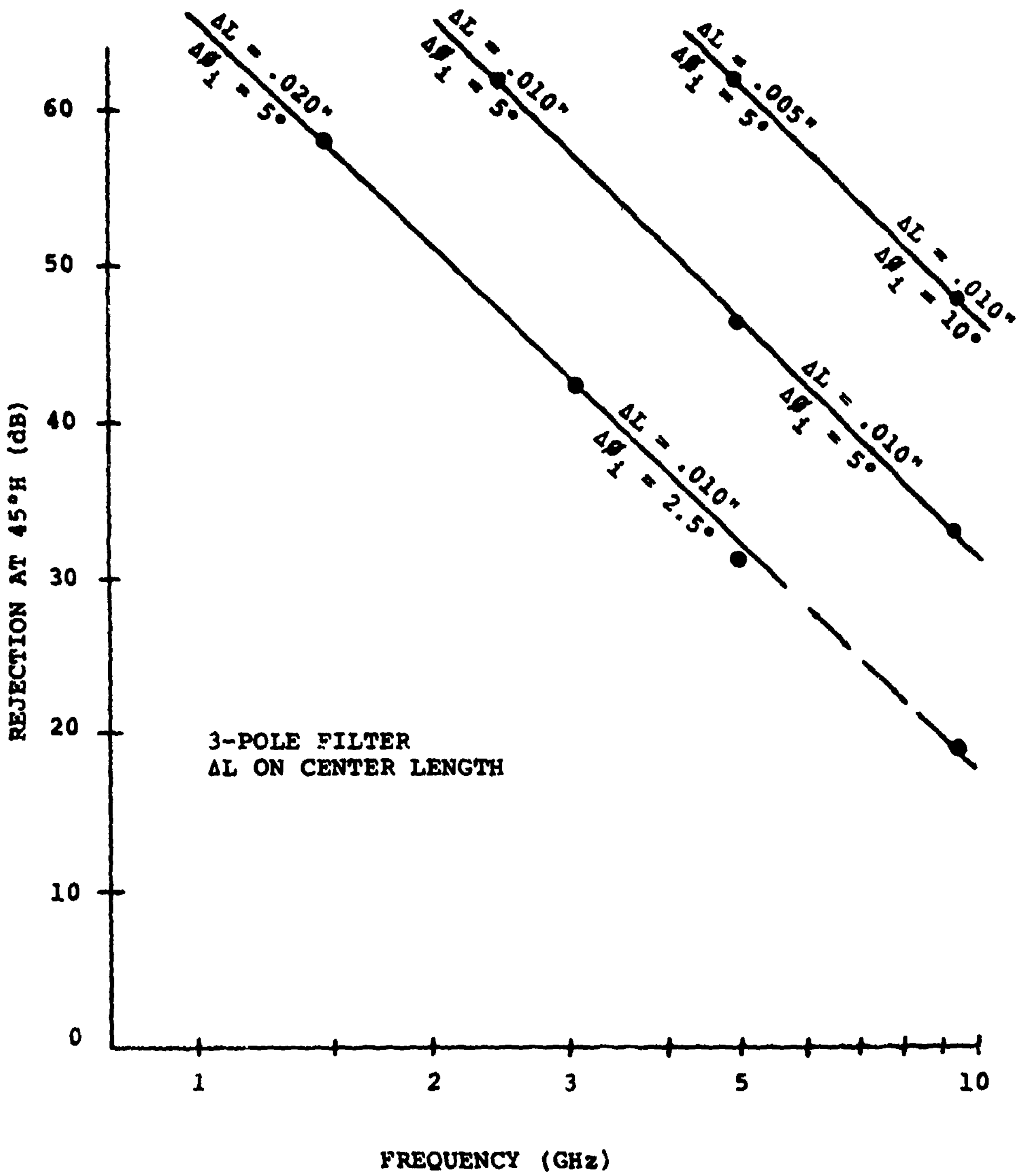

Figure 5-1 Allowable Rejection vs. Frequency

expected in making a 5 ft. square filter panel. This selection is discussed in section 5.5.

5.3 SPACING BETWEEN LAYERS

Since the spacing between layers (lengths) are the most sensitive filter dimensions, the spacing material and its manufacturing technique is an important consideration. An ideal electrical medium would have a dielectric constant of one; it would be homogenious and isotropic. In addition the medium would have the mechanical attribute of strength to support the layer susceptances, and it would also be accurately fabricated to the desired thickness.

Two alternative materials are available to provide the spacing between layers. Each approaches the ideal medium in some manner, and each fails in other ways. The first material is dielectric honeycomb. The second material is a low dielectric constant foam.

Honeycomb has good mechanical properties. It can provide the mechanical strength required to support the layer susceptances. It can be saw-cut to the desired thickness, and if needed microsanded to achieve excellent uniformity over the filter surface. It is also easy to splice sections of honeycomb together, thereby making it applicable to any filter size.

Honeycomb has a low dielectric constant, which can be expected to have repeatable values from lot to lot. Honeycomb is not isotropic, and the electrical length between filter layers for orthogonal polarizations will be slightly different. Because of the high-Q resonant nature of a strong filter, the insertion phase of such a filter may be significantly different for orthogonal linear polarizations. As a consequence of this effect, the filter may change circular polarization to elliptical. Another effect cause by the non-isotropic properties of honeycomb is that the passband reflection coefficient may be different for orthogonal linear polarization. In this investigation

linear polarization is the principal one that is considered; therefore, any filter design that employes honeycomb construction would be designed to provide the best performance with linear polarization.

Low dielectric constant foam has some properties that are inferior to honeycomb, especially for large filters. The principal deficiency is the uncertainty in obtaining a uniform dielectric constant over the entire surface of the filter. Accurate electrical measurements of the dielectric constant would be needed at small increments to find regions of excessive resin or air pockets. Secondly, to obtain a dielectric constant as low as honeycomb the foam would not possess the same mechanical strength as the honeycomb. Honeycomb is selected as the material to provide the spacing between layers.

5.4 METAL-GRID SUSCEPTANCE LAYERS

The crossed grid of conductors that forms a susceptance layer could be constructed by using a number of techniques as discussed in Section 3. Either a contacting or non-contacting grid would provide acceptable performance. The selected approach should form a flat plane of conductors, with the precise position of each plane known in order to obtain the correct thickness of honeycomb to separate the susceptance layers. A desirable feature of any crossed grid with dielectric-support would be to obviate the need to design special conducting joints at the interface between adjacent sheets of dielectric-supported conductors. Furthermore, it would be beneficial to use a fabrication technique that could be directly extended (without additional design considerations) to filter applications at lower frequencies where the filter would presumably be larger than the 5 foot square filter designed during this study.

Of the techniques discussed in Section 3, an insulated grid of round wires embedded in a dielectric supporting sheet

has no obvious size limitation. It can provide a large flat panel where the plane of wires can be maintained within tight tolerances. Since each wire is continuous across the face of the dielectric this approach requires no special conducting joints. Many different reflector antennas have been designed using a wired-skin/honeycomb construction· curved as well as flat filters can be designed using this technique.

5.5 CHOICE OF FILTER STRENGTH

A survey of potential vendors capable of fabricating a 5 x 5 foot filter using a honeycomb/wire-grid construction showed that the crucial tolerance on spacing between layers could not be reliably held to closer than about ±0.006". Based upon the concept of a 5° allowable insertion phase variation, a B_{32} filter would require the center length spacing to be maintained within ±0.0055". As was indicated in table 5-1, stronger filters such as an A_{31} filter would require a ±0.002" tolerance on the center length and a A_{32} or B_{31} filter would require ±0.0035". A weaker filter such as a C_{31} requires tolerances that can more easily be achieved by a quality plastics vendor, but provides less rejection. A B_{32} filter is therefore considered to be a good compromise between fabrication tolerances and electrical performance at 9 GHz. It is the filter that has been constructed and tested in this program.

5.6 COMPUTED PERFORMANCE OF PRACTICAL SPATIAL FILTER

The practical considerations of providing mechanical integrity requires that each metal-grid layer be embedded in a dielectric skin, and the spacing between layers be maintained by dielectric core material. Both the spacers and the skins can have an effect on the performance of the spatial filter (ref. 1).

The honeycomb has a dielectric constant only slightly greater then unity. A low dielectric constant is desired in order to retain the wave angle within the filter as close as

possible to the angle of incidence at the filter surface. The spacing between layers, first computed on the ba is of an air core, is decreased to account for the effect of the dielectric constant. Honeycomb has a slightly different dielectric constant for orthogonal planes of incidence; the average dielectric constant was used to re-compute the layer spacings.

One of the attributes of using a honeycomb construction is the ability to piece together honeycomb sections to make a filter panel much larger than the size of honeycomb stock. In order to obtain uniform electrical spacing between two layers of wire grids, the honeycomb ribbon should always be oriented in the same direction within any two-layer sandwich. Furthermore, length tolerances based on ΔR (ref. 1) show that the greatest deviation of reflection coefficient occurs when successive length deviations have alternating signs. To minimize the effect on reflection coefficient the ribbon direction was therefore oriented in the same direction for all layers.

The effect of a dielectric skin on the passband of the spatial filter can be compensated approximately by a change in susceptance of the metal grid as discussed in section 3. The effect in the reject band is to modify the E-plane characteristic as discussed in Reference 1.

When the dielectric modifications discussed above are made to the design parameters of the B_{32} filter given in table 4-2, the filter characteristics can be recomputed including the effect of the dielectric material. Figure 5-2 shows the resulting calculated H-plane and E-plane transmission characteristics. It is of interest to compare these transmission characteristics to those of the all-metal prototype filter shown in figure 4-3.

First the passband width is wider with dielectric material added to the filter. This is in part caused by refraction at the boundary between the dielectric core and free space. The bending of the incident wave as it passes into the dielectric

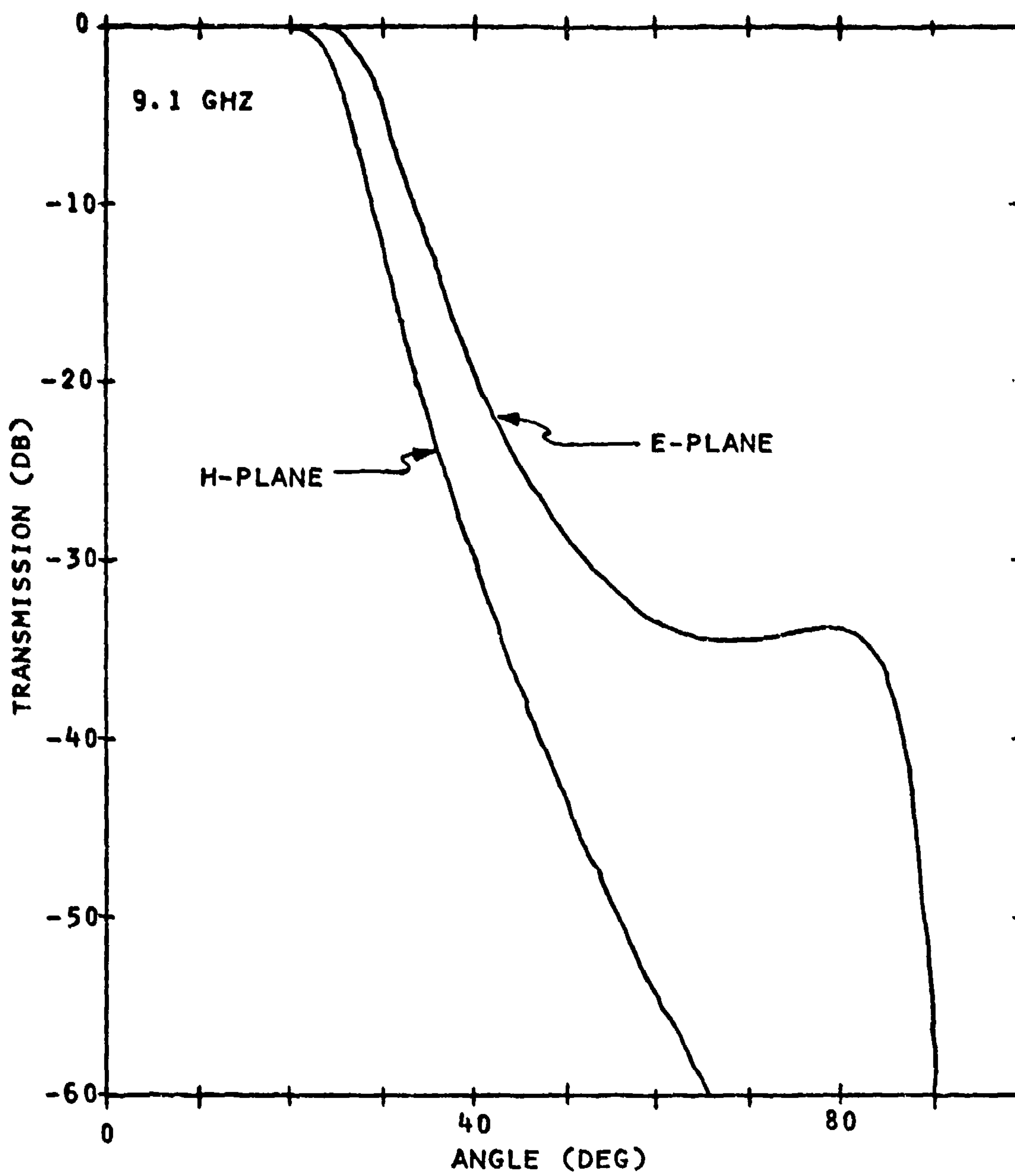

Figure 5-2 Transmission, B32 filter with dielectric

reduces the angle of incidence on the layer susceptances within the filter. The rejection a filter provides is directly related to the angle of incidence of the wave on the layer susceptances, and the rejection obtained at a given angle of free-space incidence for a filter with dielectric added will be less than it is with the all-metal prototype filter near the edge of the passband. Alternatively, the passband width of a filter with dielectric will be wider than that of the all-metal prototype filter.

The other contribution to the increase in passband width of this filter with dielectric material is caused by the approximate computational technique used to re-adjust the layer susceptances with dielectric support. The equation presented in Section 3 is a lumped susceptive representation of a dielectric skin. This formula is a good approximation for dielectric that is electrically very thin. The dielectric skin supports used in fabricating the filter for this investigation deivate sufficiently from the lumped approximation that, if a precise reproduction of the passband characteristics of the all-metal filter was needed, a more refined synthesis technique would have to be used. Since the filter with a simple synthesis provides nearly the same rejection in the region of space that is of concern in this study, it was felt that the development of a refined filter synthesis was not warranted to demonstrate the main feature of the spatial filter: the rejection of antenna far sidelobes.

The effect of dielectric on the performance of the spatial filter in the E-plane is beneficial very near grazing incidence. In this region of space the susceptance of the grid is approaching zero; however, the dielectric presents a large reflection thereby providing most of the filter's E-plane rejection. This effect is apparent when comparing Figure 5-2 with Figure 4-3.

During the first phase of this investigation measurements were made of metal grids with dielectric support in waveguides simulating angles near grazing in the E-plane (Ref. 1). The results of these measurements showed that the transmission loss of a metal grid with dielectric was less than the calculated values. The transmission calculations assume no interaction between the metal grid and the dielectric support (these calculations do include the exact transmission-line model of a dielectric skin). It was concluded from these measurements that the interaction is detrimental to the E-plane transmission characteristic, notably near 60° incidence angle. It is presumed that the reduction in transmission loss of a single grid with dielectric would also occur for incidence angles less than 60°; however, the waveguide simulator was limited to a minimum angle of incidence of 60°.

The calculated E-plane transmission characteristic shown in Figure 5-2 does not include the measured interaction effect. Therefore the actual reflection of the filter with dielectric should be less than that shown in Figure 5-2. This result is shown in Section 6 where measured performance of the spatial filter is presented.

5.7 FABRICATION TOLERANCE CONTROL

During fabrication of the spatial filter the individual skins and honeycomb were measured prior to assembly to ascertain whether the filter would meet the dimensional requirements. The thickness of the skins and honeycomb were measured using a template with periodically spaced holes that would permit readings every 3" of radius for each 30° of arc, thereby providing an extensive profile of the dimensions of the filter components. The wire spacing was also inspected.

Table 5-2 summarizes the dimensional measurements. The thickness uniformity of the honeycomb is excellent. The maximum peak-to-peak deviation over a 25 square foot surface is 0.005", while the standard deviation is only 0.0008". The skins are also quite uniform. In final assembly the skins are bonded to the honeycomb using a thin film adhesive. It was therefore concluded that the resulting sandwich should meet the ± 0.006" tolerance on layer spacing.

Although the honeycomb uniformity is excellent, the filter manufacturer mistakenly obtained honeycomb thicker than our drawing callout. This resulted in a center frequency of operation of 9.1 GHz, rather than 9.5 GHz. The filter performance was evaluated for the thicker honeycomb and it was determined that this filter would, fortunately, have performance similar to that of the original filter designed to operate at 9.5 GHz. For this reason, and because no specific X-band frequency was required for this investigation, the thicker honeycomb was accepted and construction of the filter was accomplished without the delay and risk that would have occurred if a second set of honeycomb cores had been ordered.

Table 5-2

Summary of Measurements on Dielectric Core Thickness and Dielectric Skin Thickness

Components	# of Measurements	Mean Thickness	Stand. Deviation
Skins	134	0.0348"	1.1×10^{-3}
Inner-Layer Honeycomb	82	0.5130"	8.1×10^{-4}
Outer-Layer Honeycomb			
#1	82	0.4586	7.7×10^{-4}
#2	82	0.4589	7.3×10^{-4}

SECTION 6

SPATIAL FILTER ELECTRICAL TESTS

6.1 INTRODUCTION

In general, the purpose of a test program is to demonstrate the performance of the unit under test by comparison to a specification. A specification stating the filter's passband and reject-band characteristics could be used as the only criterion for judging the spatial filter performance; however, measurements on the filter alone would not consider one of the principal issues to be studied during this investigation. This issue relates to the interaction between a filter and an antenna. The interaction between antenna and filter was examined by measuring the filter in conjunction with a reflector antenna. In addition measurements were made to determine the filter's passband and reject band characteristics. These measurements will be compared to the calculated filter performance discussed in Section 5.

6.2 MEASUREMENT OF FILTER-ANTENNA INTERACTION

There are two types of reflections from the angular filter. The first type is the reflection within the passband of the filter; the second type is the reflection in the reject band. Both of these reflections can affect the overall antenna-filter performance. Since the filter affects radiation by reflection, some of the rejected power may be trapped between the antenna and the filter. This power is initially reflected back to the antenna aperture where it may be in part absorbed by the antenna feed and in part reflected back to the filter. Some of the power reflected back to the filter may now pass through the filter. This process continues until all the reflected power is either absorbed by the antenna feed or is radiated within

the filter angular passband. Power absorbed by the feed will manifest itself as an increase of antenna reflection or VSWR. Power re-radiated within the filter passband will in general increase the near-in antenna sidelobes.

6.3 MEASUREMENT OF THE FILTER WITH A PARABOLIC REFLECTOR

One of the applications of a spatial filter is with a conventional parabolic-reflector antenna. The filter would be used to reduce the sidelobes produced by feed spillover, feed support struts, and dish deformations. Many of these sidelobes occur within the angular reject band of the filter. A typical reflector pattern illustrating the sidelobe structure is shown in figure 6-1a. If a spatial filter were placed in front of the reflector with an absorbing shroud enclosing the reflector, the ideal pattern produced by the filter-antenna combination is shown in figure 6-1b. In figure 6-1b the far sidelobes are reduced, the near-in sidelobes are unchanged, and the main beam is passed without attenuation. In practice, the near-in sidelobes will be perturbed and the main beam may be slightly attenuated.

Consider figure 6-2, which shows a flat untilted filter in front of a reflector antenna. By using ray tracing it is seen that most of the feed spillover radiation that is incident on the filter is reflected by the filter towards the periphery of the antenna. A ring or shroud of absorber placed as shown in figure 6-2 will prevent this power from radiating. The absorber will also intercept the spillover power not incident on the filter.

The filter-antenna configuration of figure 6-2 is now considered with respect to the power scattered by the feed support strut. Assuming the struts are attached to the reflector at its edge, the principle scattering components

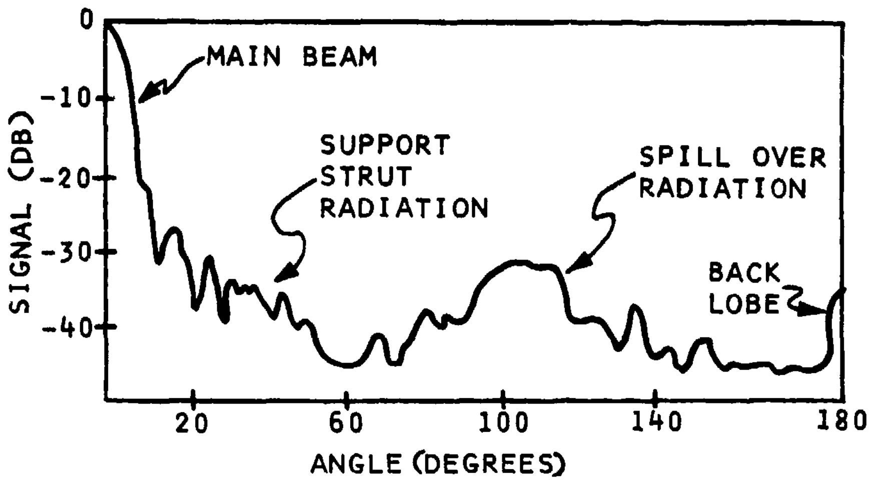

(a) Typical Reflector Pattern

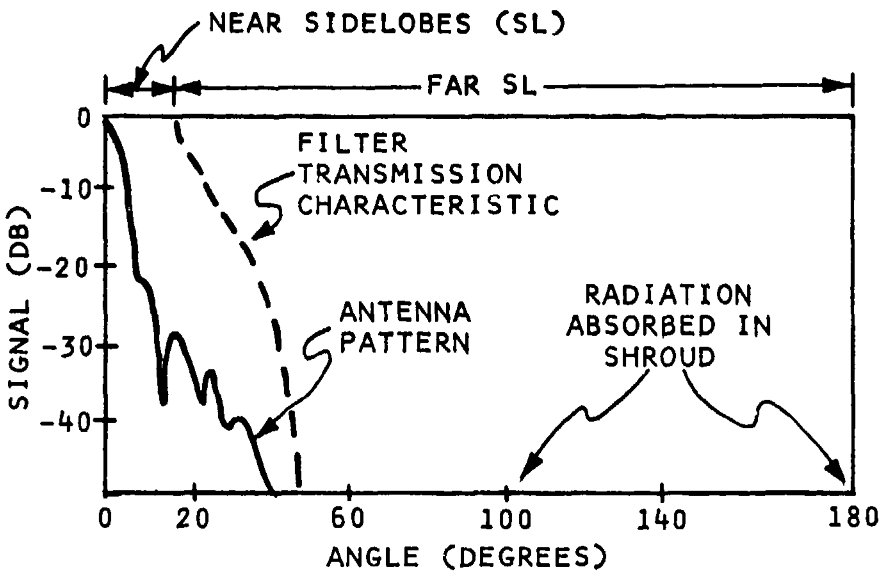

(b) Ideal Pattern of a Reflector with Filter

Figure 6-1 Ideal Performance of a Filter/Reflector Antenna Combination

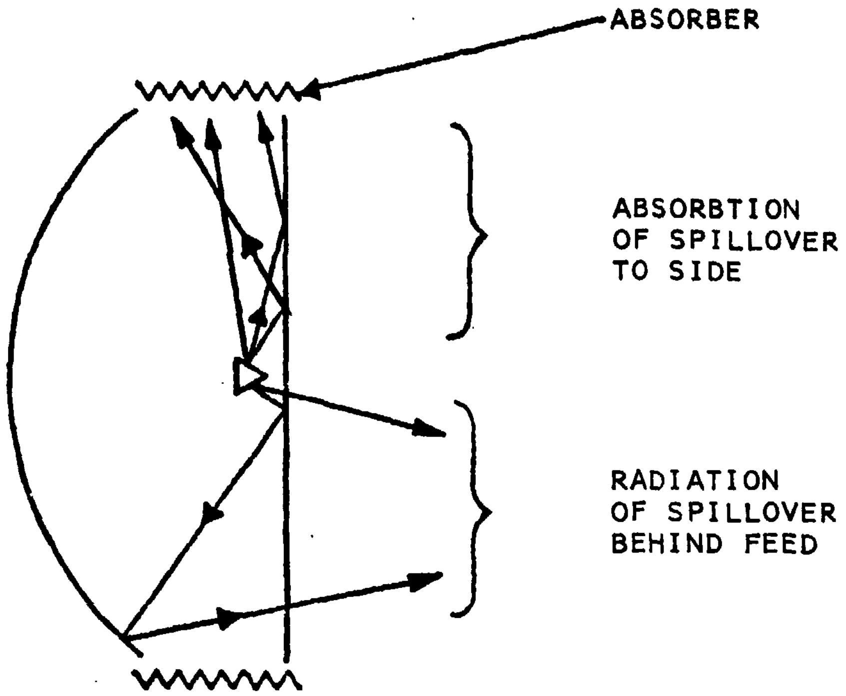

Figure 6-2 Feed Spillover Reflection Effects with Filter and Absorber

may be viewed as shown in figure 6-3. Energy is scattered over the angular region lying along the surface of the cone. The forward part of the diffraction cone will be transmitted through the passband of the filter; this portion may be represented as the familiar aperture-blocking component of the strut scattering. The component of scattering that is shown in a downward direction in figure 6-3(a), will be absorbed. The sideward component of scattering, as shown in figure 6-3(b), will in part be absorbed and in part radiate within the angular passband of the filter.

Reflections within the passband of the filter are caused principally by tolerances. The nominal filter reflection coefficient at broadside in theory is small, however, as discussed in Reference 1 tolerances in practice may cause a substantial reflection. Furthermore, the main beam of the antenna contains a substantial amount of power and therefore even a small reflection coefficient may produce reflected power levels comparable to the near-in sidelobe levels. The best approach for minimizing the sidelobes produced by passband reflection is to adhere to a tight tolerance budget, for example, as proposed in section 4 of this report.

Figure 6-4 illustrates the arrangement used for measuring the filter in conjunction with a parabolic reflector antenna. The reflector is 40 inches in diameter, and the filter is placed 2" beyond the feed for the reflector. The absorber shown in figure 6-4 is attached to a 5 ft. cubic wooden frame. A slot in the front of the frame allows the filter to be removed without disturbing the absorber panels. A standard gain horn is mounted as shown on the wooden frame. Its purpose is to compare reflector antenna signal levels with and without the filter. Figure 6-5 shows the filter on the antenna range.

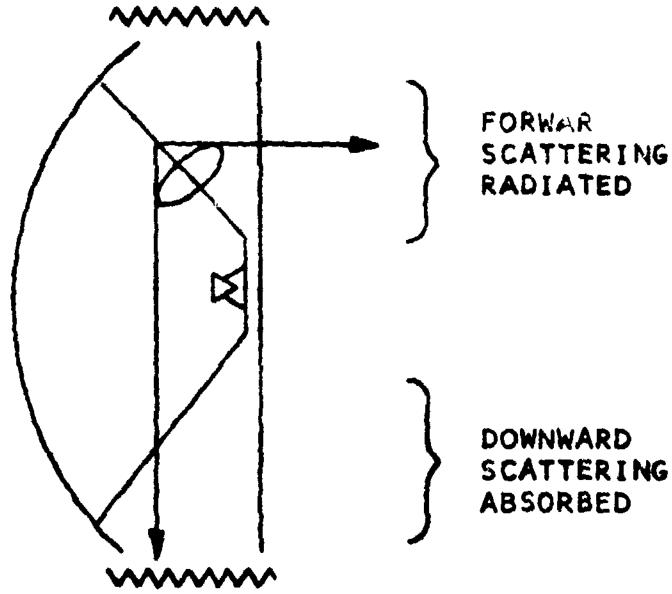

(a) SIDE VIEW OF VERTICAL-PLANE STRUTS

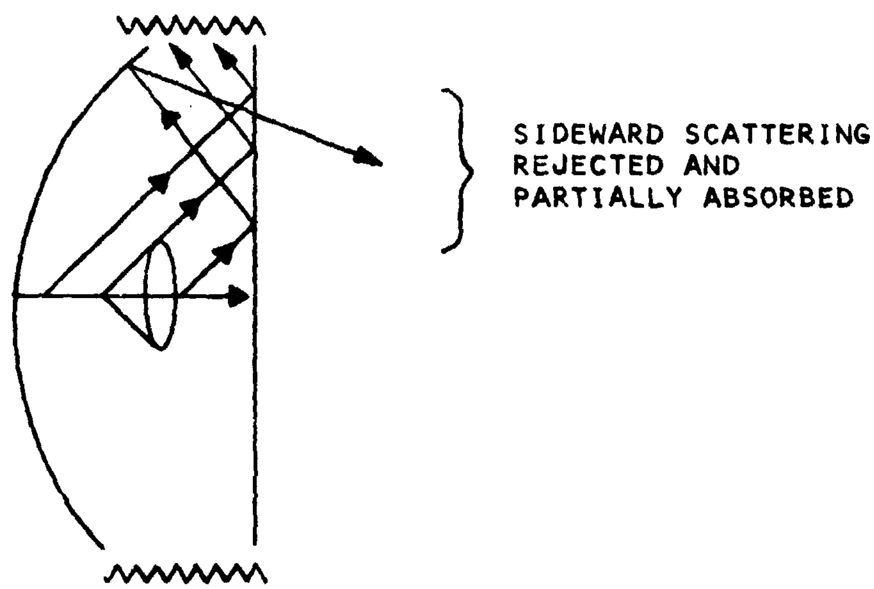

(b) TOP VIEW OF VERTICAL-PLANE STRUTS

Figure 6-3 Strut-Scattering Reflection Effects with Filter and Absorber

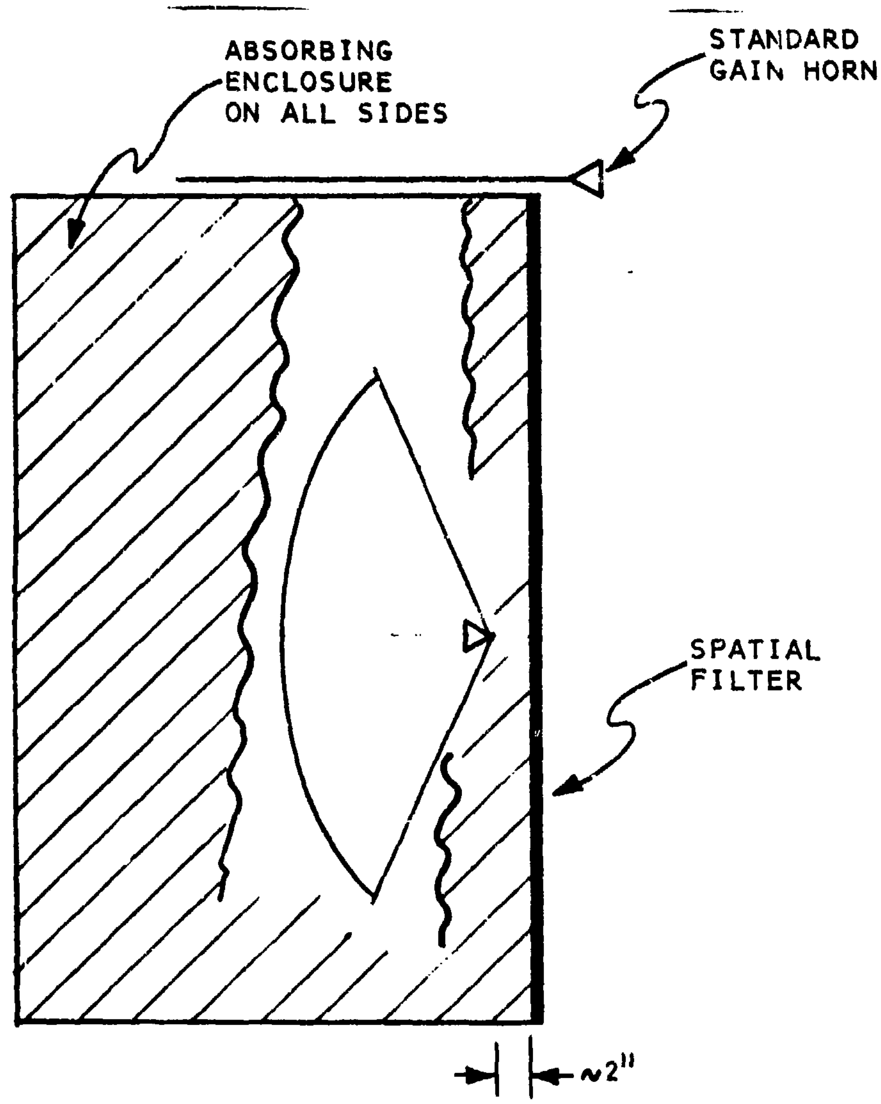

Figure 6-4 Arrangement for Measurement of Spatial Filter with Reflector Antenna

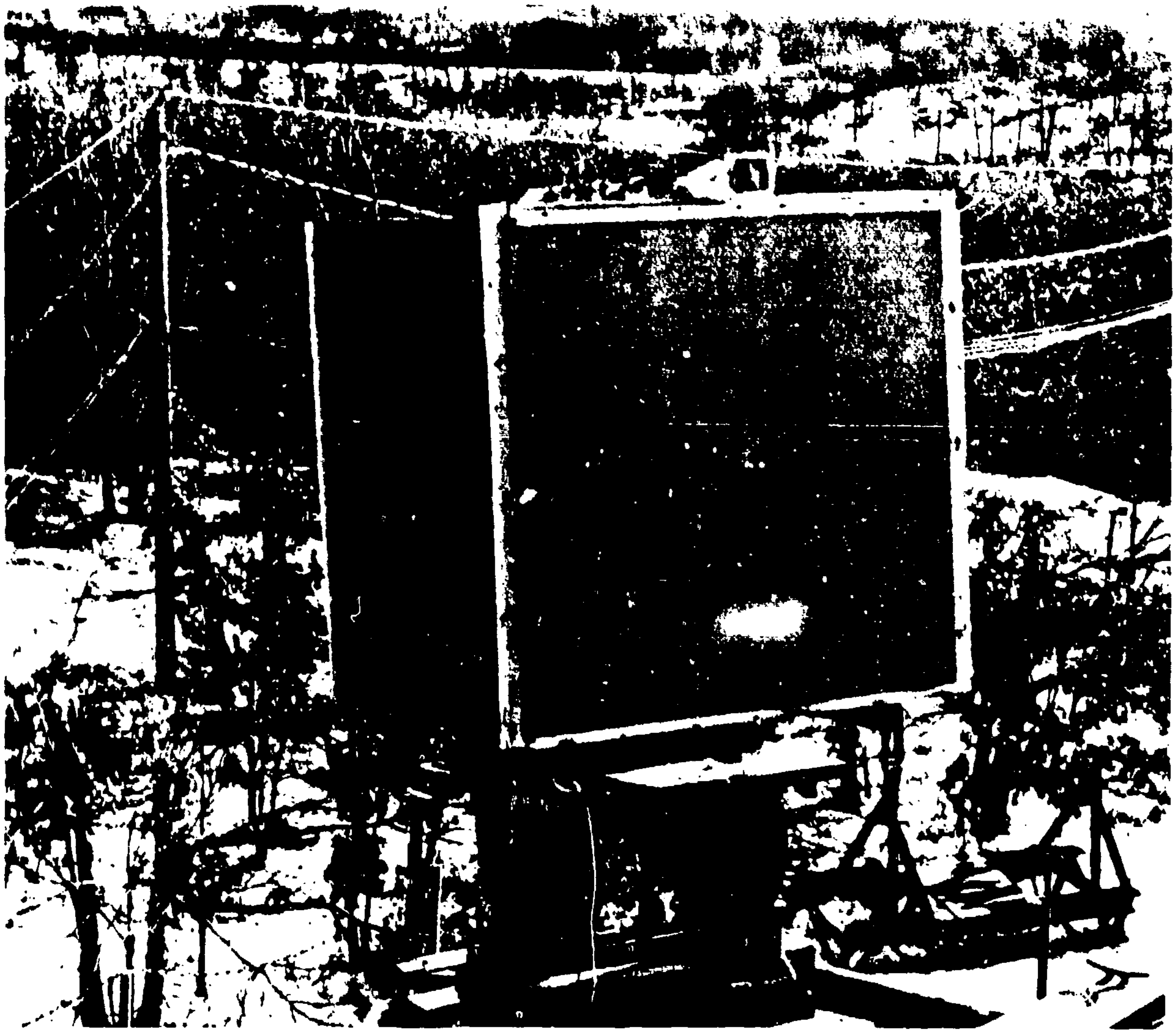

Figure 6-5 Photograph of Spatial Filter on Antenna Range

The objectives of these measurements are (1), to measure the reduction of far sidelobes; (2), to measure the change of the near-in sidelobe level; and (3), to measure the change of antenna gain when the filter is added. Appendix A presents a collection of reflector antenna patterns measured with and without the filter. As an example of the measured performance consider the following selection of patterns shown in Appendix A. Figure A-19 is a measured H-plane pattern of the reflector alone at the nominal design frequency 9.1 GHz. Figure A-27 shows the same pattern cut with the filter. In order to simplify the comparison figure 6-6 shows an overlay of the two patterns. The following items are noteworthy:

(1), beyond 30° the filter substantially reduces the antenna sidelobes; and

(2), the near-in sidelobes are perturbed by less than about $\pm$1dB at a level between -20 dB and -30 dB.

Figure 6-7 shows the results of comparing the gain of the reflector with filter to the gain of the reflector alone as a function of frequency within the frequency passband of the filter. The measurements are accurate to about $\pm$0.5 dB. The average loss of the filter over its frequency passband appears to be about 0.5 dB. Computation of the loss, assuming reasonable values for the loss tangents of the dielectric skins and honeycomb cores yields a passband loss of about 0.3 dB.

Figure A-3 is a measured E-plane pattern of the reflector alone at the nominal design frequency. Figure A-11 is the same pattern cut measured with the filter. As expected the E-plane rejection of far-sidelobes is not as substantial as the H-plane far sidelobe rejection. The change in near-in sidelobes is approximately the same as the change in H-plane sidelobes. Figure 6-8 is an overlay of the E-plane patterns discussed above.

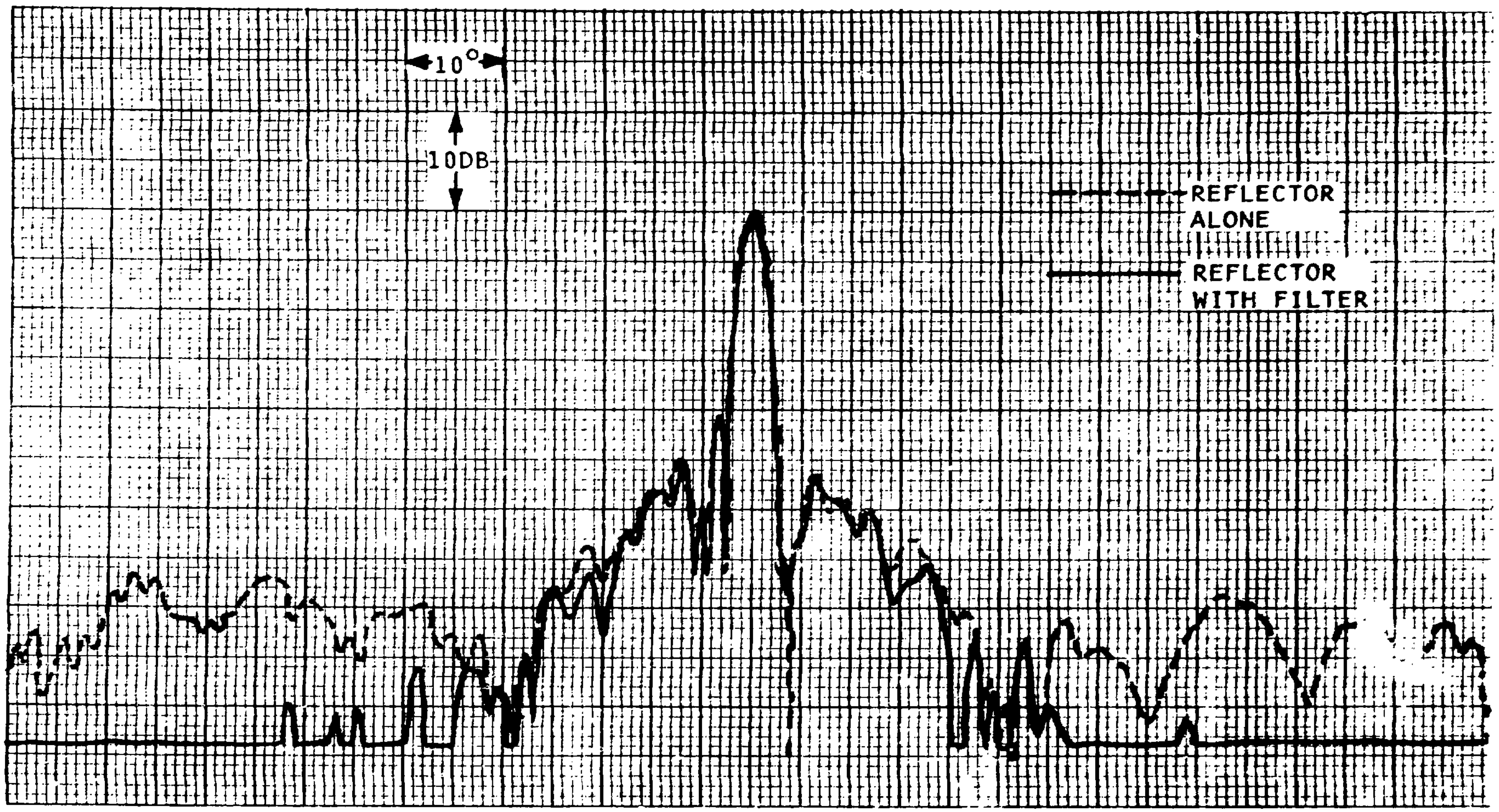

Figure 6-6 Overlay of H-Plane Reflector Antenna Patterns With and Without Filter

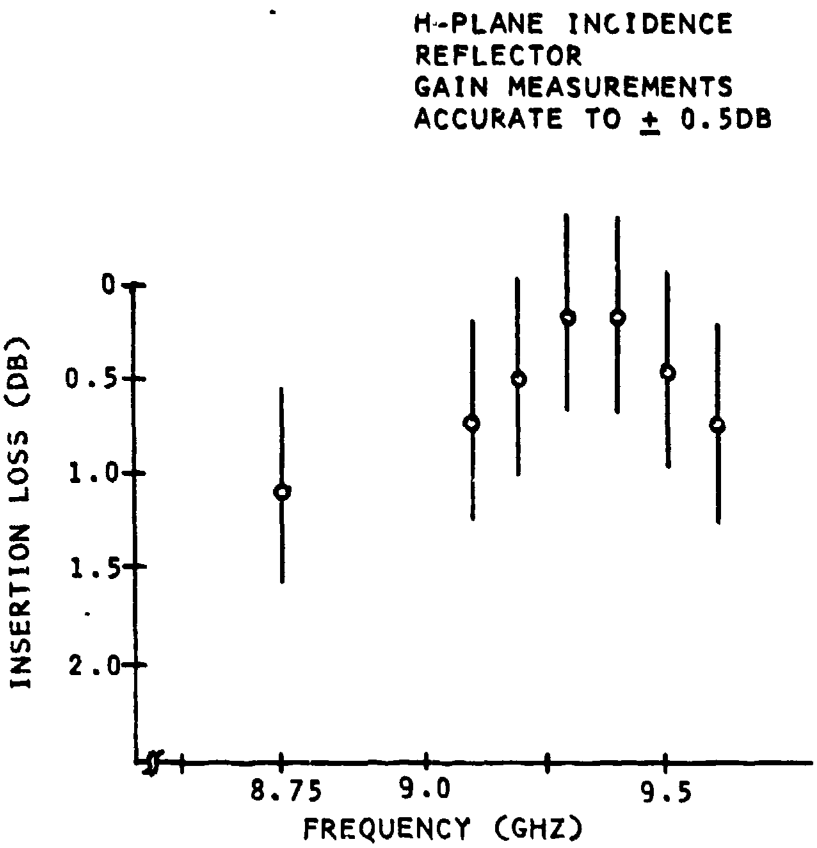

Figure 6-7 Difference in Gain of Reflector Antenna with Filter Added

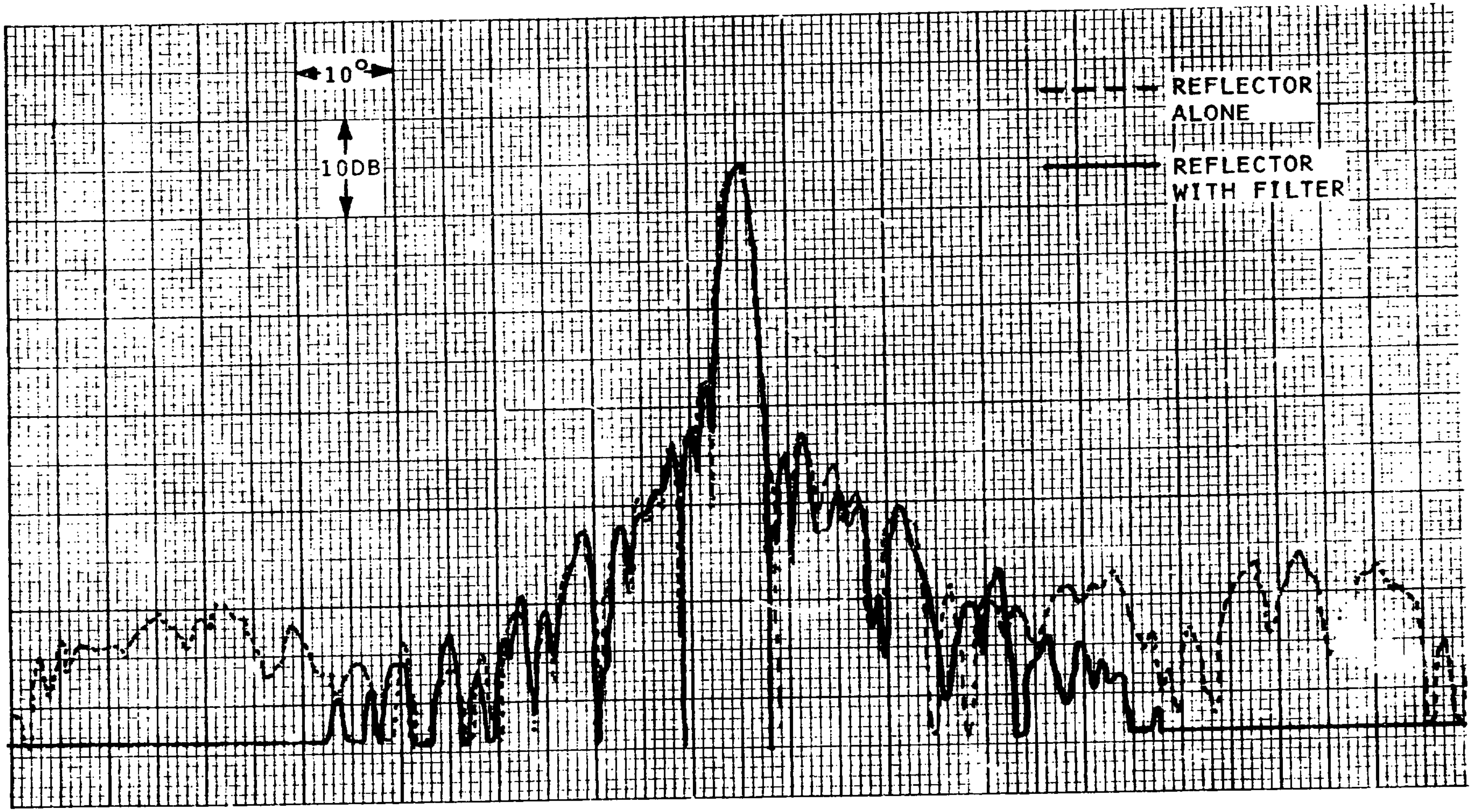

Figure 6-8 Overlay of E-Plane Reflector Antenna Patterns With and Without Filter

6.4 MEASUREMENT OF A SPATIAL FILTER WITH A REFLECTOR ANTENNA AND A GRATING

Another application of a spatial filter is with an antenna that is scanning over a limited angular region. For a scanning beam antenna, the angular passband of the filter can encompass the scan region so that the main beam is always passed but potential grating lobes may be rejected. This application was suggested by Mailloux (Reference 2).

In order to simulate a limited scan antenna, a vertical grating of metal rods was added to the test arrangement discussed in section 6-3. Figure 6-9 illustrates the grating used with the reflector antenna and the filter. The spacings between the various elements are noted on the figure. The resulting radiation pattern at 9.1 GHz is shown in Appendix B Figure B-3. The grating adds two beams at approximately $\pm 45^{\circ}$ from the main beam at about a -10 dB level with respect to the main beam. Figure B-13, is the same pattern cut as figure B-3 but with the filter in front of the antenna/grating assembly. Figure 6-10 is an overlay of these two patterns showing the effect of the filter. It is evident that the grating lobes are substantially reduced by the filter.

It appears that, upon examining the variation of gain of the patterns in Appendix B with frequency, a significant portion of the grating-lobe power that is reflected by the filter is focused onto the feed. Consider a wave at normal incidence on a grating. It produces two radiating beams at approximately $\pm 45°$ with respect to the main radiation and a similar set of reflected beams. A portion of the reflected power is focused onto the the reflector. Now let one of the radiated grating lobes be incident on the grating as a result of being reflected from

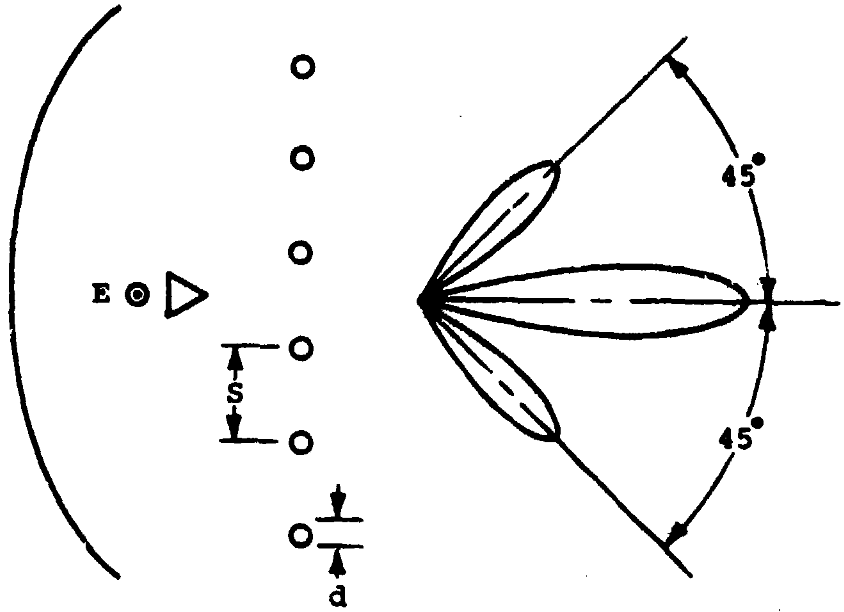

$$S = \sqrt{2}\,\lambda$$

$$\frac{d}{\lambda} = \frac{1}{4}$$

Figure 6-9 Arrangement for Test of Reflector Antenna with Grating

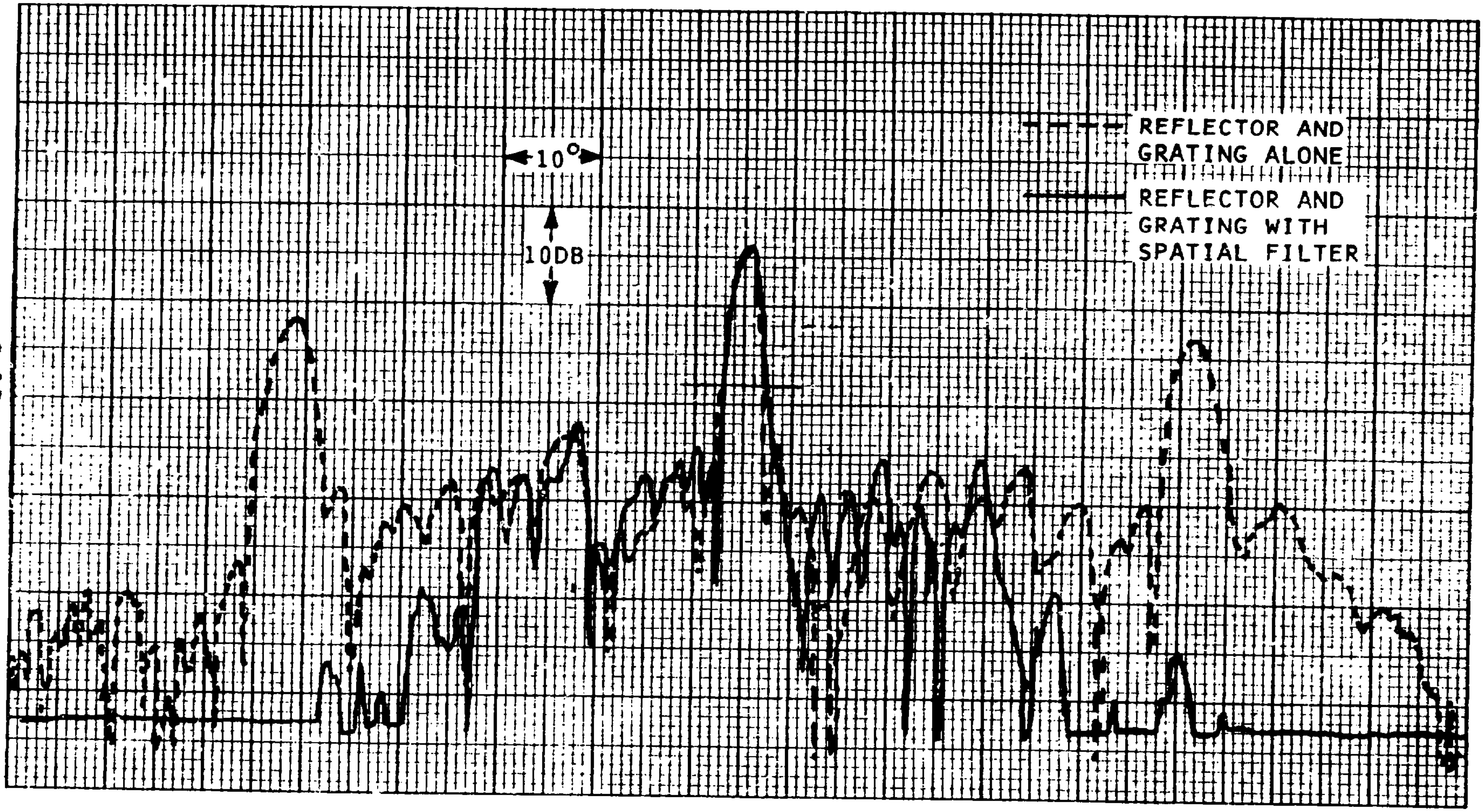

Figure 6-10 Overlay of H-Plane Patterns of Reflector Antenna with Grating With and Without Spatial Filter

the filter. The phasing across the array of rods produces its own set of beams as described above and as shown in Figure 6-11. Some of this power is also focused onto the feed. The phase differences between all contributing reflected components is evidenced by the fluctuations in antenna gain as a function of frequency. These reflected components may also contribute to the changes in the near sidelobes that can be seen in Figure 6-10.

6.5 MEASUREMENT OF TRANSMISSION CHARACTERISTIC OF FILTER

One method that may be employed to measure the transmission characteristic of the spatial filter is to measure the E-plane and H-plane patterns of a small horn with and without the filter. A horn is selected that has a much wider pattern in the E-plane and H-plane than the filter passband; therefore, a spatial filter placed in front of the horn modifies these patterns by its transmission characteristics as shown in figure 6-12. A simple comparison of the measured patterns for a particular pattern plane gives the transmission characteristic of the filter.

In Appendix C, Figures C-3 and C-17 show the H-plane and E-plane patterns of the small horn used for these tests. Figures C-10 and C-24 are the same patterns with the filter-horn combination. The difference between the pattern sets will give the H-plane and E-plane filter characteristics. The results of the subtraction are shown in Figure 6-13 for the frequency 9.1 GHz. The computed results shown in Figure 5-2 are repeated in Figure 6-13, together with the measured results. (It is noted that the dynamic range of the measurement system precluded the determination of filter characteristics at levels below -20 dB). The agreement between measured and calculated results is reasonably good in the H plane of incidence.

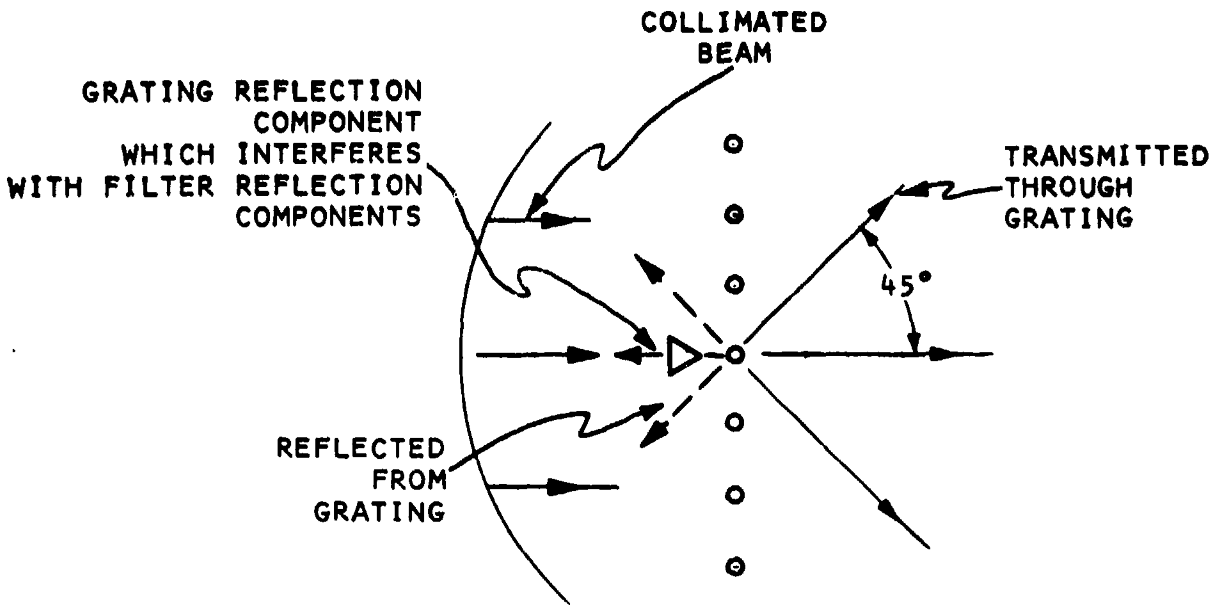

a) without filter

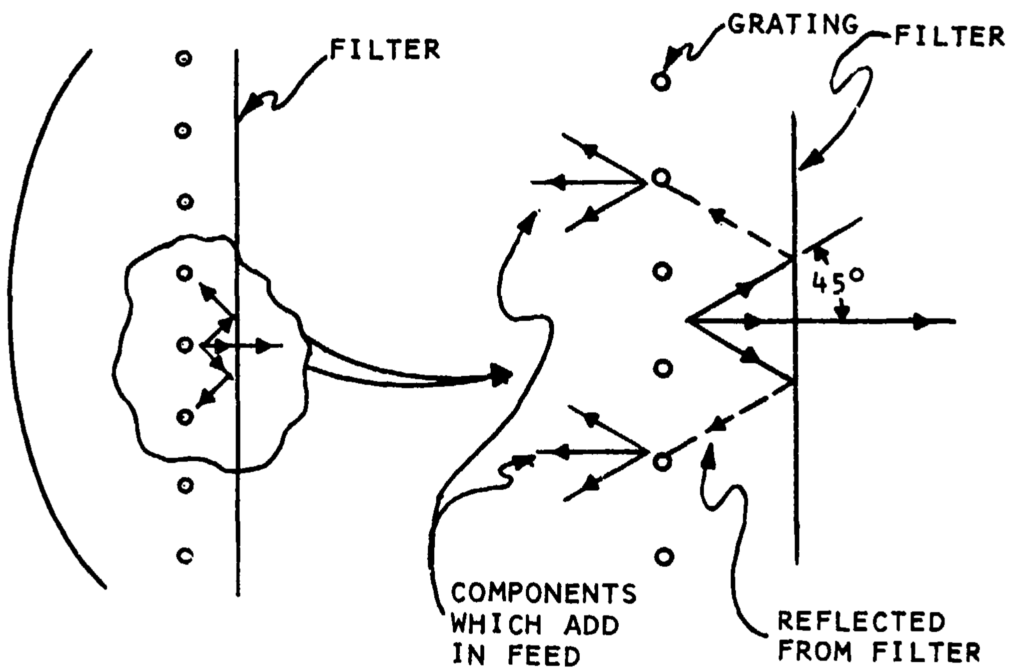

b) with filter

Figure 6-11 Grating and Filter Reflection Components that Cause Gain Variations

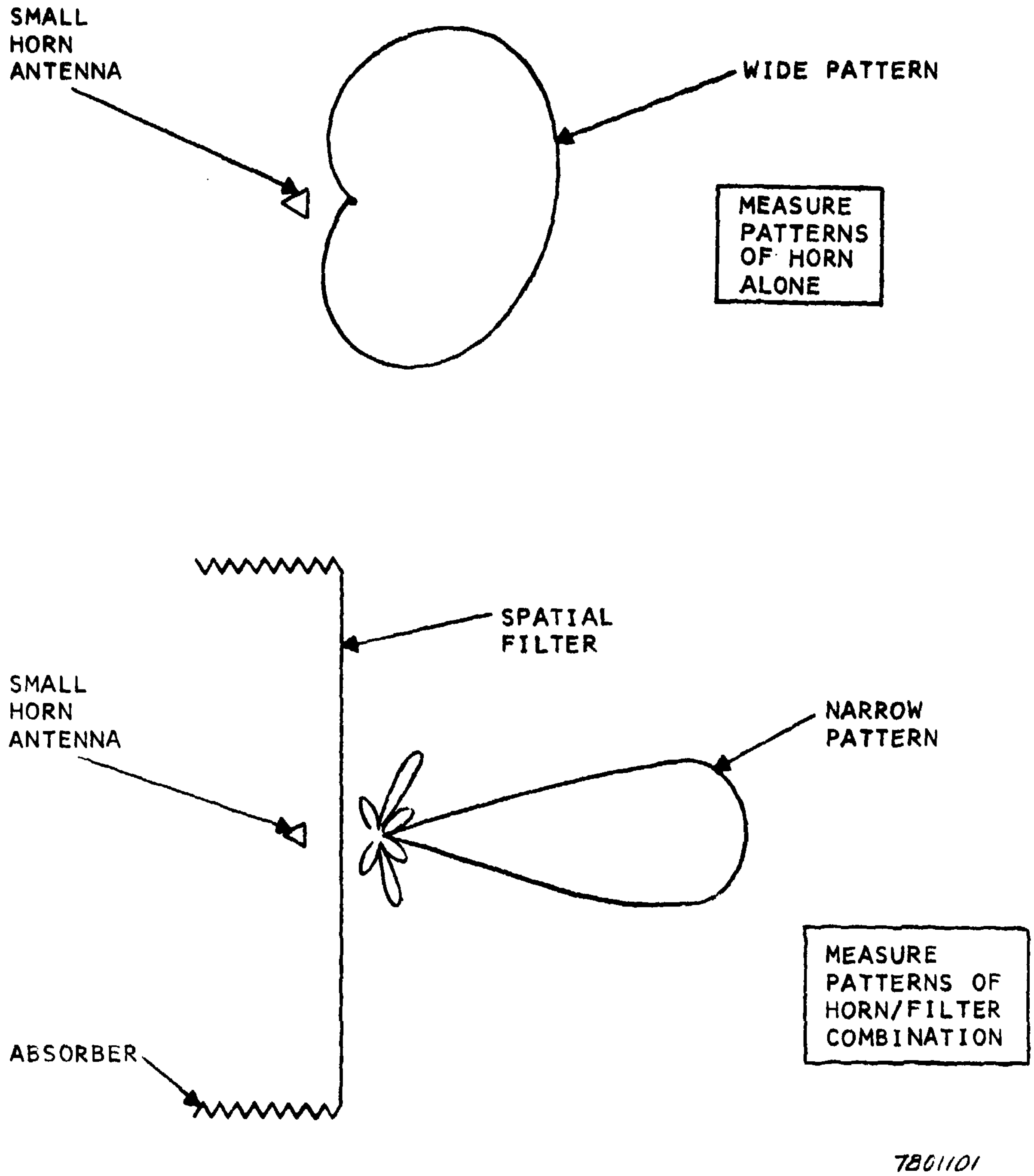

Figure 6-12 Test of Spatial Filter Transmission Characteristic

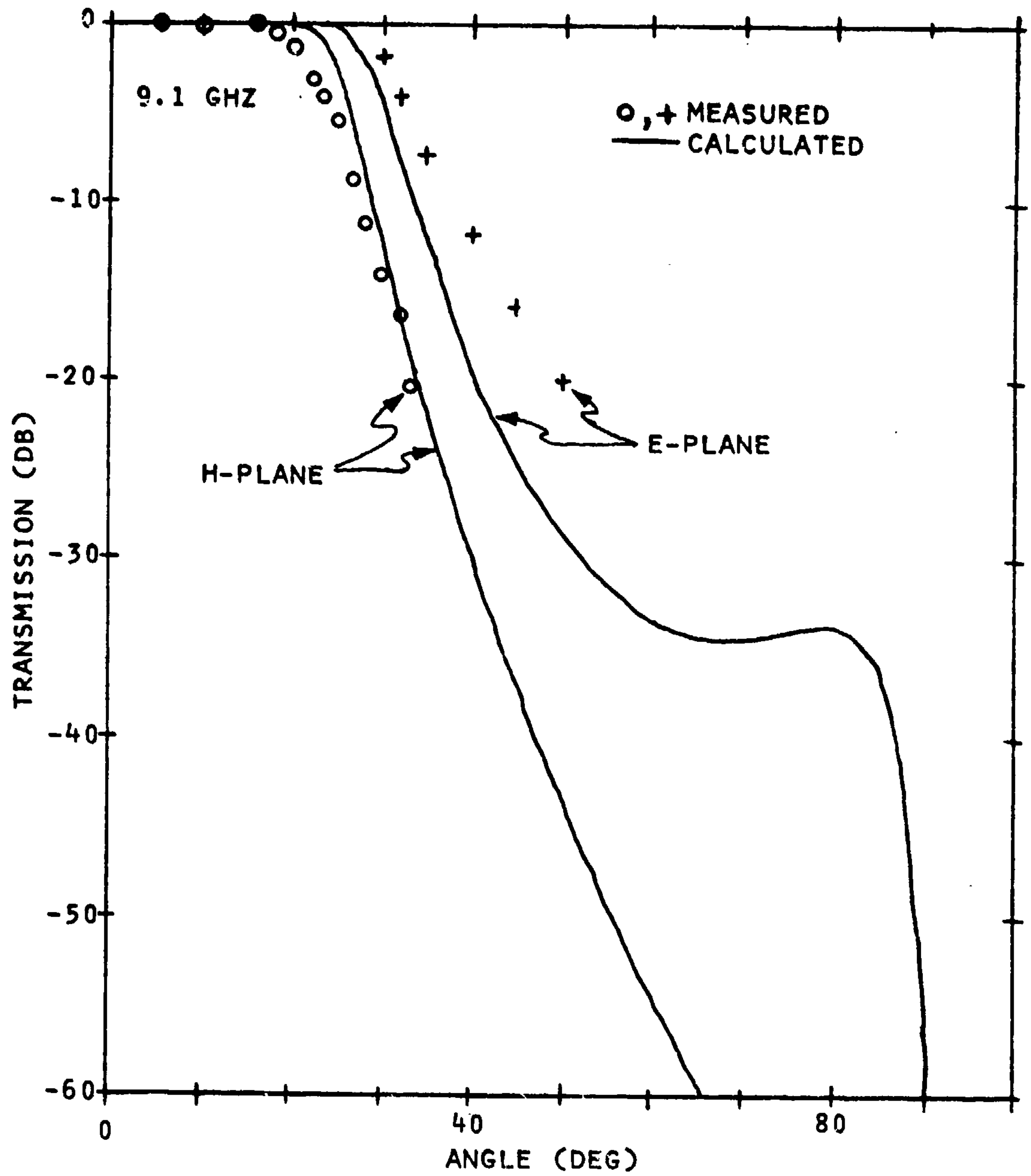

Figure 6-13 Measured H-Plane, E-Plane Transmission Characteristics, 9.1 GHz

The measured rejection in the E plane is less than the calculated rejection. This result in the E plane is not unexpected since measurements in a near-grazing E-plane simulator (Reference 1) showed that the rejection of a single crossed grid of metal wires embedded in a dielectric skin was less than the computed rejection. There is no evidence of any spurious passband in the E-plane spatial filter measurements.

Figure 6-14 shows the measured and computed H-plane filter transmission characteristics at some frequencies below and above the filter midband frequency. The basic trend of increasing angle with increasing frequency that is inherent with this type of spatial filter is apparent. The filter bandwidth for passing a wave at 0° incidence is related to the angular passband width by the following approximate relation (see Reference 1):

$$\frac{\Delta f}{f_m} \approx \theta_c^2$$

where f_m = midband frequency

θ_c = angular passband width (radians) at midband

Taking the passband width at midband (9.1 GHz) from the calculated H-plane curve shown in Figure 6-13, this relation gives a Δf of about 1 GHz, or $\pm$ 0.5 GHz from 9.1 GHz. The results shown in Figure 6-14 are reasonably close to this estimate.

In the fourth plot in Figure 6-14, the filter transmission characteristic is shown at 10.0 GHz. This frequency is substantially above the normal frequency band of the filter, so there is a substantial amount of rejection at 0° incidence angle. This case actually is an example of a spatial filter with an off-broadside passband (see Reference 1), which may be useful for certain applications.

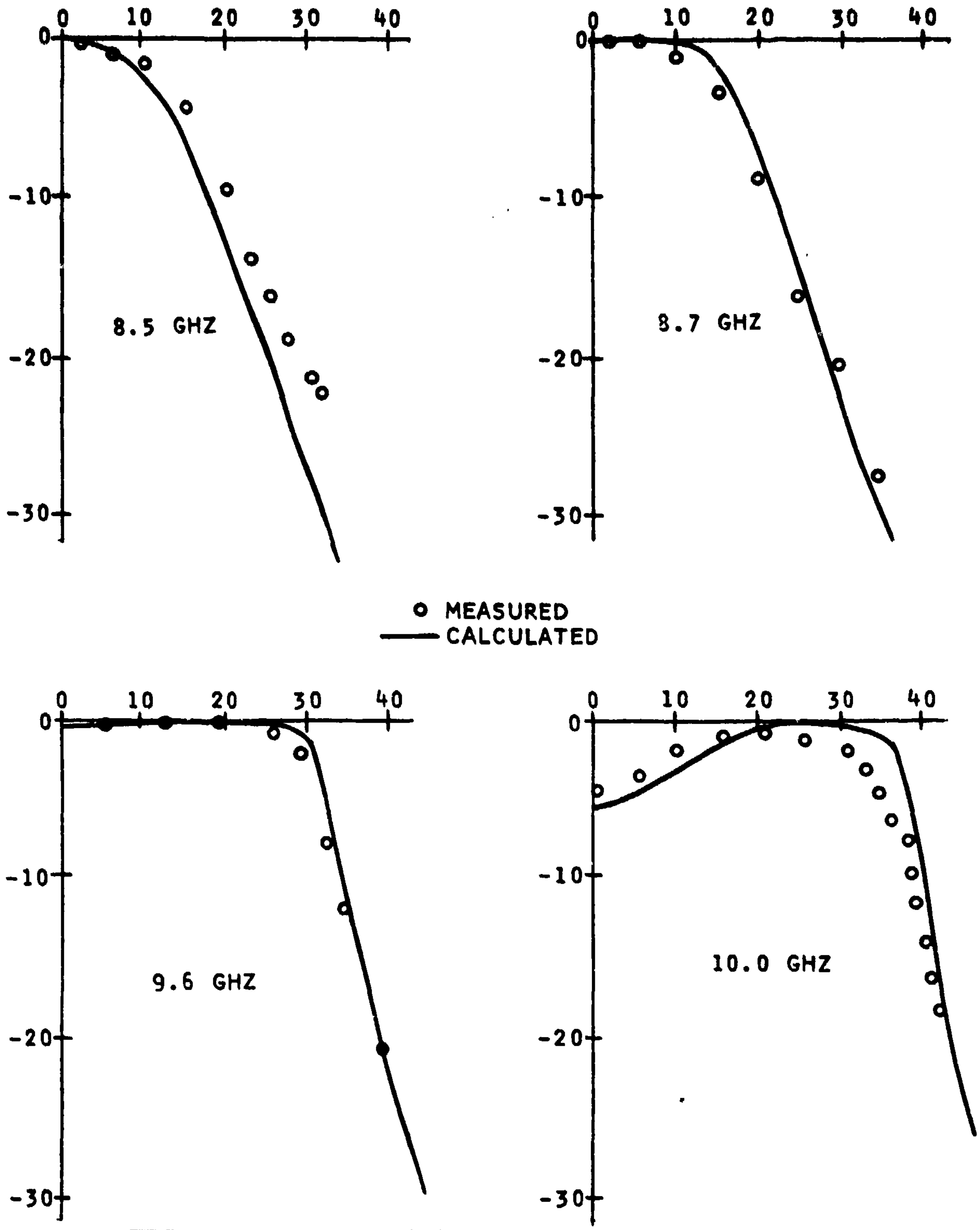

Figure 6-14 Measured and Calculated H-Plane Transmission Characterisitcs at Various Frequencies

6.6 MEASUREMENT OF THE REFLECTION COEFFICIENT AT BROADSIDE

In order to measure the reflection coefficient of the spatial filter at 0° incidence, the parabolic reflector antenna was used to illuminate the filter panel. With the filter panel oriented for 0° incidence, three sets of reflection data were recorded. The first was with the reflector radiating within the absorber enclosure shown in Figure 6-4, but without the filter. Next, reflection data was measured with the filter in place. Finally, a short-circuit reference measurement was made using a metal sheet substituted at the plane of the filter. This reference measurement was used to correct the filter reflection data for loss in the antenna system. All reflection readings were taken at closely-spaced frequencies to be certain that the measurement included the reflection ripple produced by reflection components separated by many wavelengths.

Figure 6-15 shows the measured reflection coefficient of the antenna alone (dots), and the corrected reflection coefficient of the antenna plus filter (circles). The difference between the two is shown by vertical lines and is an indication of the reflection coefficient of the filter alone (since phase was not measured, this data can only be used as a qualitative indication of the filter reflection). It is seen that over the 8.6 to 9.6 GHz frequency band of the filter, the difference between the two measurements is consistently small (less than about 0.1), while above 9.6 GHz some of the differences become substantial as would be expected from the increased filter reflection corresponding to the beginning of the reject band.

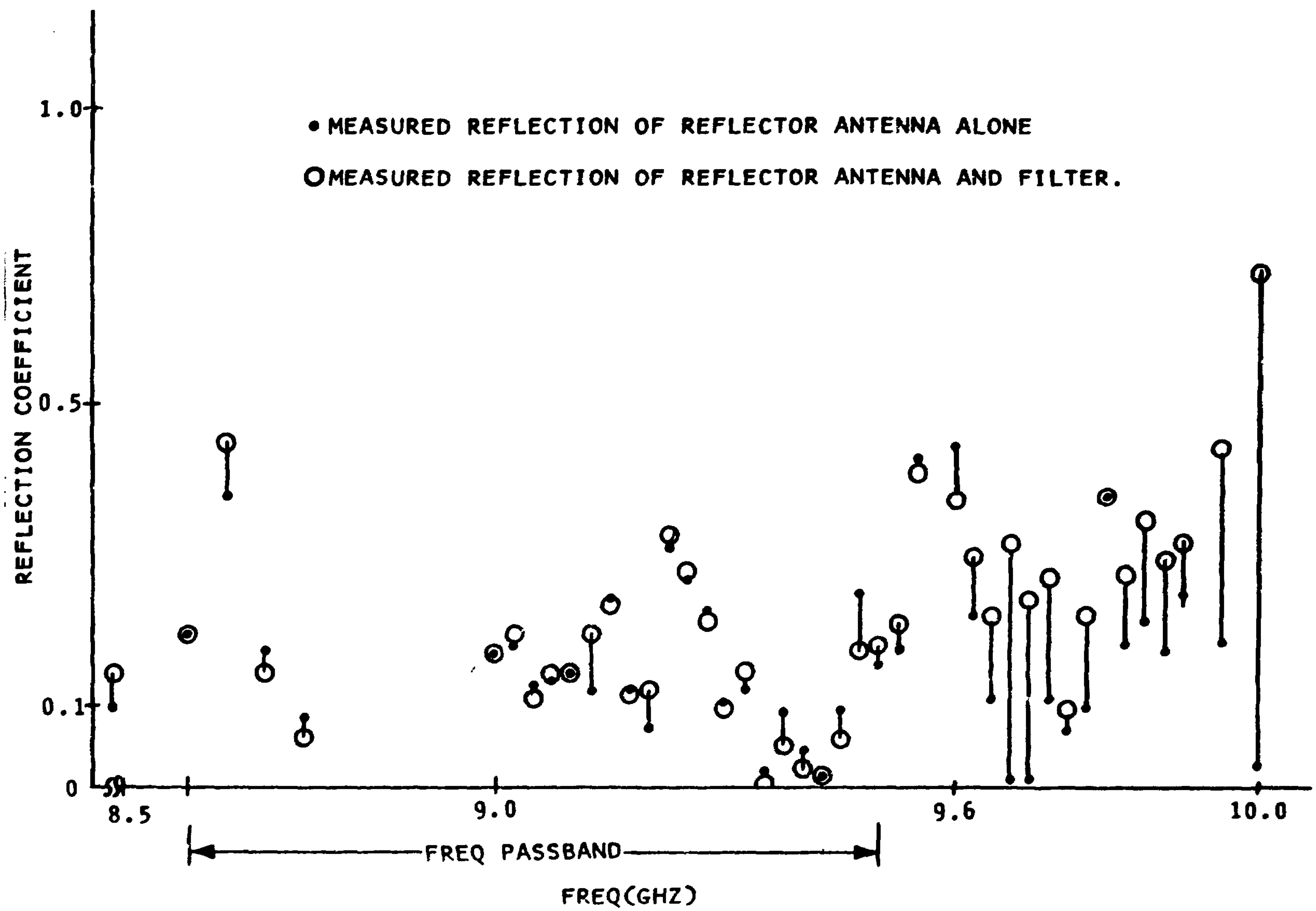

Figure 6-15 Measured Reflector Data of Filter with Reflector Antenna

SECTION 7

CONCLUSIONS

This final report describes the design, fabrication and test of a metal-grid spatial filter. The concepts, analysis, and metal-grid tests that form the basis for the design are described in the interim report (Reference 1).

The spatial filter that has been developed is a 5 x 5 foot flat panel incorporating 4 layers of crossed wire grids in a supporting structure of dielectric skins and dielectric honeycomb material. The filter operates at 9 GHz.

Tests of the spatial filter have yielded the following results:

(1) The measured rejection vs. angle of incidence in the H plane is close to the calculated rejection.

(2) In the E plane of incidence the measured rejection vs. angle is less than the calculated rejection. This result was expected from the simulator measurements of metal grids embedded in dielectric that were reported earlier (Reference 1).

(3) There was no evidence of a spurious passband in the E plane of incidence. This result also correlates with the simulator measurements reported earlier.

(4) Placing the spatial filter in front of a reflector antenna produced a significant reduction of the antenna sidelobes in the angular reject band of the filter beyond 30°.

(5) The antenna near sidelobes within the angular passband of the filter were only slightly affected by addition of the filter. This demonstrates that the choice of filter strength (amount of rejection) was sufficiently conservative,

and that the critical filter tolerances that affect insertion phase and reflection at 0° incidence were properly controlled.

(6) The filter reflection coefficient and loss at normal incidence appeared to be reasonably small.

(7) The frequency bandwidth of filter operation at normal incidence confirmed the theoretical relation between frequency bandwidth and angular passband width.

The following general conclusions are derived from the complete program of investigation of the metal-grid spatial filter:

(1) In designing a metal-grid spatial filter (or any similar type of spatial filter that relies on resonance between multiple highly-reflecting layers), the choice of filter strength should be governed by the tolerances that are achievable on spacing between the layers of metal grids. The result should be an insertion phase variation and a reflection coefficient at 0° incidence that are small enough to avoid a significant degradation of the antenna near sidelobes.

(2) This practical limitation on strength of the filter becomes less severe at lower frequencies.

(3) Since the angular passband width of this type of spatial filter is related to the frequency bandwidth of the filter, the angular passband should be chosen wide enough to satisfy the frequency bandwidth requirements.

(4) The presence of dielectric supporting material in the practical metal-grid spatial filter introduces some changes in the angular passband characteristic that should be considered if precise control of the passband characteristic is required.

(5) The rejection of a spatial filter using crossed metal grids is less in the E plane of incidence than in the

H plane. This E-plane rejection is further decreased by the addition of dielectric supporting material, except near grazing incidence.

(6) The insulated crossed grid of metal wires supported by a dielectric sandwich structure provides a practical means for achieving a dual-polarized spatial filter that can be constructed in large sizes.

SECTION 8

REFERENCES

1 - P. W. Hannan, P. L. Burgmyer, "Metal-Grid Spatial Filter", Interim Technical Report RADC-TR-79-295, by Hazeltine Corp., July 1980, AD# A089 756.

2 - R. J. Mailloux, "Synthesis of Spatial Filters with Chebyshev Characteristics", IEEE Trans. Antennas and Propagation, pp. 174-181; March, 1976.

3 - J. H. Pozgay, S. Zamoscianyk, L. R. Lewis, "Synthesis of Plane Stratified Dielectric Slab Spatial Filters Using Numerical Optimization Techniques", Final Technical Report RADC-TR-76-408 by Raytheon Co., December, 1976, AD#A037960.

4 - J. H. Pozgay, "Dielectric Spatial Filter Experimental Study", Final Technical Report RADC-TR-78-248 by Raytheon Co., November, 1978, AD# A063 260.

5 - A. C. Schell et al, "Metallic Grating Spatial Filter for Directional Beamforming Antenna" AD-D002-623; April, 1976.

6 - R. J. Mailloux, "Studies of Metallic Grid Spatial Filters", IEEE AP-S Int. Symp. Digest, p. 551; 1977.

7 - E. L. Rope, G. Tricoles, O-C Yue, "Metallic Angular Filters for Array Economy", IEEE AP-S Int. Symp. Digest, pp. 155-157; 1976.

8 - E. L. Rope, G. Tricoles, "An Angle Filter Containing Three Periodically Perforated Metallic Layers", IEEE AP-S Int. Symp. Digest, pp. 818-820; 1979.

9 - R. J. Mailloux and P. R. Franchi, "Metal Grid Angular Filters for Sidelobe Suppression", RADC-TR-79-10; January 1979, AD#A070 111.

10 - P. W. Hannan and J. F. Pedersen, "Investigation of Metal-Grid Angular Filters", Proceedings of the 1980 Antenna Applications Symposium, Allerton Park, Illinois; September 1980.

11 - G. L. Matthaei, L. Young, E. M. T. Jones, "Microwave Filters, Impedance-Matching Networks, and Coupling Structures", McGraw-Hill, pp. 85-101, 450-452; 1964.

APPENDIX A

MEASURED PATTERNS OF A REFLECTOR ANTENNA WITH AND WITHOUT THE SPATIAL FILTER

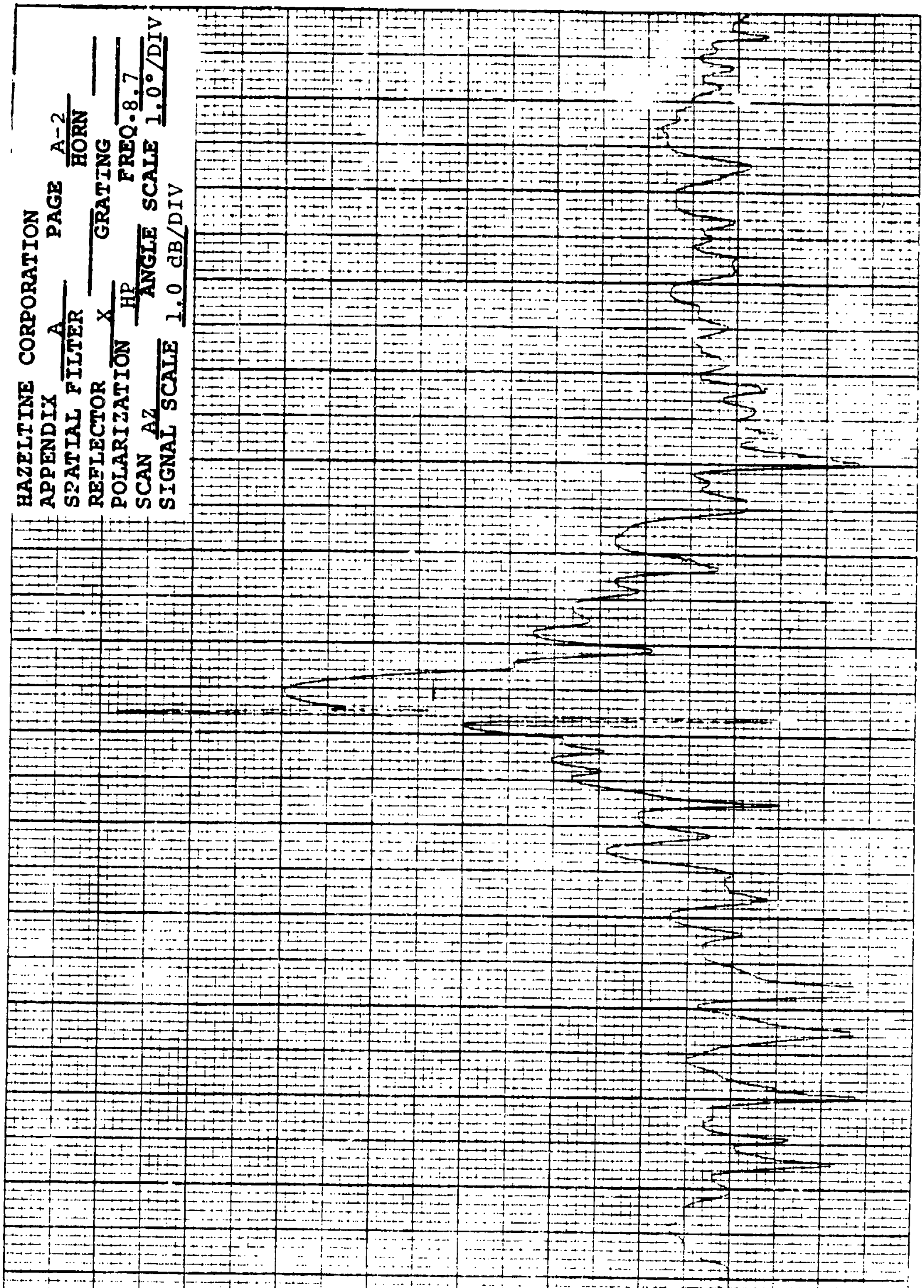
HAZELTINE CORPORATION
APPENDIX A PAGE A-2
SPATIAL FILTER HORN
REFLECTOR X GRATING
POLARIZATION HP FREQ. 8.7
SCAN AZ ANGLE SCALE 1.0°/DIV
SIGNAL SCALE 1.0 dB/DIV

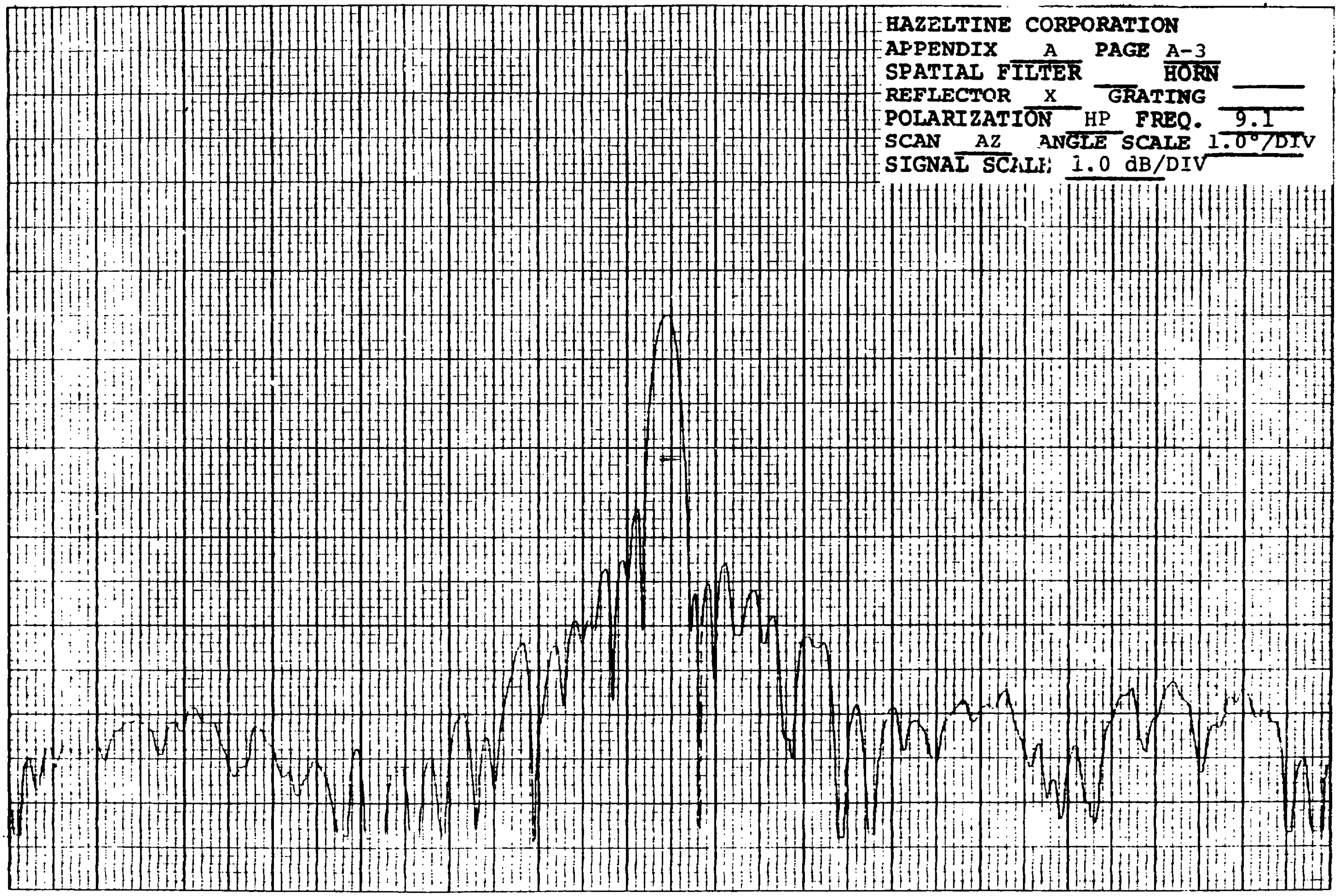
HAZELTINE CORPORATION
APPENDIX A PAGE A-3
SPATIAL FILTER HORN
REFLECTOR X GRATING
POLARIZATION HP FREQ. 9.1
SCAN AZ ANGLE SCALE 1.0°/DIV
SIGNAL SCALE 1.0 dB/DIV

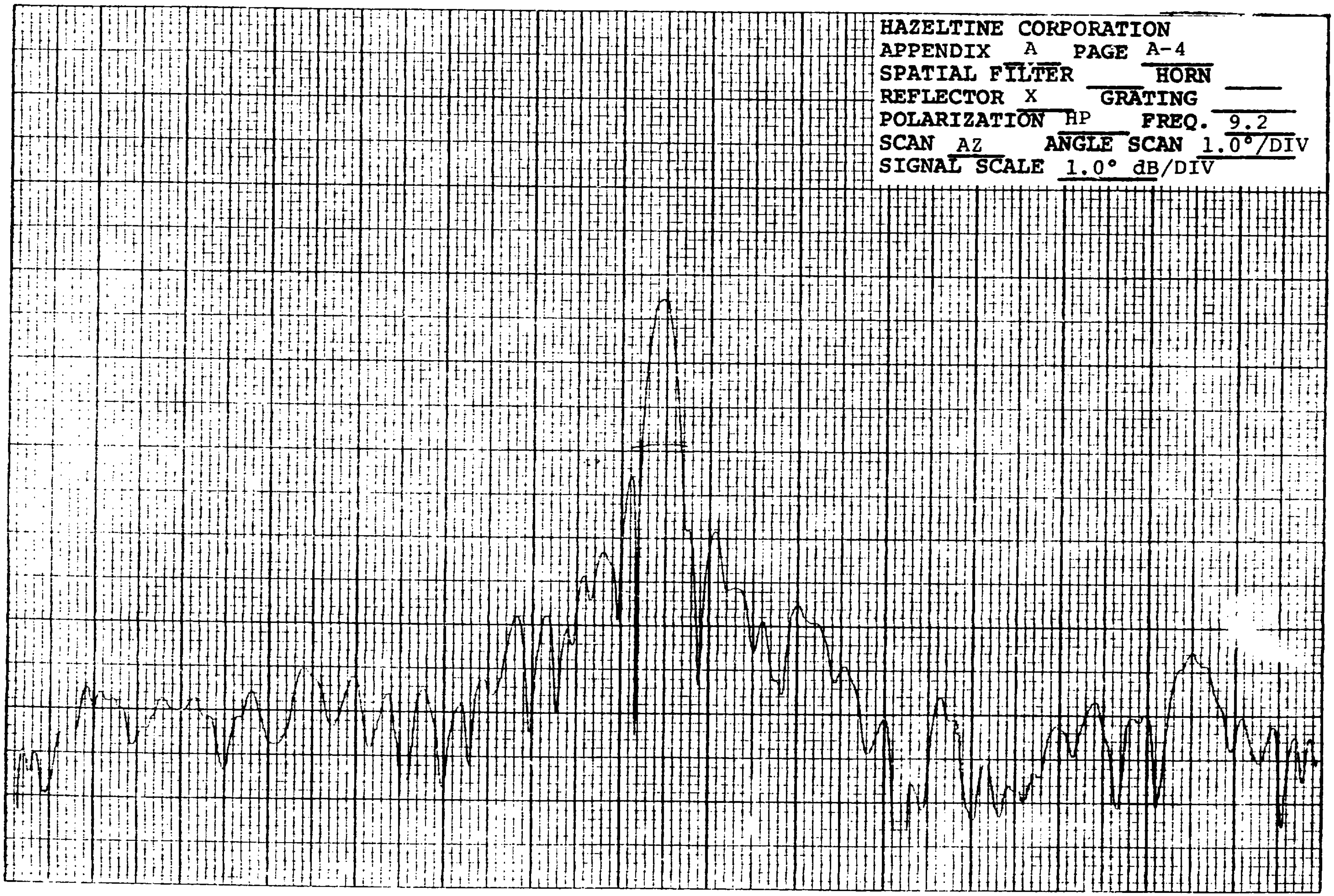
HAZELTINE CORPORATION
APPENDIX A PAGE A-4
SPATIAL FILTER ___ HORN ___
REFLECTOR X GRATING ___
POLARIZATION HP FREQ. 9.2
SCAN AZ ANGLE SCAN 1.0°/DIV
SIGNAL SCALE 1.0° dB/DIV

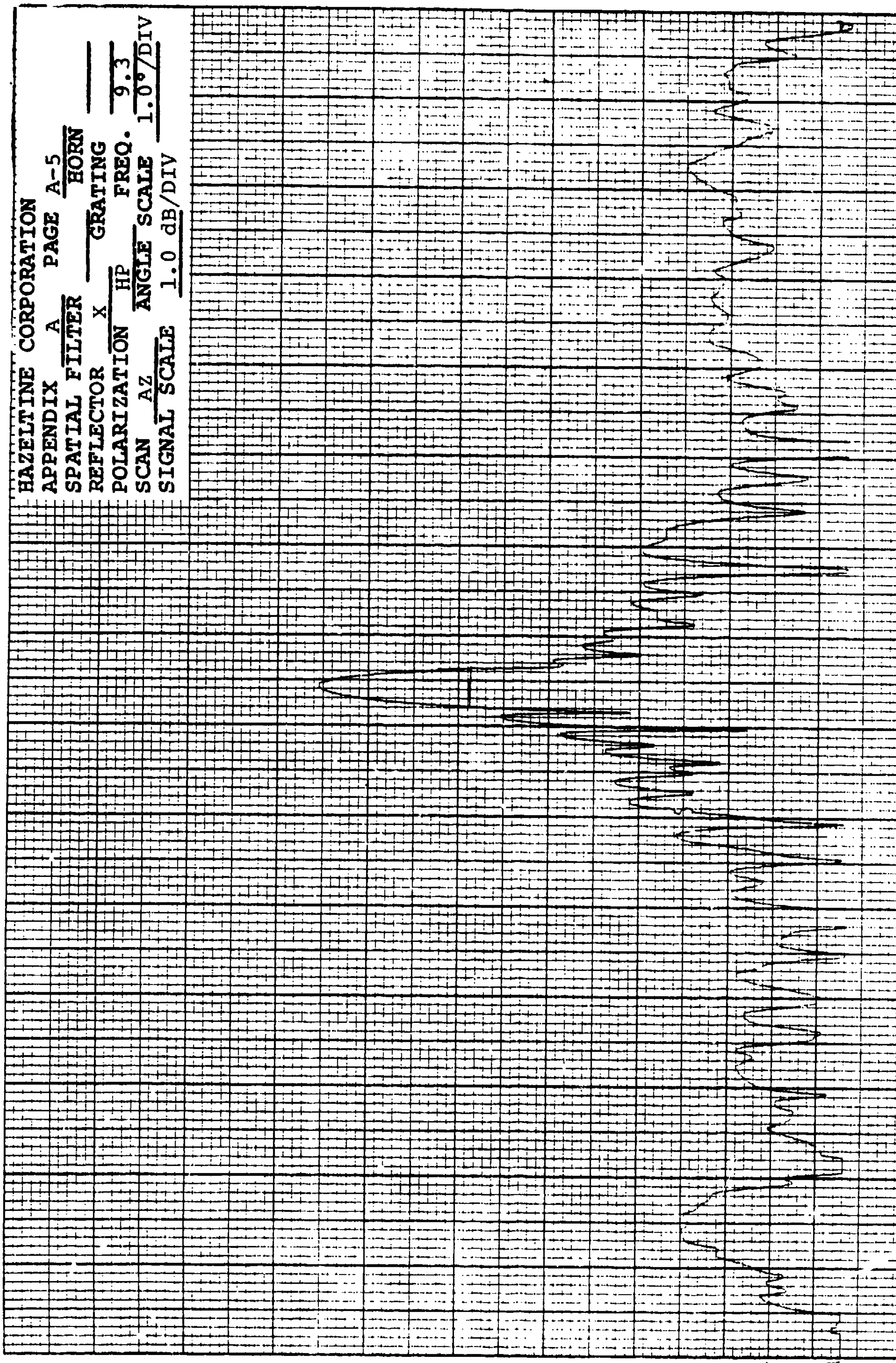
HAZELTINE CORPORATION
APPENDIX A PAGE A-5
SPATIAL FILTER HORN
REFLECTOR X GRATING
POLARIZATION HP FREQ. 9.3
SCAN AZ ANGLE SCALE 1.0°/DIV
SIGNAL SCALE 1.0 dB/DIV

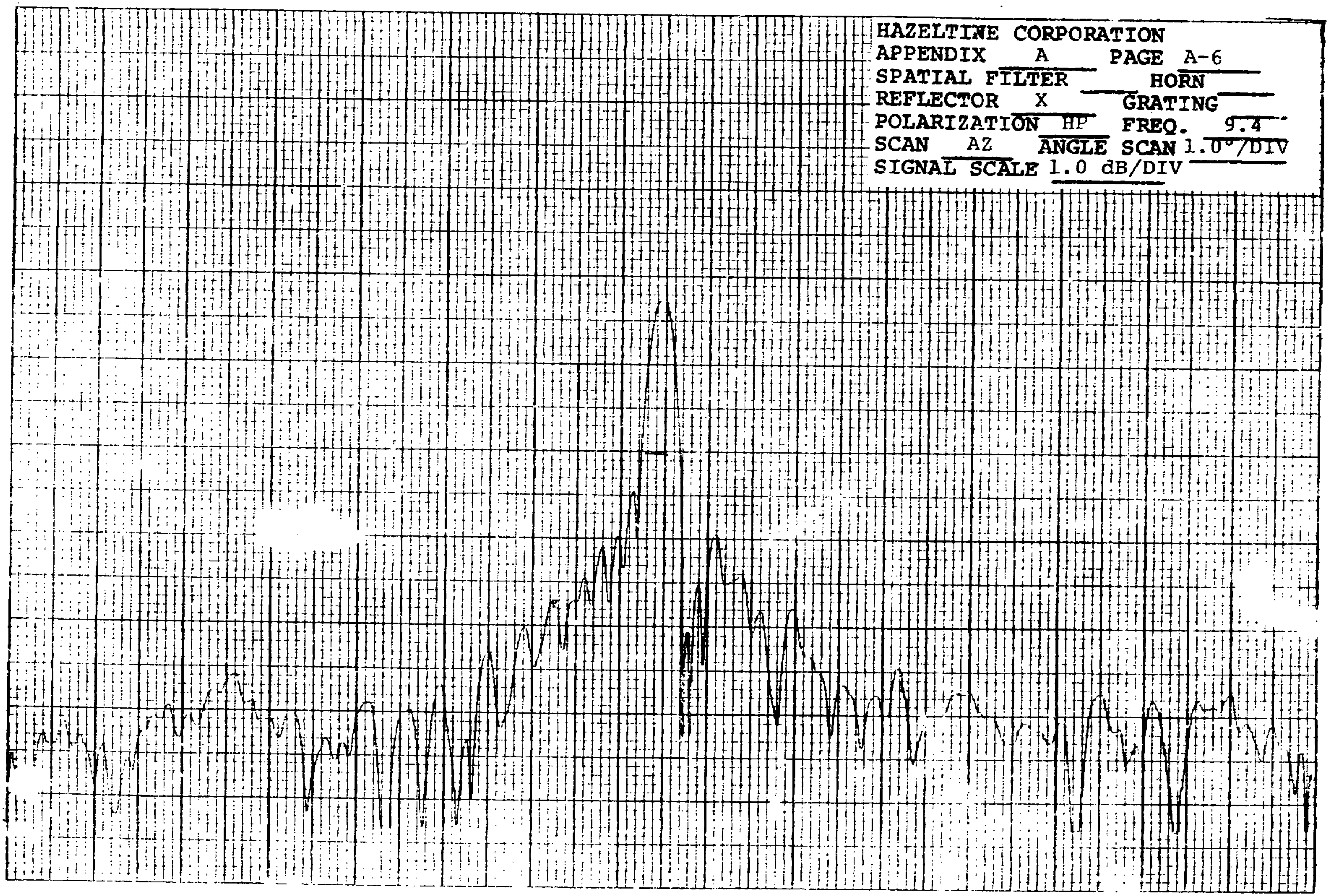
HAZELTINE CORPORATION
APPENDIX A PAGE A-6
SPATIAL FILTER HORN
REFLECTOR X GRATING
POLARIZATION HP FREQ. 9.4
SCAN AZ ANGLE SCAN 1.0°/DIV
SIGNAL SCALE 1.0 dB/DIV

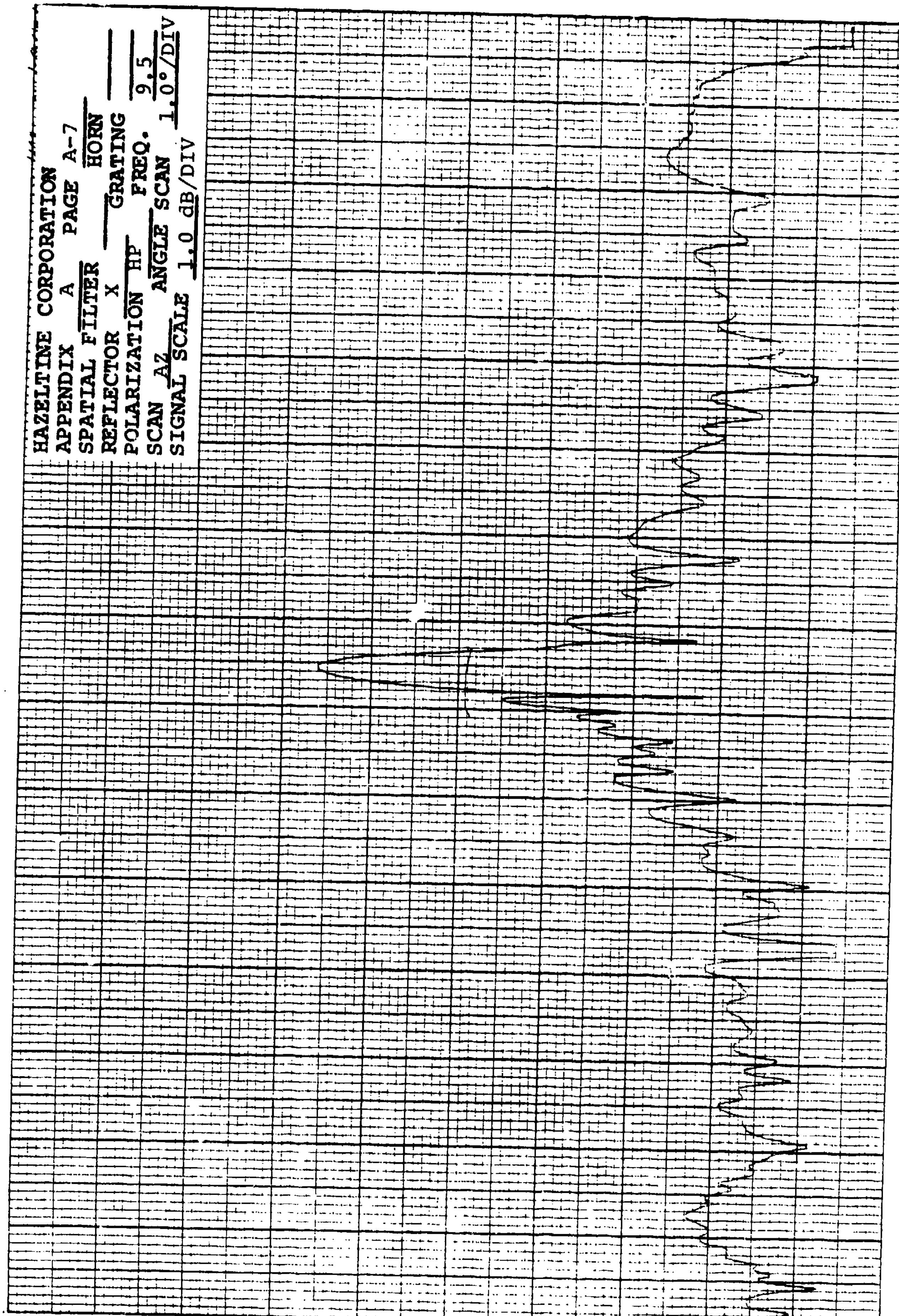
HAZELTINE CORPORATION
APPENDIX A PAGE A-7
SPATIAL FILTER HORN
REFLECTOR X GRATING
POLARIZATION HP FREQ. 9.5
SCAN AZ ANGLE SCAN 1.0°/DIV
SIGNAL SCALE 1.0 dB/DIV

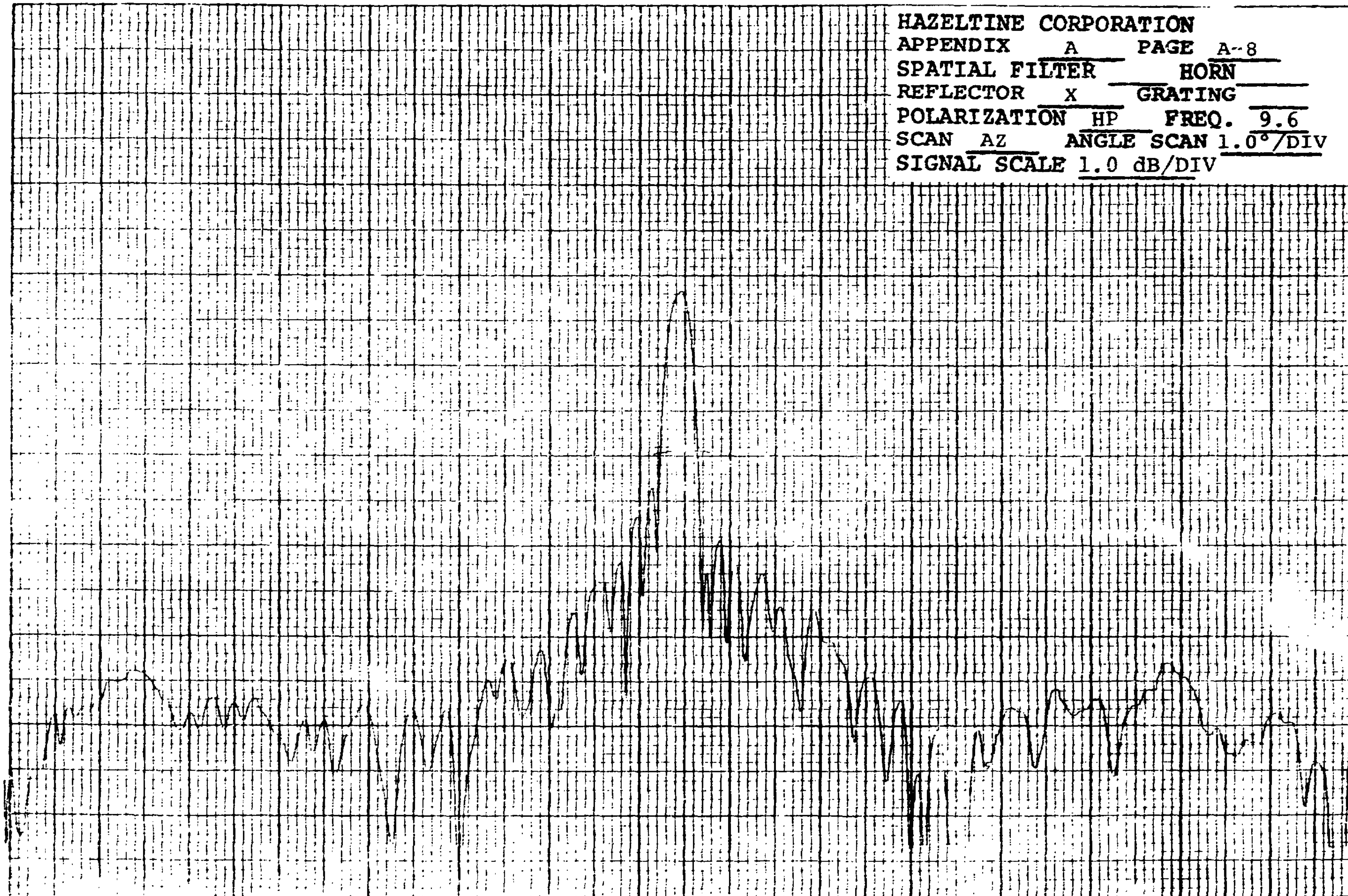
HAZELTINE CORPORATION
APPENDIX A PAGE A-8
SPATIAL FILTER HORN
REFLECTOR X GRATING
POLARIZATION HP FREQ. 9.6
SCAN AZ ANGLE SCAN 1.0°/DIV
SIGNAL SCALE 1.0 dB/DIV

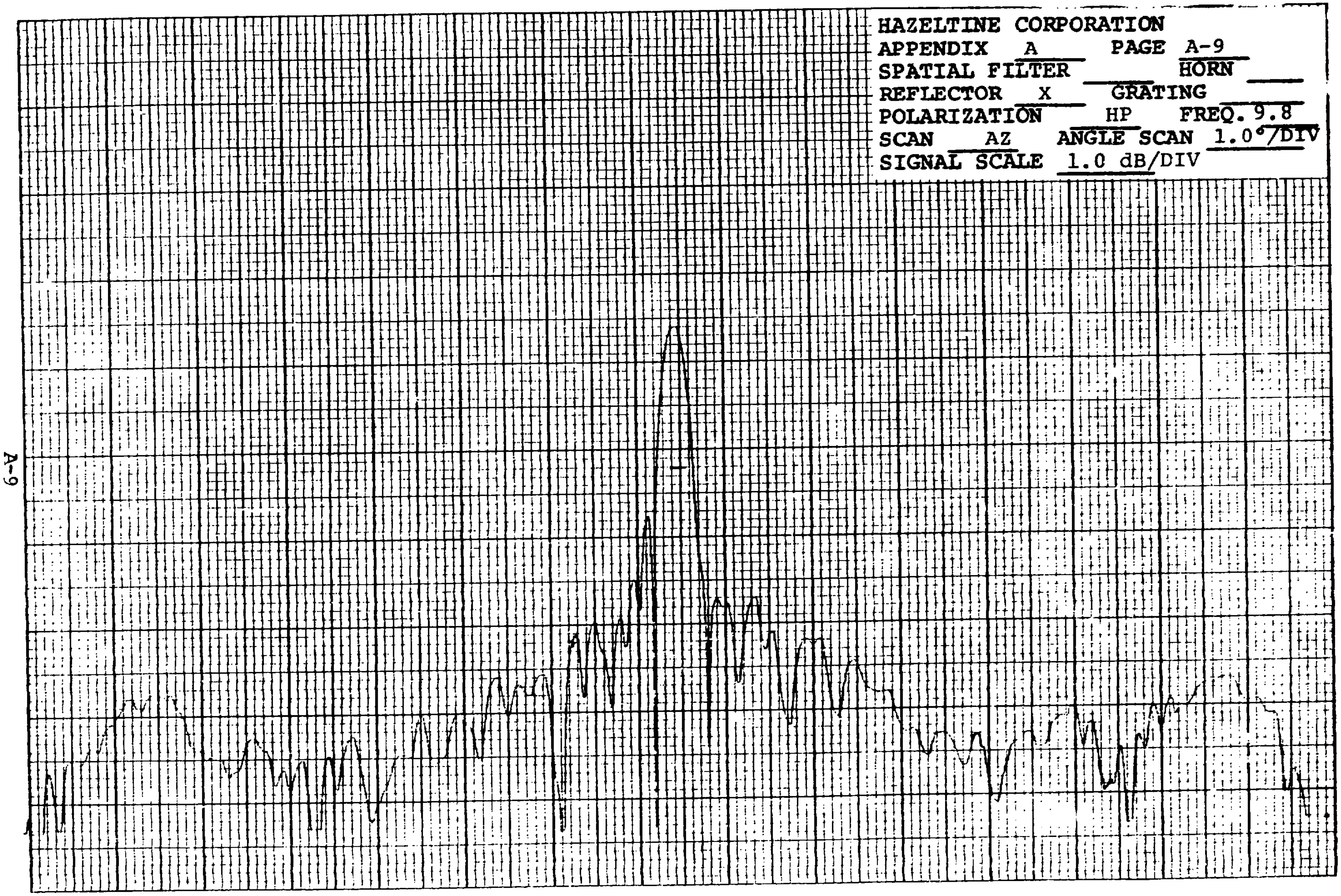
HAZELTINE CORPORATION
APPENDIX A PAGE A-9
SPATIAL FILTER HORN
REFLECTOR X GRATING
POLARIZATION HP FREQ. 9.8
SCAN AZ ANGLE SCAN 1.0°/DIV
SIGNAL SCALE 1.0 dB/DIV

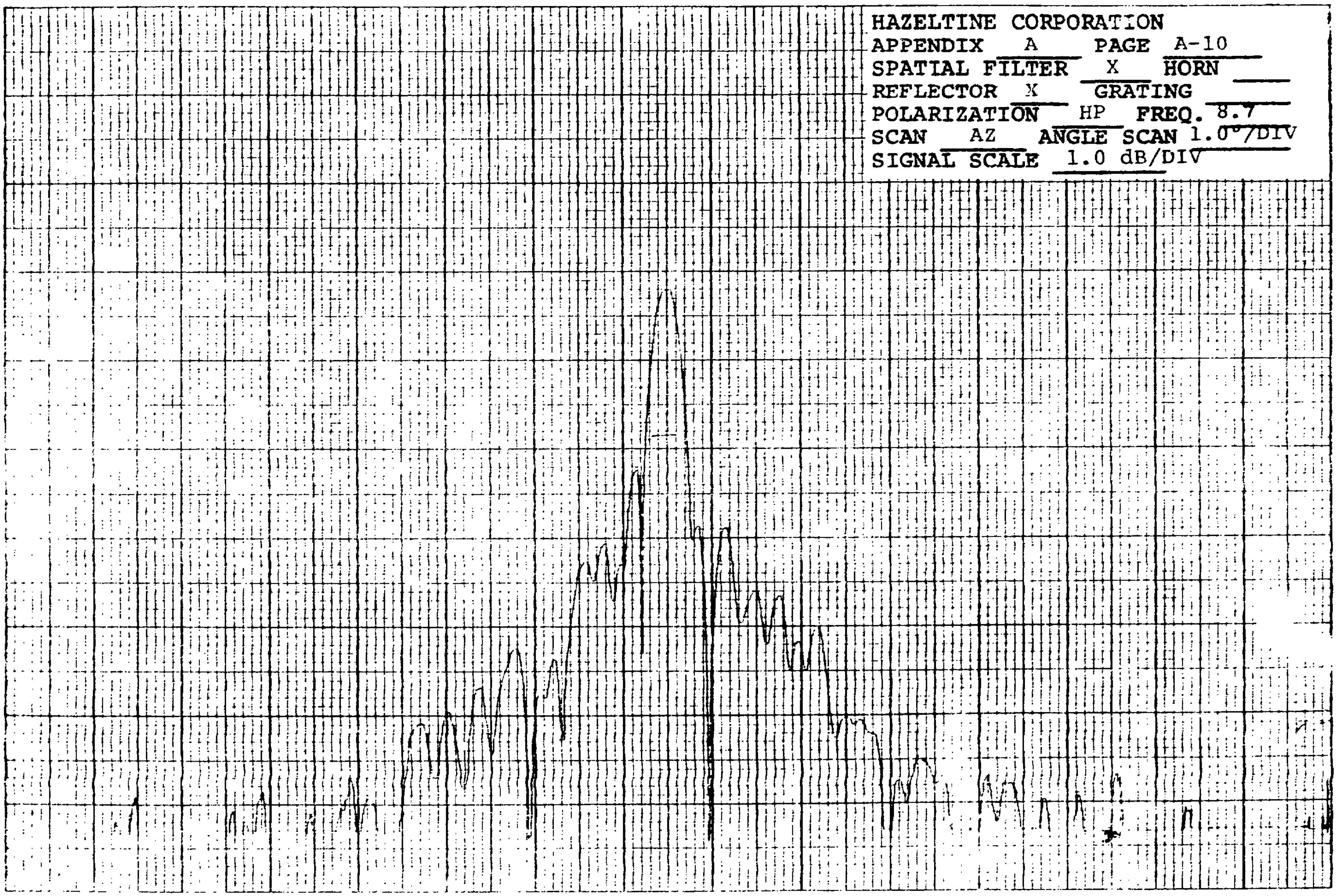
HAZELTINE CORPORATION
APPENDIX A PAGE A-10
SPATIAL FILTER X HORN
REFLECTOR X GRATING
POLARIZATION HP FREQ. 8.7
SCAN AZ ANGLE SCAN 1.0°/DIV
SIGNAL SCALE 1.0 dB/DIV

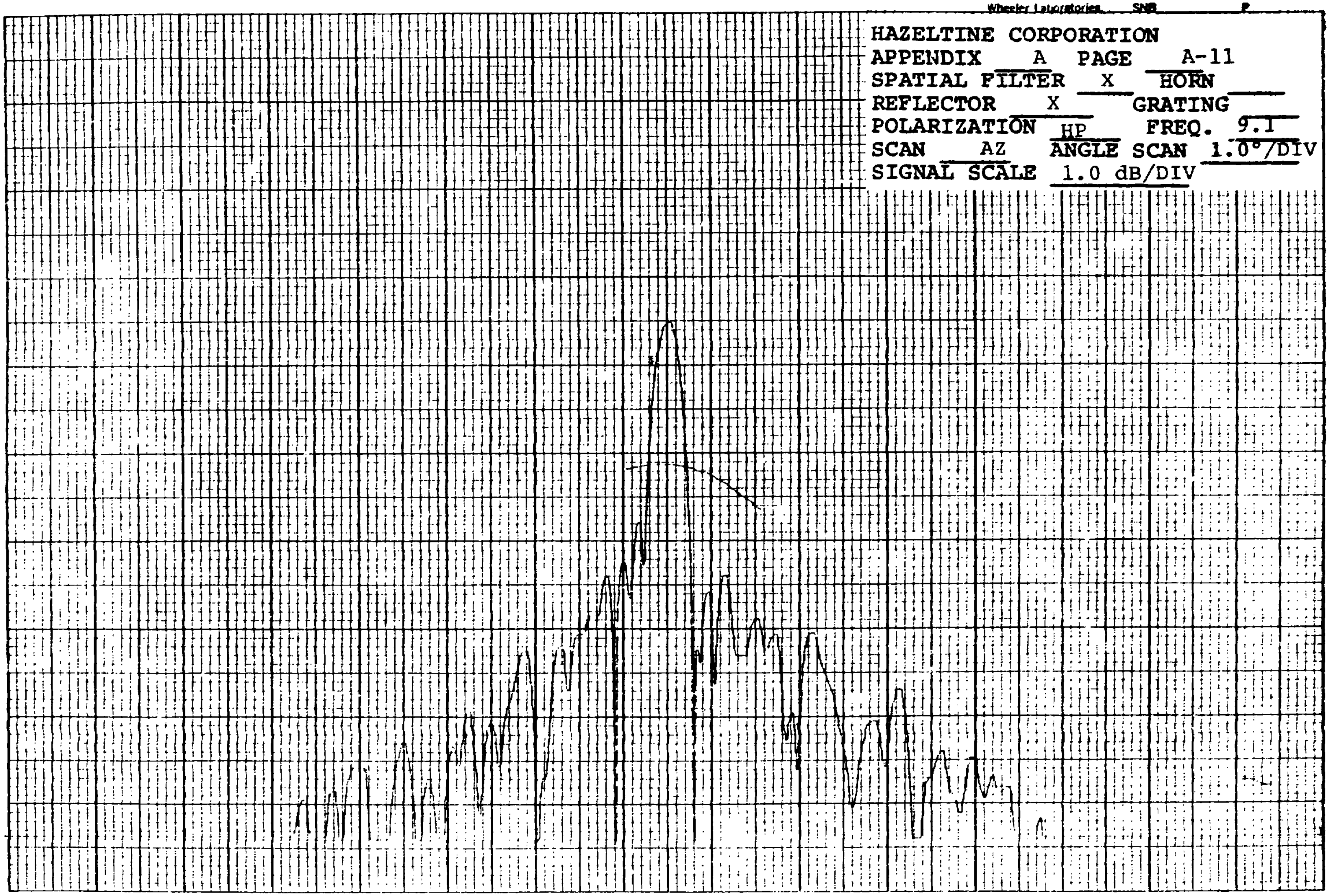
Wheeler Laboratories SNB P
HAZELTINE CORPORATION
APPENDIX A PAGE A-11
SPATIAL FILTER X HORN
REFLECTOR X GRATING
POLARIZATION HP FREQ. 9.1
SCAN AZ ANGLE SCAN 1.0°/DIV
SIGNAL SCALE 1.0 dB/DIV

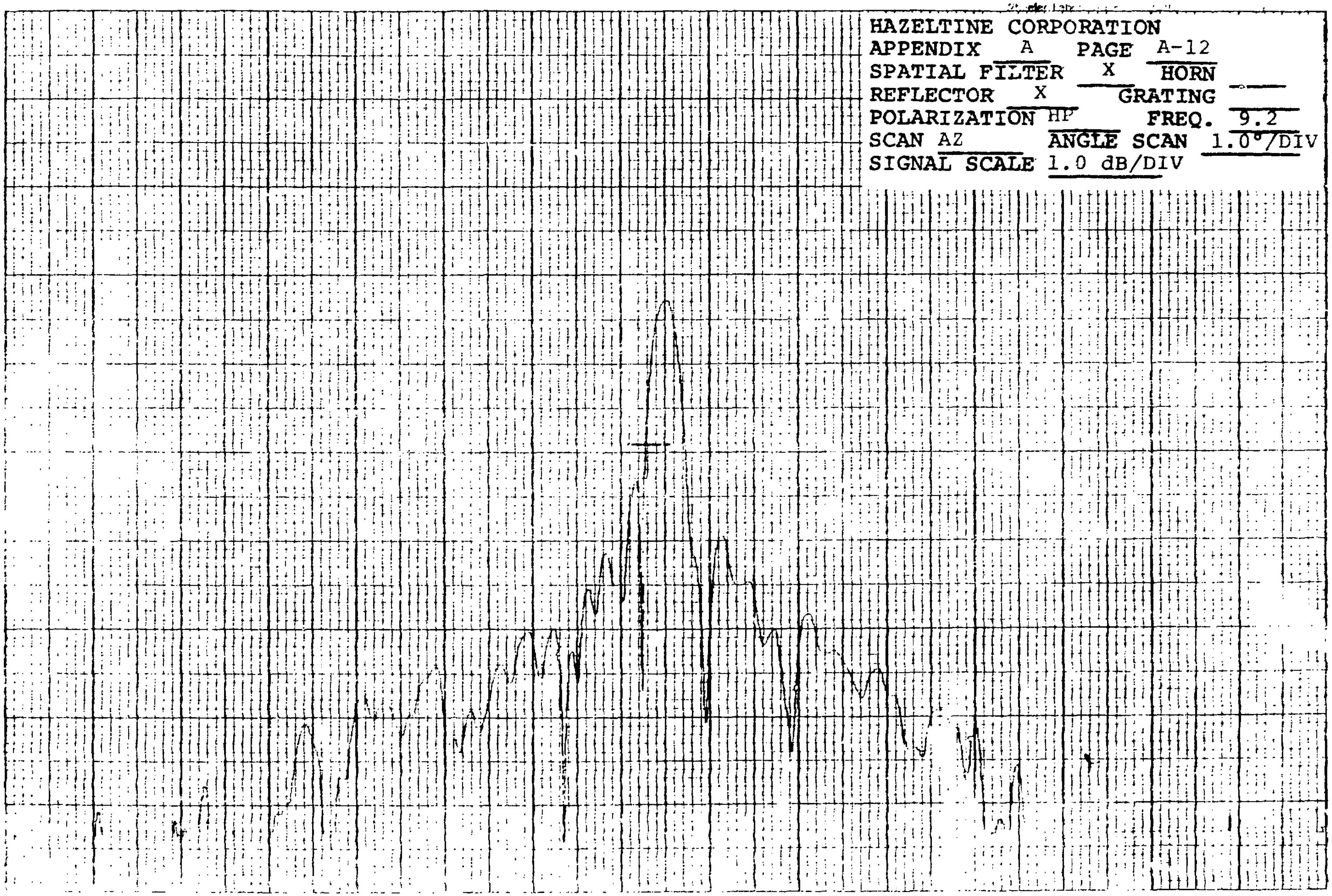
HAZELTINE CORPORATION
APPENDIX A PAGE A-12
SPATIAL FILTER X HORN
REFLECTOR X GRATING
POLARIZATION HP FREQ. 9.2
SCAN AZ ANGLE SCAN 1.0°/DIV
SIGNAL SCALE 1.0 dB/DIV

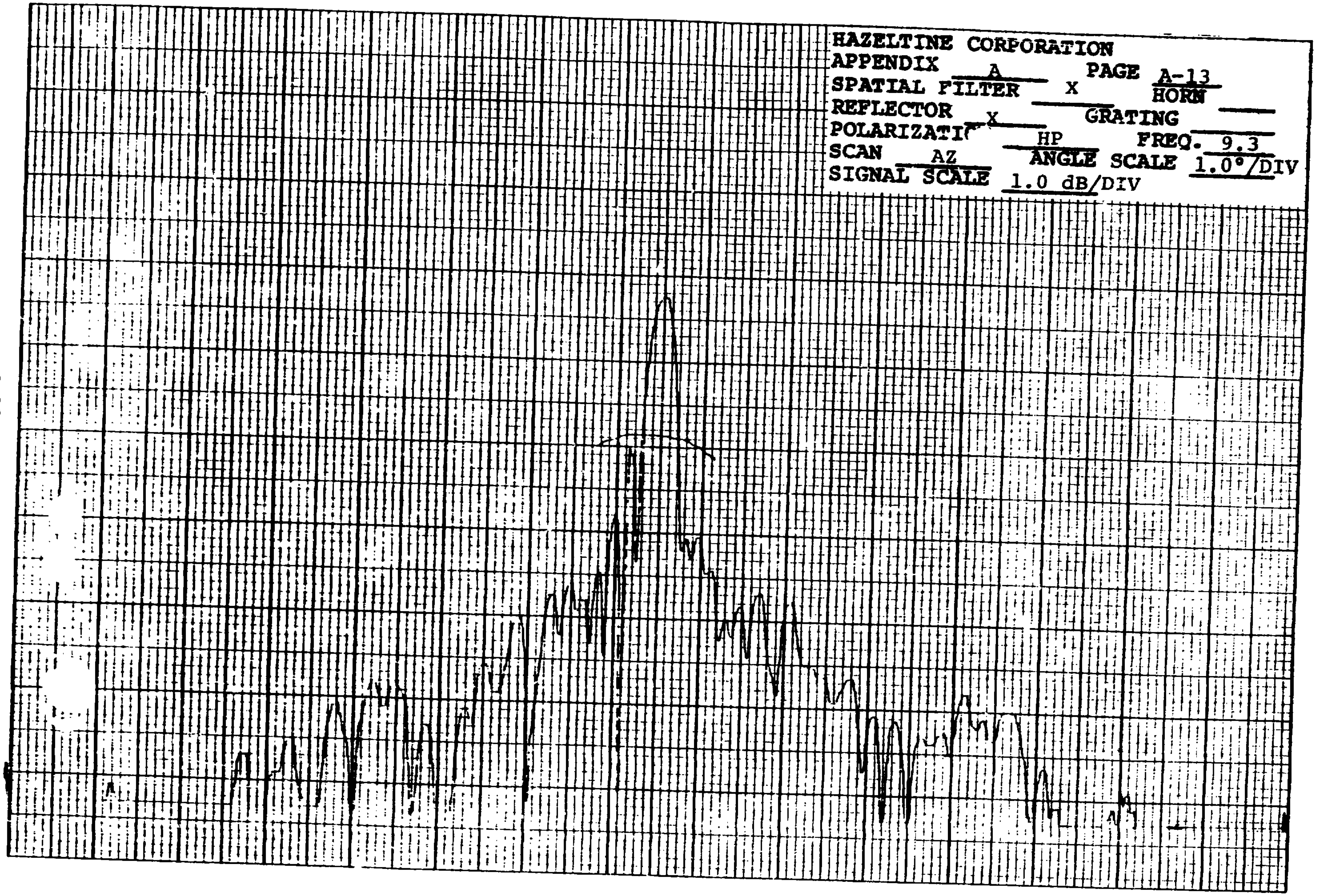
HAZELTINE CORPORATION
APPENDIX A PAGE A-13
SPATIAL FILTER X HORN
REFLECTOR X GRATING
POLARIZATI HP FREQ. 9.3
SCAN AZ ANGLE SCALE 1.0°/DIV
SIGNAL SCALE 1.0 dB/DIV

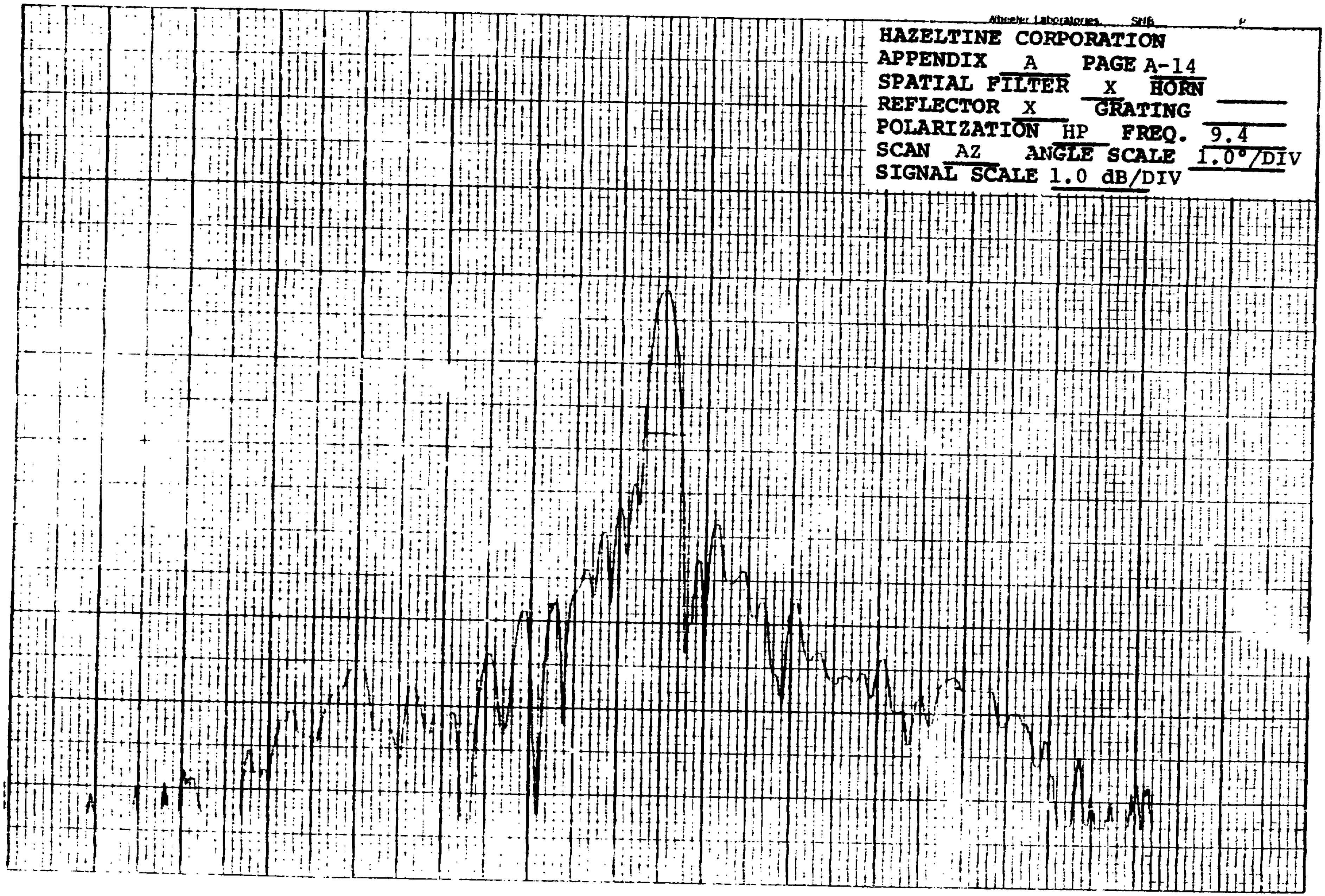
Wheeler Laboratories
HAZELTINE CORPORATION
APPENDIX A PAGE A-14
SPATIAL FILTER X HORN
REFLECTOR X GRATING
POLARIZATION HP FREQ. 9.4
SCAN AZ ANGLE SCALE 1.0°/DIV
SIGNAL SCALE 1.0 dB/DIV

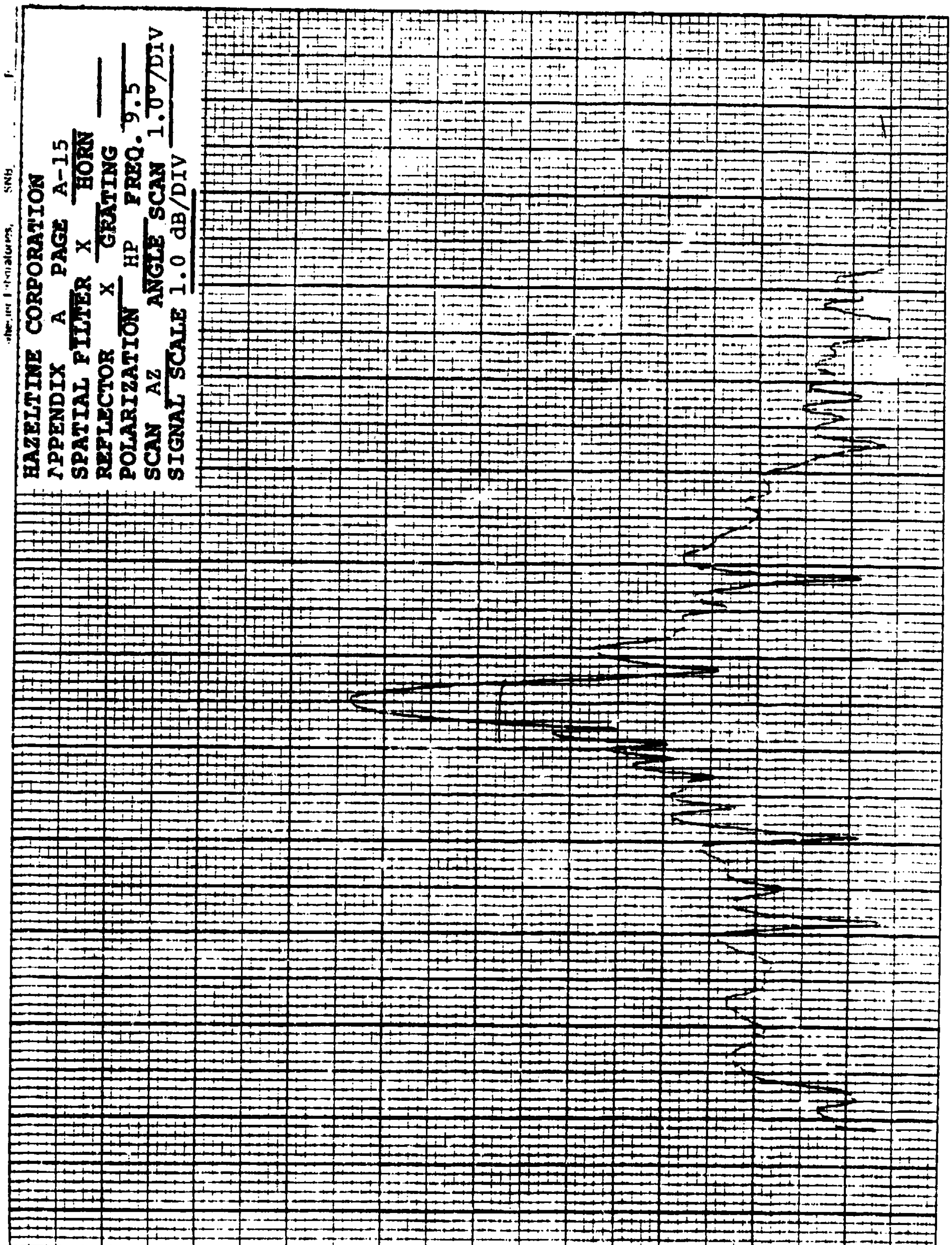
HAZELTINE CORPORATION
APPENDIX A PAGE A-15
SPATIAL FILTER X HORN
REFLECTOR X GRATING
POLARIZATION HP FREQ. 9.5
SCAN AZ ANGLE SCAN 1.0°/DIV
SIGNAL SCALE 1.0 dB/DIV

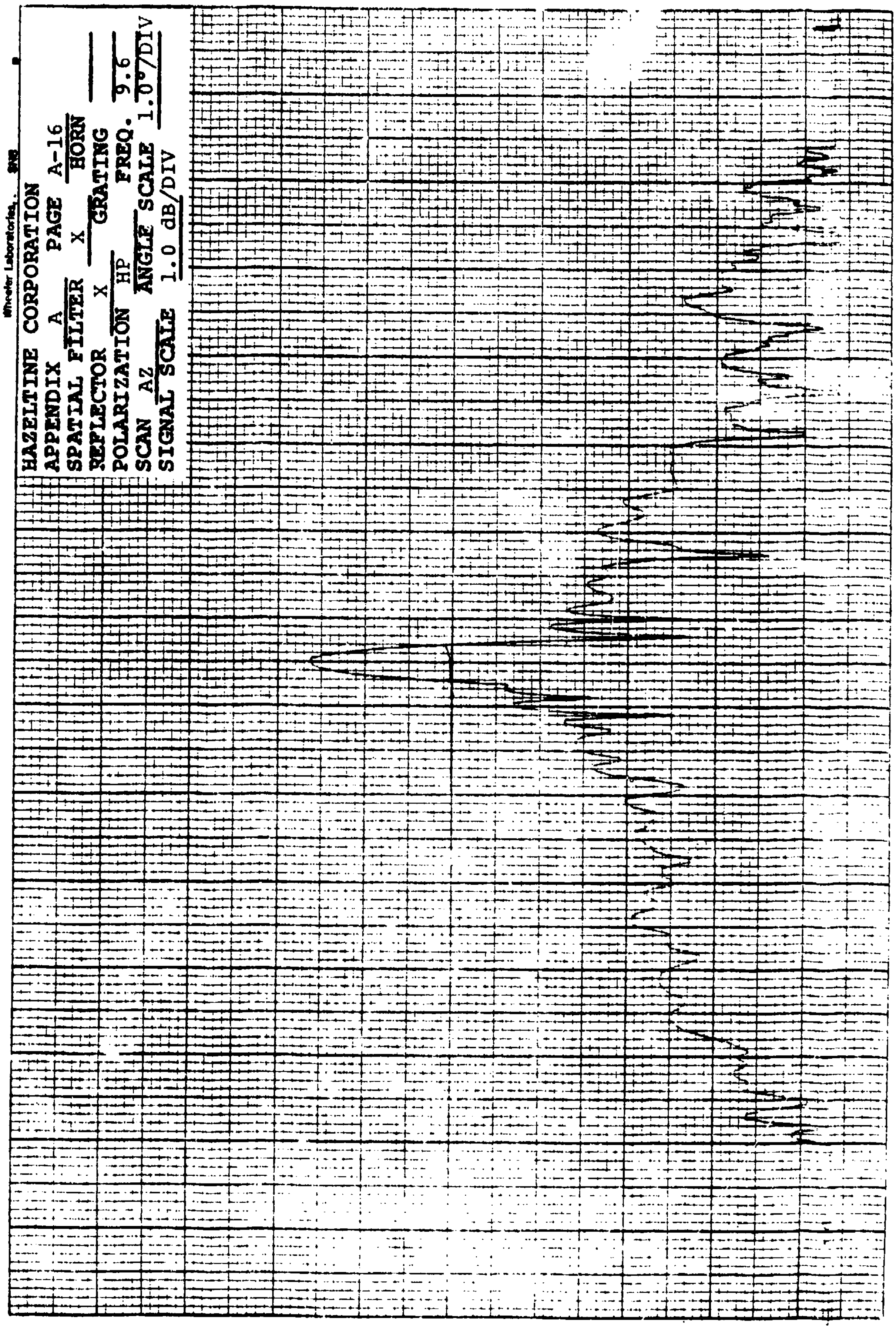
Wheeler Laboratories
HAZELTINE CORPORATION
APPENDIX A PAGE A-16
SPATIAL FILTER X HORN
REFLECTOR X GRATING
POLARIZATION HP FREQ. 9.6
SCAN AZ ANGLE SCALE 1.0°/DIV
SIGNAL SCALE 1.0 dB/DIV

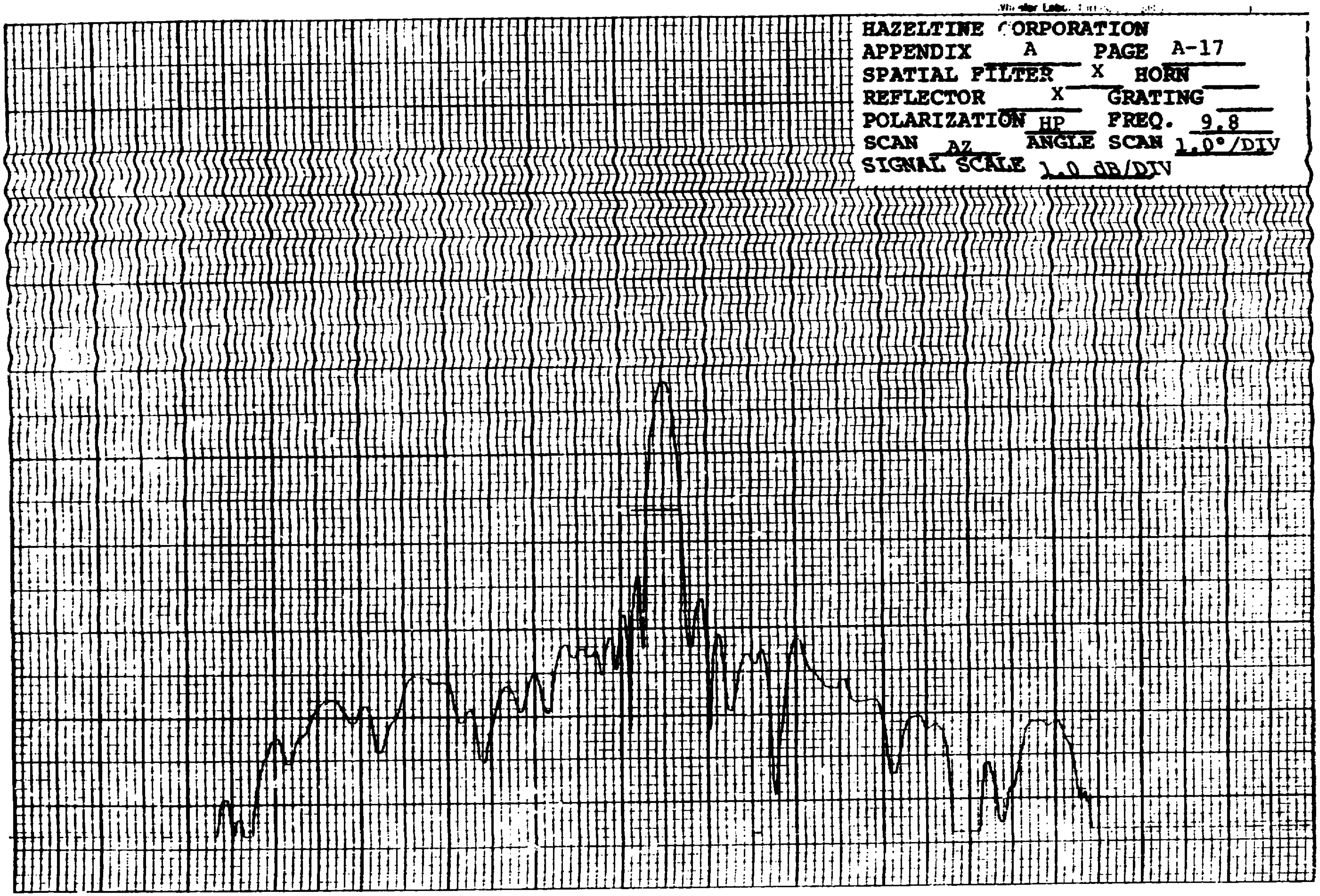
HAZELTINE CORPORATION
APPENDIX A PAGE A-17
SPATIAL FILTER X HORN
REFLECTOR X GRATING
POLARIZATION HP FREQ. 9.8
SCAN AZ ANGLE SCAN 1.0°/DIV
SIGNAL SCALE 1.0 dB/DIV

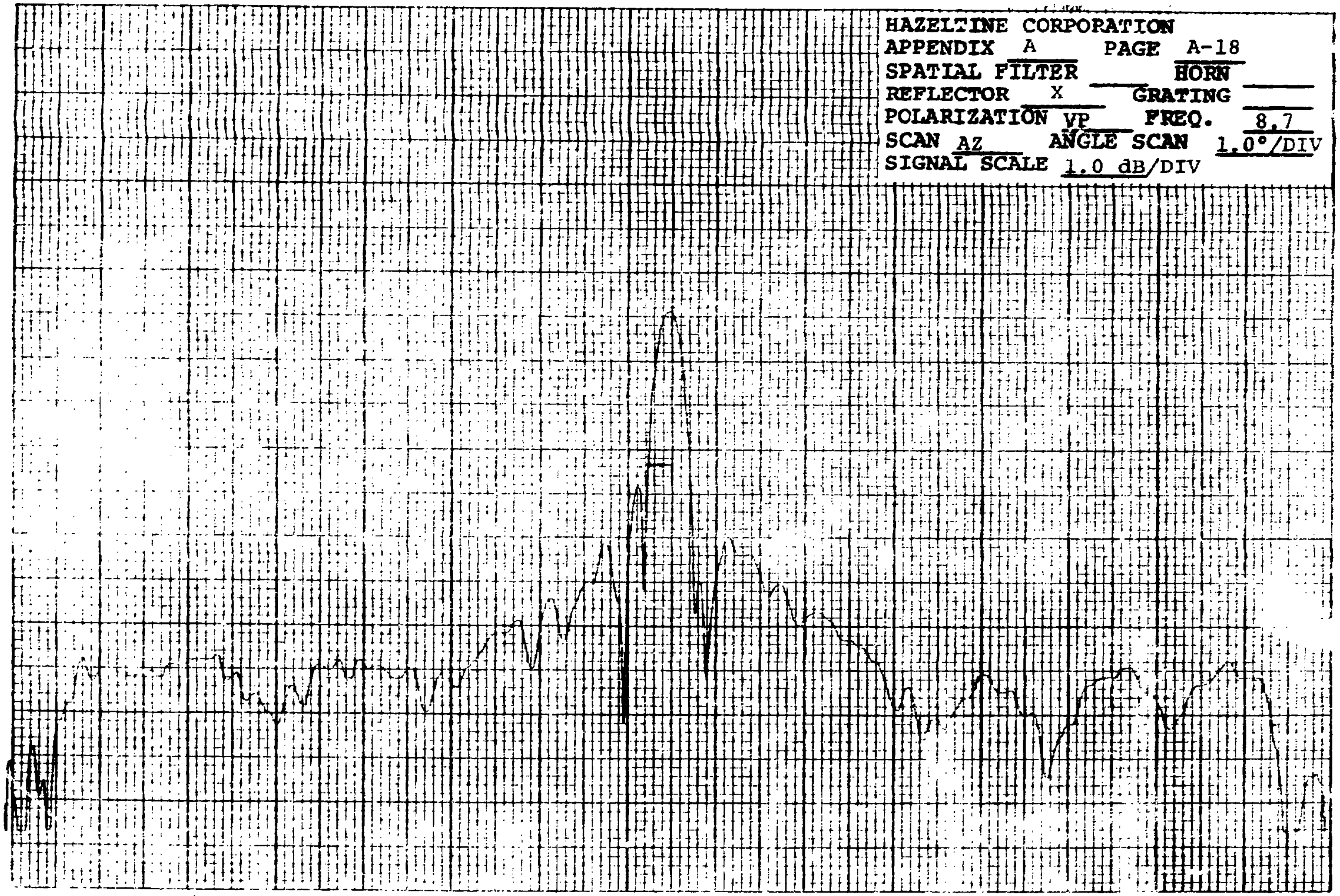
HAZELTINE CORPORATION
APPENDIX A PAGE A-18
SPATIAL FILTER HORN
REFLECTOR X GRATING
POLARIZATION VP FREQ. 8.7
SCAN AZ ANGLE SCAN 1.0°/DIV
SIGNAL SCALE 1.0 dB/DIV

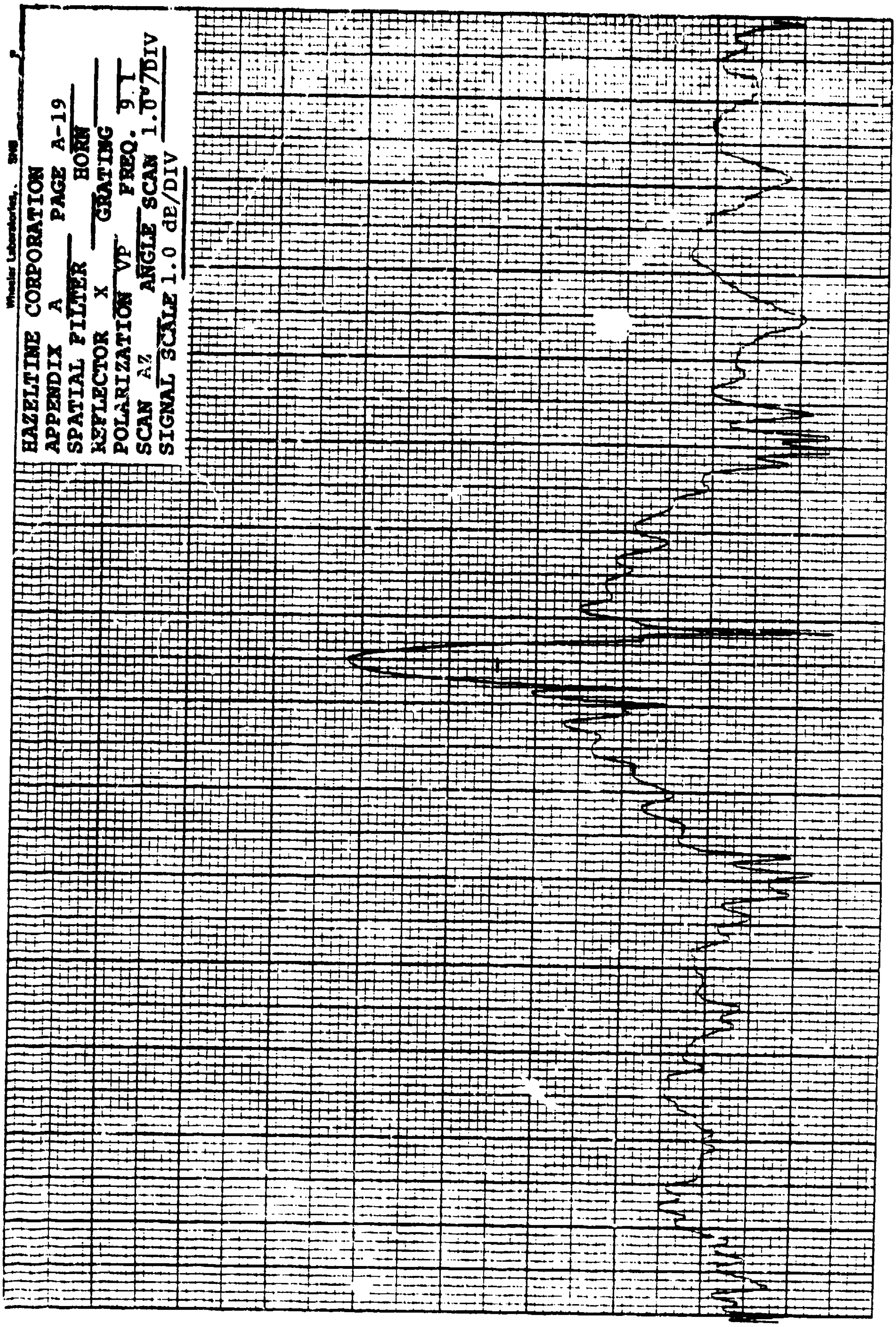
HAZELTINE CORPORATION
APPENDIX A PAGE A-19
SPATIAL FILTER HORN
REFLECTOR X GRATING
POLARIZATION VP FREQ. 9.1
SCAN AZ ANGLE SCAN 1.0°/DIV
SIGNAL SCALE 1.0 dB/DIV

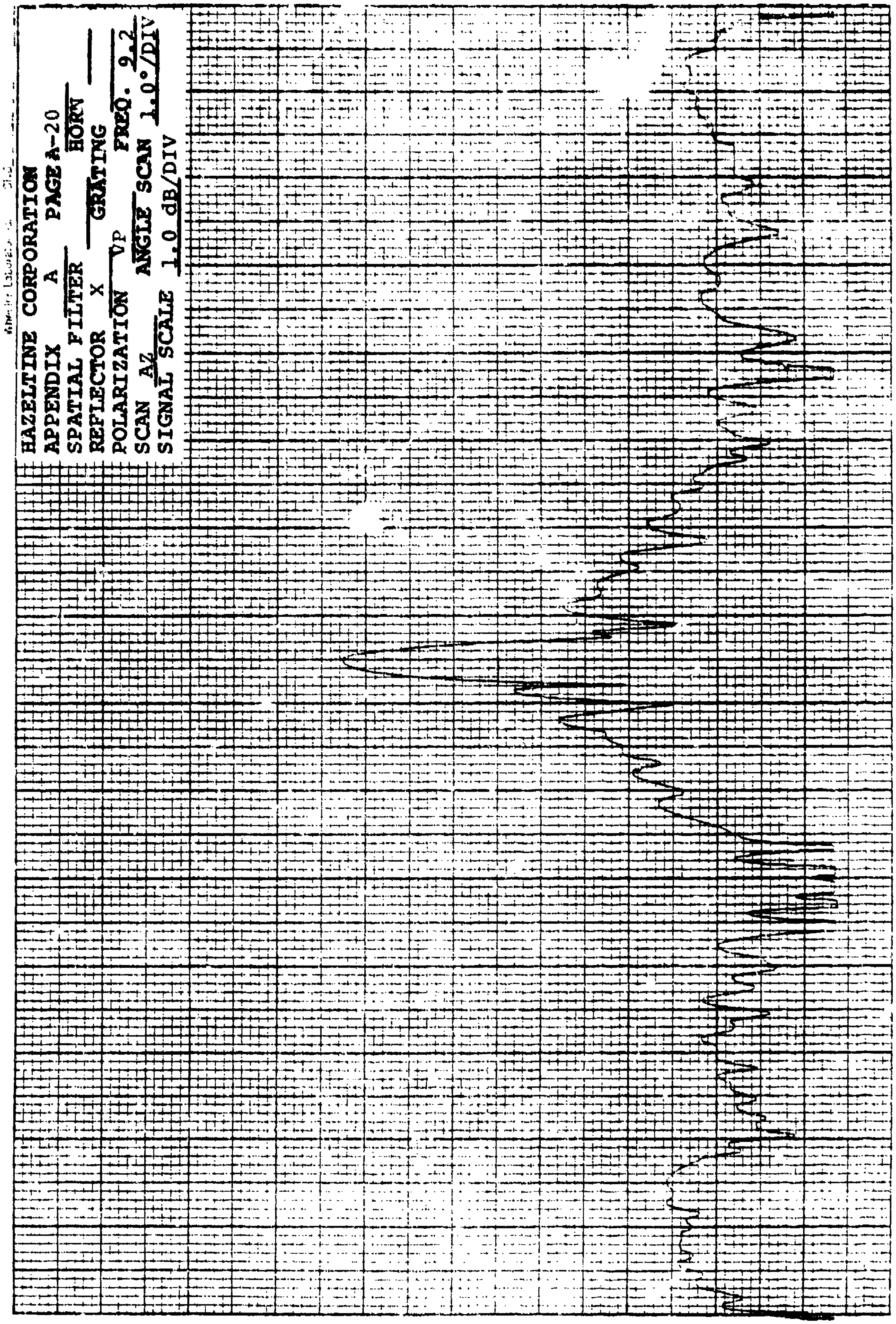
HAZELTINE CORPORATION
APPENDIX A PAGE A-20
SPATIAL FILTER HORN
REFLECTOR X GRATING
POLARIZATION VP FREQ. 9.2
SCAN AZ ANGLE SCAN 1.0°/DIV
SIGNAL SCALE 1.0 dB/DIV

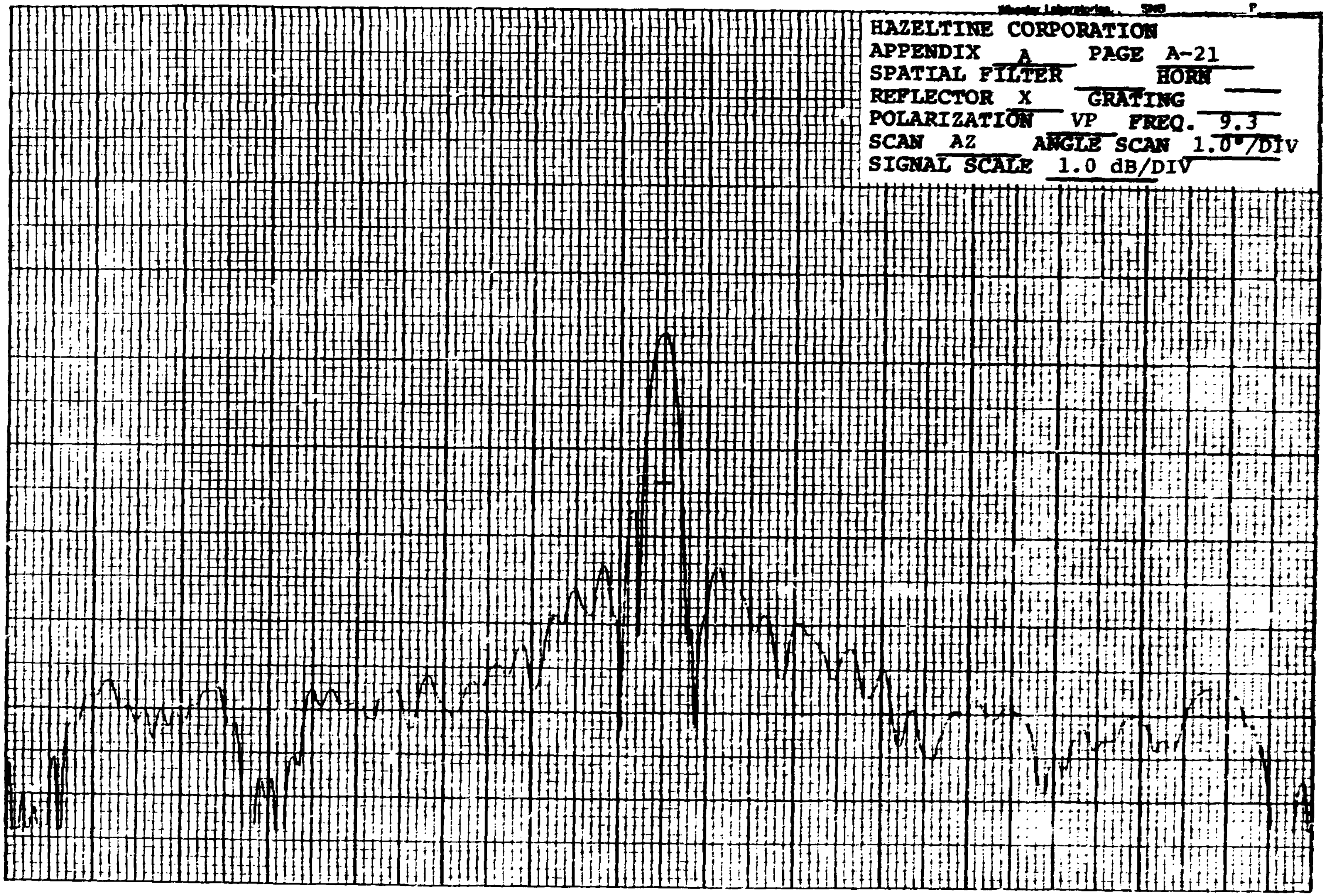
HAZELTINE CORPORATION
APPENDIX A PAGE A-21
SPATIAL FILTER HORN
REFLECTOR X GRATING
POLARIZATION VP FREQ. 9.3
SCAN AZ ANGLE SCAN 1.0°/DIV
SIGNAL SCALE 1.0 dB/DIV

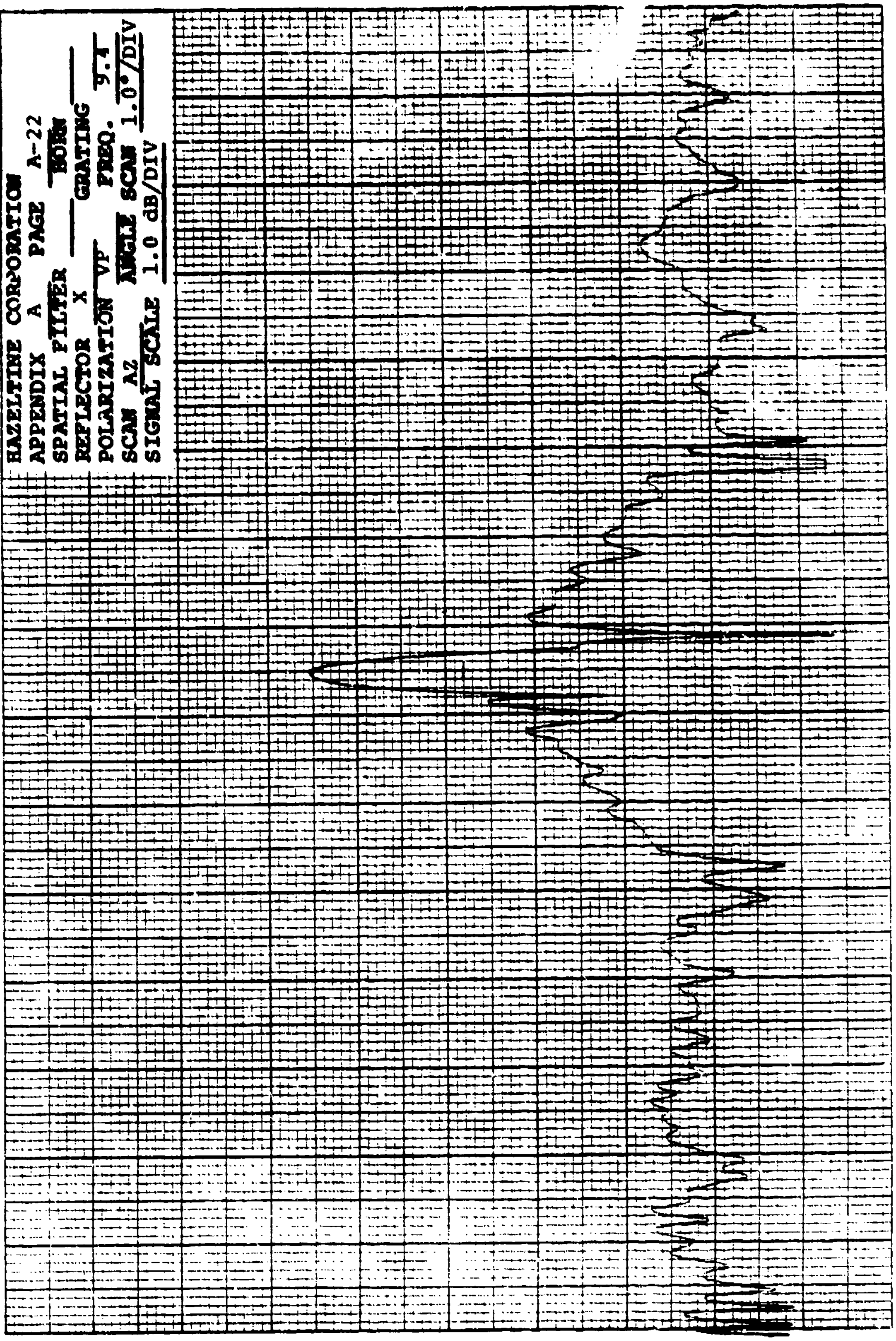
Wheeler Laboratories
HAZELTINE CORPORATION
APPENDIX A PAGE A-22
SPATIAL FILTER HORN
REFLECTOR X GRATING
POLARIZATION VP FREQ. 9.4
SCAN AZ ANGLE SCAN 1.0°/DIV
SIGNAL SCALE 1.0 dB/DIV

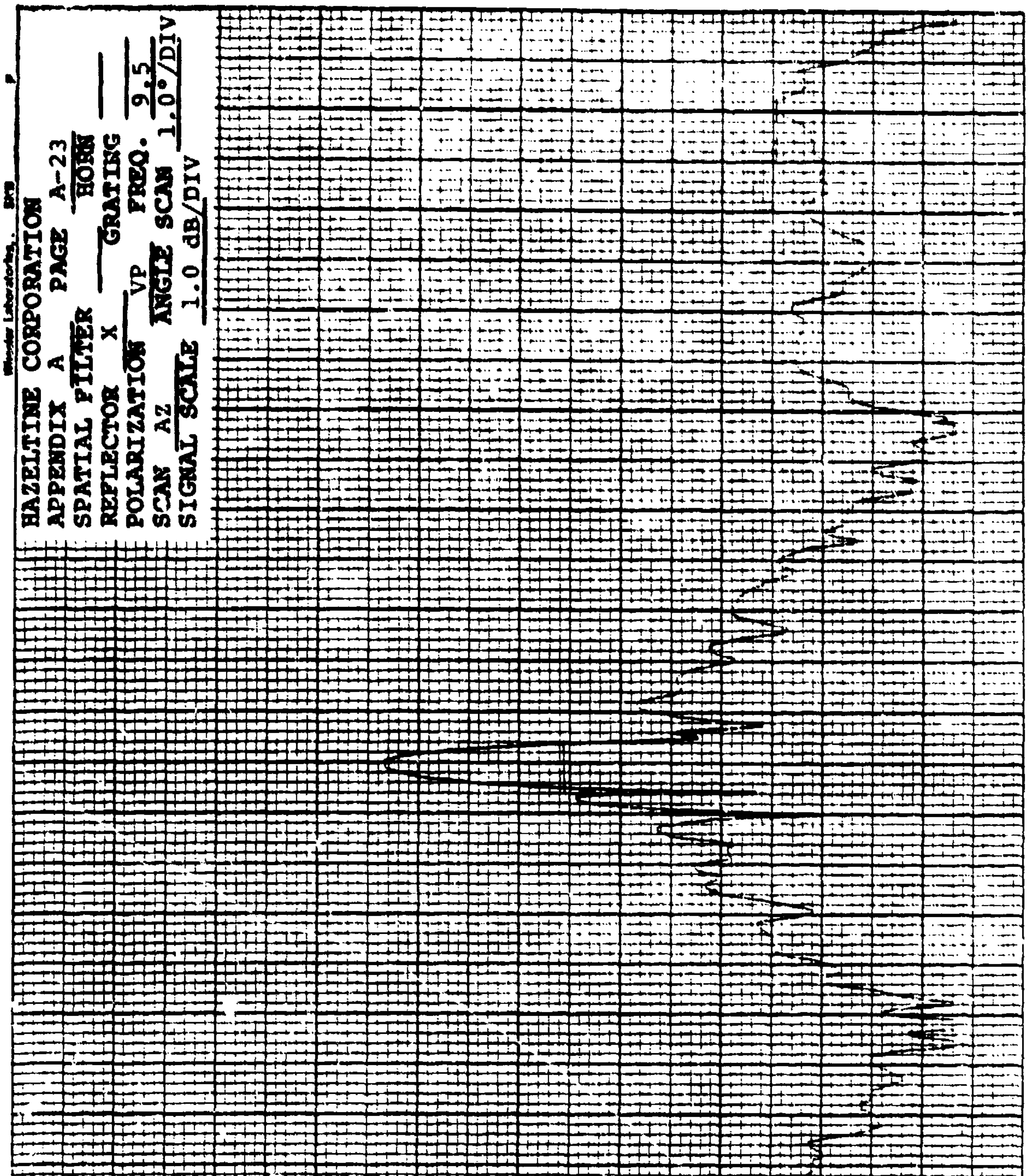
HAZELTINE CORPORATION
APPENDIX A PAGE A-23
SPATIAL FILTER HORN
REFLECTOR X GRATING
POLARIZATION VP FREQ. 9.5
SCAN AZ ANGLE SCAN 1.0°/DIV
SIGNAL SCALE 1.0 dB/DIV

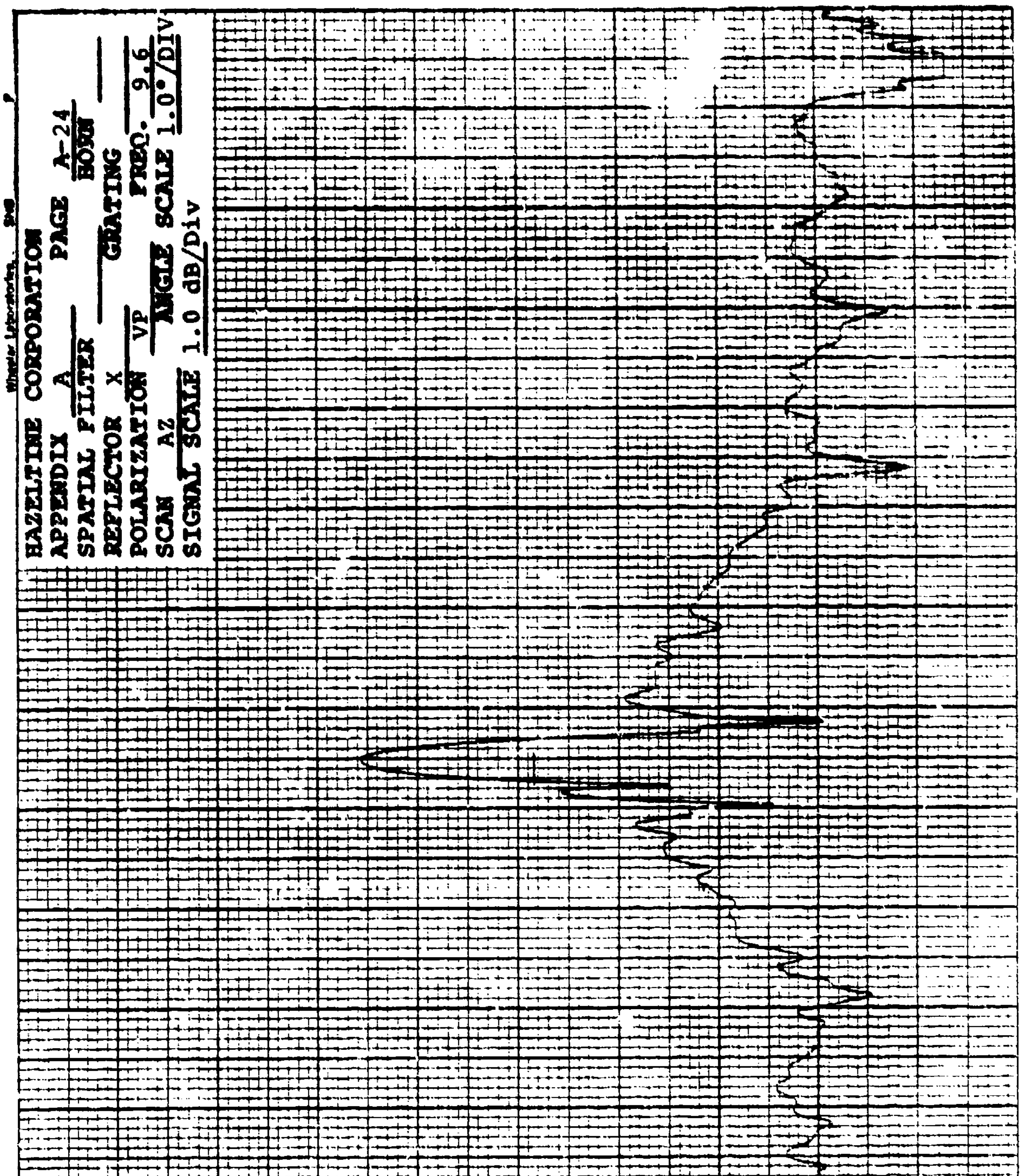
HAZELTINE CORPORATION
APPENDIX A PAGE A-24
SPATIAL FILTER HORN
REFLECTOR X GRATING
POLARIZATION VP FREQ. 9.6
SCAN AZ ANGLE SCALE 1.0°/DIV
SIGNAL SCALE 1.0 dB/Div

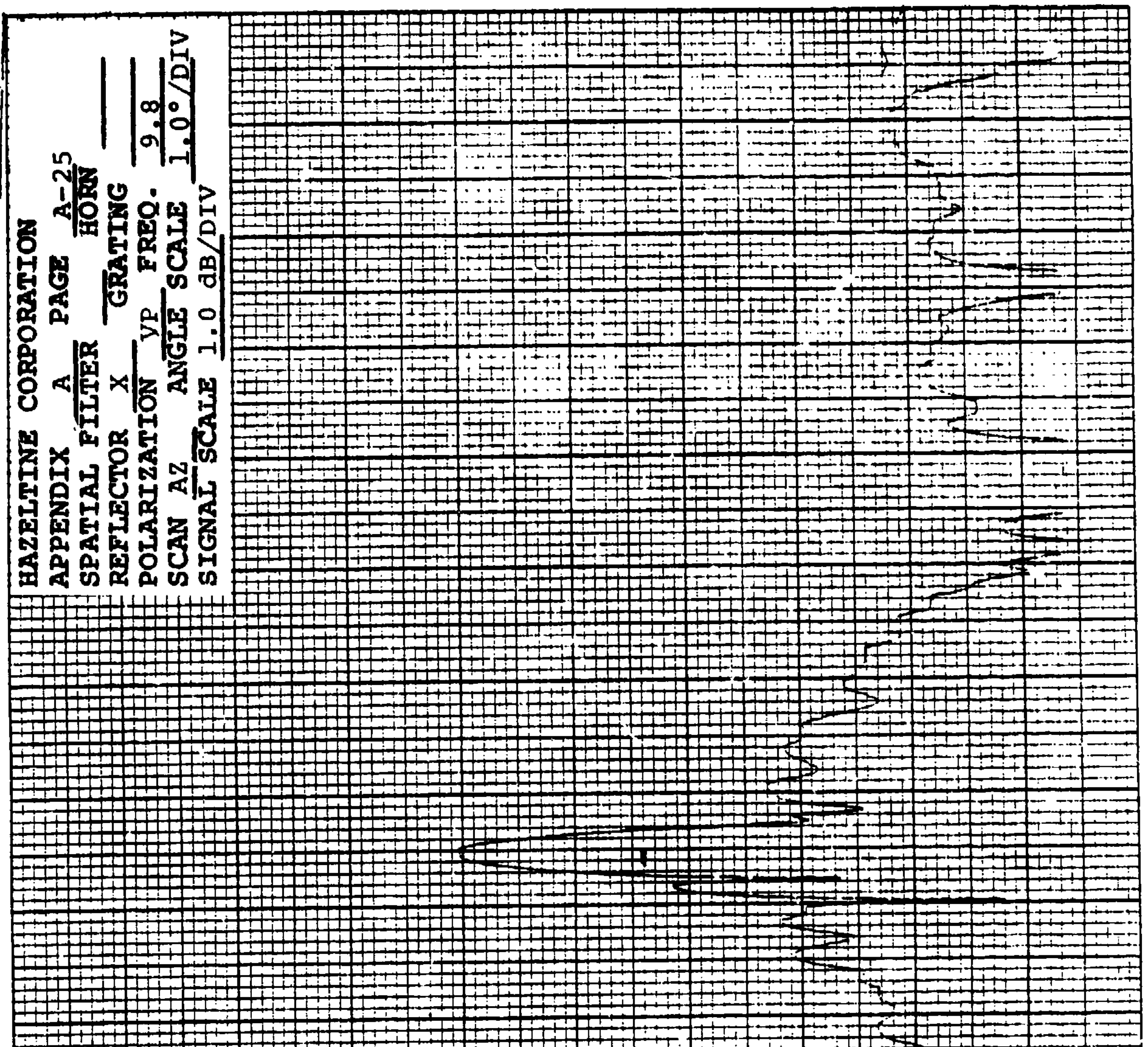
Wheeler Laboratories, . SNB P
HAZELTINE CORPORATION
APPENDIX A PAGE A-25
SPATIAL FILTER HORN
REFLECTOR X GRATING
POLARIZATION VP FREQ. 9.8
SCAN AZ ANGLE SCALE 1.0°/DIV
SIGNAL SCALE 1.0 dB/DIV

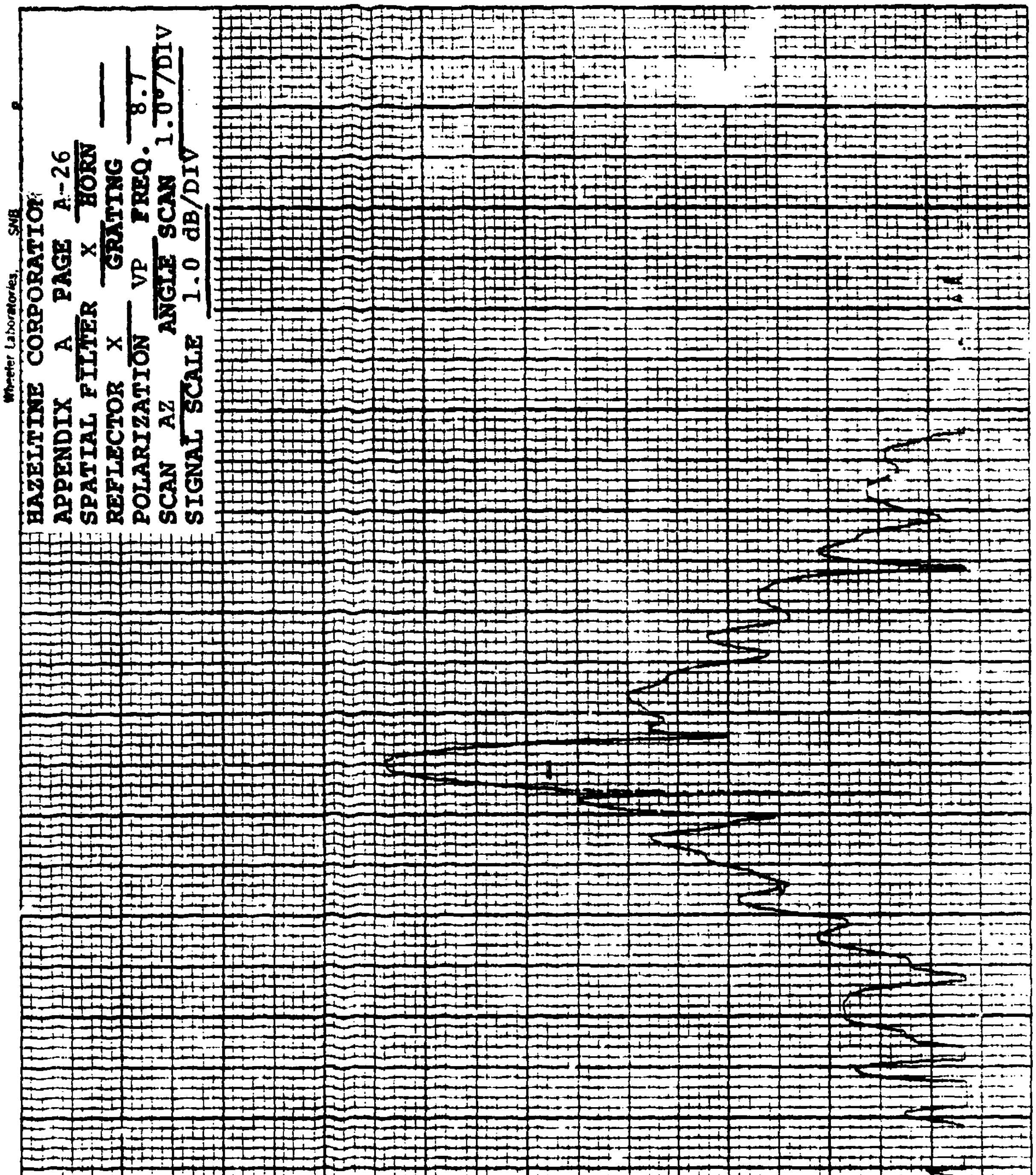
Wheeler Laboratories, SNB
HAZELTINE CORPORATION
APPENDIX A PAGE A-26
SPATIAL FILTER X HORN
REFLECTOR X GRATING
POLARIZATION VP FREQ. 8.7
SCAN AZ ANGLE SCAN 1.0°/DIV
SIGNAL SCALE 1.0 dB/DIV

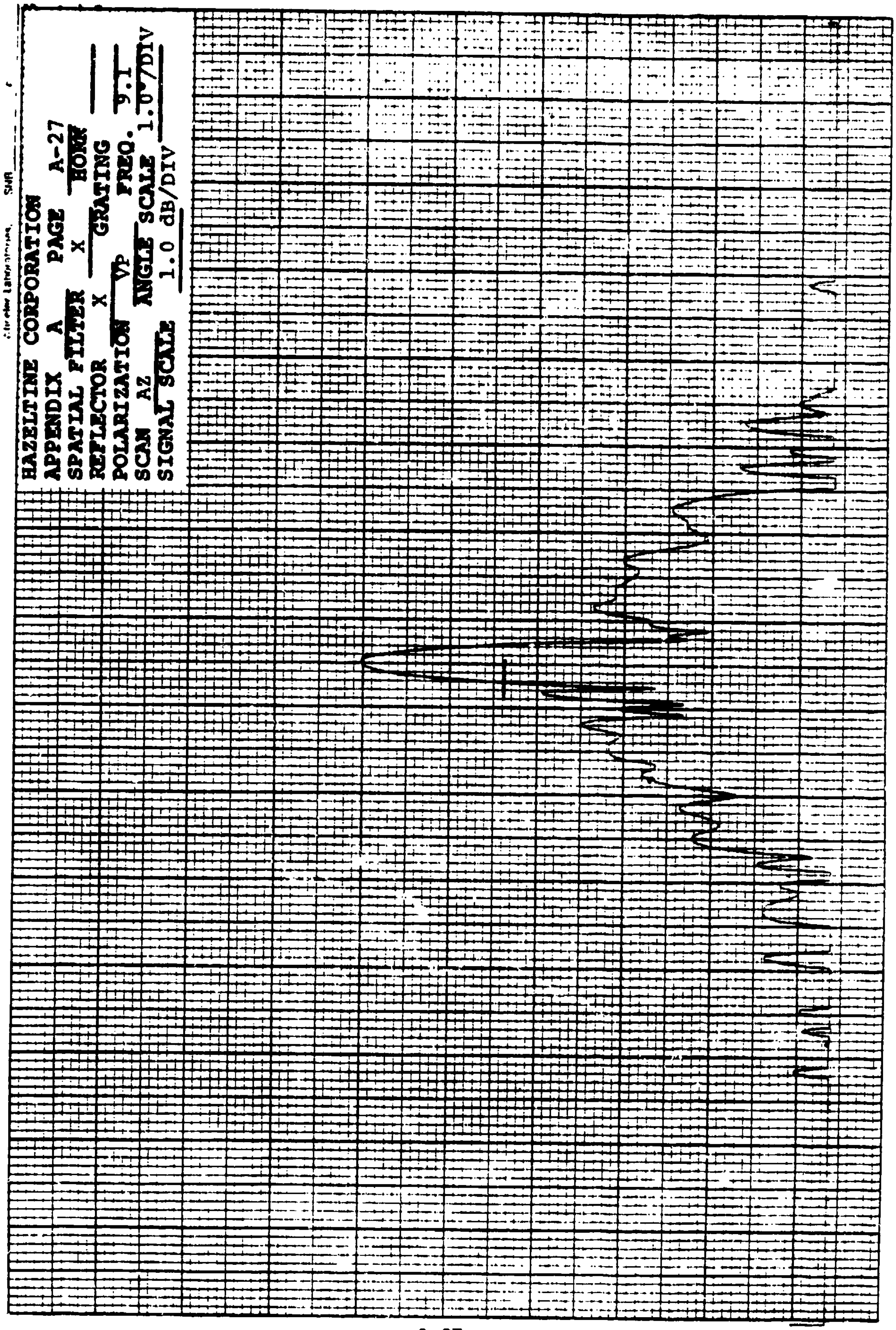
HAZELTINE CORPORATION
APPENDIX A PAGE A-27
SPATIAL FILTER X HORN
REFLECTOR X GRATING
POLARIZATION VP FREQ. 9.1
SCAN AZ ANGLE SCALE 1.0°/DIV
SIGNAL SCALE 1.0 dB/DIV

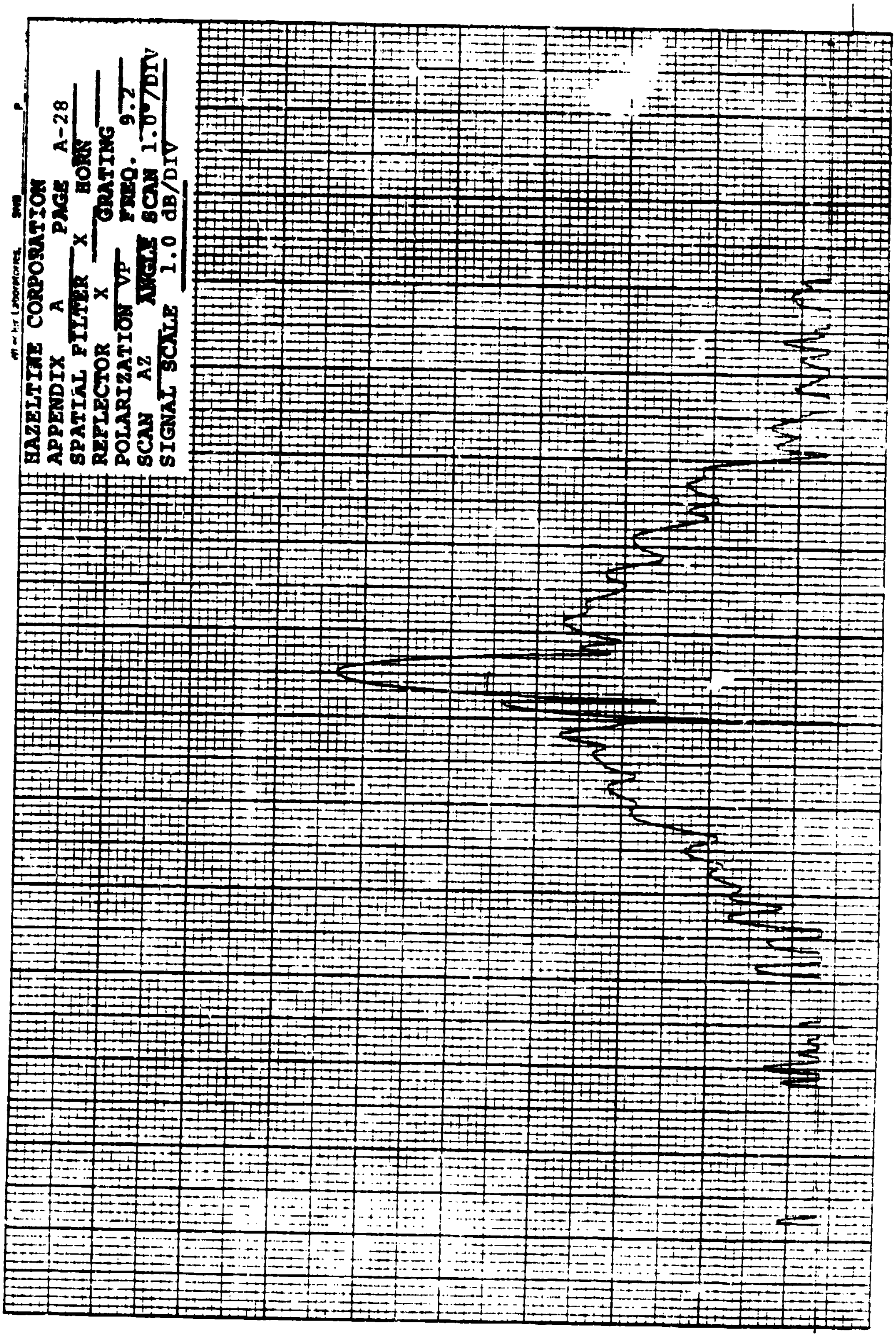
HAZELTINE CORPORATION
APPENDIX A PAGE A-28
SPATIAL FILTER X HORN
REFLECTOR X GRATING
POLARIZATION VP FREQ. 9.2
SCAN AZ ANGLE SCAN 1.0°/DIV
SIGNAL SCALE 1.0 dB/DIV

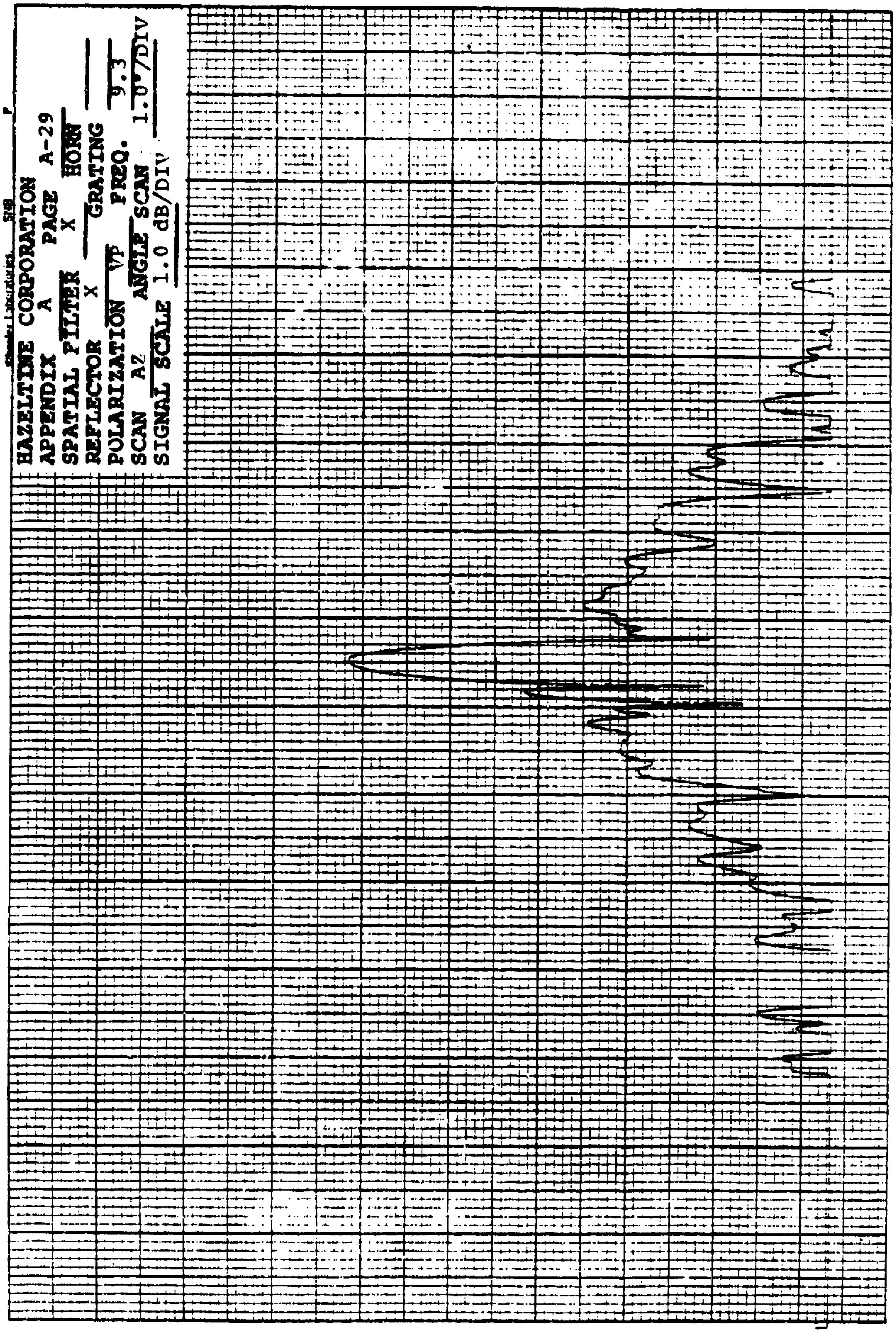
HAZELTINE CORPORATION
APPENDIX A PAGE A-29
SPATIAL FILTER X HORN
REFLECTOR X GRATING
POLARIZATION VP FREQ. 9.3
SCAN AZ ANGLE SCAN 1.0°/DIV
SIGNAL SCALE 1.0 dB/DIV

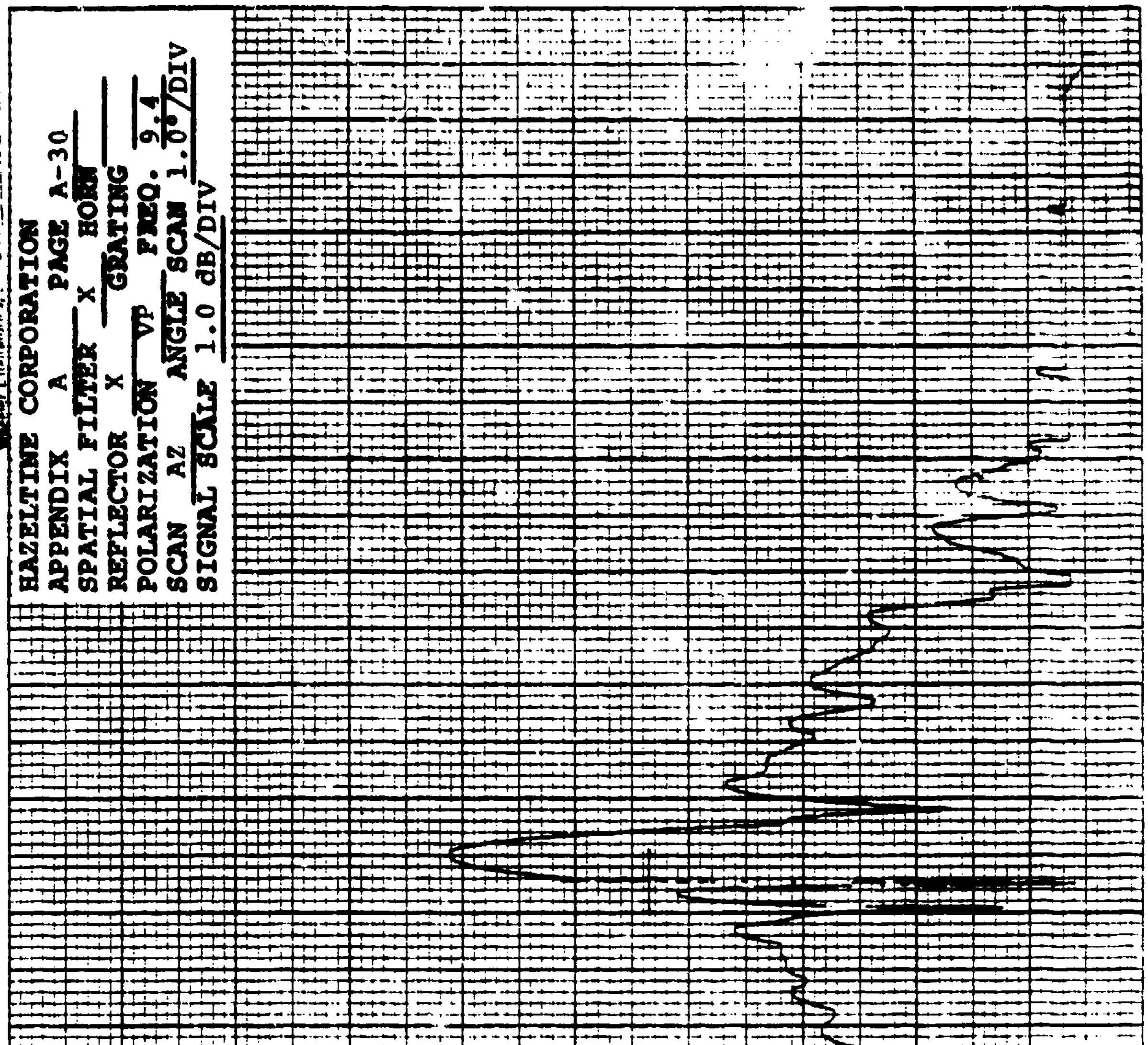
HAZELTINE CORPORATION
APPENDIX A PAGE A-30
SPATIAL FILTER X HORN
REFLECTOR X GRATING
POLARIZATION VP FREQ. 9.4
SCAN AZ ANGLE SCAN 1.0°/DIV
SIGNAL SCALE 1.0 dB/DIV

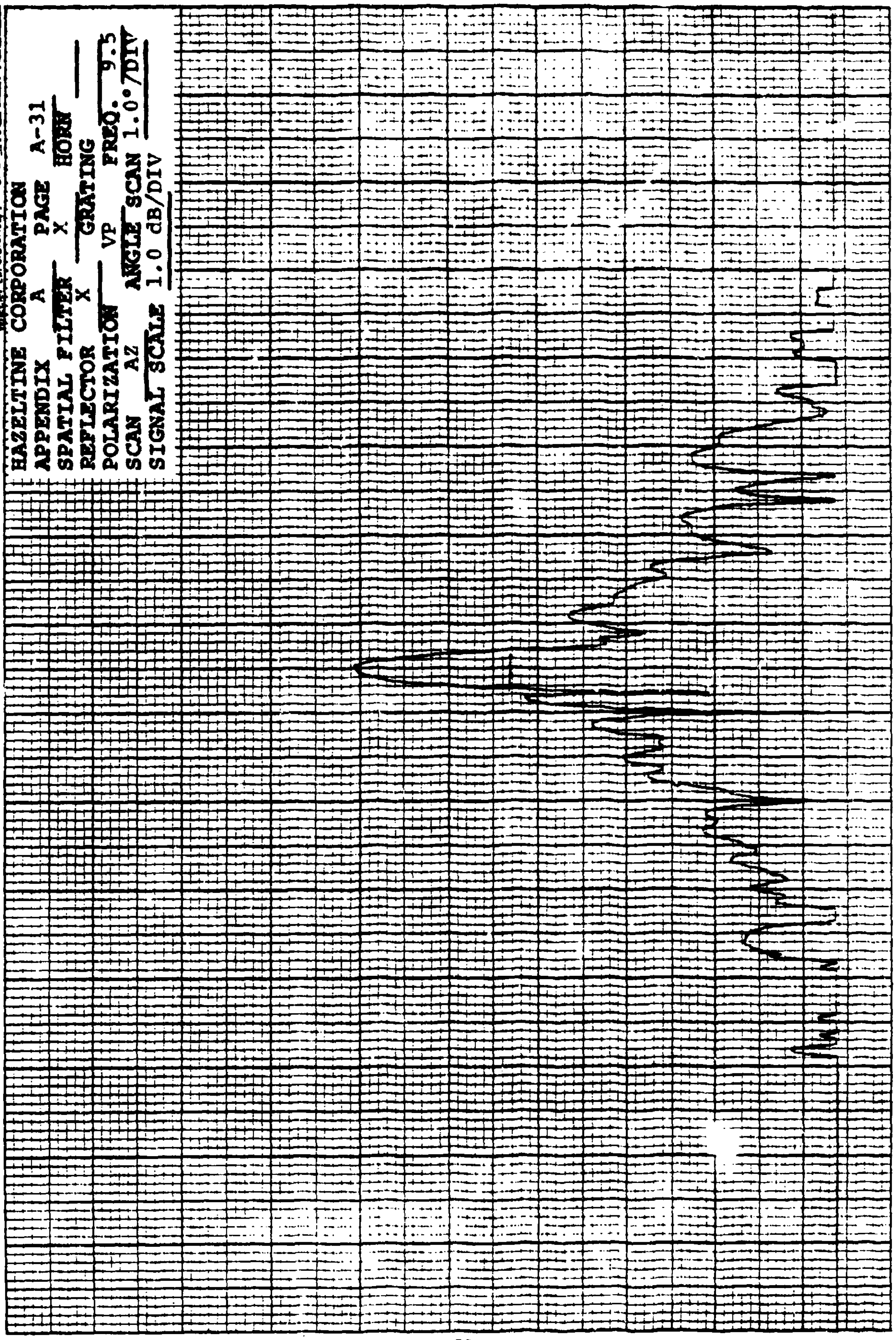
HAZELTINE CORPORATION
APPENDIX A PAGE A-31
SPATIAL FILTER X HORN
REFLECTOR X GRATING
POLARIZATION VP FREQ. 9.5
SCAN AZ ANGLE SCAN 1.0°/DIV
SIGNAL SCALE 1.0 dB/DIV

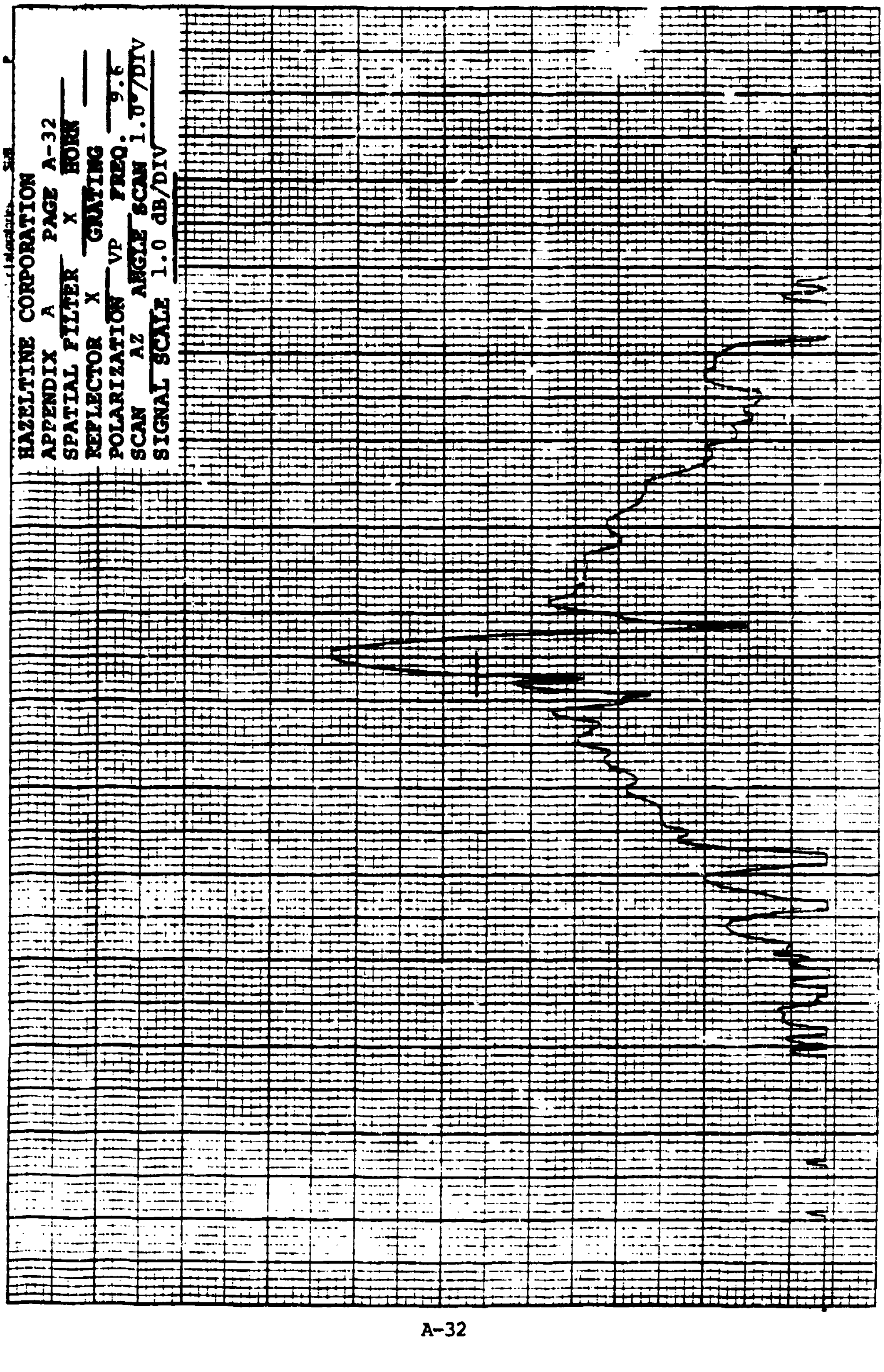
HAZELTINE CORPORATION
APPENDIX A PAGE A-32
SPATIAL FILTER X HORN
REFLECTOR X GRATING
POLARIZATION VP FREQ. 9.6
SCAN AZ ANGLE SCAN 1.0°/DIV
SIGNAL SCALE 1.0 dB/DIV

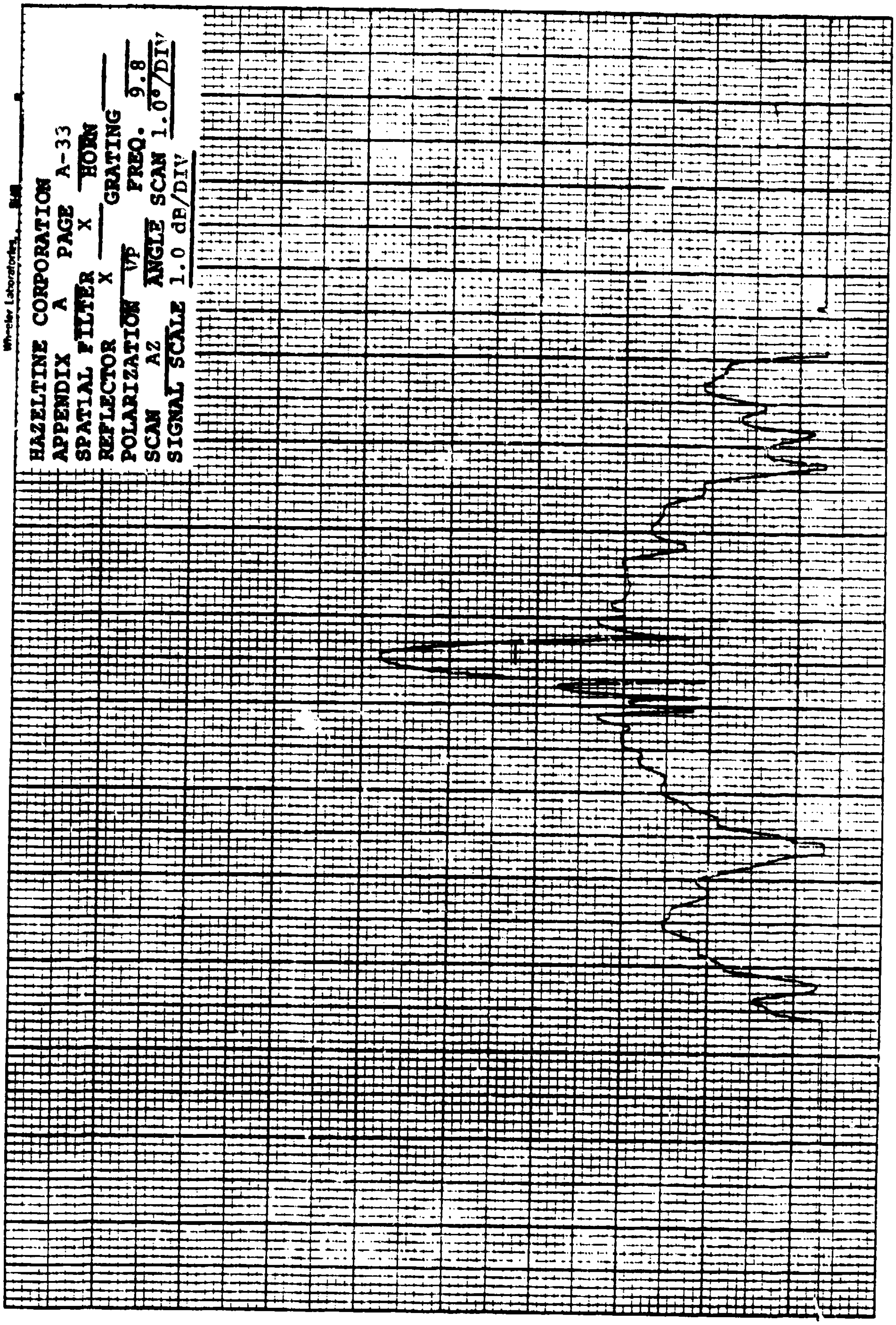
Wheeler Laboratories
HAZELTINE CORPORATION
APPENDIX A PAGE A-33
SPATIAL FILTER X HORN
REFLECTOR X GRATING
POLARIZATION VP FREQ. 9.8
SCAN AZ ANGLE SCAN 1.0°/DIV
SIGNAL SCALE 1.0 dB/DIV

APPENDIX B

MEASURED PATTERNS OF A REFLECTOR ANTENNA WITH A GRATING WITH AND WITHOUT THE SPATIAL FILTER

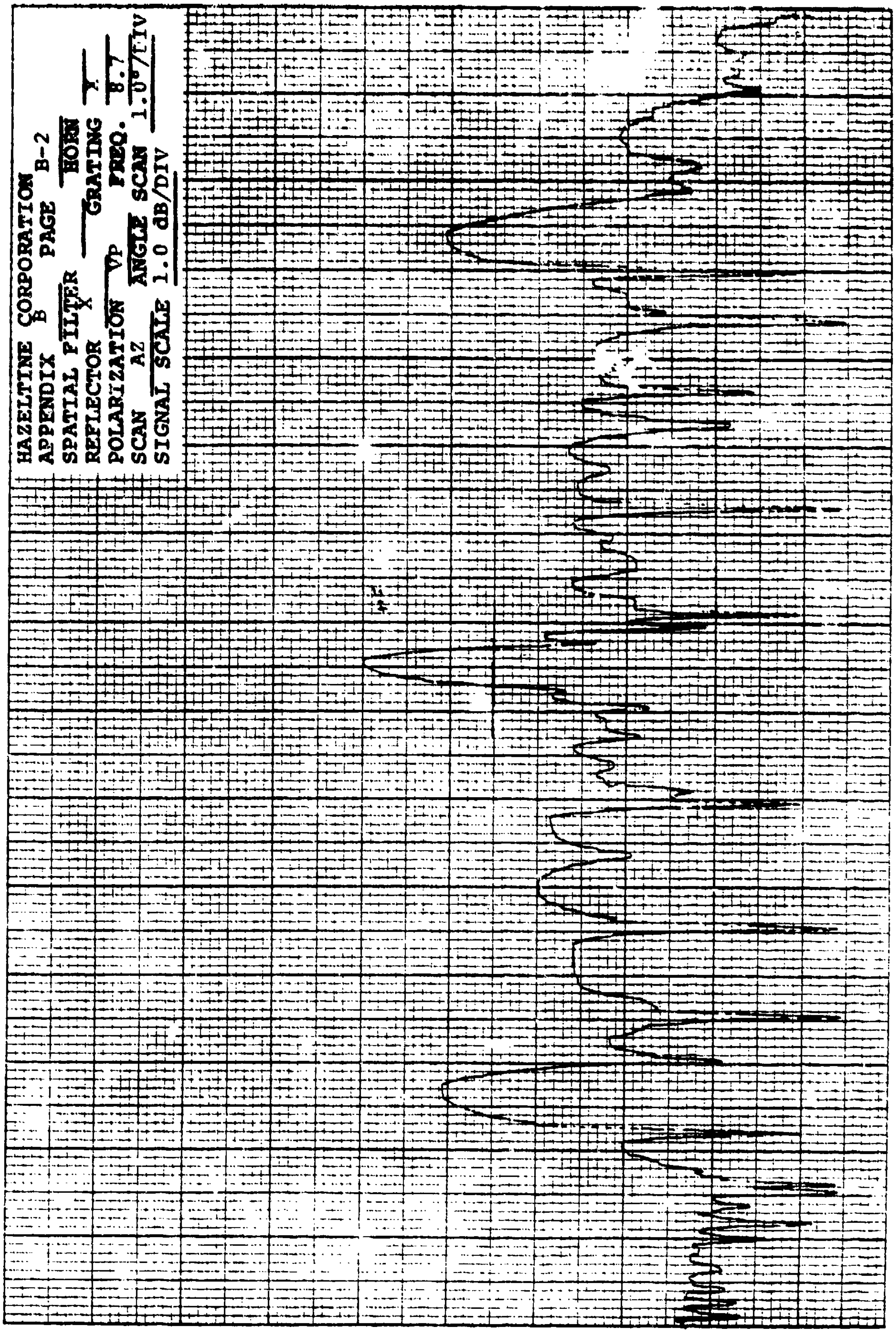
HAZELTINE CORPORATION
APPENDIX B PAGE B-2
SPATIAL FILTER HORN
REFLECTOR X GRATING Y
POLARIZATION VP FREQ. 8.7
SCAN AZ ANGLE SCAN 1.0°/DIV
SIGNAL SCALE 1.0 dB/DIV

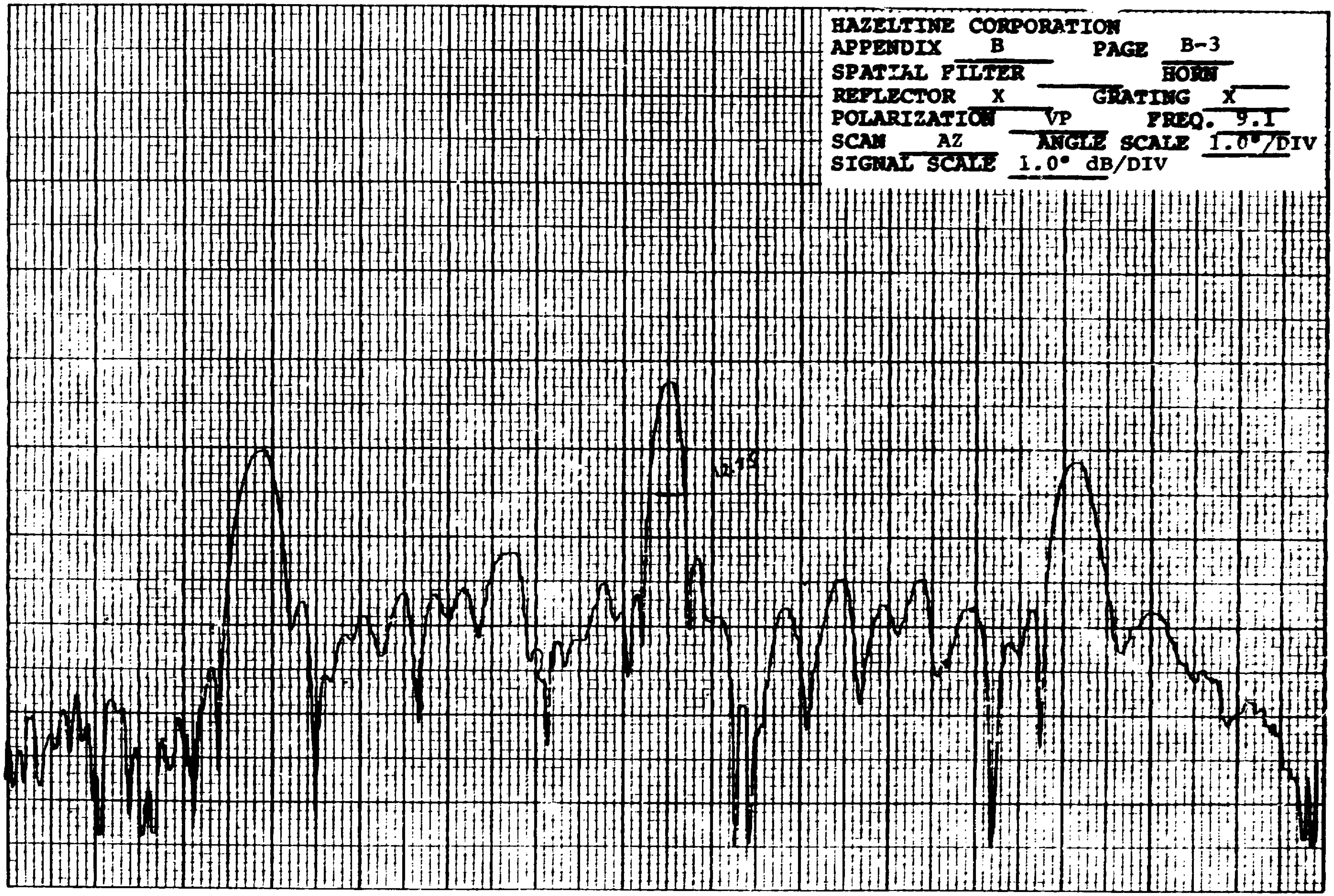
HAZELTINE CORPORATION
APPENDIX B PAGE B-3
SPATIAL FILTER HORN
REFLECTOR X GRATING X
POLARIZATION VP FREQ. 9.1
SCAN AZ ANGLE SCALE 1.0°/DIV
SIGNAL SCALE 1.0° dB/DIV

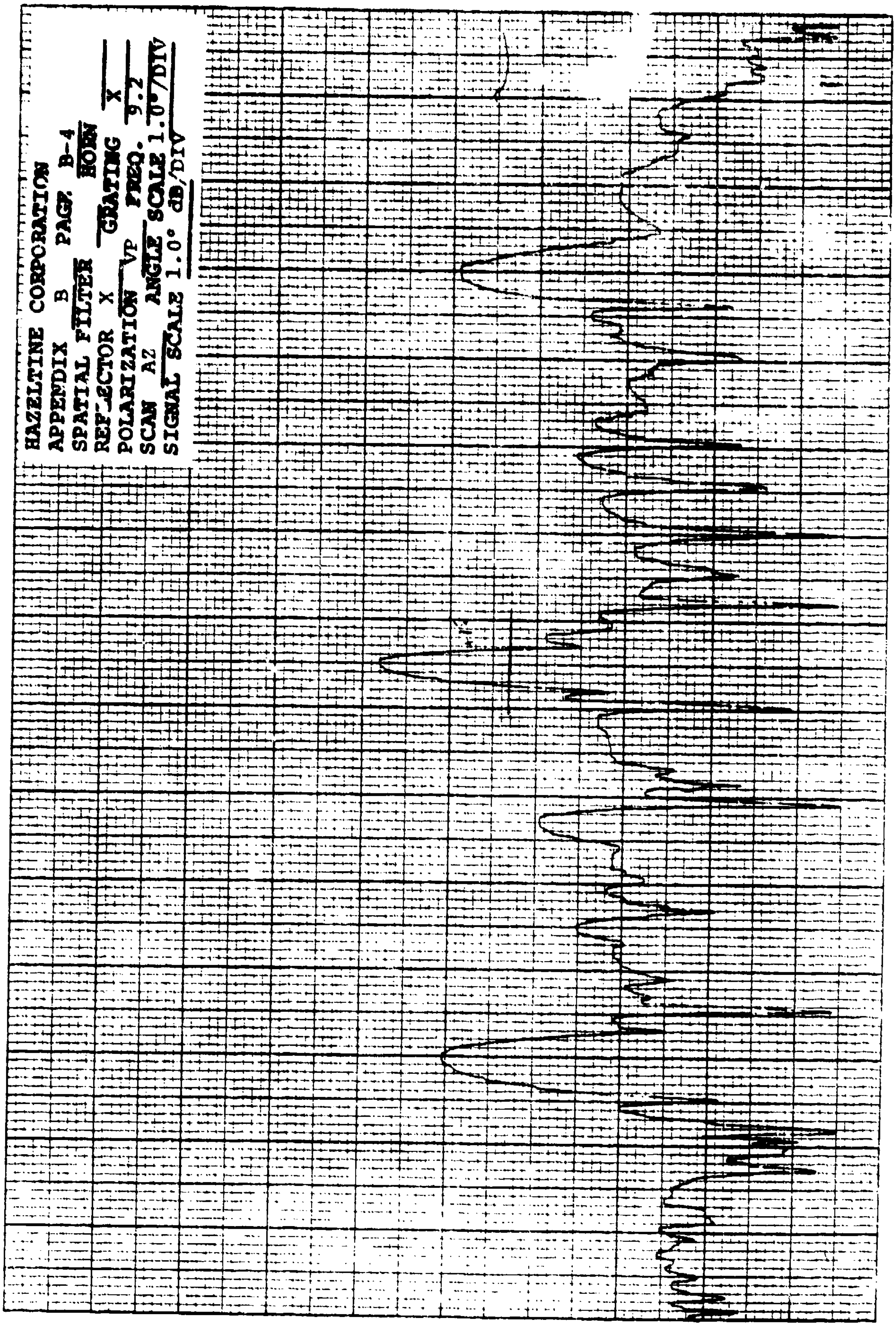
HAZELTINE CORPORATION
APPENDIX B PAGE B-4
SPATIAL FILTER HORN
REFLECTOR X GRATING X
POLARIZATION VP FREQ. 9.2
SCAN AZ ANGLE SCALE 1.0°/DIV
SIGNAL SCALE 1.0° dB/DIV

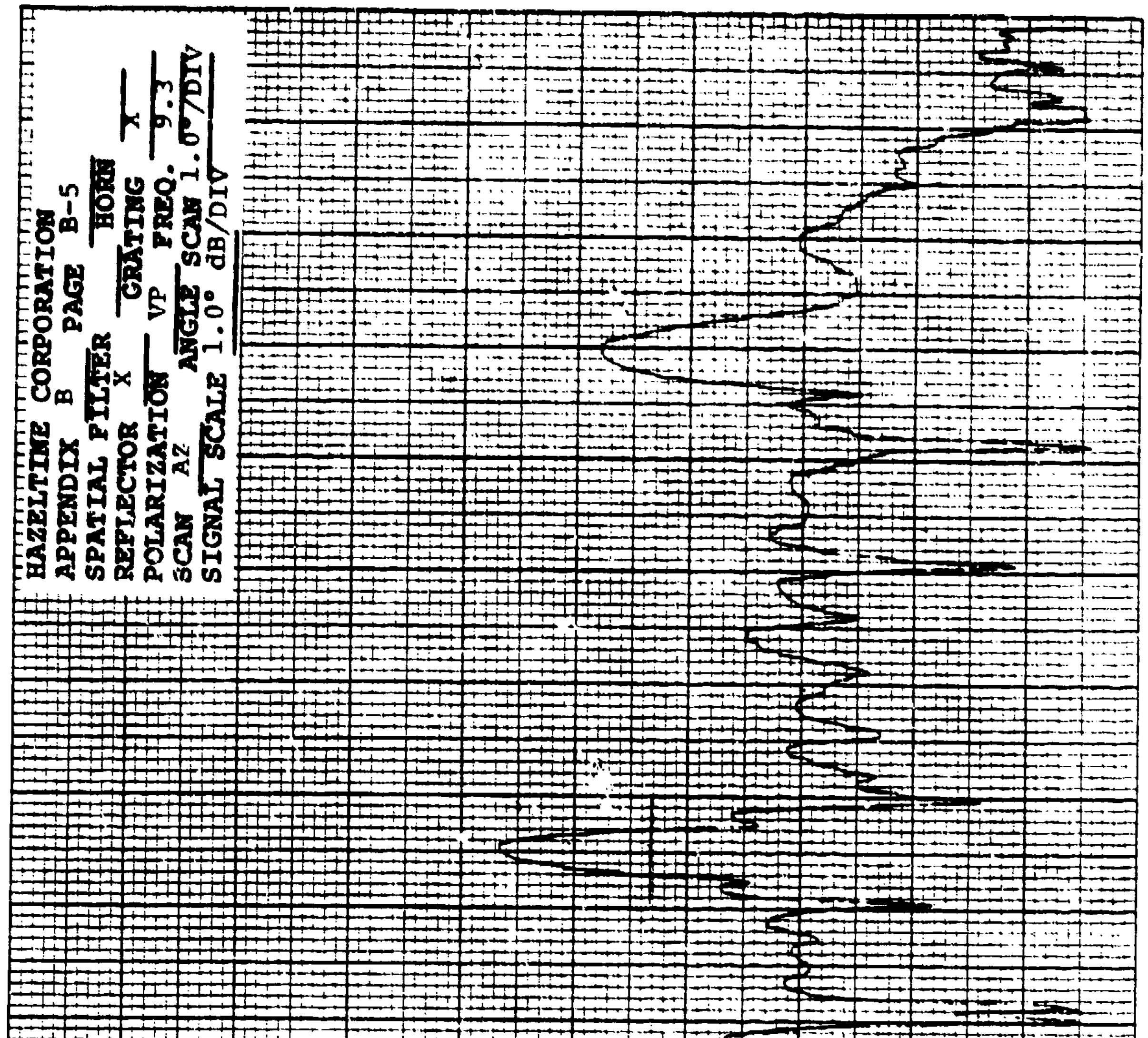
HAZELTINE CORPORATION
APPENDIX B PAGE B-5
SPATIAL FILTER HORN
REFLECTOR X GRATING X
POLARIZATION VP FREQ. 9.3
SCAN AZ ANGLE SCAN 1.0°/DIV
SIGNAL SCALE 1.0° dB/DIV

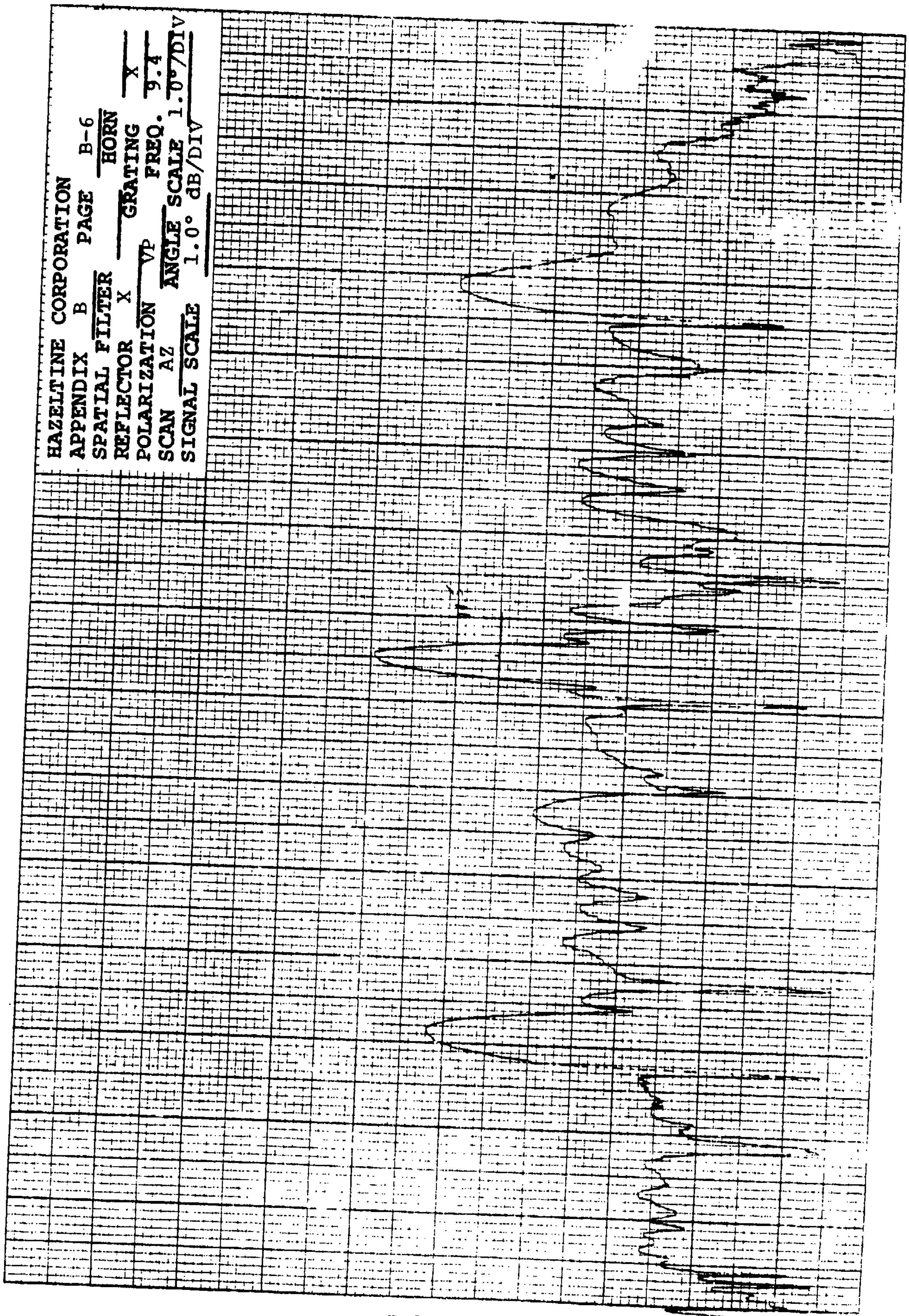
HAZELTINE CORPORATION
APPENDIX B PAGE B-6
SPATIAL FILTER HORN
REFLECTOR X GRATING X
POLARIZATION VP FREQ. 9.4
SCAN AZ ANGLE SCALE 1.0°/DIV
SIGNAL SCALE 1.0° dB/DIV

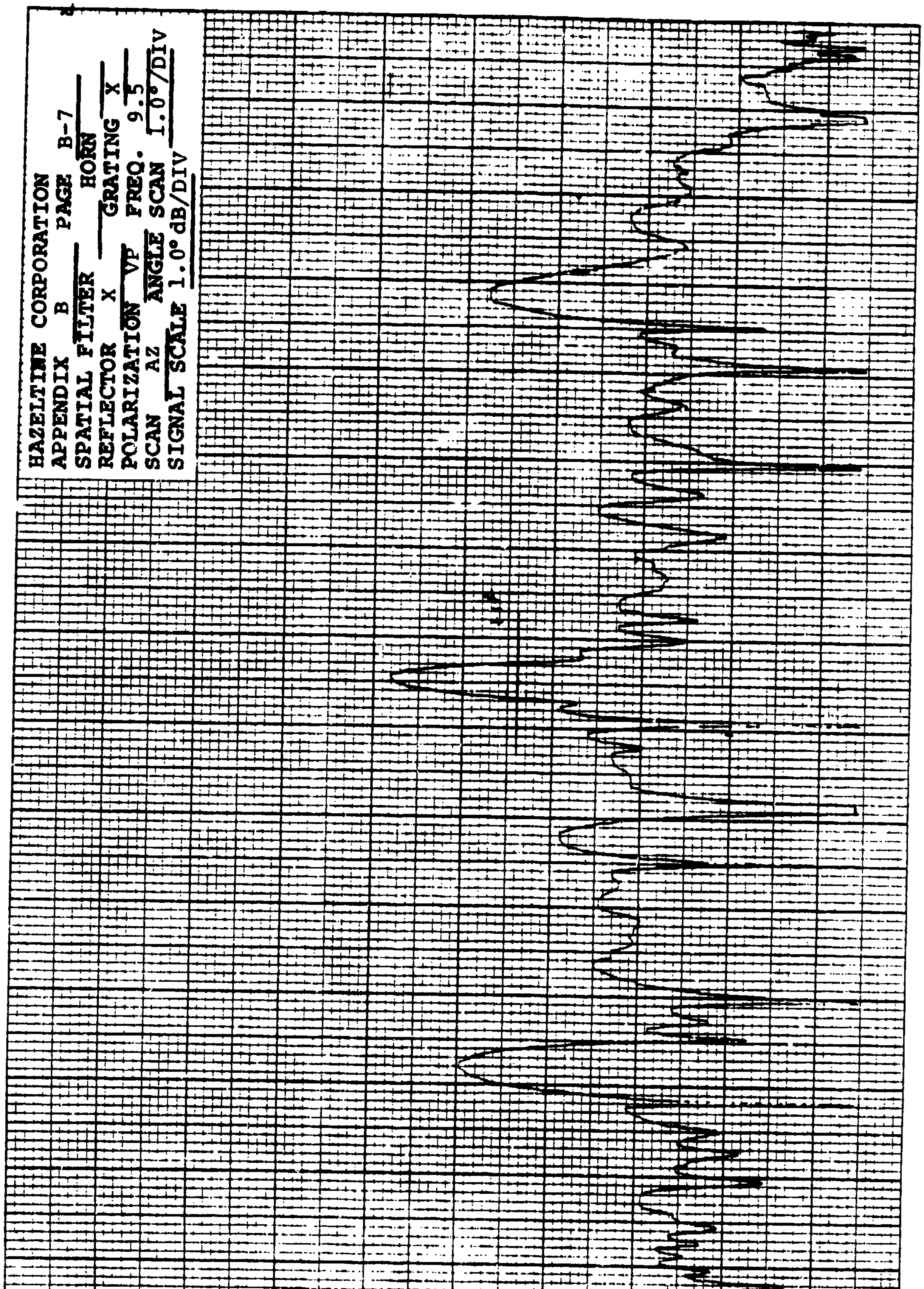
HAZELTINE CORPORATION
APPENDIX B PAGE B-7
SPATIAL FILTER HORN
REFLECTOR X GRATING X
POLARIZATION VP FREQ. 9.5
SCAN AZ ANGLE SCAN 1.0°/DIV
SIGNAL SCALE 1.0° dB/DIV

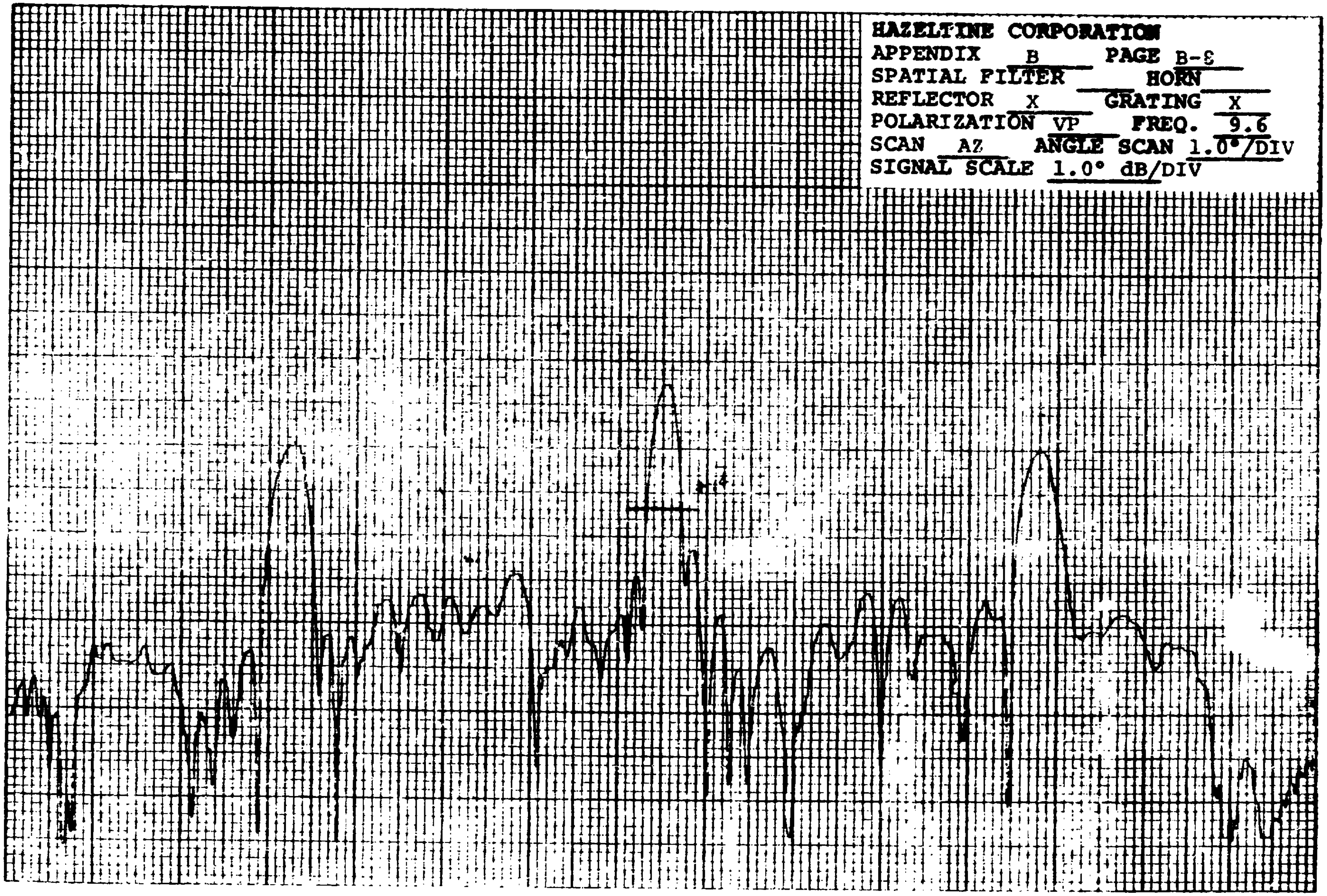
HAZELTINE CORPORATION
APPENDIX B PAGE B-8
SPATIAL FILTER HORN
REFLECTOR X GRATING X
POLARIZATION VP FREQ. 9.6
SCAN AZ ANGLE SCAN 1.0°/DIV
SIGNAL SCALE 1.0° dB/DIV

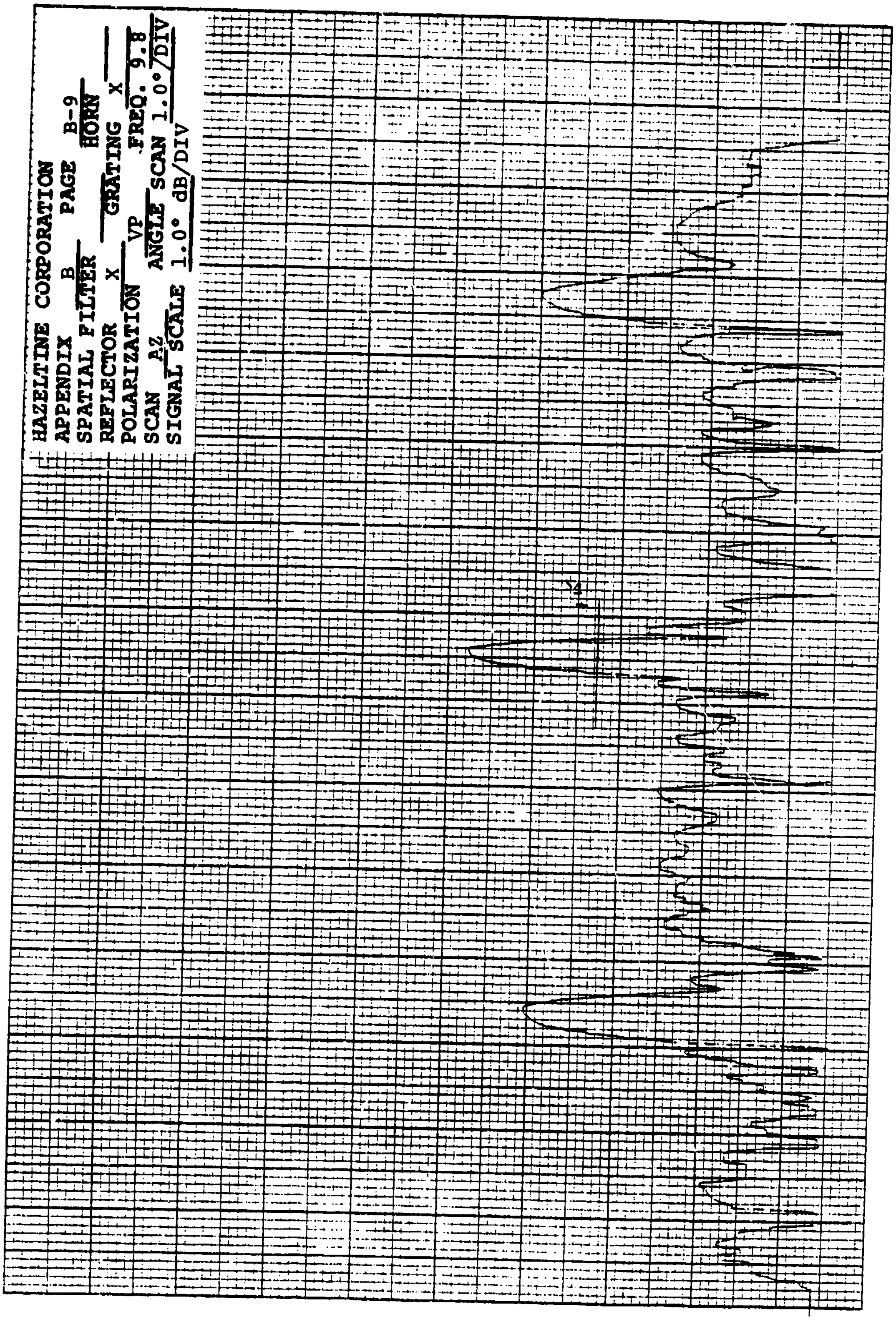
HAZELTINE CORPORATION
APPENDIX B PAGE B-9
SPATIAL FILTER HORN
REFLECTOR X GRATING X
POLARIZATION VP FREQ. 9.8
SCAN AZ ANGLE SCAN 1.0°/DIV
SIGNAL SCALE 1.0° dB/DIV

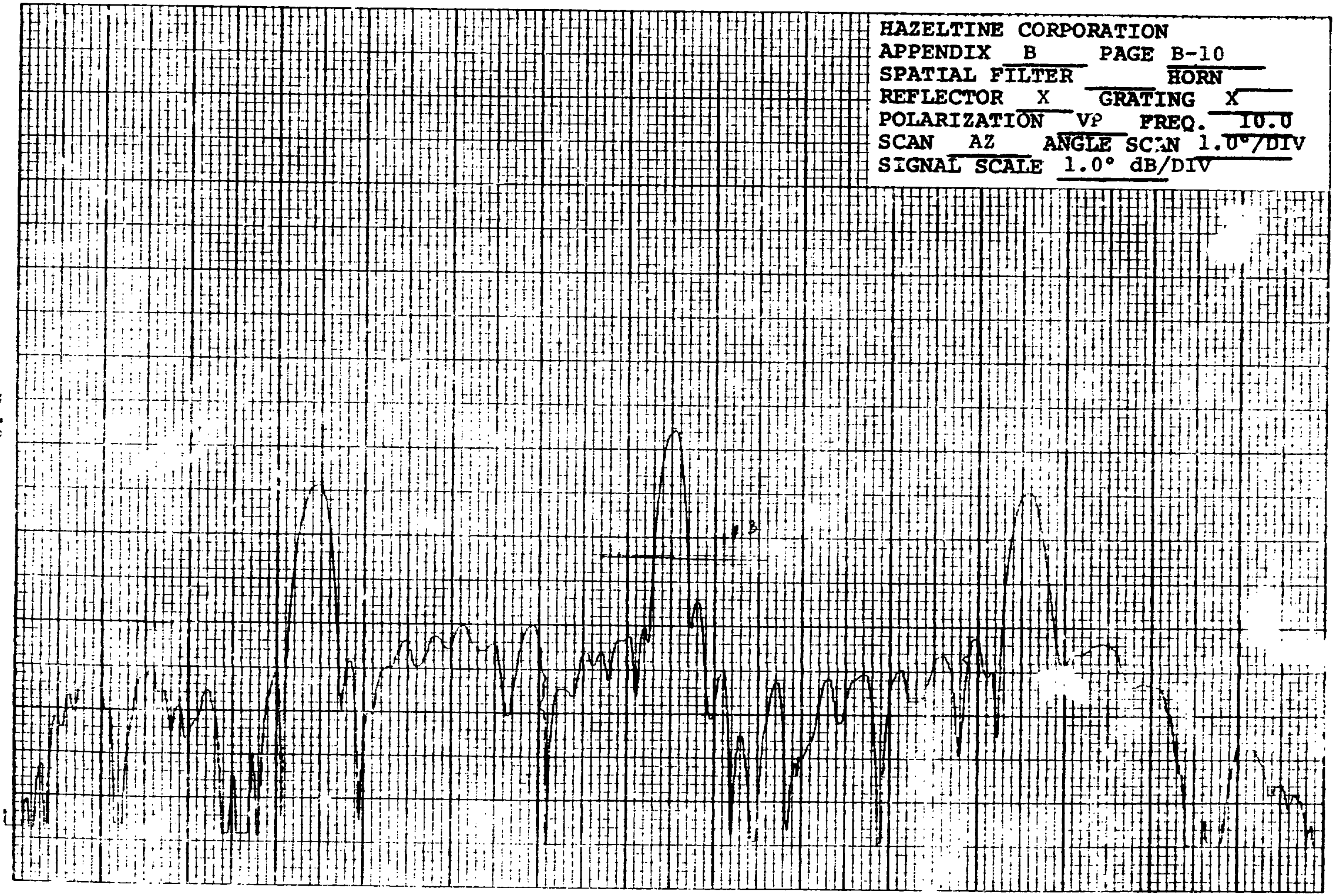
HAZELTINE CORPORATION
APPENDIX B PAGE B-10
SPATIAL FILTER HORN
REFLECTOR X GRATING X
POLARIZATION VP FREQ. 10.0
SCAN AZ ANGLE SCAN 1.0°/DIV
SIGNAL SCALE 1.0° dB/DIV
B

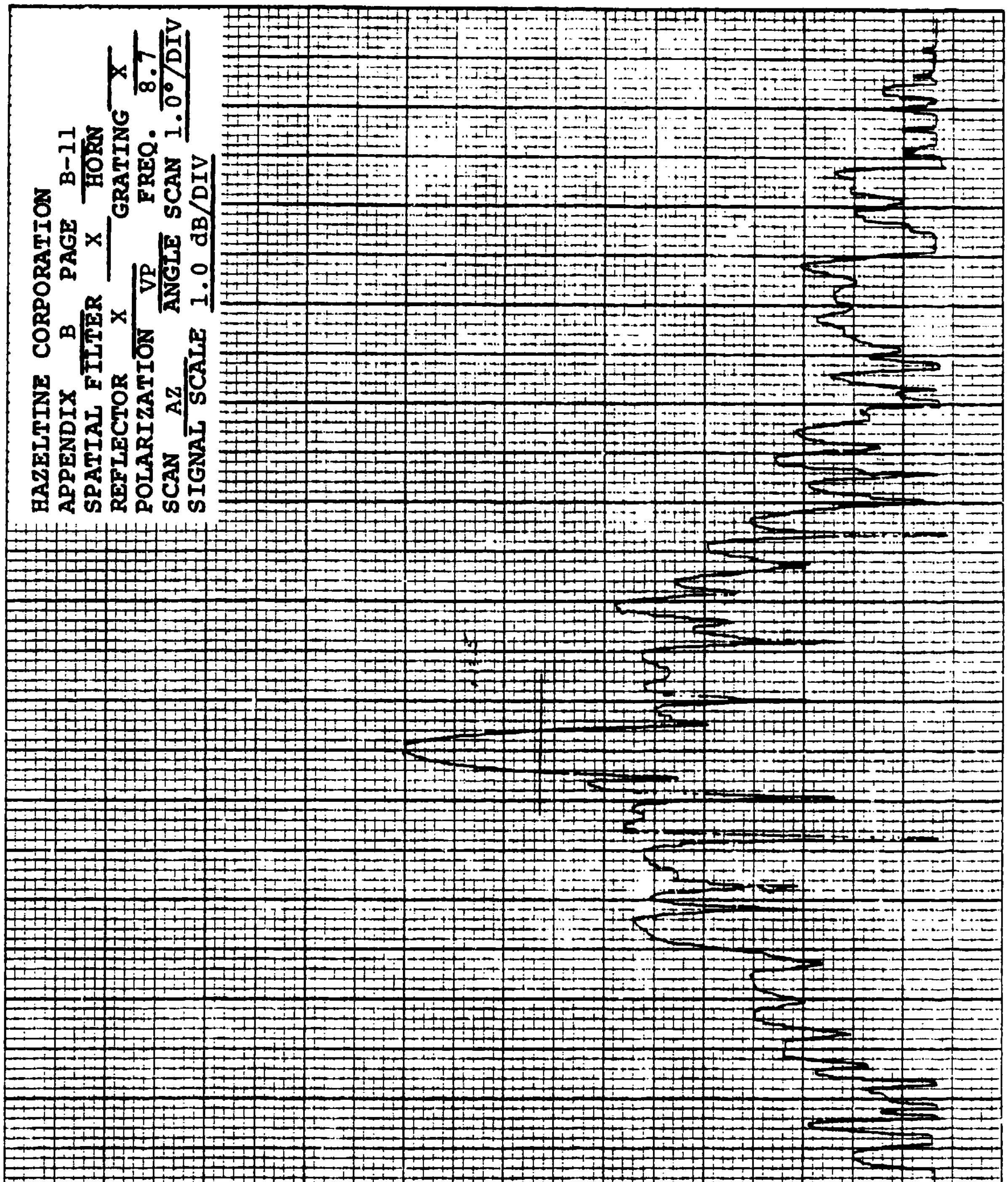
HAZELTINE CORPORATION
APPENDIX B PAGE B-11
SPATIAL FILTER X HORN
REFLECTOR X GRATING X
POLARIZATION VP FREQ. 8.7
SCAN AZ ANGLE SCAN 1.0°/DIV
SIGNAL SCALE 1.0 dB/DIV

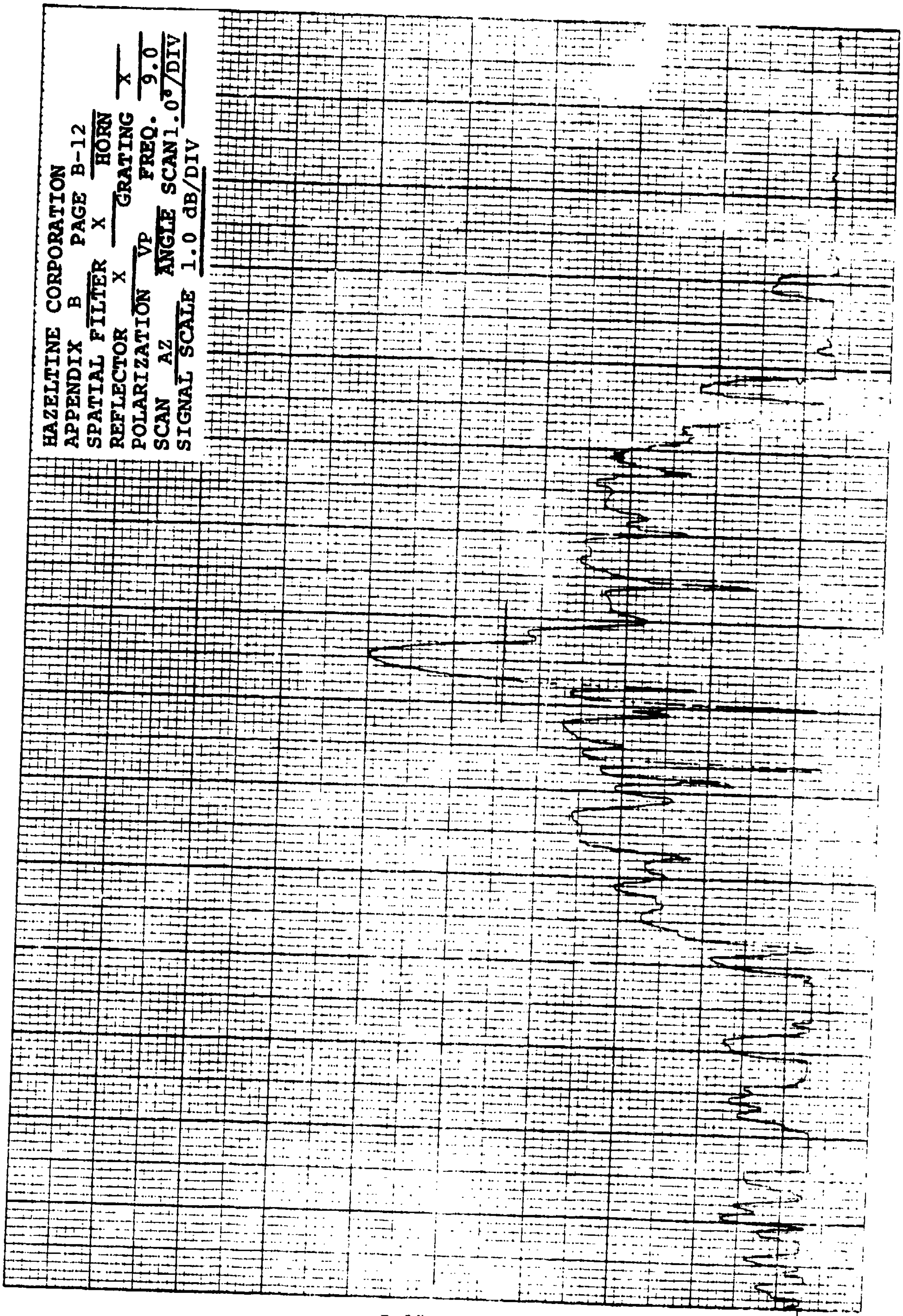

HAZELTINE CORPORATION
APPENDIX B PAGE B-12
SPATIAL FILTER X HORN
REFLECTOR X GRATING X
POLARIZATION VP FREQ. 9.0
SCAN AZ ANGLE SCAN 1.0°/DIV
SIGNAL SCALE 1.0 dB/DIV

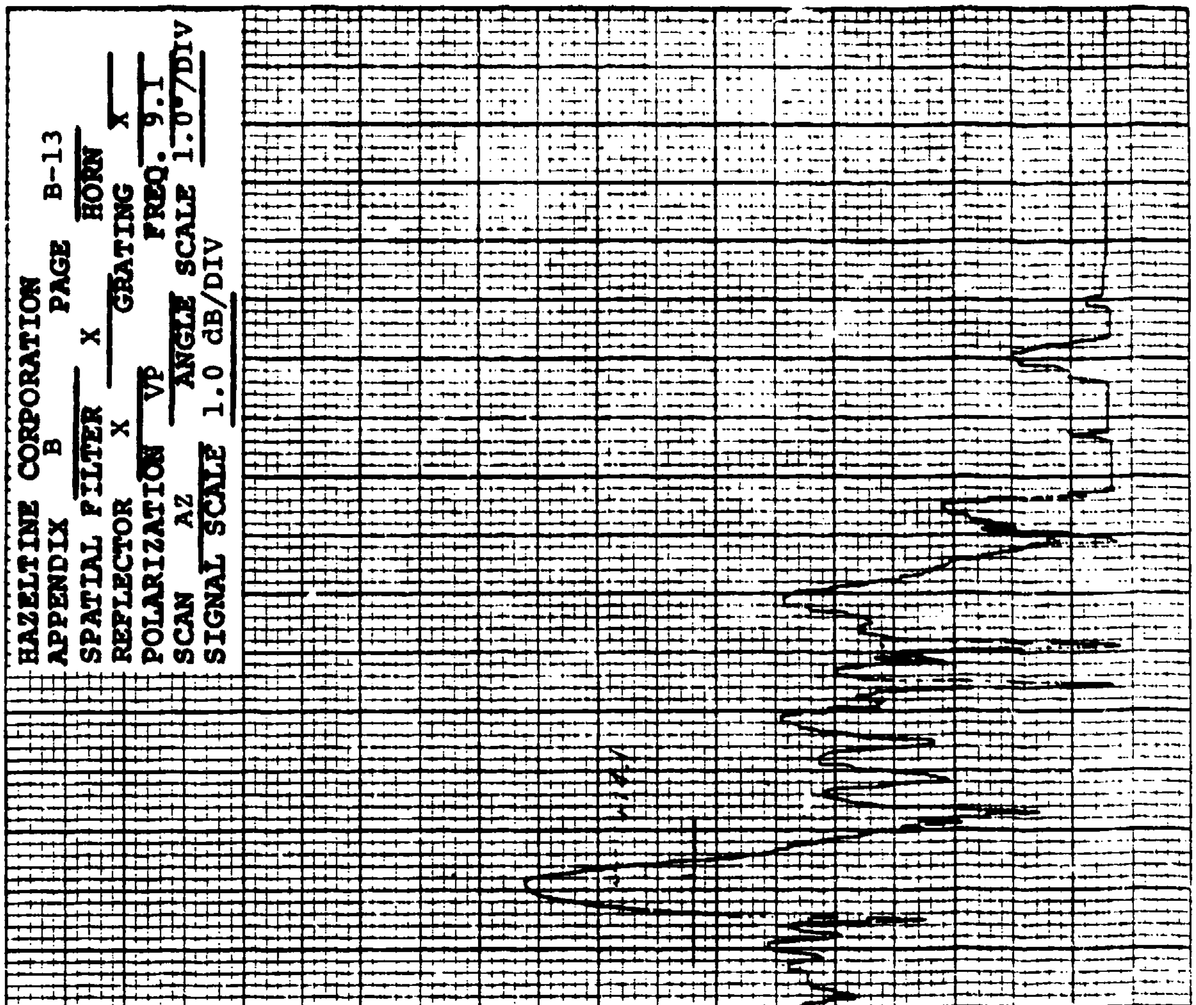
HAZELTINE CORPORATION
APPENDIX B PAGE B-13
SPATIAL FILTER X HORN
REFLECTOR X GRATING X
POLARIZATION VP FREQ. 9.1
SCAN AZ ANGLE SCALE 1.0°/DIV
SIGNAL SCALE 1.0 dB/DIV

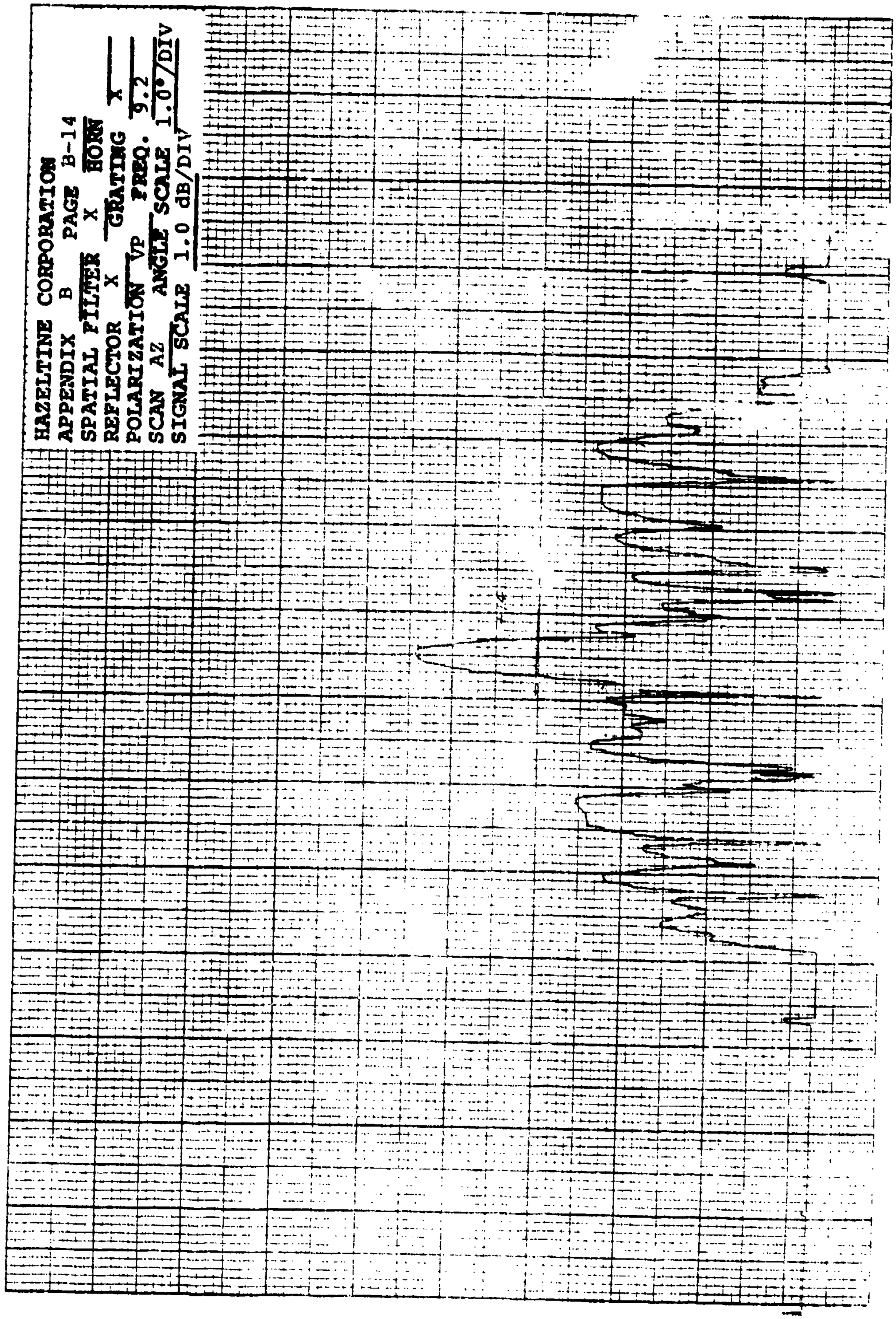
HAZELTINE CORPORATION
APPENDIX B PAGE B-14
SPATIAL FILTER X HORN
REFLECTOR X GRATING X
POLARIZATION VP FREQ. 9.2
SCAN AZ ANGLE SCALE 1.0°/DIV
SIGNAL SCALE 1.0 dB/DIV

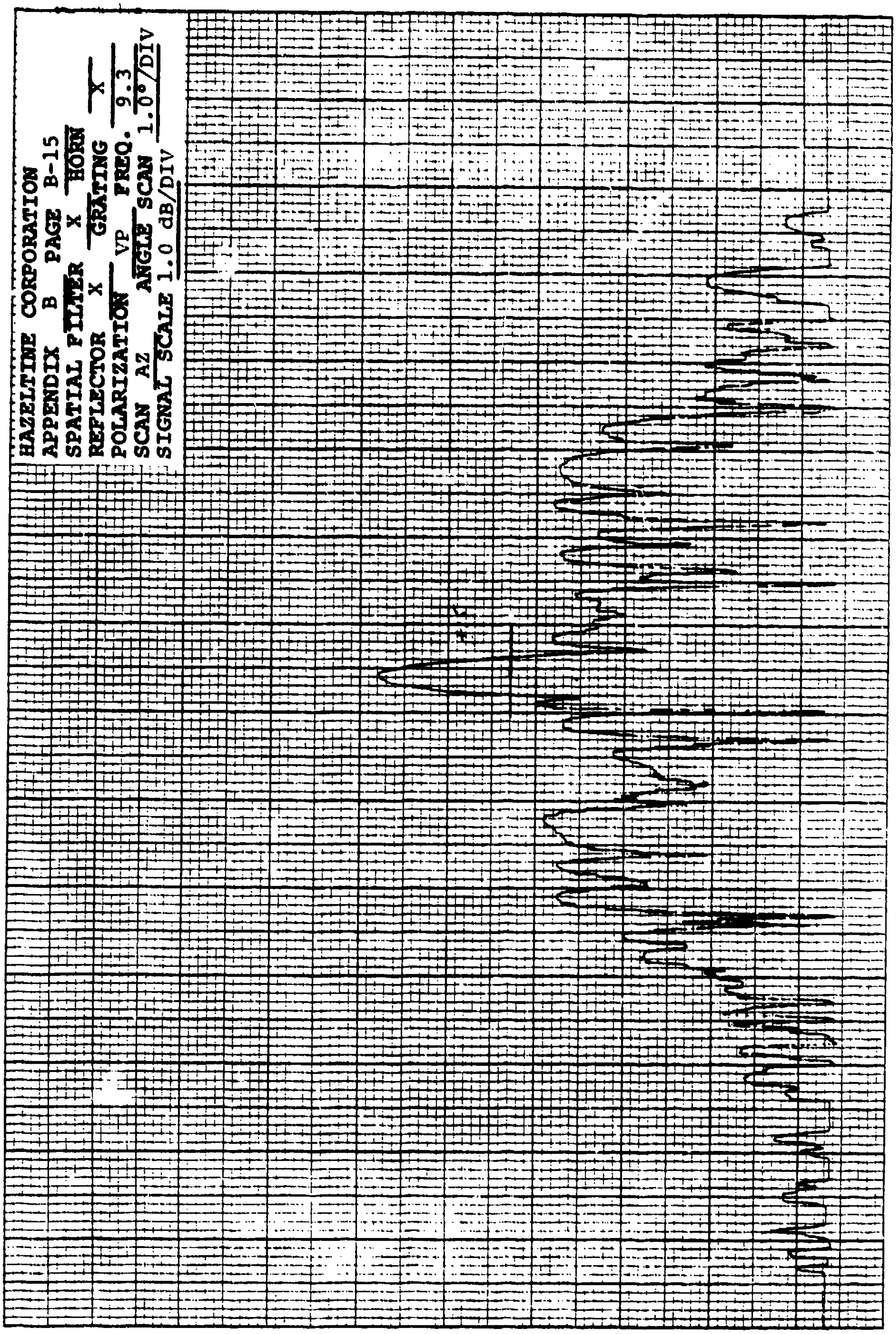
HAZELTINE CORPORATION
APPENDIX B PAGE B-15
SPATIAL FILTER X HORN
REFLECTOR X GRATING X
POLARIZATION VP FREQ. 9.3
SCAN AZ ANGLE SCAN 1.0°/DIV
SIGNAL SCALE 1.0 dB/DIV

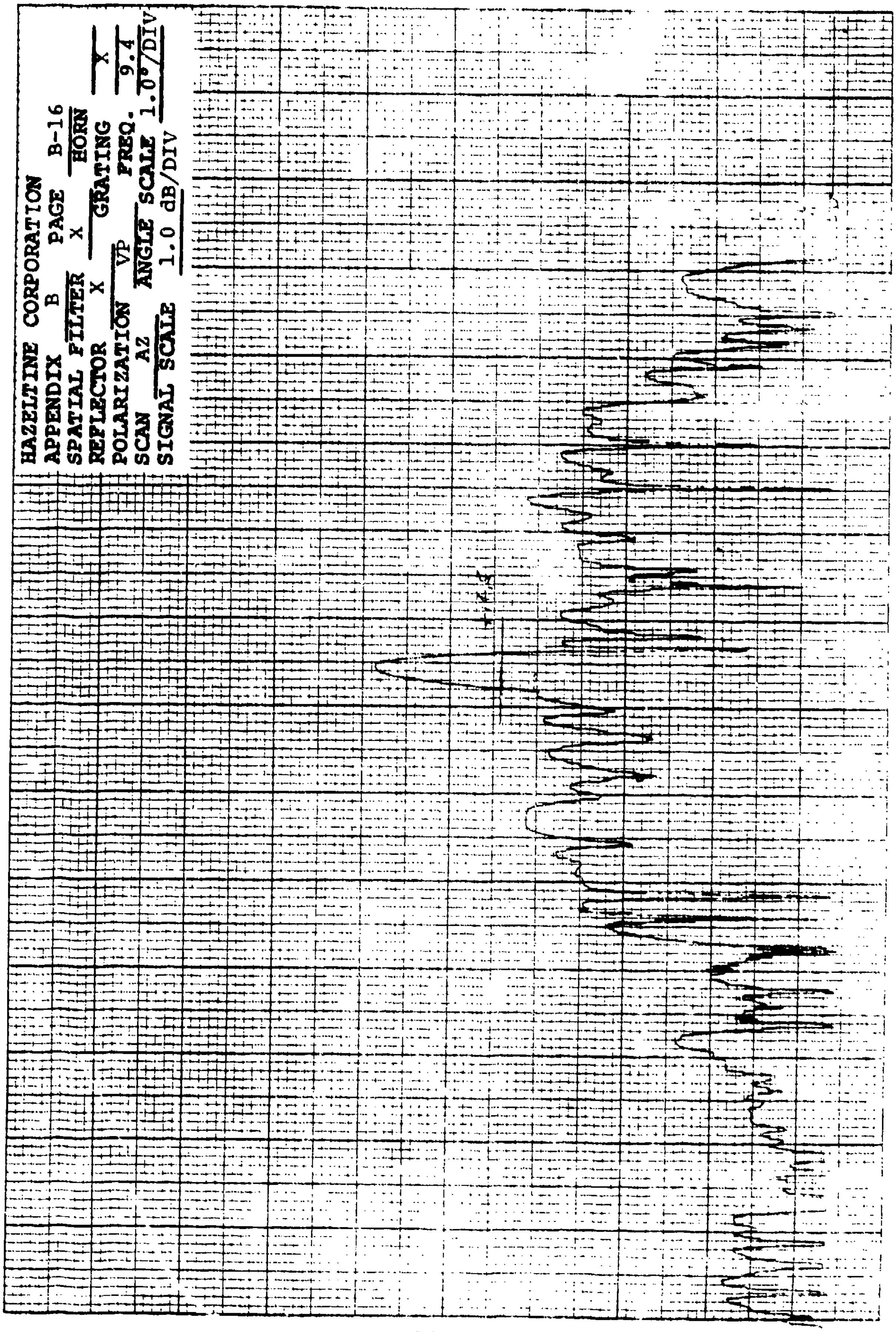
HAZELTINE CORPORATION
APPENDIX B PAGE B-16
SPATIAL FILTER X HORN
REFLECTOR X GRATING X
POLARIZATION VP FREQ. 9.4
SCAN AZ ANGLE SCALE 1.0°/DIV
SIGNAL SCALE 1.0 dB/DIV

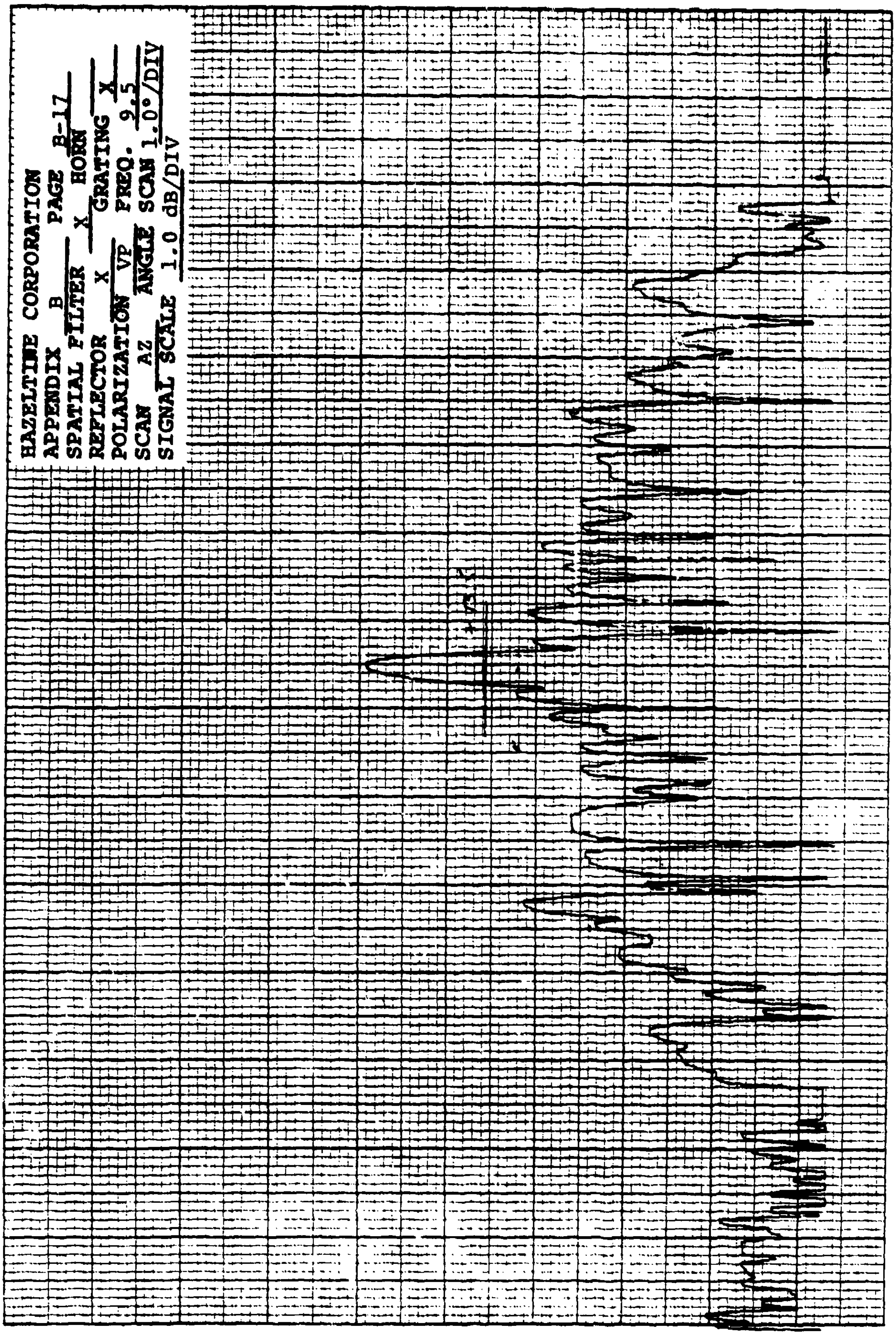
HAZELTINE CORPORATION
APPENDIX B PAGE B-17
SPATIAL FILTER X HORN
REFLECTOR X GRATING X
POLARIZATION VP FREQ. 9.5
SCAN AZ ANGLE SCAN 1.0°/DIV
SIGNAL SCALE 1.0 dB/DIV

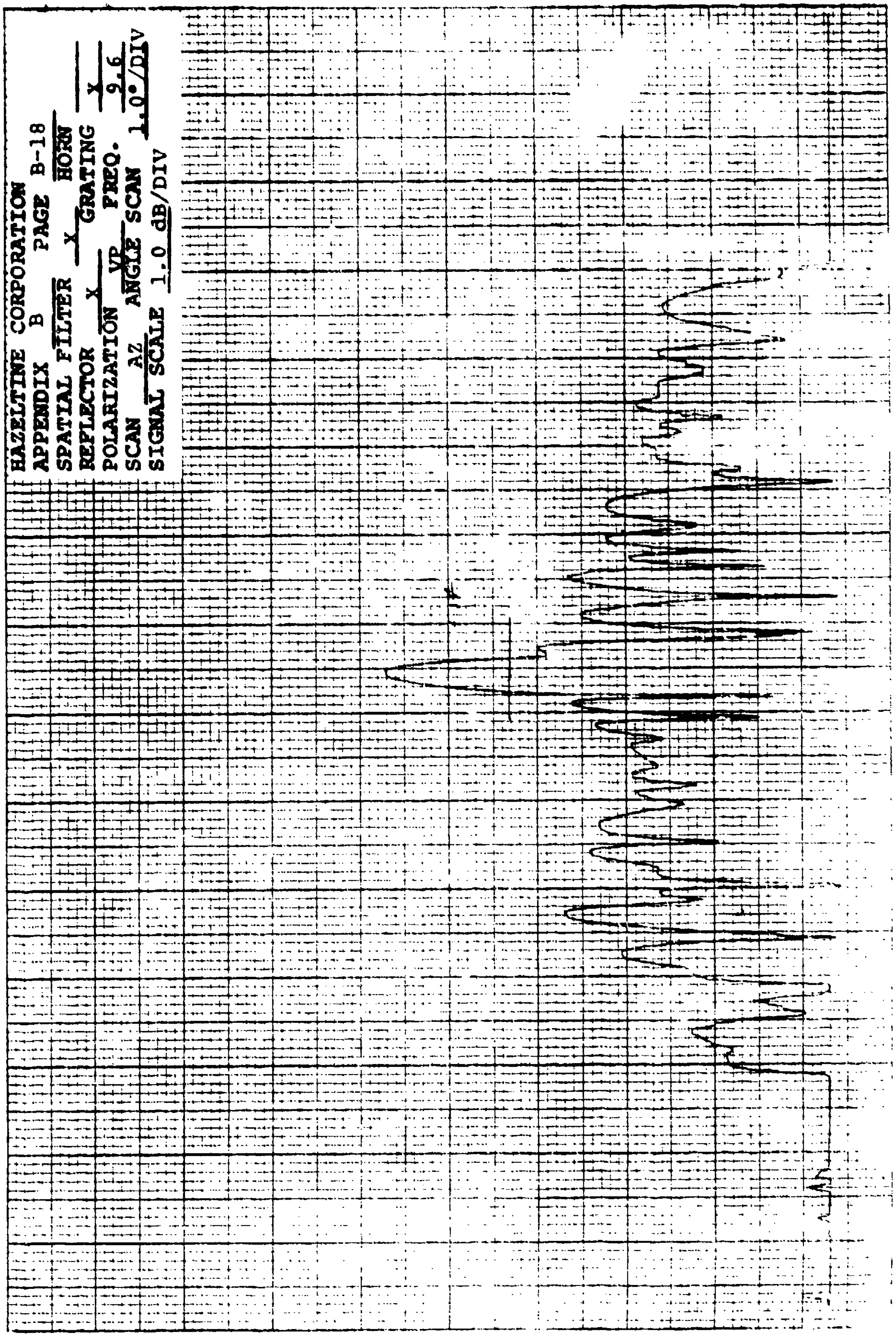
HAZELTINE CORPORATION
APPENDIX B PAGE B-18
SPATIAL FILTER X HORN
REFLECTOR X GRATING X
POLARIZATION VP FREQ. 9.6
SCAN AZ ANGLE SCAN 1.0°/DIV
SIGNAL SCALE 1.0 dB/DIV

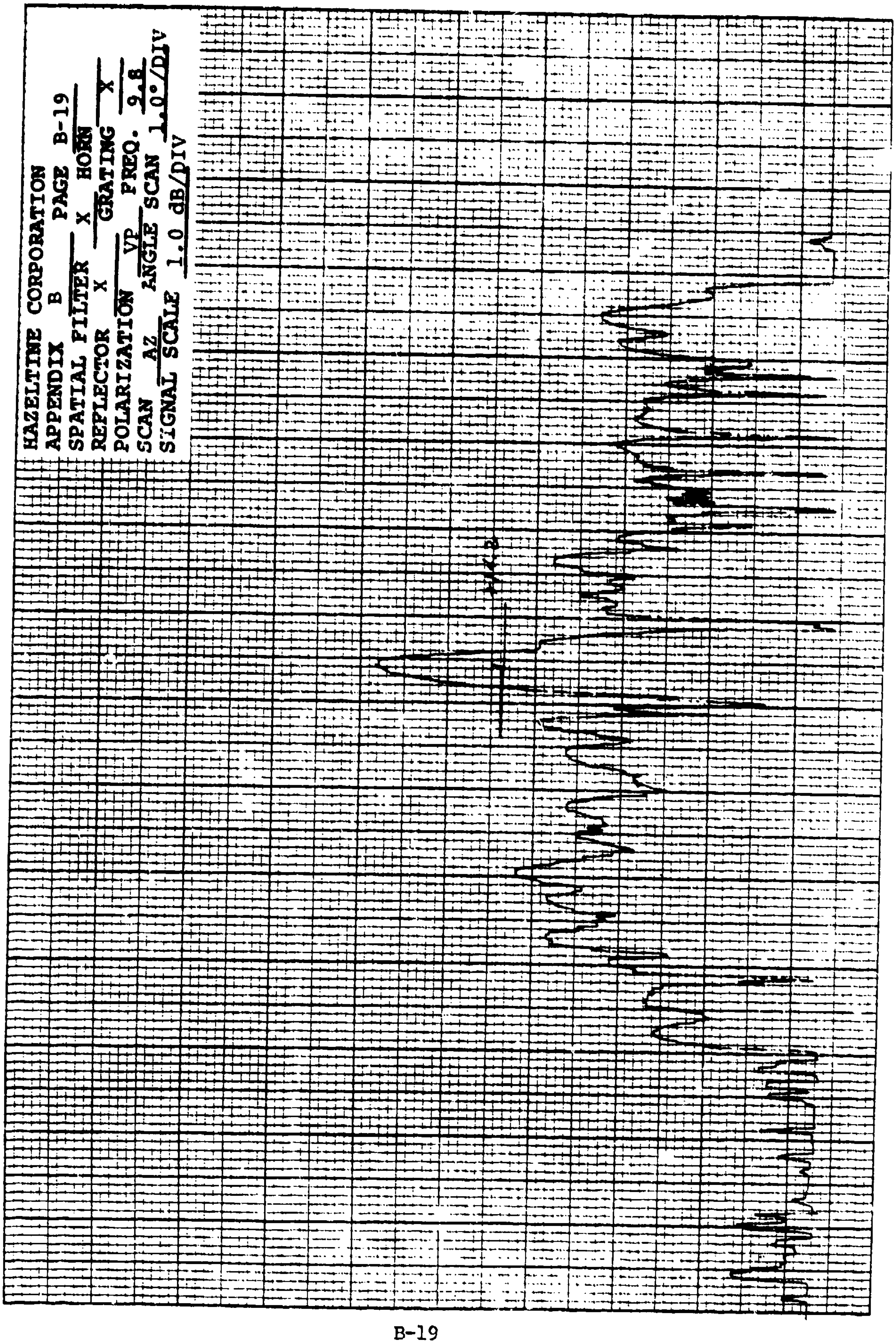
HAZELTINE CORPORATION
APPENDIX B PAGE B-19
SPATIAL FILTER X HORN
REFLECTOR X GRATING X
POLARIZATION VP FREQ. 9.8
SCAN AZ ANGLE SCAN 1.0°/DIV
SIGNAL SCALE 1.0 dB/DIV

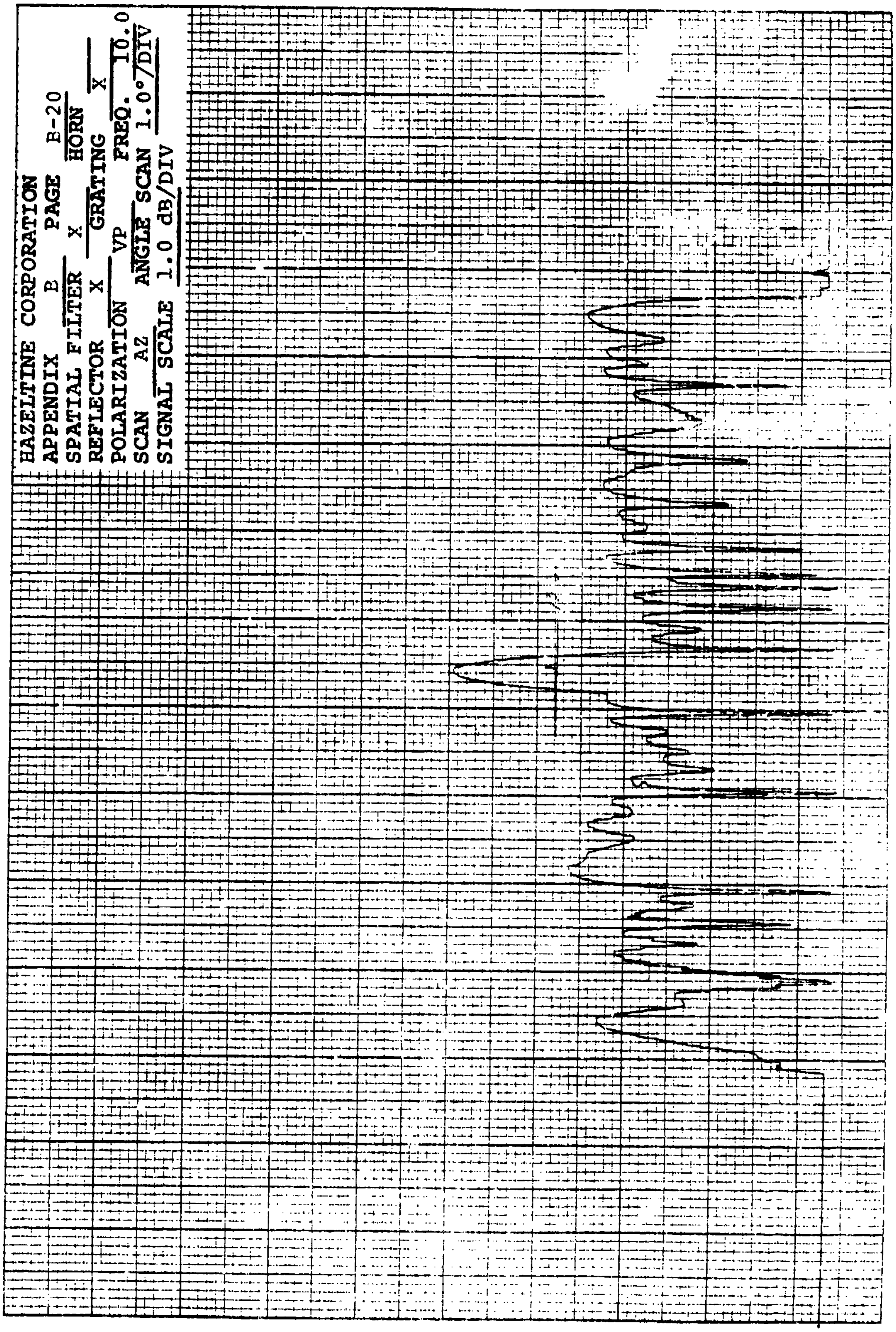
HAZELTINE CORPORATION
APPENDIX B PAGE B-20
SPATIAL FILTER X HORN
REFLECTOR X GRATING X
POLARIZATION VP FREQ. 10.0
SCAN AZ ANGLE SCAN 1.0°/DIV
SIGNAL SCALE 1.0 dB/DIV

APPENDIX C

MEASURED PATTERNS OF A HORN WITH AND WITHOUT THE SPATIAL FILTER

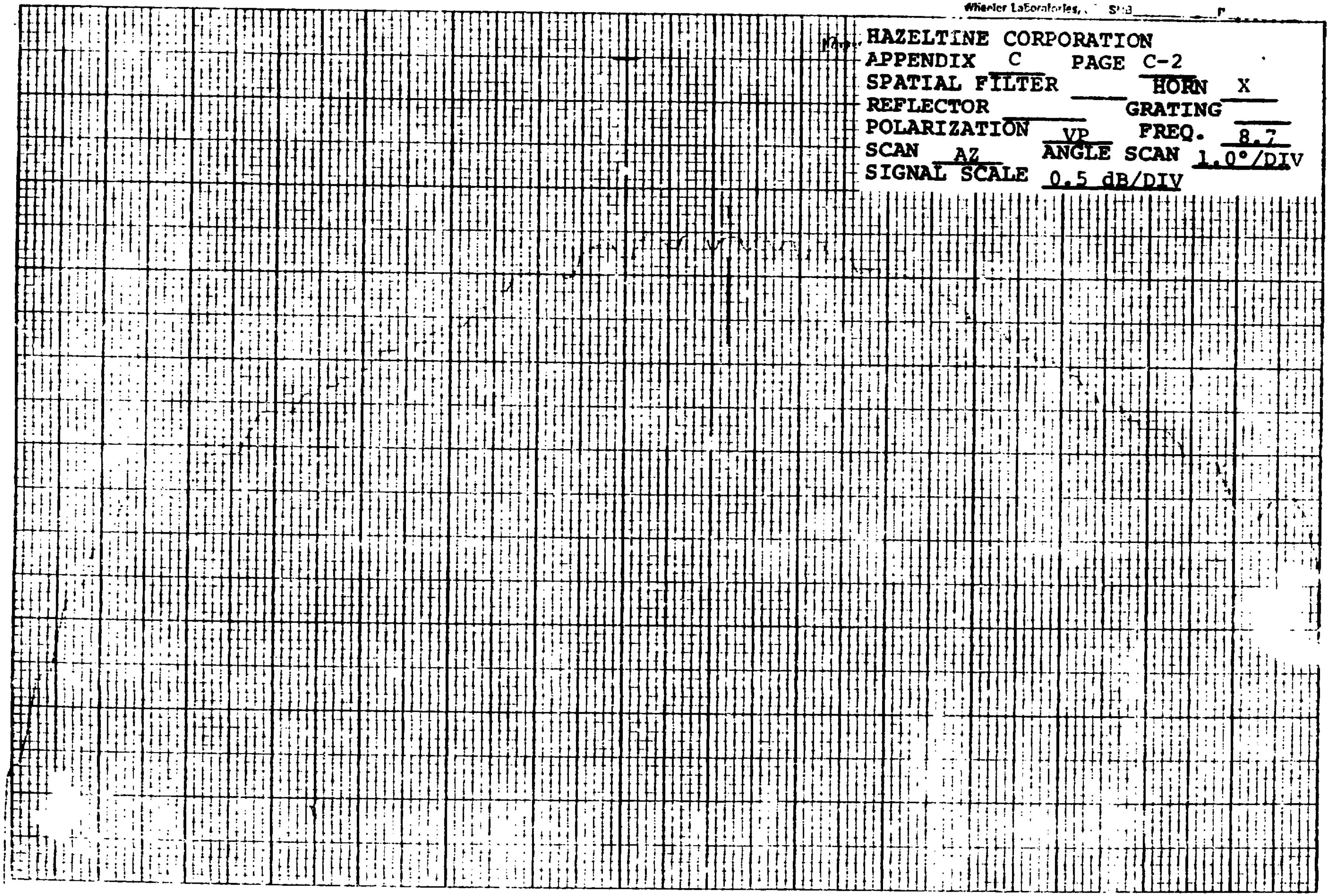
Wheeler Laboratories, . S:3
HAZELTINE CORPORATION
APPENDIX C PAGE C-2
SPATIAL FILTER HORN X
REFLECTOR GRATING
POLARIZATION VP FREQ. 8.7
SCAN AZ ANGLE SCAN 1.0°/DIV
SIGNAL SCALE 0.5 dB/DIV

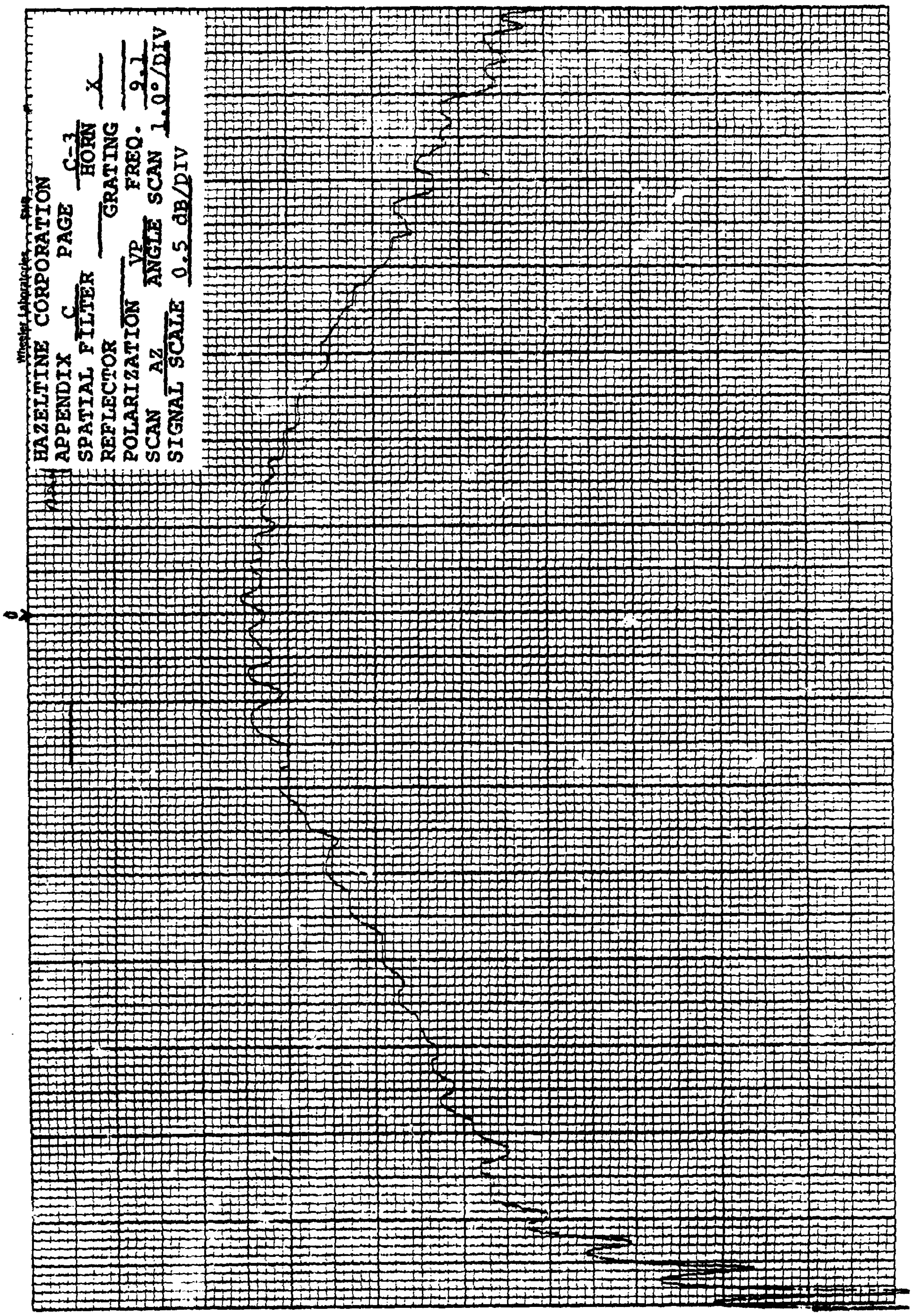
HAZELTINE CORPORATION
APPENDIX C PAGE C-3
SPATIAL FILTER HORN X
REFLECTOR GRATING
POLARIZATION VP FREQ. 9.1
SCAN AZ ANGLE SCAN 1.0°/DIV
SIGNAL SCALE 0.5 dB/DIV

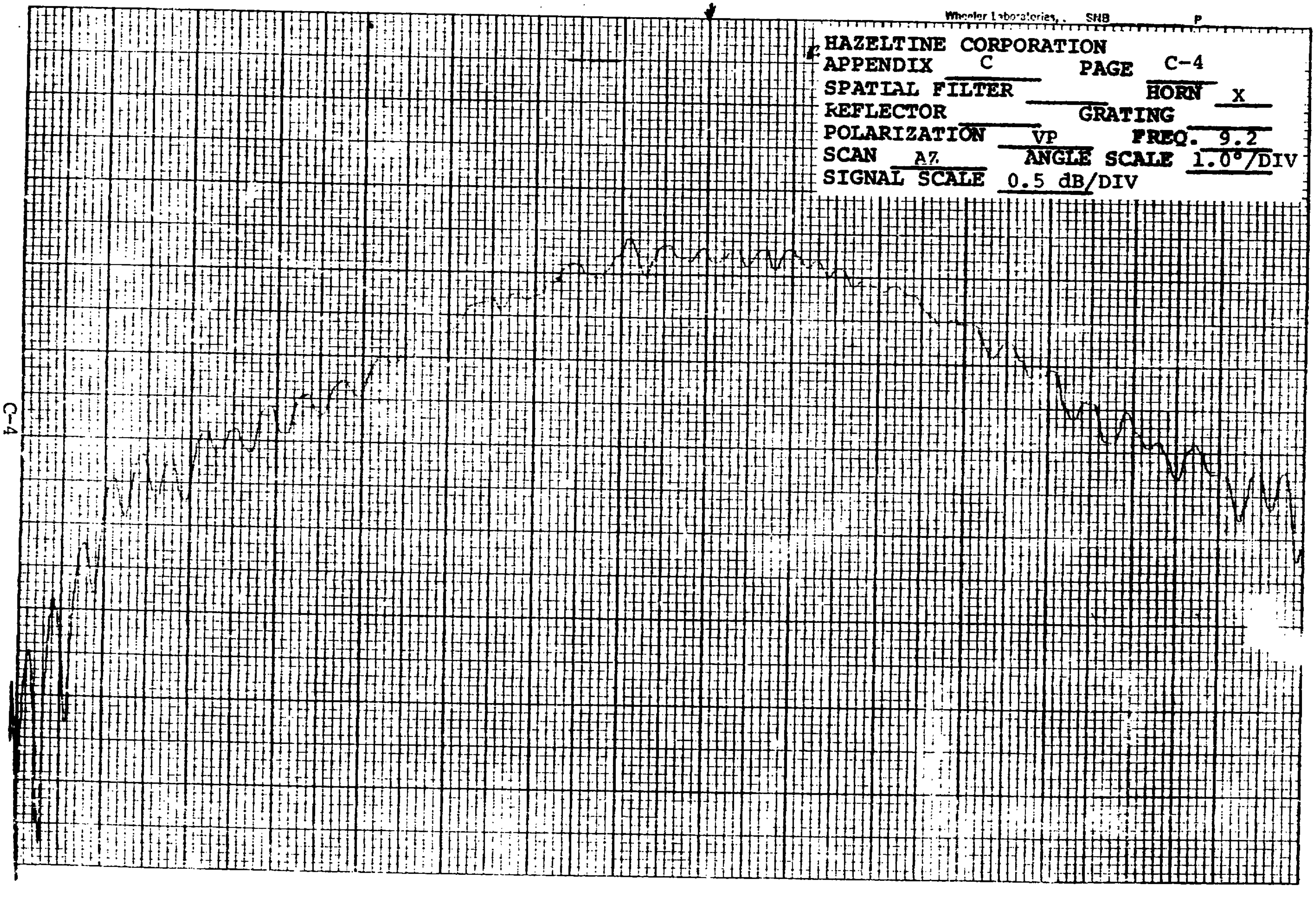
Wheeler Laboratories, SNB P
HAZELTINE CORPORATION
APPENDIX C PAGE C-4
SPATIAL FILTER HORN X
REFLECTOR GRATING
POLARIZATION VP FREQ. 9.2
SCAN AZ ANGLE SCALE 1.0°/DIV
SIGNAL SCALE 0.5 dB/DIV

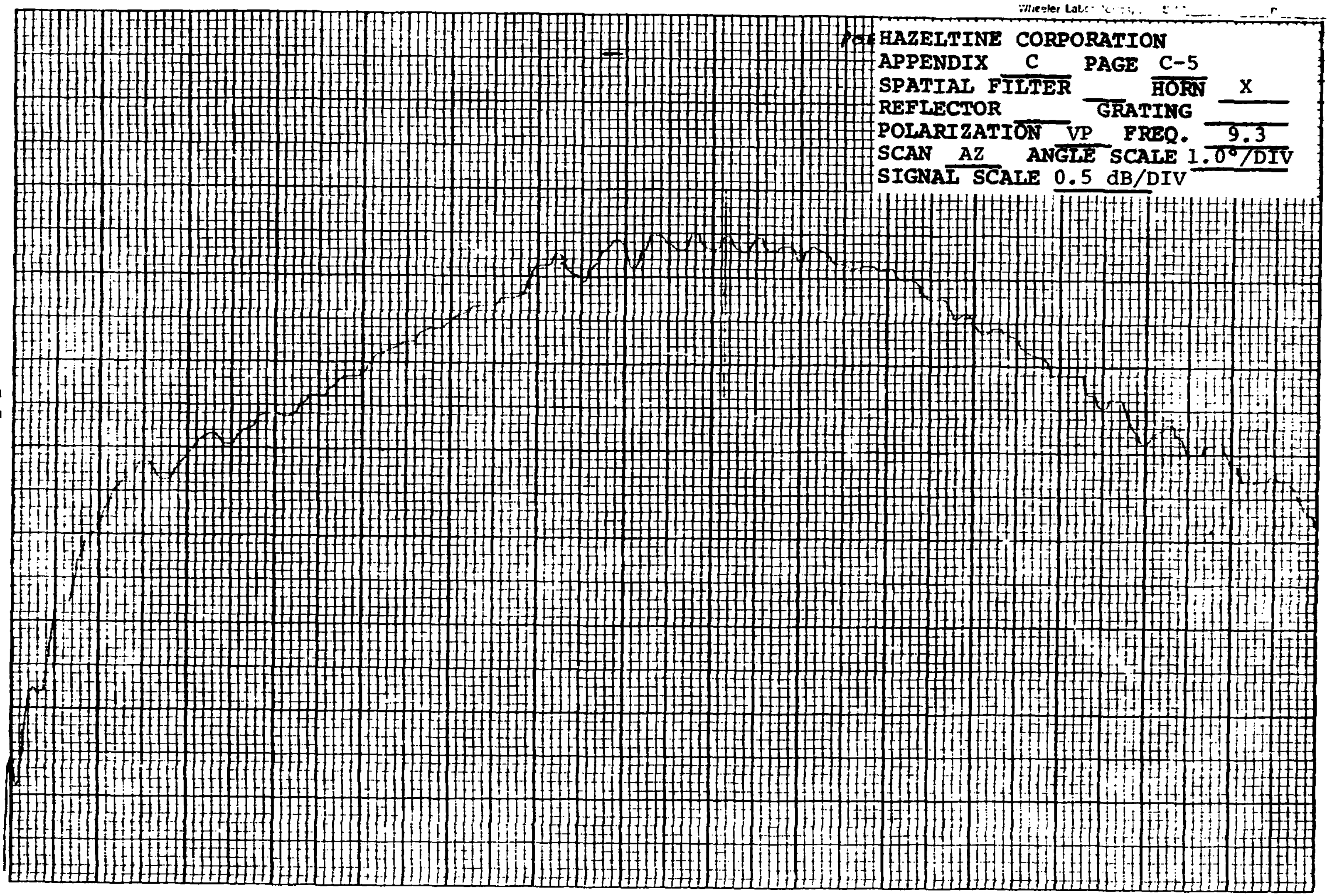
HAZELTINE CORPORATION
APPENDIX C PAGE C-5
SPATIAL FILTER ___ HORN X
REFLECTOR ___ GRATING ___
POLARIZATION VP FREQ. 9.3
SCAN AZ ANGLE SCALE 1.0°/DIV
SIGNAL SCALE 0.5 dB/DIV

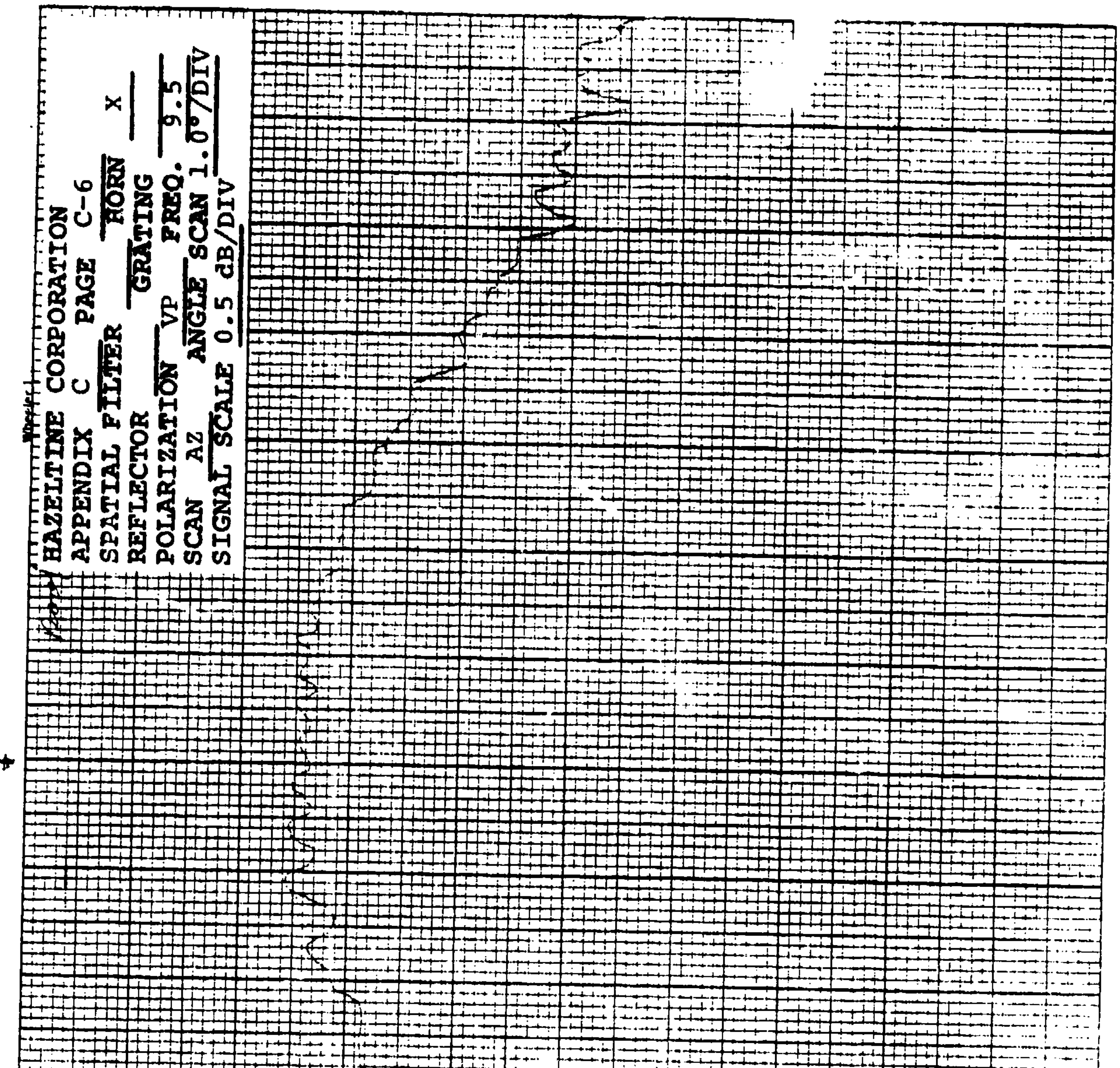
HAZELTINE CORPORATION
APPENDIX C PAGE C-6
SPATIAL FILTER HORN X
REFLECTOR GRATING
POLARIZATION VP FREQ. 9.5
SCAN AZ ANGLE SCAN 1.0°/DIV
SIGNAL SCALE 0.5 dB/DIV

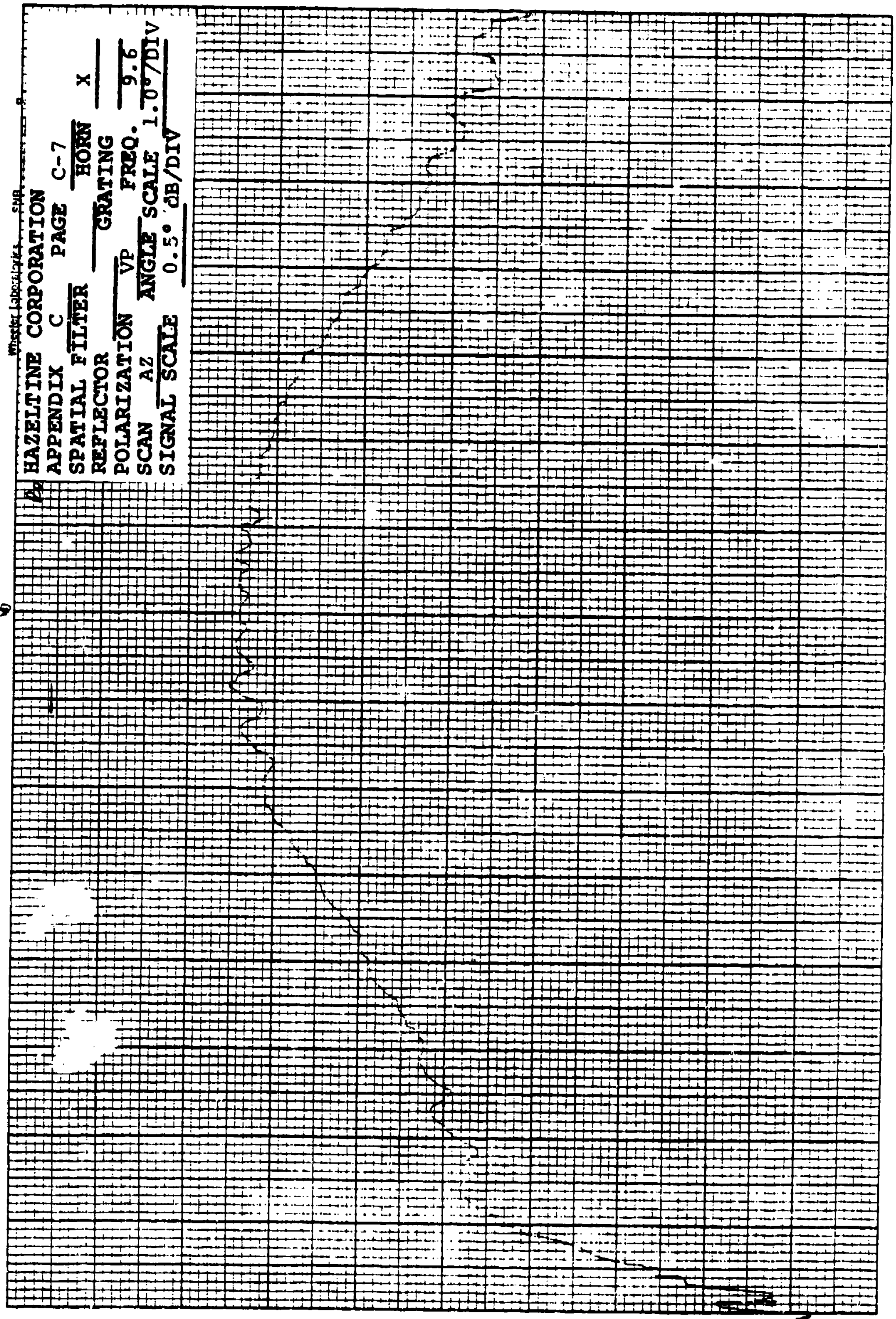
Wheeler Laboratories
HAZELTINE CORPORATION
APPENDIX C PAGE C-7
SPATIAL FILTER HORN
REFLECTOR GRATING X
POLARIZATION VP FREQ. 9.6
SCAN Az ANGLE SCALE 1.0°/DIV
SIGNAL SCALE 0.5° dB/DIV

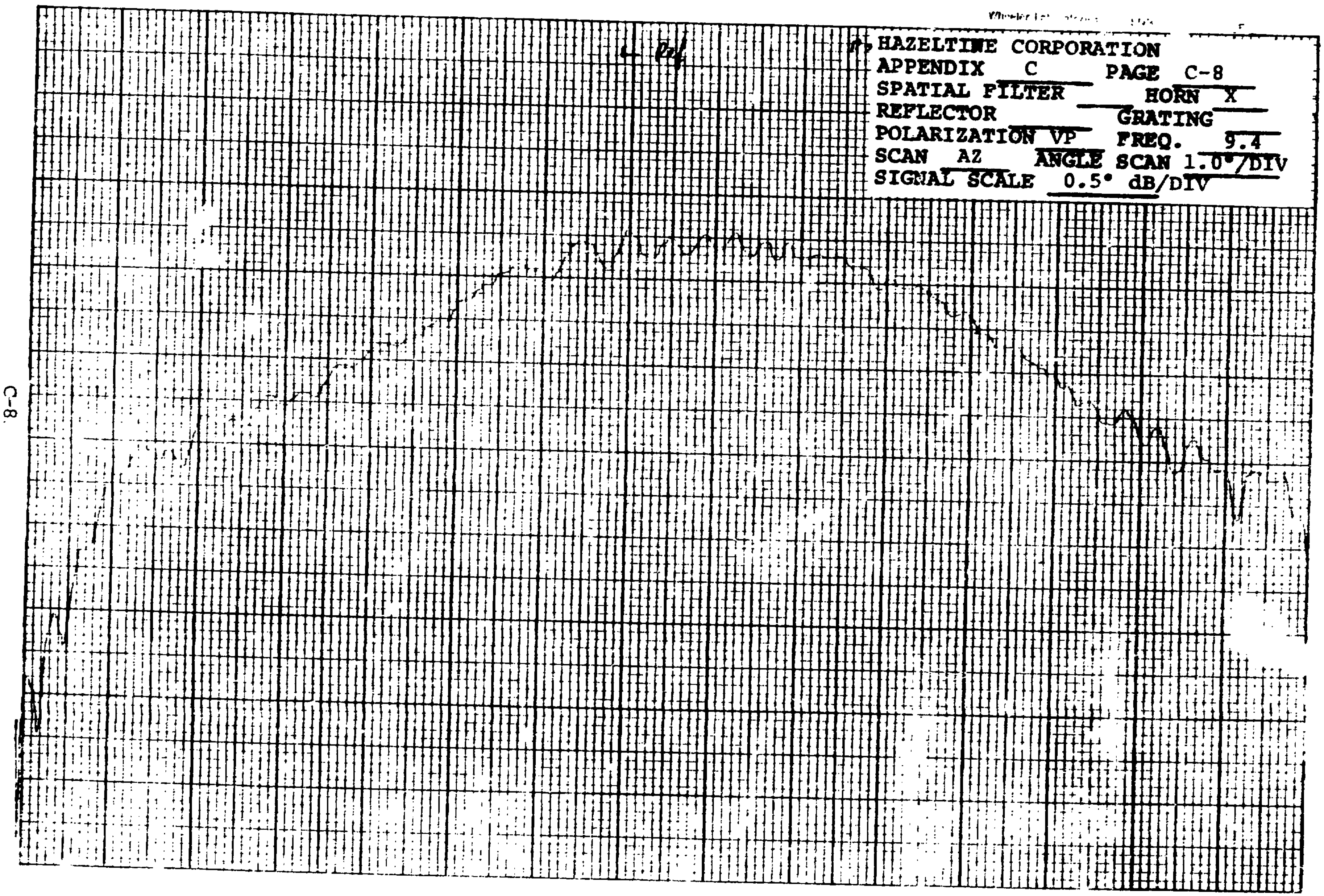

HAZELTINE CORPORATION
APPENDIX C PAGE C-8
SPATIAL FILTER HORN X
REFLECTOR GRATING
POLARIZATION VP FREQ. 9.4
SCAN AZ ANGLE SCAN 1.0°/DIV
SIGNAL SCALE 0.5° dB/DIV

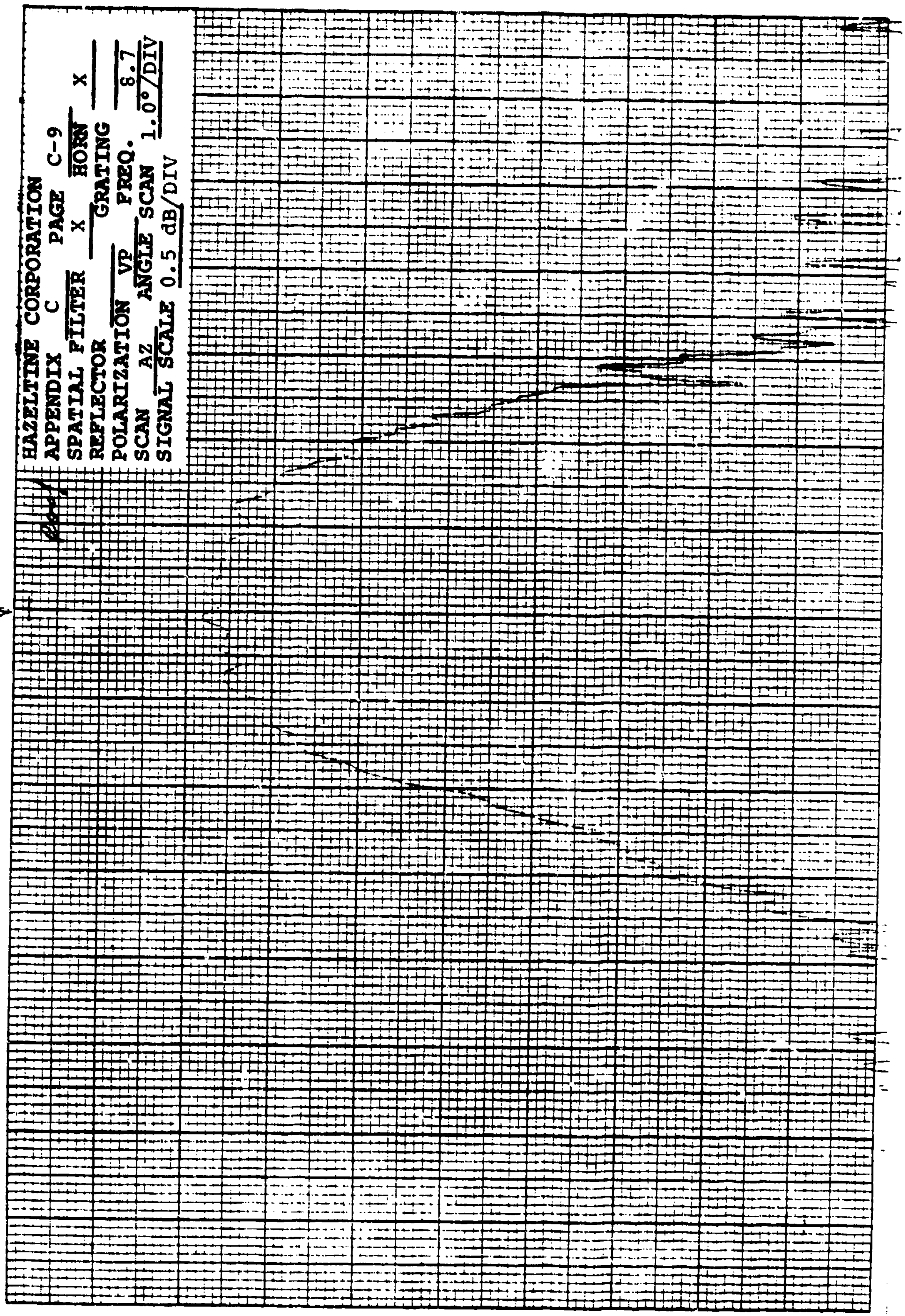
HAZELTINE CORPORATION
APPENDIX C PAGE C-9
SPATIAL FILTER X HORN X
REFLECTOR GRATING
POLARIZATION VP FREQ. 8.7
SCAN AZ ANGLE SCAN 1.0°/DIV
SIGNAL SCALE 0.5 dB/DIV

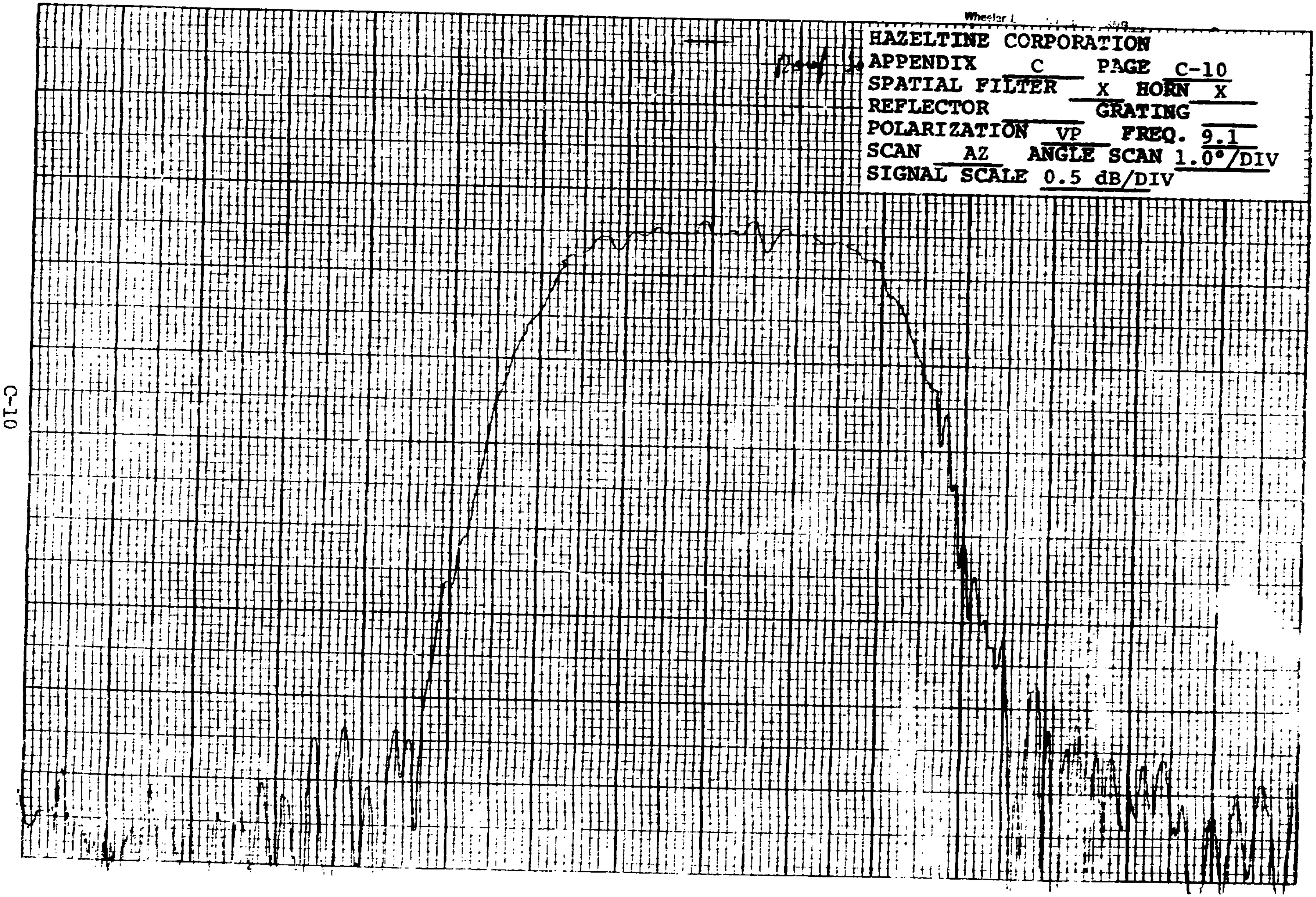
HAZELTINE CORPORATION
APPENDIX C PAGE C-10
SPATIAL FILTER X HORN X
REFLECTOR GRATING
POLARIZATION VP FREQ. 9.1
SCAN AZ ANGLE SCAN 1.0°/DIV
SIGNAL SCALE 0.5 dB/DIV

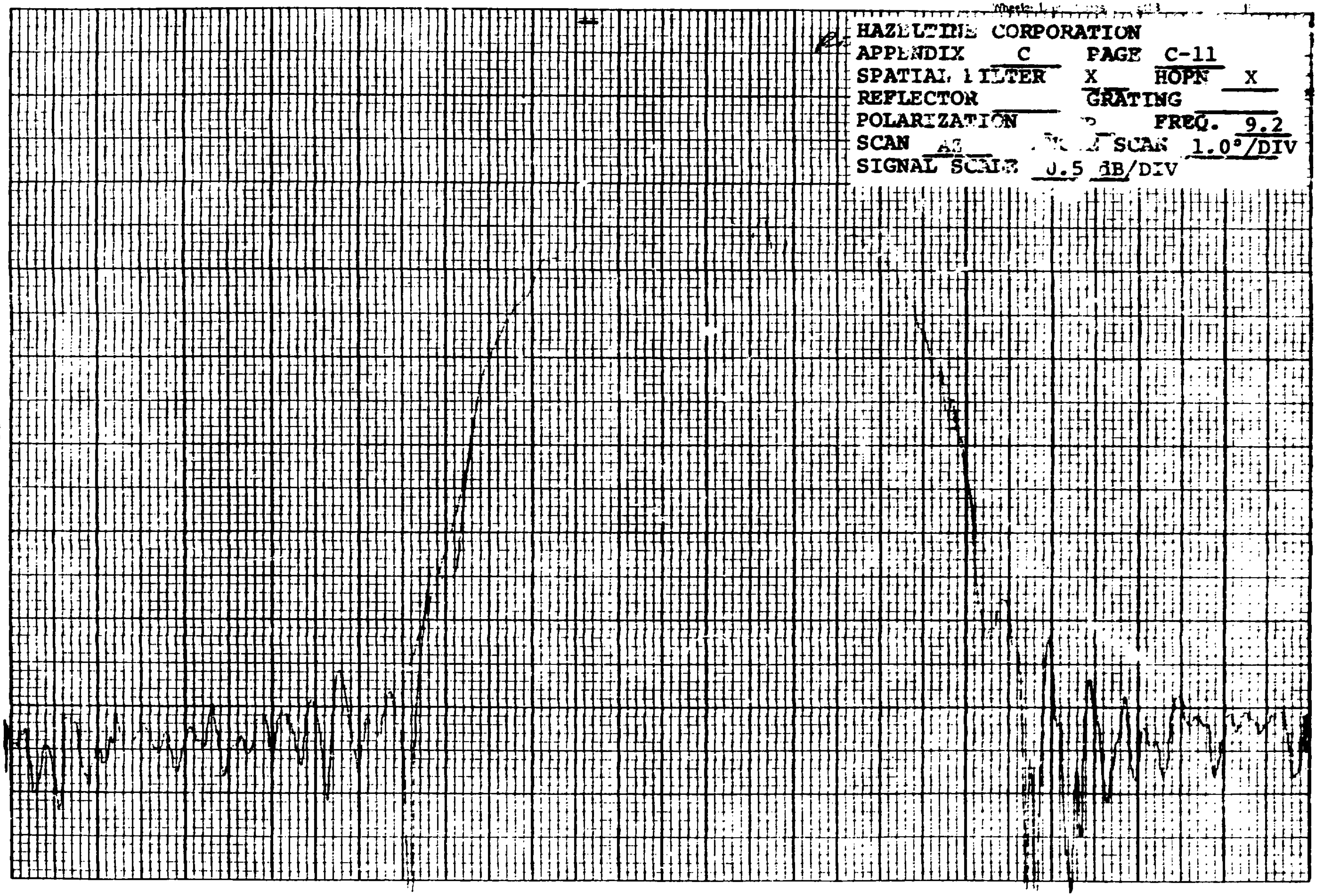
HAZELTINE CORPORATION
APPENDIX C PAGE C-11
SPATIAL FILTER X HORN X
REFLECTOR GRATING
POLARIZATION FREQ. 9.2
SCAN AZ SCAN 1.0°/DIV
SIGNAL SCALE 0.5 dB/DIV

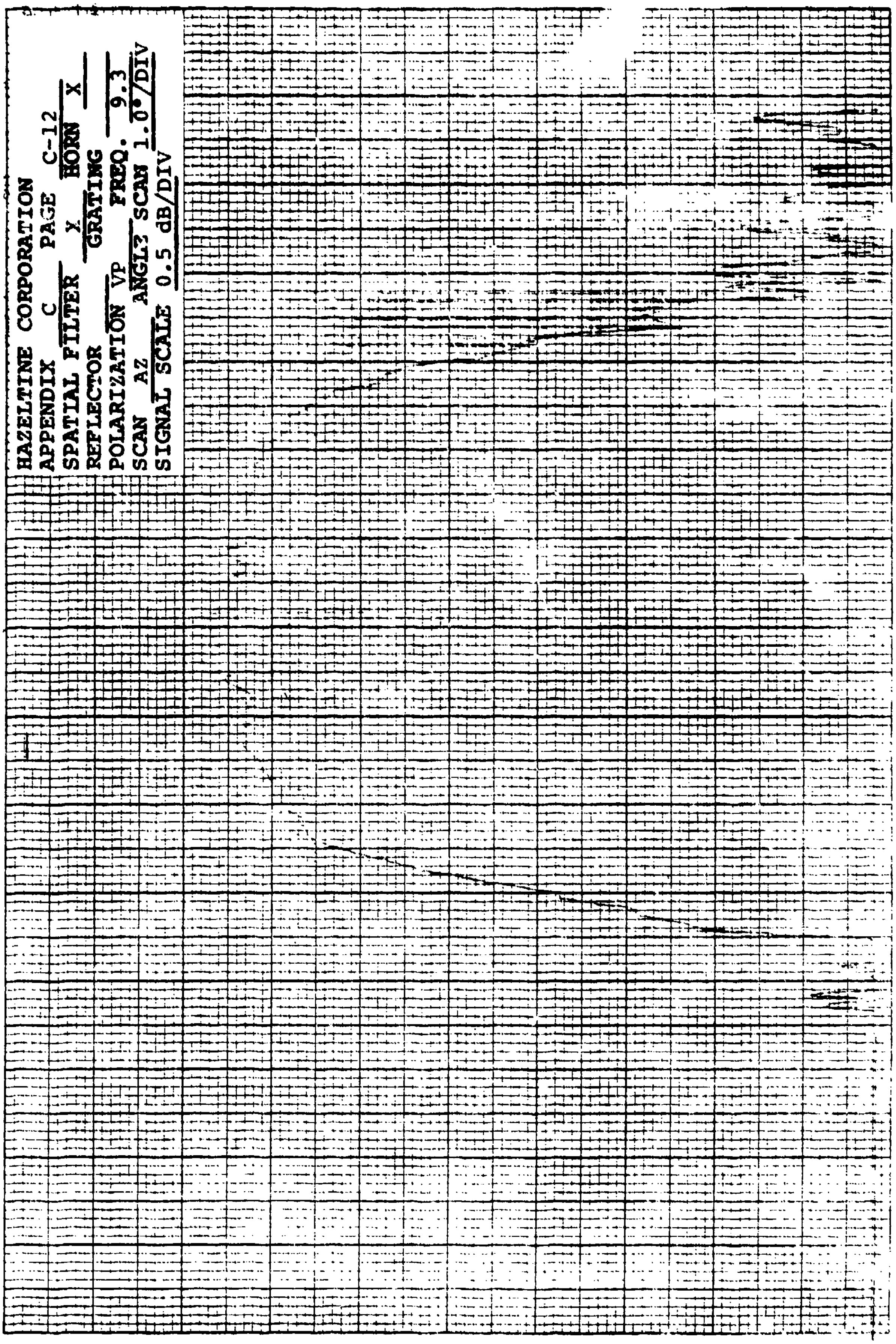
HAZELTINE CORPORATION
APPENDIX C PAGE C-12
SPATIAL FILTER X HORN X
REFLECTOR GRATING
POLARIZATION VP FREQ. 9.3
SCAN AZ ANGLE SCAN 1.0°/DIV
SIGNAL SCALE 0.5 dB/DIV

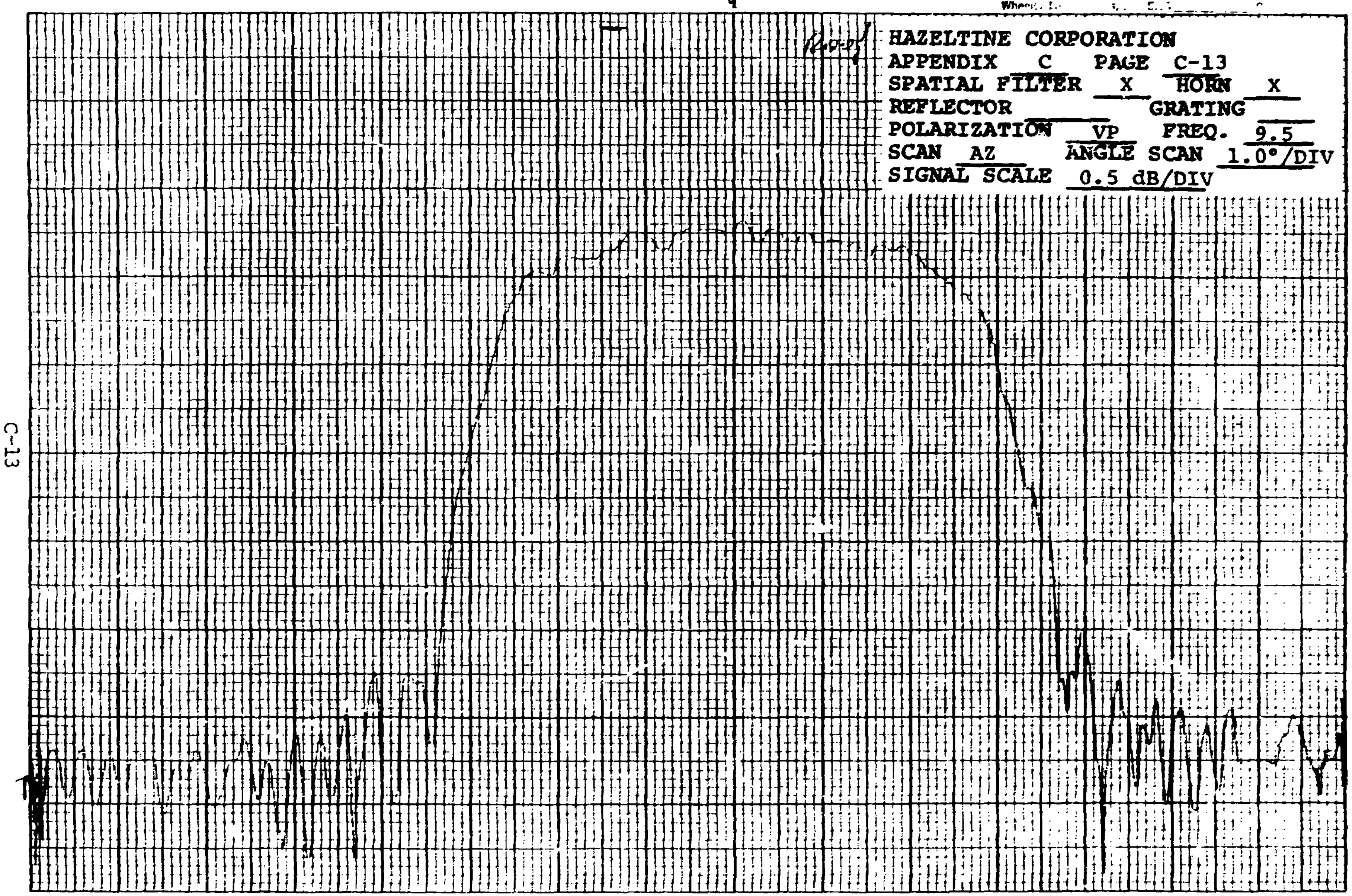
HAZELTINE CORPORATION
APPENDIX C PAGE C-13
SPATIAL FILTER X HORN X
REFLECTOR GRATING
POLARIZATION VP FREQ. 9.5
SCAN AZ ANGLE SCAN 1.0°/DIV
SIGNAL SCALE 0.5 dB/DIV

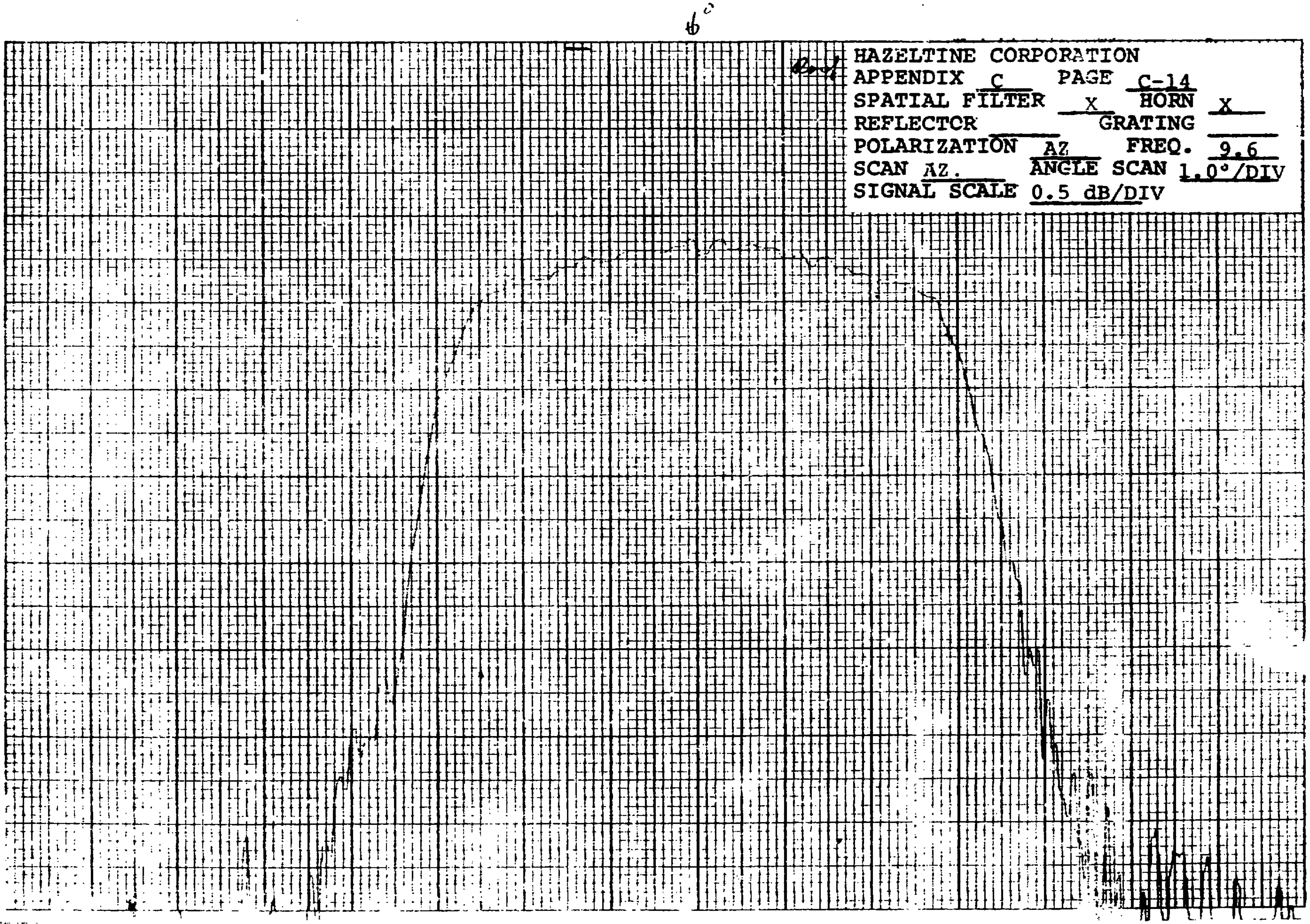
HAZELTINE CORPORATION
APPENDIX C PAGE C-14
SPATIAL FILTER X HORN X
REFLECTOR GRATING
POLARIZATION AZ FREQ. 9.6
SCAN AZ. ANGLE SCAN 1.0°/DIV
SIGNAL SCALE 0.5 dB/DIV
6°

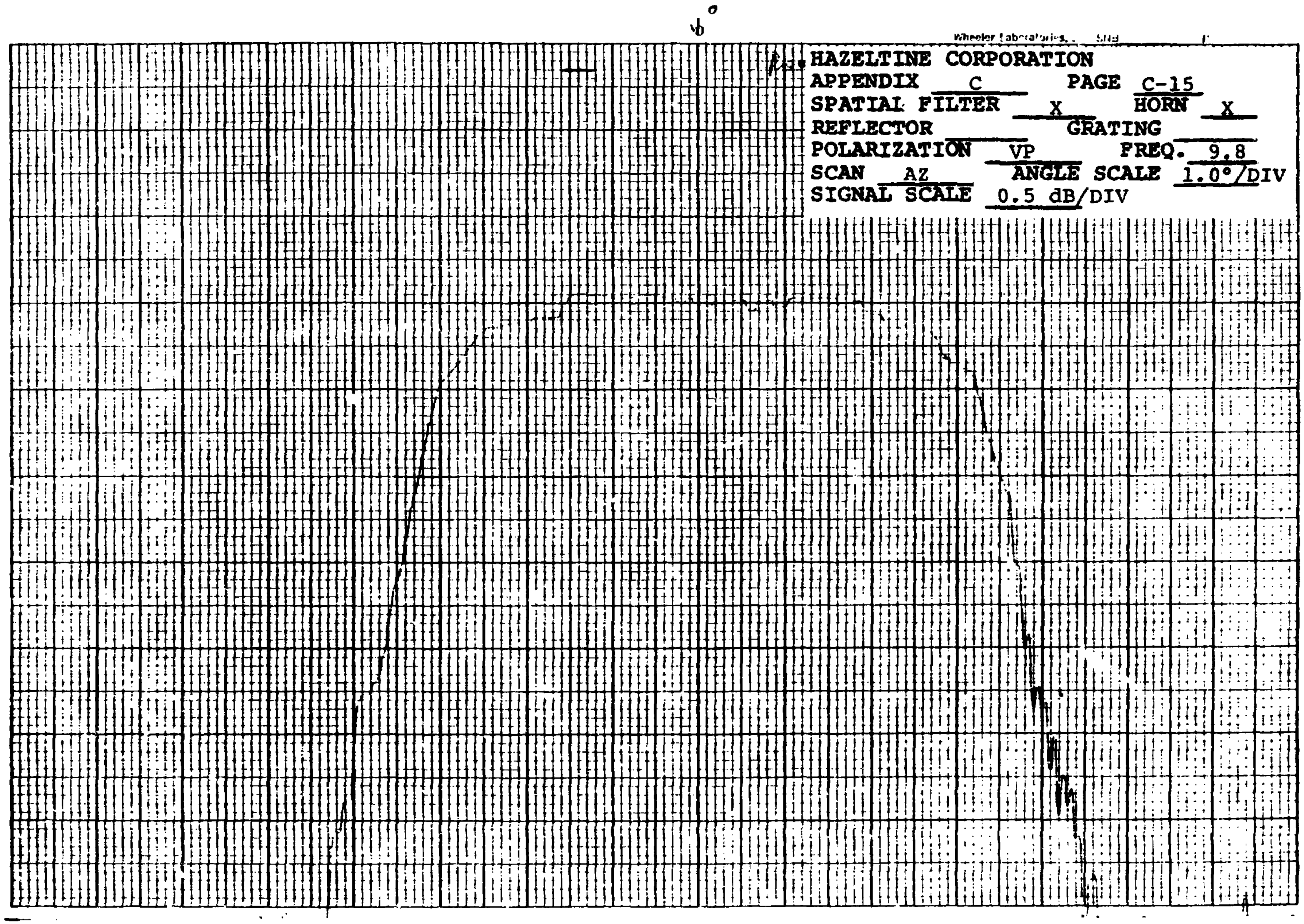
Wheeler Laboratories
HAZELTINE CORPORATION
APPENDIX C PAGE C-15
SPATIAL FILTER X HORN X
REFLECTOR GRATING
POLARIZATION VP FREQ. 9.8
SCAN AZ ANGLE SCALE 1.0°/DIV
SIGNAL SCALE 0.5 dB/DIV

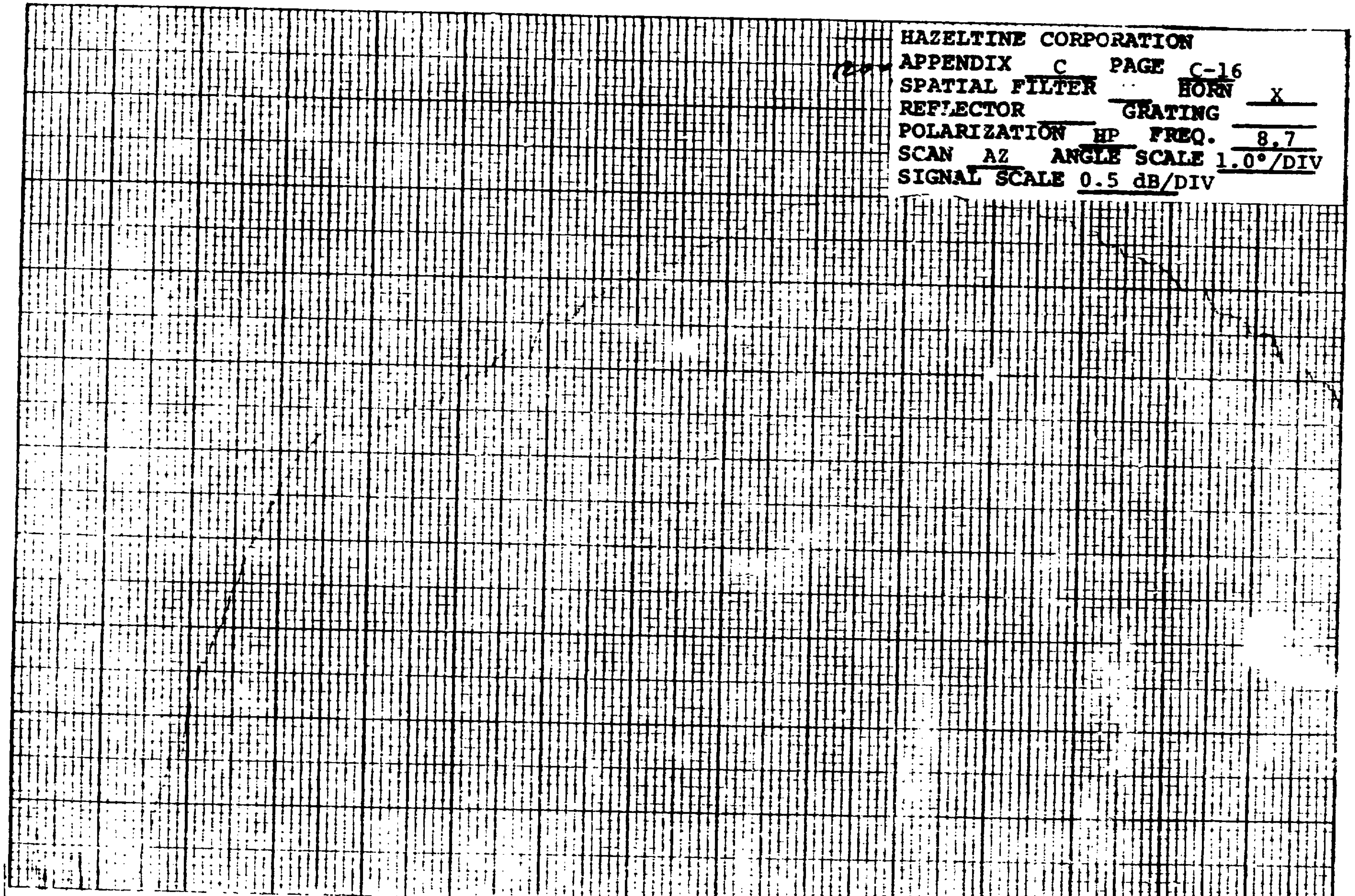
HAZELTINE CORPORATION
APPENDIX C PAGE C-16
SPATIAL FILTER HORN X
REFLECTOR GRATING
POLARIZATION HP FREQ. 8.7
SCAN AZ ANGLE SCALE 1.0°/DIV
SIGNAL SCALE 0.5 dB/DIV

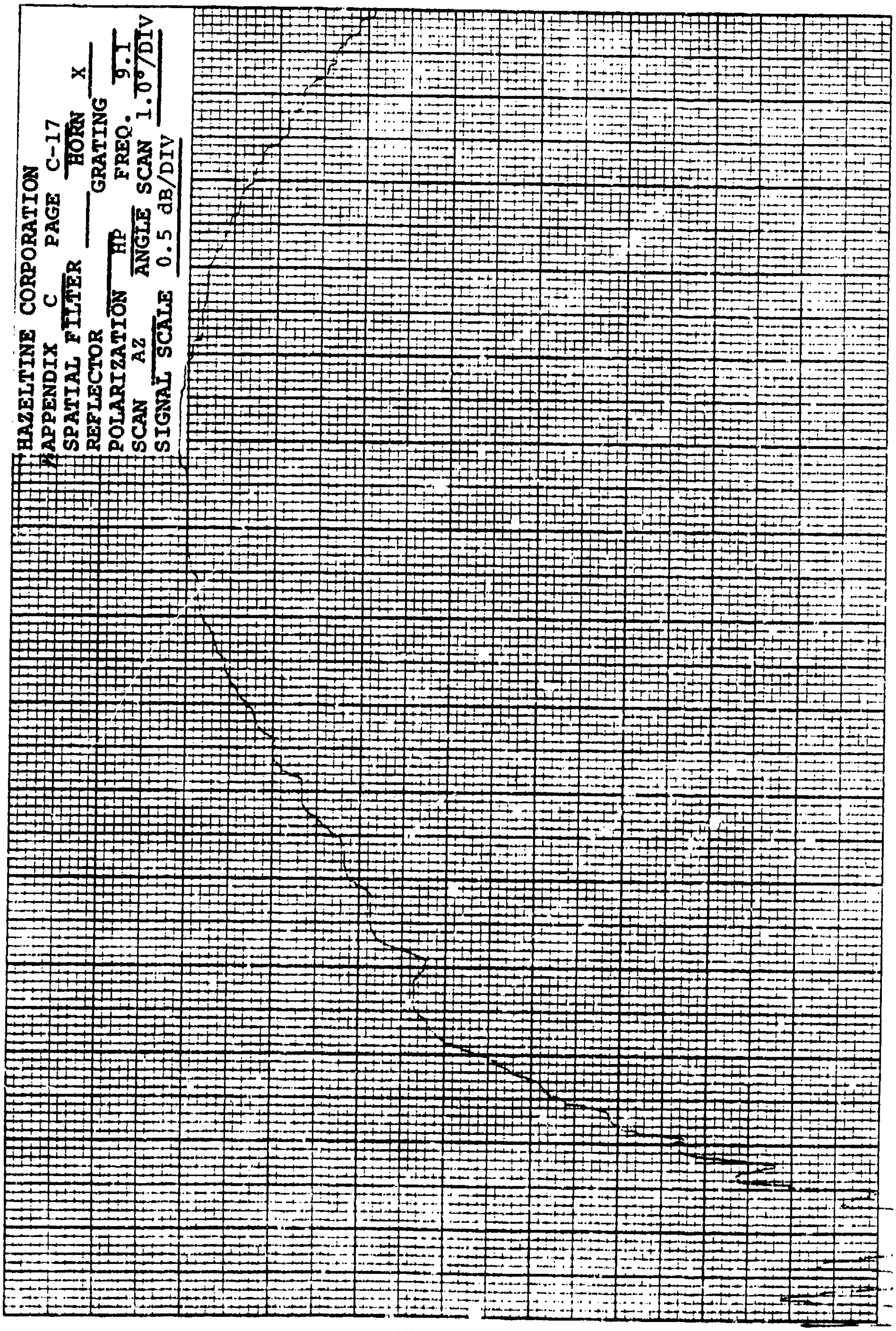
HAZELTINE CORPORATION
APPENDIX C PAGE C-17
SPATIAL FILTER HORN X
REFLECTOR GRATING
POLARIZATION HP FREQ. 9.1
SCAN AZ ANGLE SCAN 1.0°/DIV
SIGNAL SCALE 0.5 dB/DIV

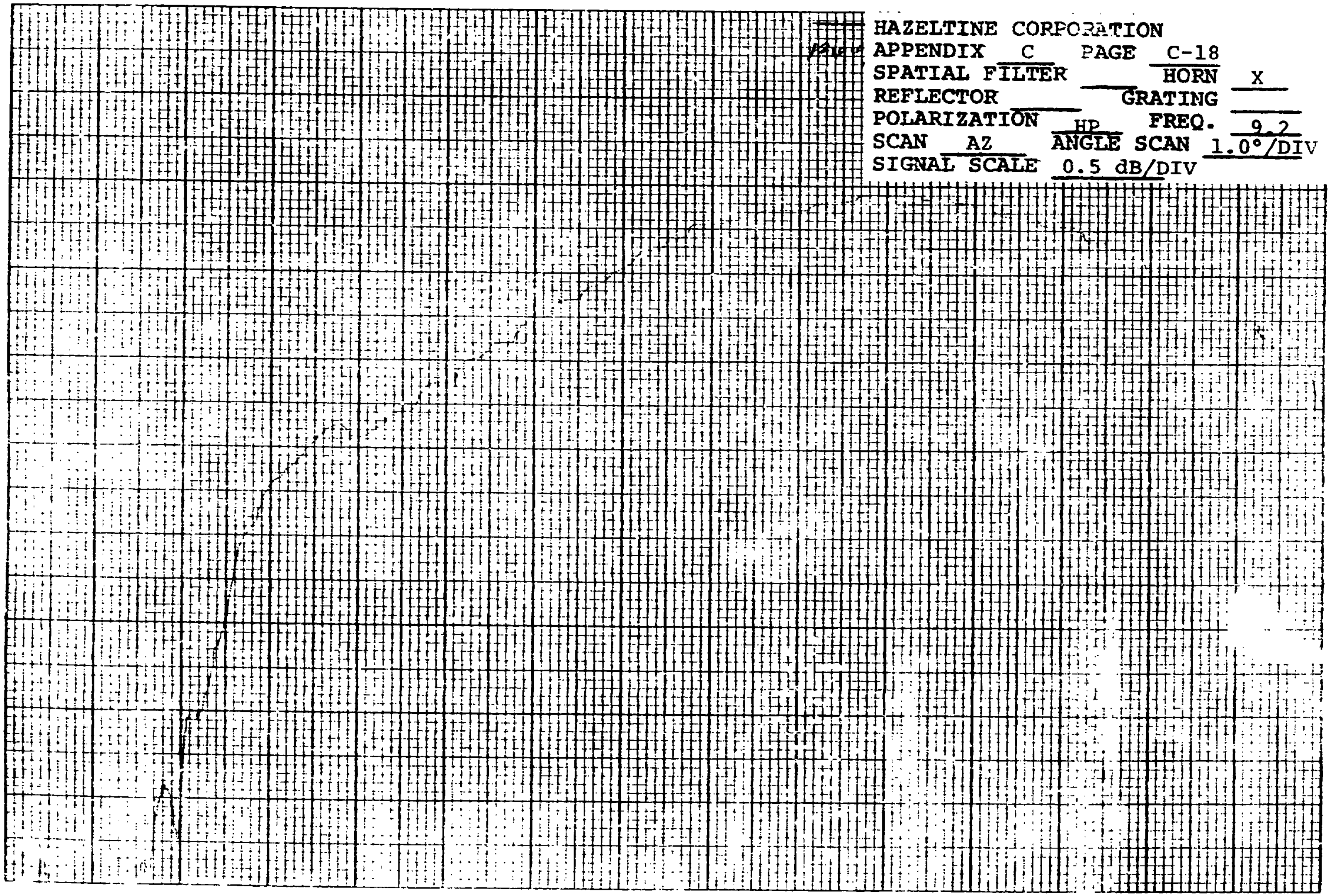
HAZELTINE CORPORATION
APPENDIX C PAGE C-18
SPATIAL FILTER HORN X
REFLECTOR GRATING
POLARIZATION HP FREQ. 9.2
SCAN AZ ANGLE SCAN 1.0°/DIV
SIGNAL SCALE 0.5 dB/DIV

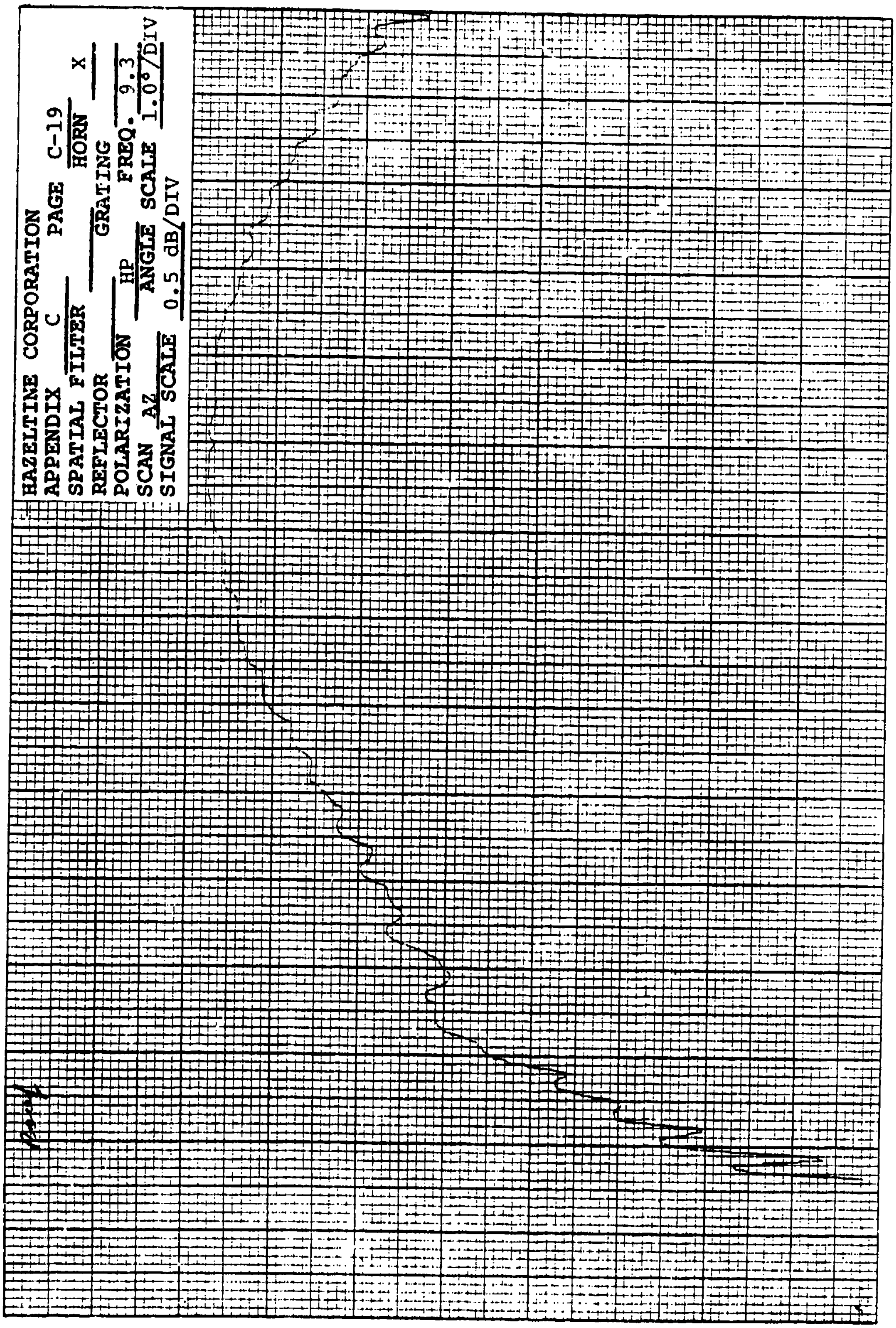
HAZELTINE CORPORATION
APPENDIX C PAGE C-19
SPATIAL FILTER HORN X
REFLECTOR GRATING
POLARIZATION HP FREQ. 9.3
SCAN AZ ANGLE SCALE 1.0°/DIV
SIGNAL SCALE 0.5 dB/DIV

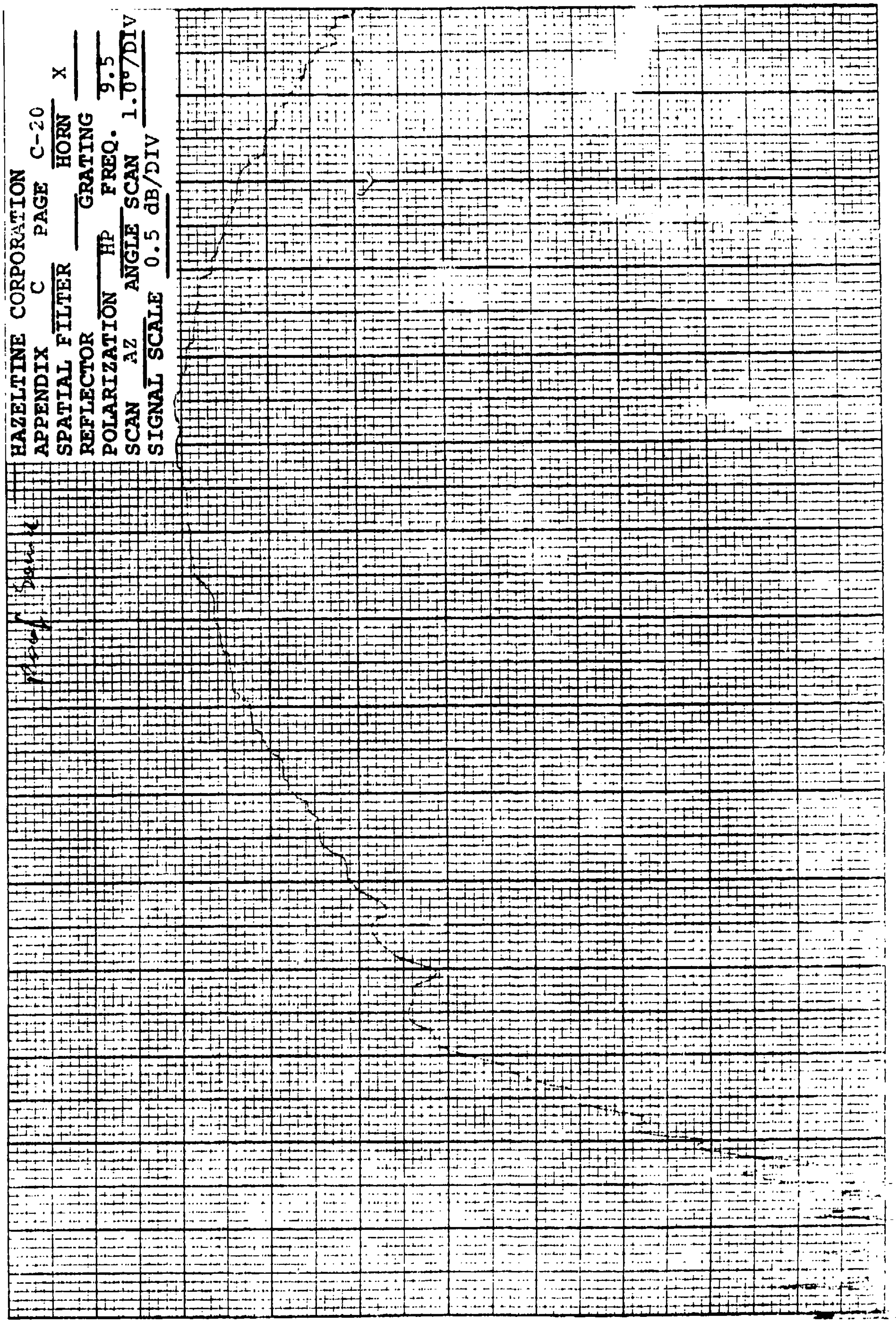
HAZELTINE CORPORATION
APPENDIX C PAGE C-20
SPATIAL FILTER HORN X
REFLECTOR GRATING
POLARIZATION HP FREQ. 9.5
SCAN AZ ANGLE SCAN 1.0°/DIV
SIGNAL SCALE 0.5 dB/DIV

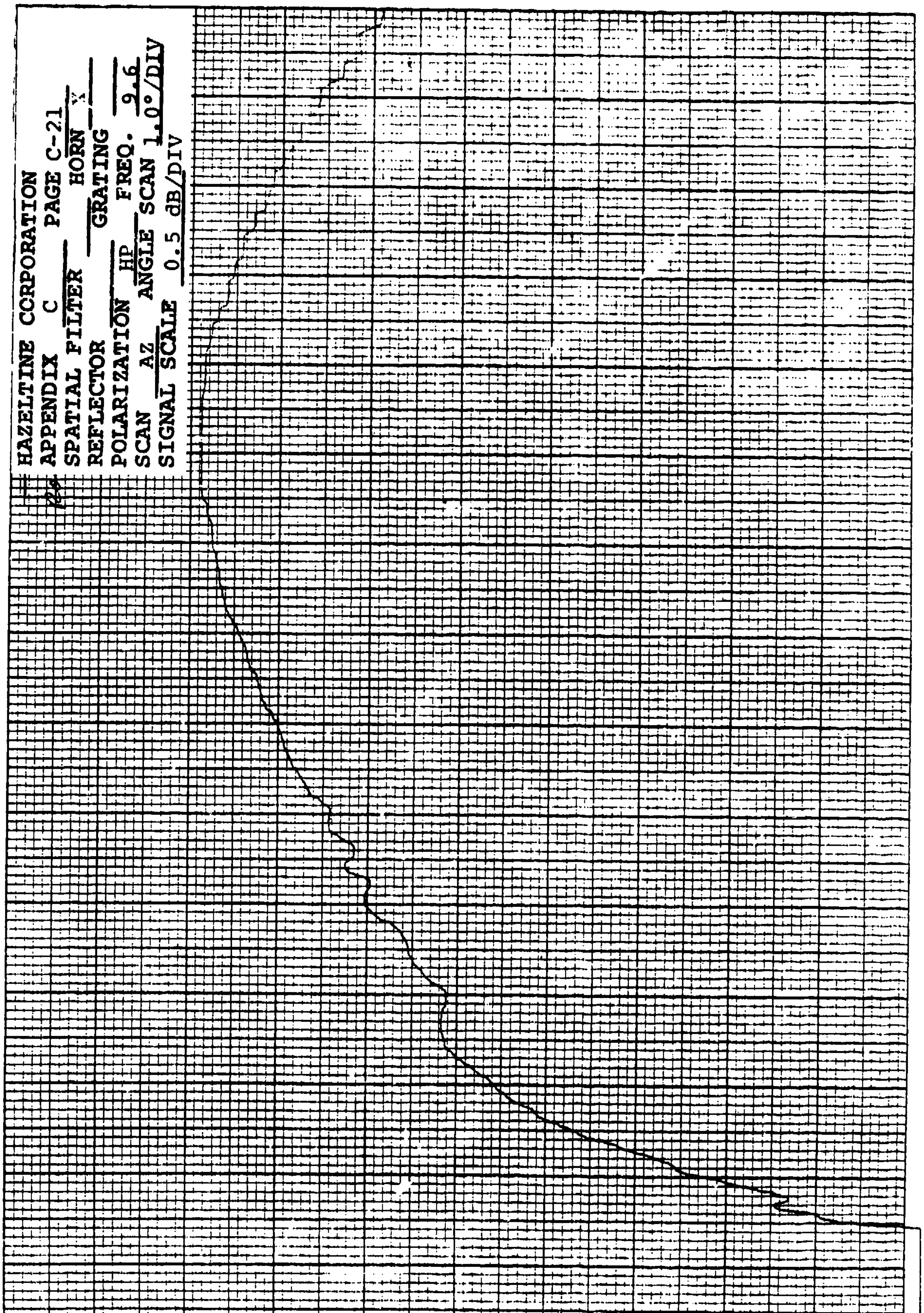

HAZELTINE CCRPORATION
APPENDIX C PAGE C-21
SPATIAL FILTER HORN X
REFLECTOR GRATING
POLARIZATION HP FREQ. 9.6
SCAN AZ ANGLE SCAN 1.0°/DIV
SIGNAL SCALE 0.5 dB/DIV

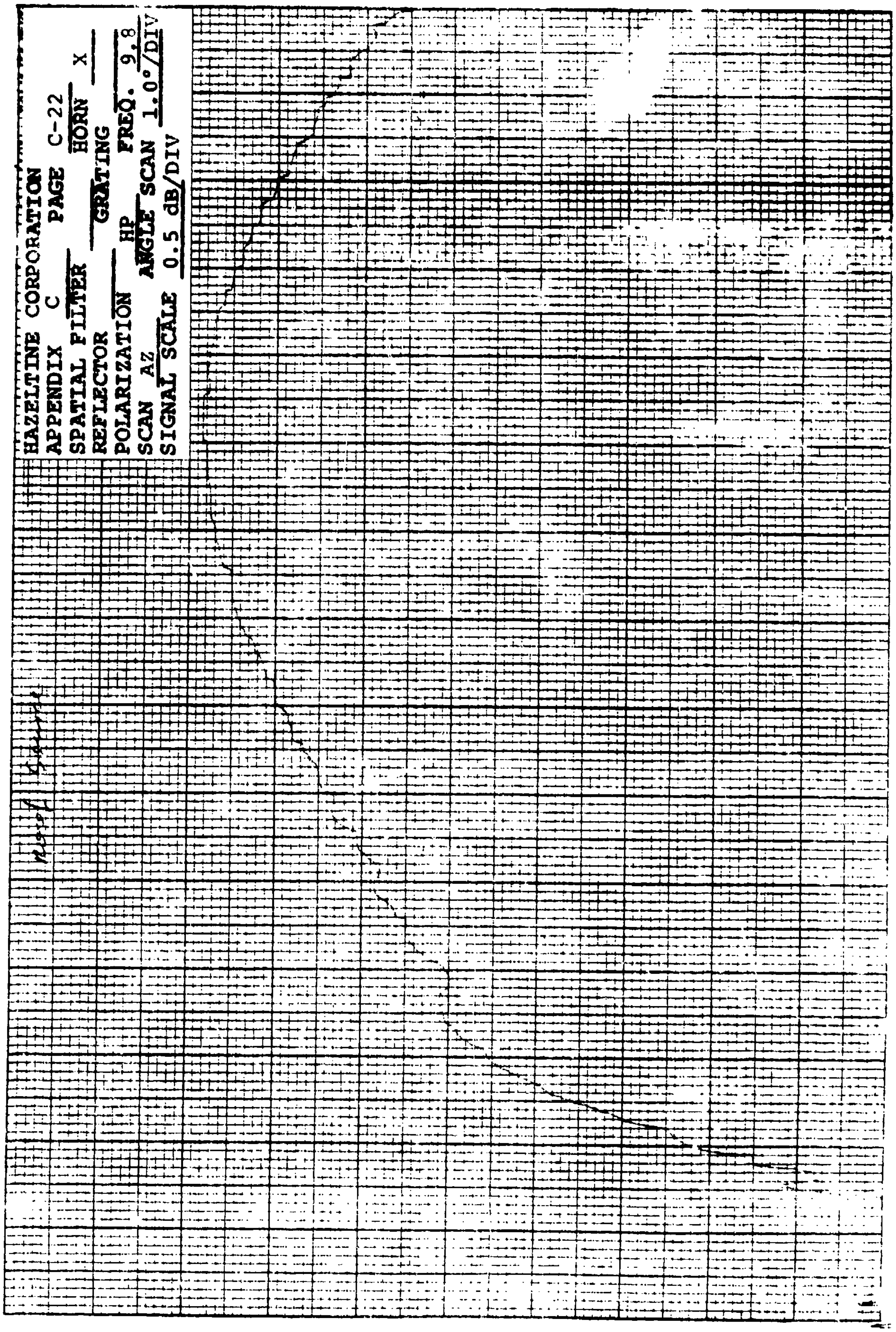
HAZELTINE CORPORATION
APPENDIX C PAGE C-22
SPATIAL FILTER HORN X
REFLECTOR GRATING
POLARIZATION HP FREQ. 9.8
SCAN AZ ANGLE SCAN 1.0°/DIV
SIGNAL SCALE 0.5 dB/DIV

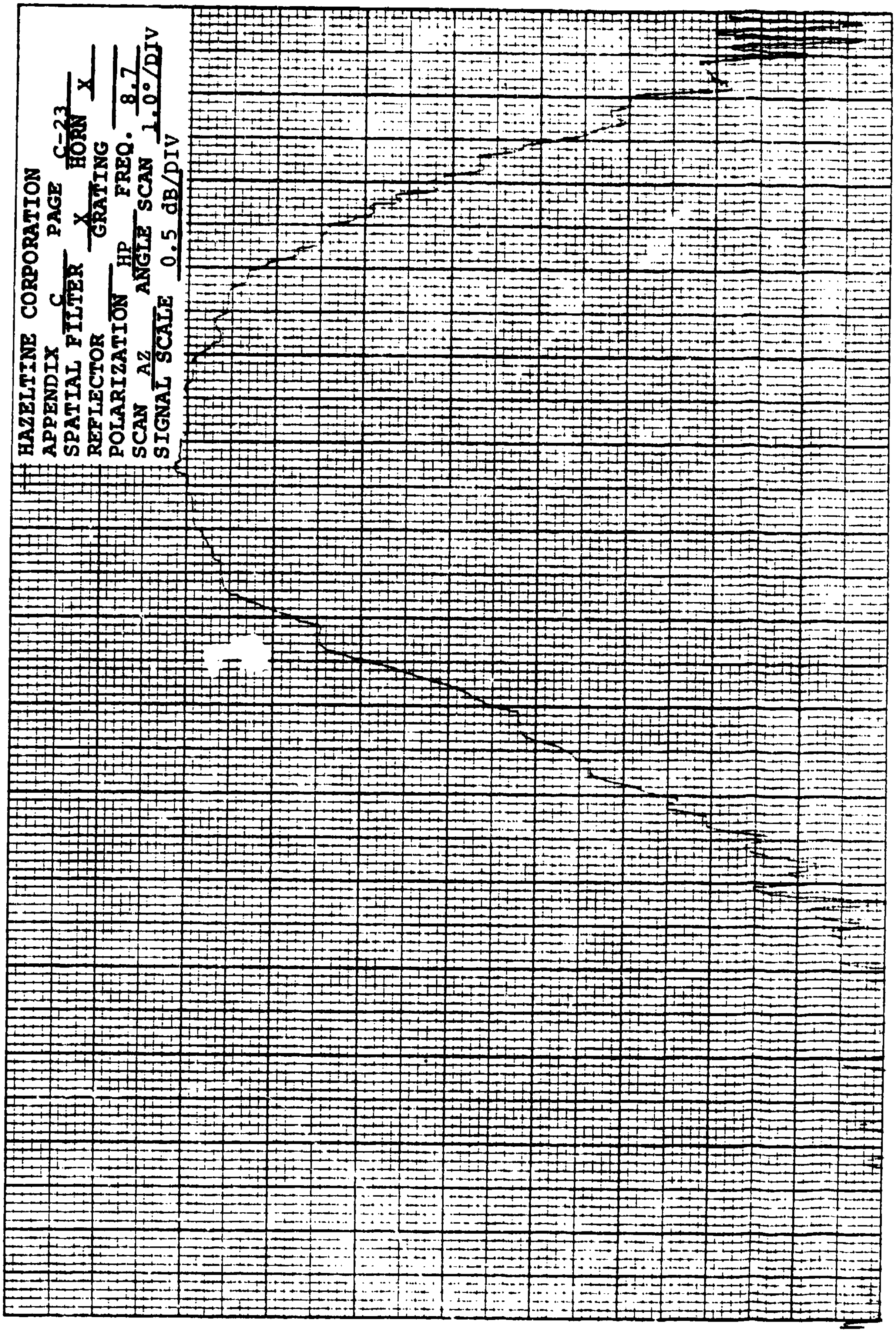
HAZELTINE CORPORATION
APPENDIX C PAGE C-23
SPATIAL FILTER X HORN X
REFLECTOR GRATING
POLARIZATION HP FREQ. 8.7
SCAN AZ ANGLE SCAN 1.0°/DIV
SIGNAL SCALE 0.5 dB/DIV

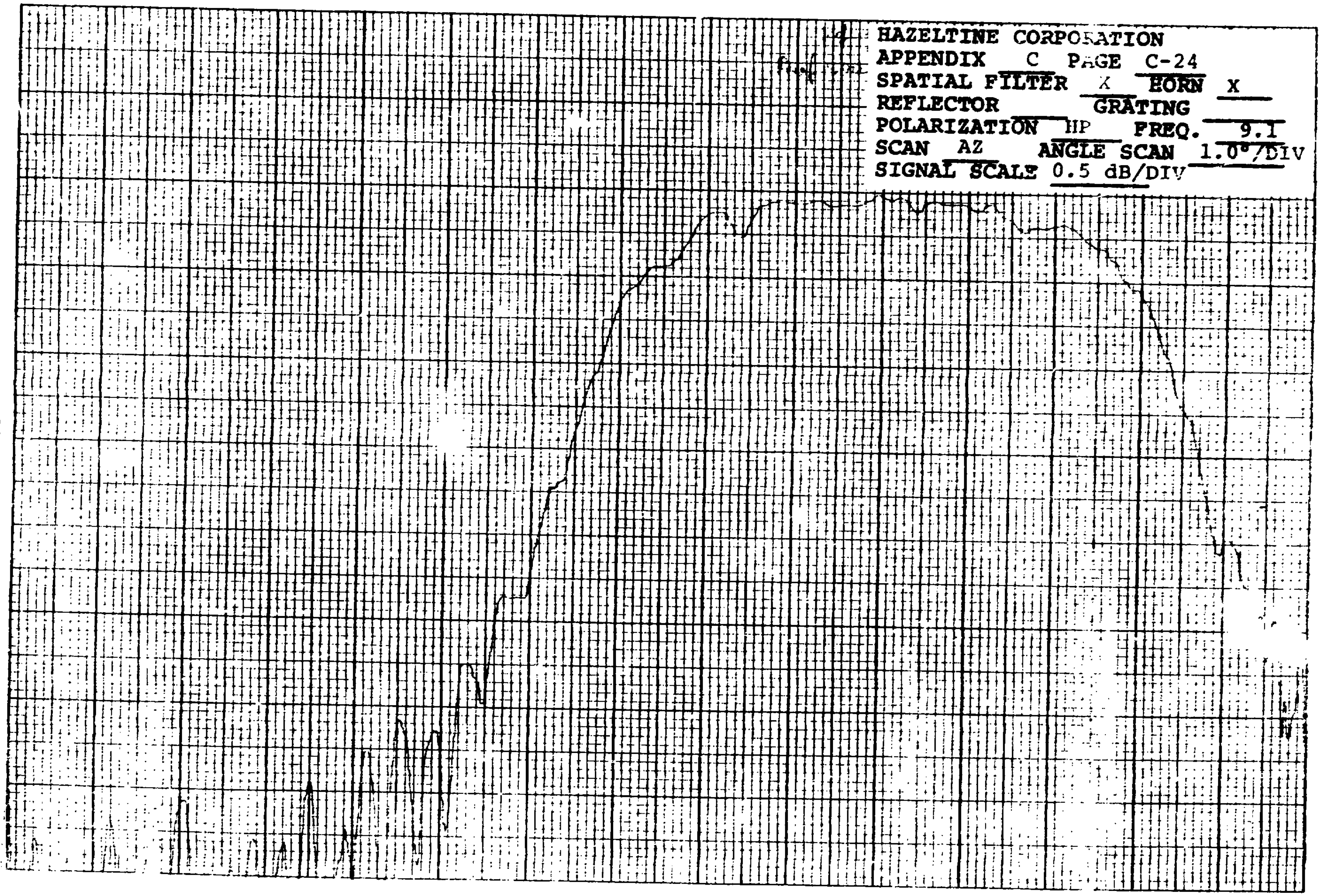
HAZELTINE CORPORATION
APPENDIX C PAGE C-24
SPATIAL FILTER X HORN X
REFLECTOR GRATING
POLARIZATION HP FREQ. 9.1
SCAN AZ ANGLE SCAN 1.0°/DIV
SIGNAL SCALE 0.5 dB/DIV

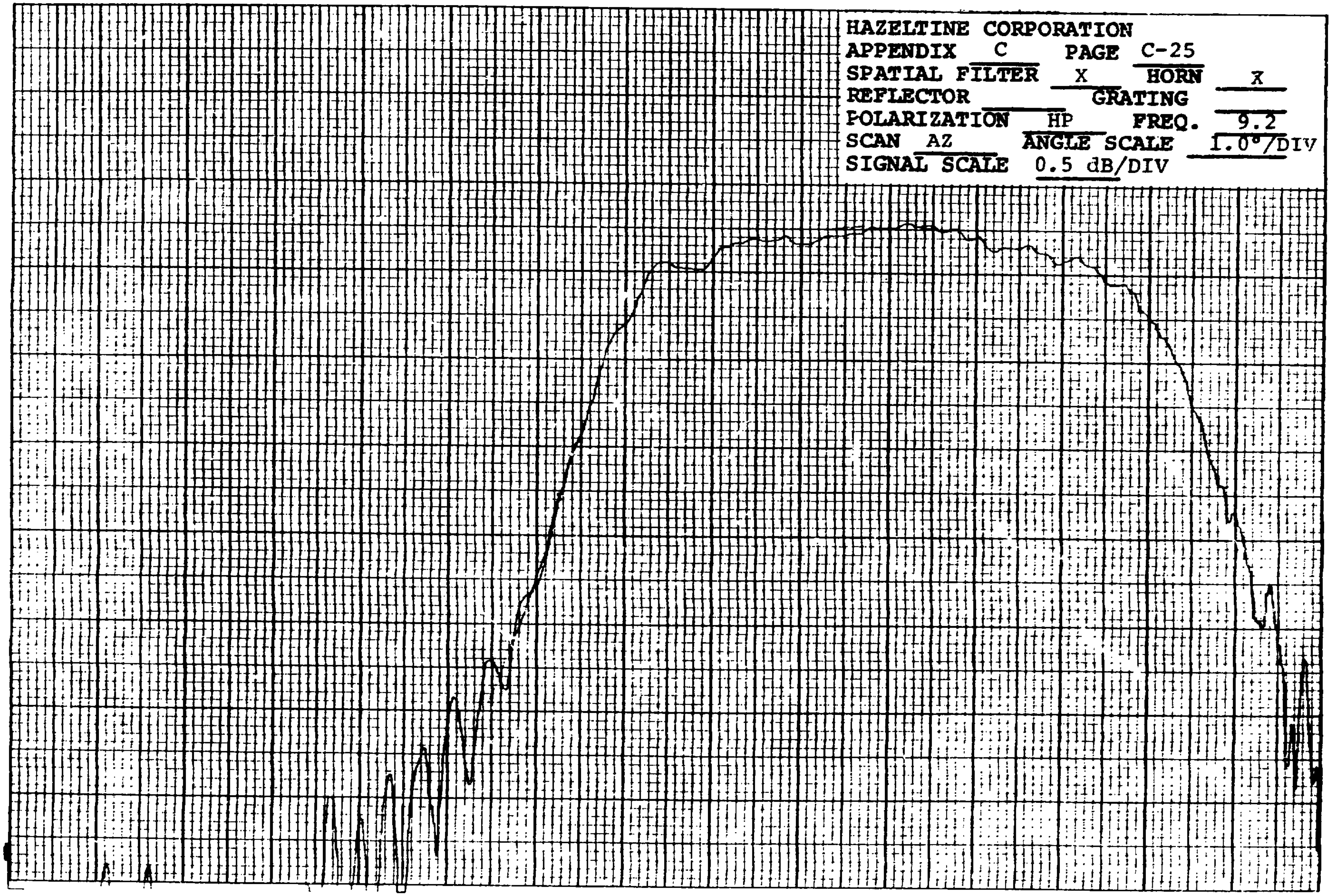
HAZELTINE CORPORATION
APPENDIX C PAGE C-25
SPATIAL FILTER X HORN X
REFLECTOR GRATING
POLARIZATION HP FREQ. 9.2
SCAN AZ ANGLE SCALE 1.0°/DIV
SIGNAL SCALE 0.5 dB/DIV

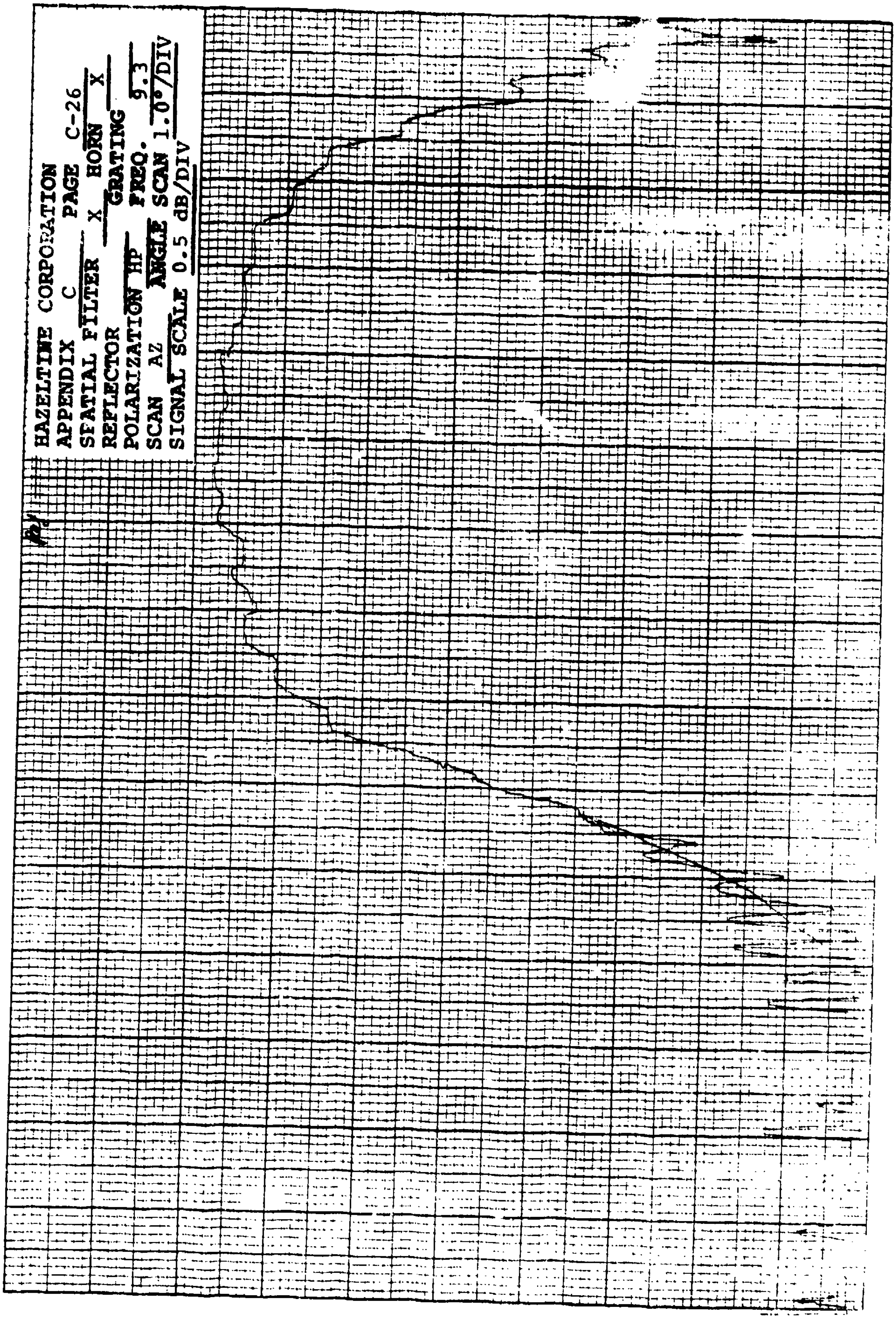
HAZELTINE CORPORATION
APPENDIX C PAGE C-26
SPATIAL FILTER X HORN X
REFLECTOR GRATING
POLARIZATION HP FREQ. 9.3
SCAN AZ ANGLE SCAN 1.0°/DIV
SIGNAL SCALE 0.5 dB/DIV

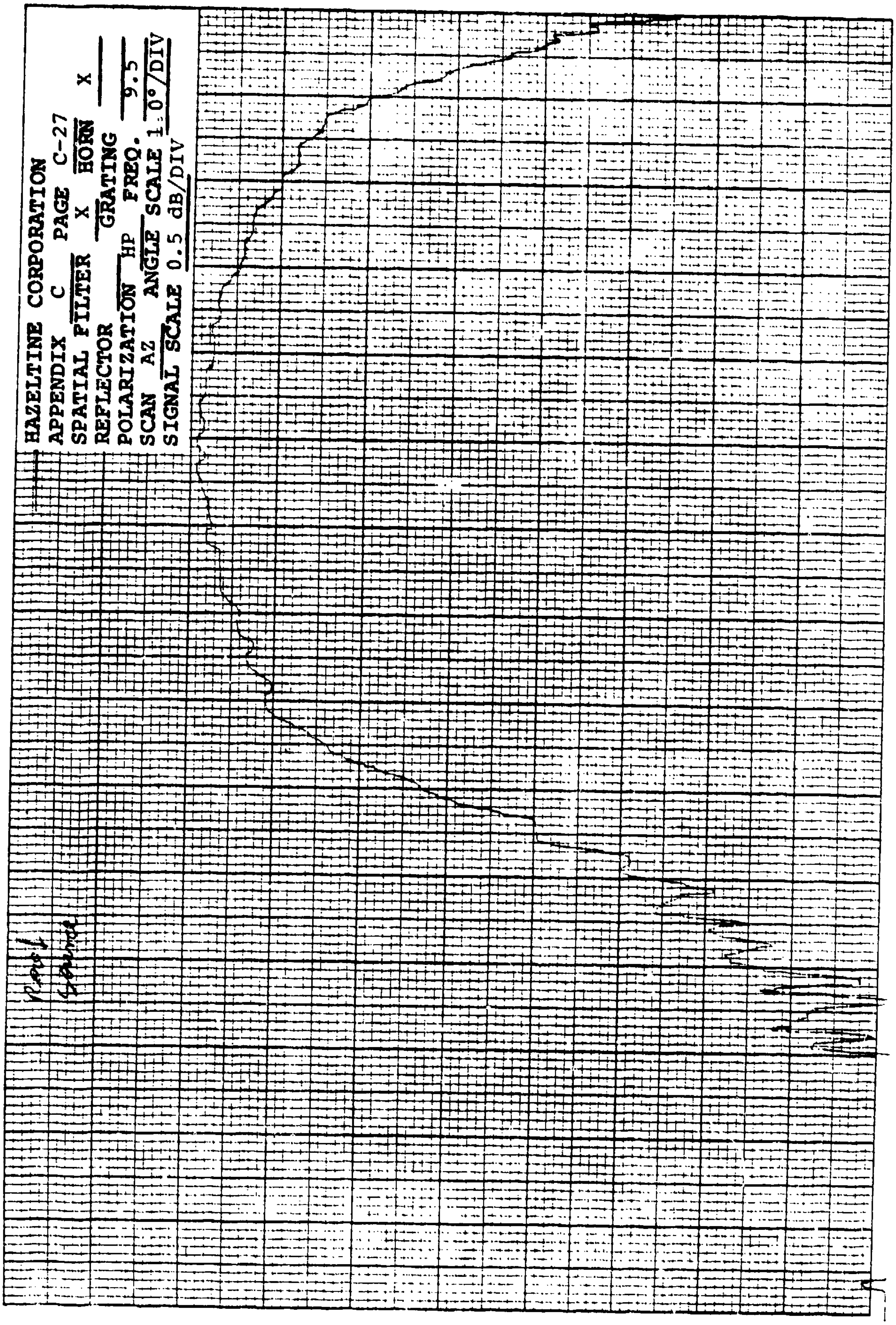
HAZELTINE CORPORATION
APPENDIX C PAGE C-27
SPATIAL FILTER X HORN X
REFLECTOR GRATING
POLARIZATION HP FREQ. 9.5
SCAN AZ ANGLE SCALE 1.0°/DIV
SIGNAL SCALE 0.5 dB/DIV
Real Source

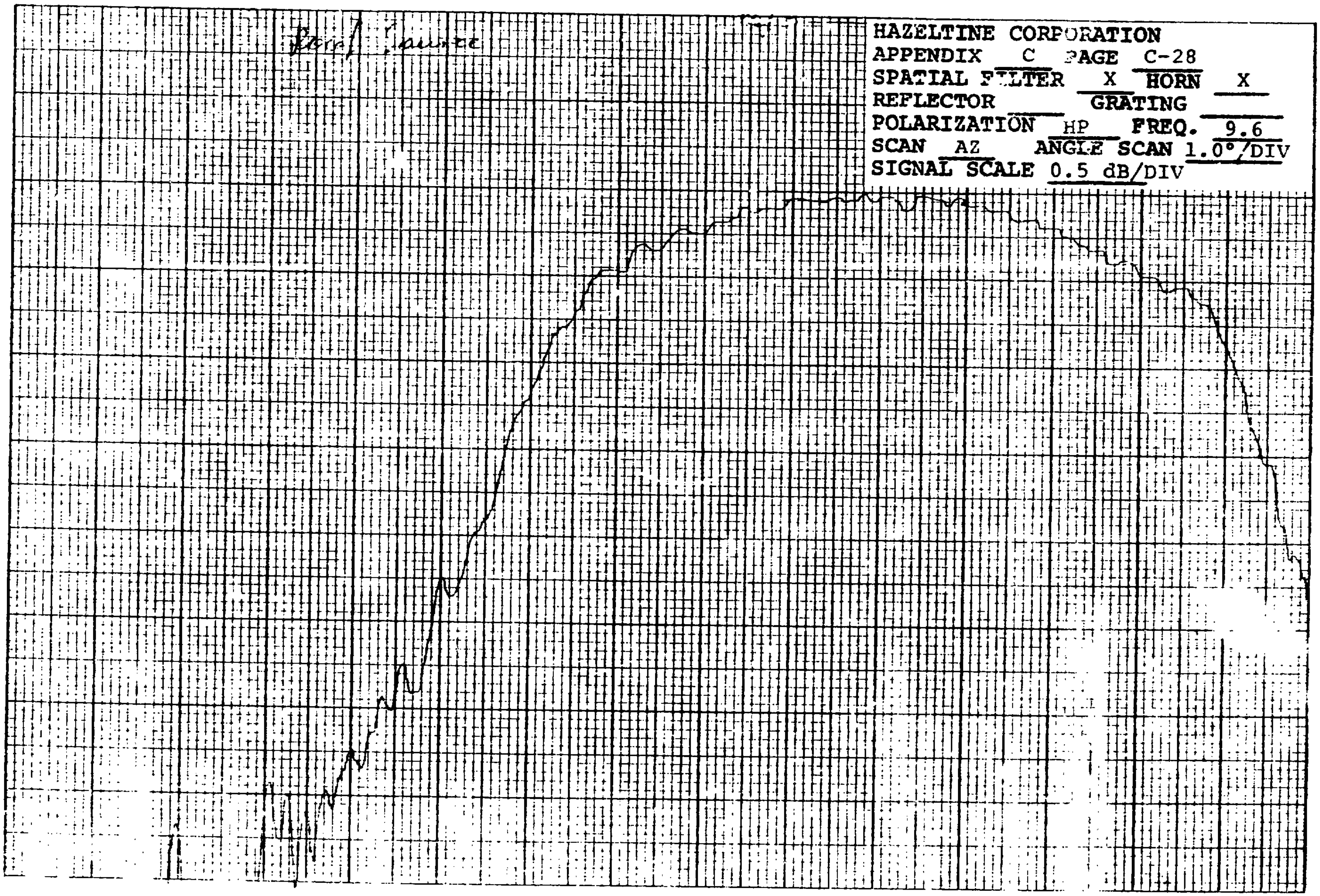
HAZELTINE CORPORATION
APPENDIX C PAGE C-28
SPATIAL FILTER X HORN X
REFLECTOR GRATING
POLARIZATION HP FREQ. 9.6
SCAN AZ ANGLE SCAN 1.0°/DIV
SIGNAL SCALE 0.5 dB/DIV

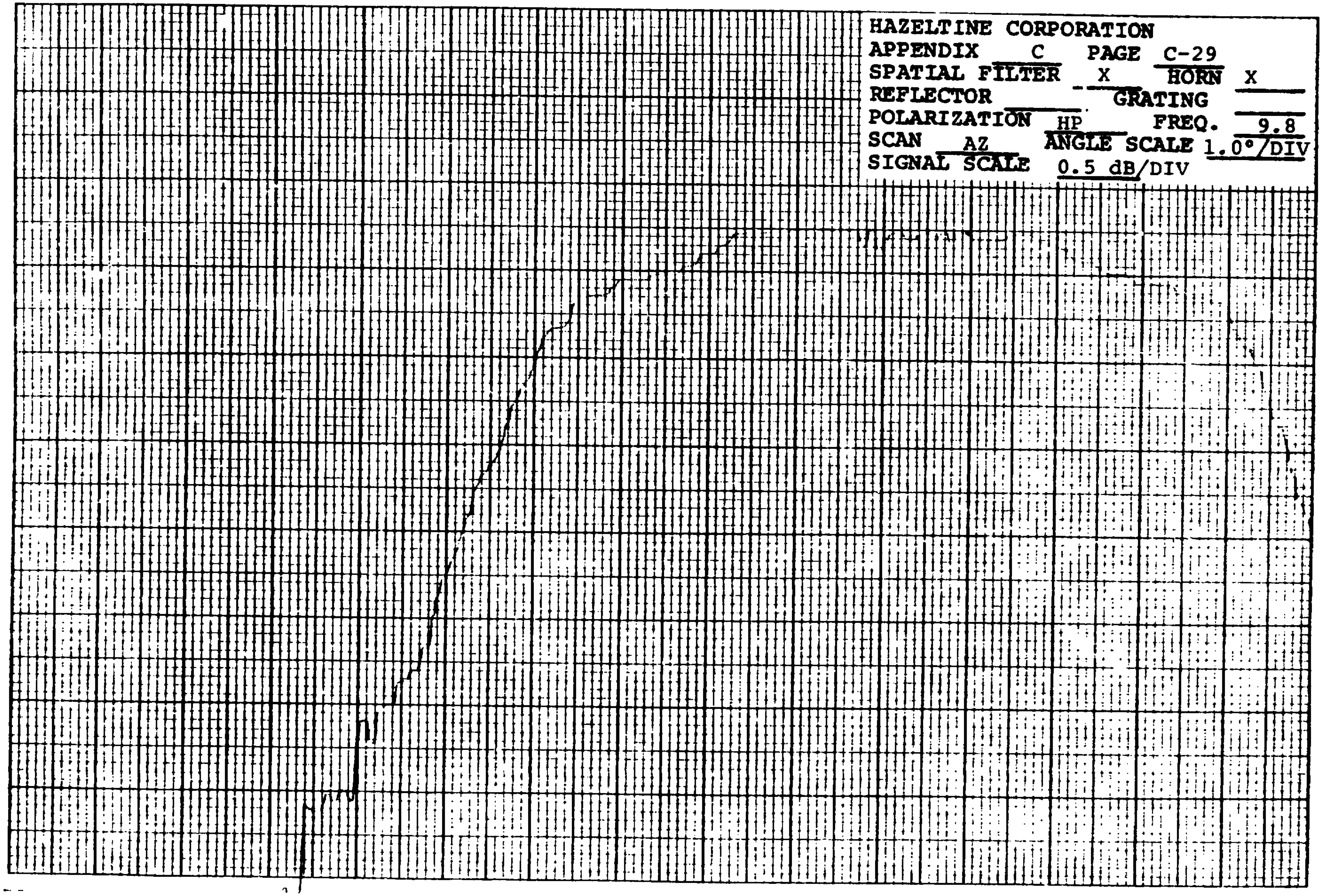
HAZELTINE CORPORATION
APPENDIX C PAGE C-29
SPATIAL FILTER X HORN X
REFLECTOR - GRATING
POLARIZATION HP FREQ. 9.8
SCAN AZ ANGLE SCALE 1.0°/DIV
SIGNAL SCALE 0.5 dB/DIV

MISSION
of
Rome Air Development Center

RADC plans and executes research, development, test and selected acquisition programs in support of Command, Control Communications and Intelligence (C^3I) activities. Technical and engineering support within areas of technical competence is provided to ESD Program Offices (POs) and other ESD elements. The principal technical mission areas are communications, electromagnetic guidance and control, surveillance of ground and aerospace objects, intelligence data collection and handling, information system technology, ionospheric propagation, solid state sciences, microwave physics and electronic reliability, maintainability and compatibility.

Printed by
United States Air Force
Hanscom AFB, Mass. 01731